University of Southampton

Faculty of Engineering and Physical Sciences

Institute of Sound and Vibration Research

A Study of the Suspension-Seat-Occupant System Dynamics under Tri-Axial Translational Vibration

by

Weitan Yin

ORCID ID: 0000-0002-1598-5514

Thesis for the degree of Doctor of Philosophy

July 2022

University of Southampton

Abstract

Faculty of Engineering and Physical Sciences
Institute of Sound and Vibration Research

Thesis for the degree of Doctor of Philosophy

A Study of the Suspension-Seat-Occupant System Dynamics under Tri-Axial Translational Vibration

by Weitan Yin

Most previous studies on the biodynamic response and the seating dynamics were limited to single-axial excitations. How the suspension-seat-occupant system behaves in the multi-axial vibrational environment is less reported. The objective of this study is to advance the understanding of the effect of the excitation magnitude and the backrest inclination angle on the biodynamic response of the seated human body and the transmissibility of the suspension seat with tri-axial translational excitation.

An experimental study was carried out with single-axial excitations at various magnitudes up to 1.0 ms^{-2} (r.m.s.) to examine the effect of the backrest inclination angles on the biodynamic response in fore-aft, lateral and vertical directions when the human body was sitting in the rigid seat. It was found that, at different excitation magnitudes, the apparent masses in the three translational directions were affected by the increased backrest inclination angle up to 20°. Such an inclination angle also affected the degree of the nonlinearity caused by changing excitation magnitude.

The experimental study on the human body seated in the rigid seat also investigated under tri-axial excitations the effect of the excitation magnitude in fore-aft, lateral and vertical directions (up to 1.0 ms^{-2} r.m.s. in each axis) and the backrest inclination angle on the biodynamic response. The increased excitation magnitude in one (named as “primary-axis”) of three translational axes and that in the other two (named as “secondary-axes”) axes both led to the decrease of the resonance frequency of the apparent mass in the “primary-axis” under the conditions tested. Interactive effects were found between the excitation magnitudes in different directions: the reduction of the resonance frequency of the apparent mass with the increased excitation magnitude in the “primary-axis” became smaller when the excitation magnitude in the “secondary-axes” was increased, and vice versa. Furthermore, the effect of backrest inclination angle under tri-axial vibration on the apparent mass was found to be comparable with that under single-axial vibration. Results showed that the backrest inclination and the excitation magnitude had combined effect on the degree of nonlinearity of the apparent mass.

The effect of the excitation magnitude and the backrest inclination angle on the transmissibility of the suspension seat with the seated subject was further studied with tri-axial excitation. Under the conditions tested, the suspension seat with loaded inert mass exhibited nonlinear behaviour in all three translational directions subject to the change of the excitation magnitude in the “primary-axis”. The interaction between the excitation magnitude in the “primary-axis” and that in the “secondary-axes” were observed in the transmissibilities of the suspension seat with seated occupant. The backrest inclination angle also affected the moduli of the seat transmissibilities at the backrest.

Based on the experimental studies, a linear multi-body biodynamic model of the seated human body exposed to tri-axial vibration was developed. With a rigorous calibration procedure, the model was shown to be capable of representing the tri-axial biodynamic responses of human body supported by either upright or inclined backrest. Four vibration modes of the human body, which contributed to the resonances of the lateral, fore-aft and vertical apparent masses respectively, were identified through a modal analysis with the calibrated biodynamic model.

Finally, linear multi-body models of the suspension mechanism with inert mass, the suspension seat with inert mass, and suspension seat with occupant under tri-axial excitation were developed. Results showed that the suspension-seat-occupant model was capable of predicting the fore-aft

and vertical seat transmissibilities at the seat pan and backrest under tri-axial excitation when the subject was seated. The parameters of the seat model (e.g., the contact stiffness at the seat-occupant interface) to which the seat transmissibilities were most sensitive were identified, providing useful information for the seat design to improve ride comfort.

Keywords: Whole-Body Vibration, multi-axes vibration, apparent mass, biodynamic modelling, suspension seat, seating dynamics, seat transmissibility, multi-body modelling

Table of Contents

Table of Tables

Table of Tables

Table of Figures

Table of Figures

Table of Figures

Table of Figures

Research Thesis: Declaration of Authorship

Print name: Weitan Yin

Title of thesis: A study of the Suspension-Seat-Occupant System dynamics under tri-axial translational vibration

I declare that this thesis and the work presented in it are my own and has been generated by me as the result of my own original research.

I confirm that:

1. This work was done wholly or mainly while in candidature for a research degree at this University;
2. Where any part of this thesis has previously been submitted for a degree or any other qualification at this University or any other institution, this has been clearly stated;
3. Where I have consulted the published work of others, this is always clearly attributed;
4. Where I have quoted from the work of others, the source is always given. With the exception of such quotations, this thesis is entirely my own work;
5. I have acknowledged all main sources of help;
6. Where the thesis is based on work done by myself jointly with others, I have made clear exactly what was done by others and what I have contributed myself;
7. Parts of this work have been published as:

Yin W. and Qiu Y. (2018) Dynamic modelling of a suspension seat for predicting nonlinear vertical transmissibility of the seat, Presented on the *53rd United Kingdom Conference on Human Responses to Vibration*, Ascot, United Kingdom

Yin W. and Qiu Y. (2019) Effect of backrest inclination on the apparent mass at the seat pan and backrest during vertical vibration, Presented on the *54th United Kingdom Conference on Human Responses to Vibration*, Edinburgh, United Kingdom

Yin W. and Qiu Y. (2021) Comparison of the vertical transmissibility of the suspension seat under single-axial vertical vibration and tri-axial vibration: effect of the magnitude of in-line vertical and horizontal vibration, Presented on the *27th International Congress on Sound and Vibration*, Czech Rep.

Yin, W., Ding, J. and Qiu, Y. (2021) Nonlinear dynamic modelling of a suspension seat for predicting the vertical seat transmissibility. *Mathematical Problems in Engineering*, vol. 2021, Article ID 3026108.

Signature: .....Date:.....

Acknowledgements

I would like to express my sincerest gratitude to my supervisors Dr. Yi Qiu and Dr. Neil Ferguson for their enthusiastic supervision and constant support during my PhD research. It was a pleasure to work with them.

I would like to thank Mr Peter Russell and Mr Gary Parker for their support in my laboratory experiments.

I am grateful to Dr. Yeping Xiong and Dr. Ying Ye, who took part in my PhD reviews and gave me valuable suggestions for me to improve my research work.

Many thanks to all the members of the Dynamics Group for spending time with me and helping me.

I would like to thank Mr Juyue Ding, Prof. Xichan Zhu, and Prof. Hongyan Wang, for recommending me to do my PhD study in ISVR.

Finally, I would like to thank my parents and other family members for their love, encouragement, and support.

Definitions and Abbreviations

a_1, …, a_q ..... Inputs of the multi-input-single-output model

a_{ij} ..... Acceleration measured in *i* axis at *j* position in the experimental study

a_w ..... Frequency weighted acceleration

a_x, a_y, a_z ..... Excitation in the x, y, and z-axis in the experimental study

A_1, …, A_q ..... Fourier transforms of the inputs a_1, …, a_q

A^{Bi} ..... Coordinate of the contact point *A* in the coordinate system of body B_i

$A_{i.(i-1)!}$ ..... Fourier transforms of the *i*th conditioned input

AM ..... Modulus of the apparent mass

B_i ..... The *i*th rigid body of the model

c ..... Damping

$\boldsymbol{C}$ ..... Damping matrix

E_0 ..... Correlation coefficient of the linear regression model

E_1 ..... Constant of the linear regression model

$f_{0.25}$, $f_{1.0}$ ..... Resonance frequency of the apparent mass or seat transmissibility measured when the excitation magnitude in the "primary-axis" was 0.25 ms^{-2} (r.m.s.) and 1.0 ms^{-2} (r.m.s.)

$f_{upright}$, $f_{20°}$ ..... Resonance frequency of the apparent mass or seat transmissibility measured when the backrest was upright and inclined by 20°

$f_{ij(x)}$, $f_{ij(y)}$, $f_{ij(z)}$ ..... Force in the x, y, and z-axis between the rigid bodies *i* and *j* in the models

f_{sec_0}, f_{sec_1} ..... Resonance frequency of the apparent mass or seat transmissibility measured when the excitation magnitude in the "secondary-axes" was 0 ms^{-2} and 1.0 ms^{-2} (r.m.s.)

$\boldsymbol{f}_{ij}$ ..... Force vector transmitted between the rigid bodies *i* and *j* in the models

F ..... Force measured in the experimental study

g_{error} ..... Error function

G ..... Auto-spectrum or Cross-spectrum of the signals in the experimental study

H ..... Stature of the human body

H_{1b}, …, H_{qb} ..... Transfer functions between the original inputs and output of the multi-input-single-output model

I ..... Moment of inertia

k ..... Stiffness

$\boldsymbol{K}$ ..... Stiffness matrix

l ..... Length of the rigid body

$\boldsymbol{l}_{ij}$ ..... Displacement between the rigid bodies i and j in the models

L_{rj} ..... Transfer functions between conditioned signal r and signal j of the multi-input-single-output model

m ..... Mass of the rigid body

$\boldsymbol{M}$ ..... Mass matrix

n ..... Number of frequency points

$\boldsymbol{N}$ ..... Unit vector

$\boldsymbol{O}_i^O$ ..... The coordinate of mass centre $\boldsymbol{O}_i$ in the global coordinate system

PC ..... Percentage change of the modulus associated with the resonance frequency of the apparent mass or seat transmissibility

P_j ..... The jth parameter of the seat model in the sensitivity analysis

R^2 ..... R-squared goodness-of-fit measure of the linear regression

$Re(*), Im(*)$ ..... The real and imaginary part of *, respectively

R_i ..... The ith response in the sensitivity analysis

R_{nl} ..... The ratio of the resonance frequency of the apparent mass or seat transmissibility under two different conditions

res_i ..... Resonance frequency of the apparent mass at the seat pan in the i-axis (i=x, y, z)

$SEAT$ ..... SEAT value

$\boldsymbol{T}$ ..... Transformation matrix for the acceleration and force at the backrest

T_R ..... Transfer function of the models

TR ..... Transmissibility of the suspension mechanism or the suspension seat

w.....Weighting factor

x_i, y_i, z_i.....Displacements of the ith rigid body in the x, y, and z-axis

x_{i0}, y_{i0}, z_{i0}.....Coordinates of the mass centre of the of the ith rigid body at the static position in the x, y, and z-axis

$x_{A_i}^{B_j}$, $y_{A_i}^{B_j}$, $y_{A_i}^{B_j}$.....The x, y, and z coordinates of the contact point A_i in the relative coordinate system of B_j

$\boldsymbol{X}$.....Input matrix

$X_{backrest}$, $X_{seatpan}$, X_{floor}.....X-axis of the backrest coordinate system, the seat pan coordinate system, and the floor coordinate system in the experimental study, respectively

$Z_{backrest}$, $Z_{seatpan}$, Z_{floor}.....Z-axis of the backrest coordinate system, the seat pan coordinate system, and the floor coordinate system in the experimental study, respectively

α.....Backrest inclination angle

β.....Roll angle around x-axis

γ^2.....Coherence

θ.....Pitch angle around y-axis

Ψ.....Sensitivity index

$\boldsymbol{\Psi}$.....Sensitivity matrix

ω.....Frequency in rad

Superscript

s.....Seat pan coordinate system in the experimental study

b.....Backrest coordinate system in the experimental study

Subscript

apms.....Apparent mass

b:q!.....The part of the output that is related to all the inputs

br.....Backrest

c.....Seat pan cushion

calc.....Calculated apparent mass or seat transmissibility using models

f.....floor

ilm ..... Excitation magnitude in the “primary-axis”

l ..... Suspension linkage on the left

m ..... Inert mass

meas ..... Measured apparent mass or seat transmissibility in the experimental study

mech ..... Suspension mechanism

p, *pitch* ..... Pitch motion

r, *roll*..... Roll motion

s..... Seat input to the human body model

sec ..... Excitation magnitude in the “secondary-axes”

seat ..... Suspension-seat-occupant model (for the sensitivity matrix)

seat-inert ..... Suspension seat loaded with inert mass

seat-body ..... Suspension seat with seated human body

sp ..... Sprung mass of the suspension top plate

stat..... Static position of the rigid bodies of the model

susp..... Suspension mechanism

TR..... Change of the seat transmissibility

x, *y*, *z* ..... Direction of the acceleration, force, apparent mass, transmissibility, or length

Abbreviation

APMS ..... Apparent mass

BMI..... Body mass index

DoF..... Degree of freedom

FE ..... Finite element

GA ..... Genetic algorithm

ISVR..... Institute of Sound and Vibration Research

LPM..... Lumped parameter model

MISO ..... Multi-input-single-output

PSD .....Power spectral density

r.m.s. .....Root-mean-square

SEAT .....Seat Effective Attenuation Transmissibility

SISO .....Single-input-single-output

VDV .....Vibration dose value

WBV .....Whole-Body Vibration

Chapter 1 GENERAL INTRODUCTION

1.1 Motivation

The human body seated in vehicles are often exposed to the seat-transmitted Whole-Body Vibration (WBV). The exposure to the WBV may have adverse effect on the ride comfort and health of the seated occupants. For example, it is an important factor that leads to the low back pain widely reported among the occupational heavy vehicle drivers (Alperovitch-Najenson et al., 2010; Robb and Mansfield, 2007). WBV has also been found to have a significant effect on the induction of drowsiness of the drivers (Zou et al., 2021), and the stress on lumbar spine which may increase the risk of musculoskeletal disorders at lower back (Singh et al., 2019). It is worthy of studying the biodynamic response of the seated human body to the WBV and the transmission of the WBV through the seat-occupant system on the heavy vehicles, so that measures can be taken to attenuate the vibration transmitted to the seated human body and reduce the adverse effects of the WBV.

The biodynamic response to the WBV varies with different frequencies (Griffin, 1990), which is affected by multiple factors. To reduce the WBV exposure more effectively in the frequency range where the human body is most sensitive, various studies have been carried out to investigate the effect of the influencing factors on the biodynamic response. Two of the most important factors that have been widely studied are the magnitude of excitation (e.g., Nawayseh and Griffin (2003); Qiu and Griffin (2012); Wu et al. (2021)), and the condition of the backrest support (e.g., Mandapuram et al. (2005); Toward and Griffin (2009); Liu and Qiu (2021)). The dynamic properties of the seat may interact with the biodynamic response of the human body it supports, and affect the WBV transmitted to the occupant. Many studies have been carried out to study the seat-occupant system dynamics, i.e., the seating dynamics, and it is found that the seat transmissibility was also affected by the excitation magnitude and backrest inclination (e.g., Jalil and Griffin (2007); Zhang et al. (2016); Qiu (2017)).

Most existing studies on the dynamic characteristics of the human body and seat-occupant system have been carried out under single-axial vibration. In real life, the occupant seated in the heavy vehicles may be exposed to WBV in multiple translational directions (Chaudhary et al., 2015; Jonsson et al., 2015; Johnson et al., 2019). Due to the coupling of the biodynamic responses in different directions and its nonlinearity, the dynamic behaviour of the seated human body under tri-axial translational vibration may be more complicated than the superposition of that under single-axial vibration. Despite some previous studies on the biodynamic response to dual-axial (Qiu

and Griffin, 2012; Zheng et al., 2019) or tri-axial translational excitation (Mansfield and Maeda, 2007; Mandapuram et al., 2012), the effects of a series of changes of the excitation magnitude in different directions and the backrest inclination angle, still remain to be further studied under tri-axial translational excitation.

Suspension seats have been widely used in heavy vehicles to attenuate the vertical vibration transmitted to the seated human body. The transmissibility of the suspension seat is affected by the vertical excitation magnitude, which has been reported in many laboratory studies that were limited to single-axial vertical excitation and with an upright backrest (Qiu, 2017; Adam et al., 2019a). How would the seat performance in terms of the vibration attenuation be affected by the magnitude of the additional horizontal vibration commonly existing on the heavy vehicles have been rarely reported. How does the backrest inclination angle affect the transmissibility of the suspension seat in x, y and z-axis has not been reported either.

In addition to experimental studies, the biodynamic response and the seat transmissibility may be studied using mathematical models. Various models based on the experimental data have been proposed to study the apparent mass or the seat transmissibility under single- or dual-axial vibration (e.g., Nawayseh and Griffin (2009); Qiu and Griffin (2011); Liu et al. (2015); Desai et al. (2021a)). Whether the apparent masses of the seated subject or the transmissibilities of the suspension seat in three translational directions with tri-axial translational excitation could be reflected by models, still remains to be investigated.

1.2 Research scope

This thesis consists of nine chapters.

Chapter 1 presents an introduction of the motivation and a general scope of this research.

In Chapter 2, a review of literature is given to show some of the relevant research progress on both the experimental study and the modelling of the biodynamic response to WBV and the seat transmissibility.

In Chapter 3, an experimental study of the biodynamic response under single-axial excitations in three translational directions is introduced. The effect of a series of changes of the backrest inclination angle on the apparent masses in three translational directions under various magnitudes of single-axial excitation have been investigated. Interactive effects between the excitation magnitude and backrest inclination angle on the apparent masses have been detected, by investigating how the extent of the change in the apparent mass that was due to the increase of one of these two factors could be affected by the other.

Chapter 4 introduces an experimental study on how the apparent masses of the seated human body in either x, y or z-axis under tri-axial translational excitation could be affected by a series of changes of the magnitude of excitation in the two additional axes and the angle of backrest inclination. The interaction between the effect of the excitation magnitude in one of the three axis and that in the two additional axes, and between the effects of the magnitudes of the tri-axial excitation and the backrest inclination angle, are also examined and discussed.

Chapter 5 describes a laboratory study on the dynamic characteristics of the suspension seat and the seat transmissibilities with seated subjects in both vertical and horizontal directions under tri-axial translational excitation. It also investigated how do they change with the increased excitation magnitude in different axes and the increased angle of backrest inclination.

In Chapter 6, a three-dimensional linear multi-body biodynamic model of the seated human body exposed to tri-axial translational vibration is proposed. The model is calibrated using the apparent masses measured at the seat pan and backrest in three translational directions during the experimental study presented in Chapter 4. The modal analysis is conducted on the calibrated model to study the association of biodynamic response with the resonances of the apparent mass.

Chapter 7 introduces a three-dimensional linear suspension seat model that is developed based on the measured transmissibilities of the suspension mechanism and the suspension seat with loaded inert mass in three translational directions. Then, a linear suspension-seat-occupant model is developed by coupling this suspension seat model and the human body model proposed in Chapter 6, and is calibrated using the suspension seat transmissibilities measured with the seated subject during the experimental study introduced in Chapter 5. The sensitivity of the parameters of the calibrated suspension-seat-occupant model is analysed to find the model parameter that affect the simulation results the most.

In Chapter 8, the general discussion of the main findings of this thesis from an overall perspective is provided.

Chapter 9 summarizes the major conclusions of this research, and proposes a few suggestions for the future studies.

Chapter 2 REVIEW OF LITERATURE

2.1 Tri-axial Whole-Body Vibration (WBV) environment on the heavy vehicles

The Whole-Body Vibration (WBV) is defined as the vibration of the human body occurring when a greater part of the body weight is supported by a vibrating surface (Griffin, 1990). The WBV transmitted through the seat can lead to discomfort of the seated occupants, interference with their activities and even cause health problems (Krajnak, 2018). Many occupational vehicle drivers are vulnerable to these adverse effects of the WBV, as they are exposed to the long-term, high-level vibration transmitted through the seat during daily work. It has been found that the exposure to WBV was one of the major factors that lead to low back pain among the drivers (Bernard and Putz-Anderson, 1997) with a strong statistical connection (Tiemessen et al., 2008). Furthermore, the exposure to WBV is also related to some types of musculoskeletal, cardiovascular and gastrointestinal disorders (Fritz, 2000). Among the occupational drivers of different vehicles, the coach or bus drivers are especially at high risk of developing low-back pain and other sorts of back disorders (Alperovitch-Najenson et al., 2010). Johanning (1998) suggested that the back disorder was one of the most important factors for the medical impairment and early permanent disability among mass transit vehicle drivers.

Depending on the vibrational environment on the vehicle and the dynamic properties of the seat, the WBV transmitted to the seated occupant in different types of vehicles is also different. To improve the ride comfort by reducing the WBV, a general understanding of the vibrational environment on the specific type of vehicle is necessary. Many field studies have been carried out to measure and evaluate the WBV exposure of the heavy vehicle drivers using the current standards such as ISO 2631-1:1997, which takes into account the frequency-dependent sensitivity of the human body to the WBV in different directions.

According to the reported field studies, the vibration in the horizontal (x and y) axes measured on the suspension seats of the heavy vehicles played an important role in affecting the ride comfort together with the vertical vibration. Blood et al. (2010) measured the WBV exposure of the bus drivers seated on different seats in the x, y and z-axis, and found that it was affected by both the seat design and road surface. They also reported that the magnitude of WBV in the vertical direction was larger than that in fore-aft or lateral direction, but the effect of these horizontal vibration on the ride comfort was not negligible, as the weighted r.m.s. acceleration in the fore-aft or lateral direction was more than 25% of that in the vertical direction. Similar observation was reported by

Jonsson et al. (2015) who measured the WBV exposure on different combinations of bus types and seat types, and Rao et al. (2018) who measured the WBV exposure of the drivers seated in a minibus with different backrest inclination angles. For other types of heavy vehicles, the drivers' exposure to horizontal WBV may be even more severe. Kabir et al. (2017) evaluated the WBV exposure of the tractor operators working on four kinds of land surfaces and reported that the exposure to the vibration in the x and y-axis were greater than that in the z-axis in all the cases. The dominance of the horizontal WBV over that in the vertical direction was also reported by Du et al. (2018) who did a field measurement of the WBV exposure on a truck. It was suggested that on heavy vehicles, the magnitude of vibration in the horizontal directions were generally greater compared to that in cars (Sayed et al., 2013). Due to the tri-axial vibrational environment on the heavy vehicles found in the field studies, the laboratory study on the biodynamic response of the seated occupant and the seating dynamics under tri-axial translational vibration would be beneficial for the improvement of the ride comfort in real life.

2.2 Biodynamic response of the seated human body to the WBV

The biodynamic response of the seated human body to the WBV is closely related to the ride comfort, and has been widely investigated over the years. To exclude the interaction between the human body biodynamics and the dynamic characteristics of the seat supporting the human body, the study is normally carried out on the rigid seats, on which the moduli of the seat transmissibilities in the translational directions are close to 1 in the low frequency range where the human body is most sensitive to the WBV (Griffin, 1990). Many studies on the biodynamic response to the WBV were carried out by measuring the physical indices, such as the apparent masses and body transmissibilities. It can also help develop appropriate human body models for the prediction of the biodynamic response.

Due to the convenience of the measurement, the apparent mass is the most frequently used index for the study of the biodynamic responses to WBV in the translational directions. The apparent mass is defined as the complex ratio between the force and the acceleration measured at the point where the vibration is transmitted to the human body. In case of random excitation, the apparent mass could be calculated using the cross- and auto-power spectra as follows:

$$M(f) = S_{aF}(f)/S_{aa}(f) \tag{2.1}$$

Where M, S_{aF}, S_{aa} and f stand for the apparent mass, the cross spectral density between the acceleration and force, the power spectral density (PSD) of the acceleration, and frequency, respectively.

Generally speaking, the response of the seated human body to WBV depends on the inter-subject biomechanical characteristics, and can be affected by various external influencing factors, such as the magnitude and direction of the excitation, and the support of the backrest.

2.2.1 In-line and cross-axis apparent masses under single-axial excitation

Under single-axial vertical excitation, the in-line vertical apparent mass of the seated human body at the seat pan generally exhibits a peak between 4-6 Hz regardless of the existence of the backrest support (Mansfield and Maeda, 2007; Huang et al., 2020; Liu and Qiu, 2021), which is shown in Figure 2.1. Under single-axial fore-aft excitation, the in-line fore-aft apparent mass measured at the seat pan generally exhibits a fundamental resonance (in this thesis, the "fundamental resonance" refers to the resonance with the lowest frequency, sic passim) at about 4 Hz when the human body is supported by the backrest, and at about 0.7 Hz without backrest (Mansfield and Maeda, 2006; Qiu and Griffin, 2012). In the lateral direction, the resonance frequency of the in-line lateral apparent mass also depends on the backrest: it usually occurs at about 1.5 Hz with backrest or 0.7 Hz without backrest (Fairley and Griffin, 1990; Mandapuram et al., 2005). Figure 2.2 shows the normalized apparent masses in the horizontal directions under different conditions of backrest support. The normalization was carried out by dividing the measured modulus of the apparent mass of each subject with the static sitting weight.

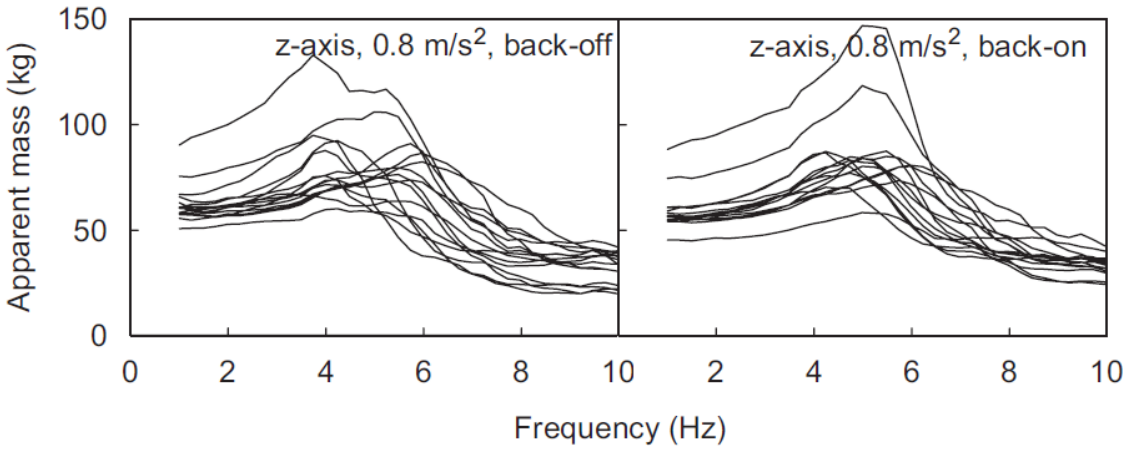

Figure 2.1 Vertical apparent masses of 15 subjects with ("back-on") and without ("back-off") support of an upright backrest under single-axial vertical vibration (Mansfield and Maeda, 2007)

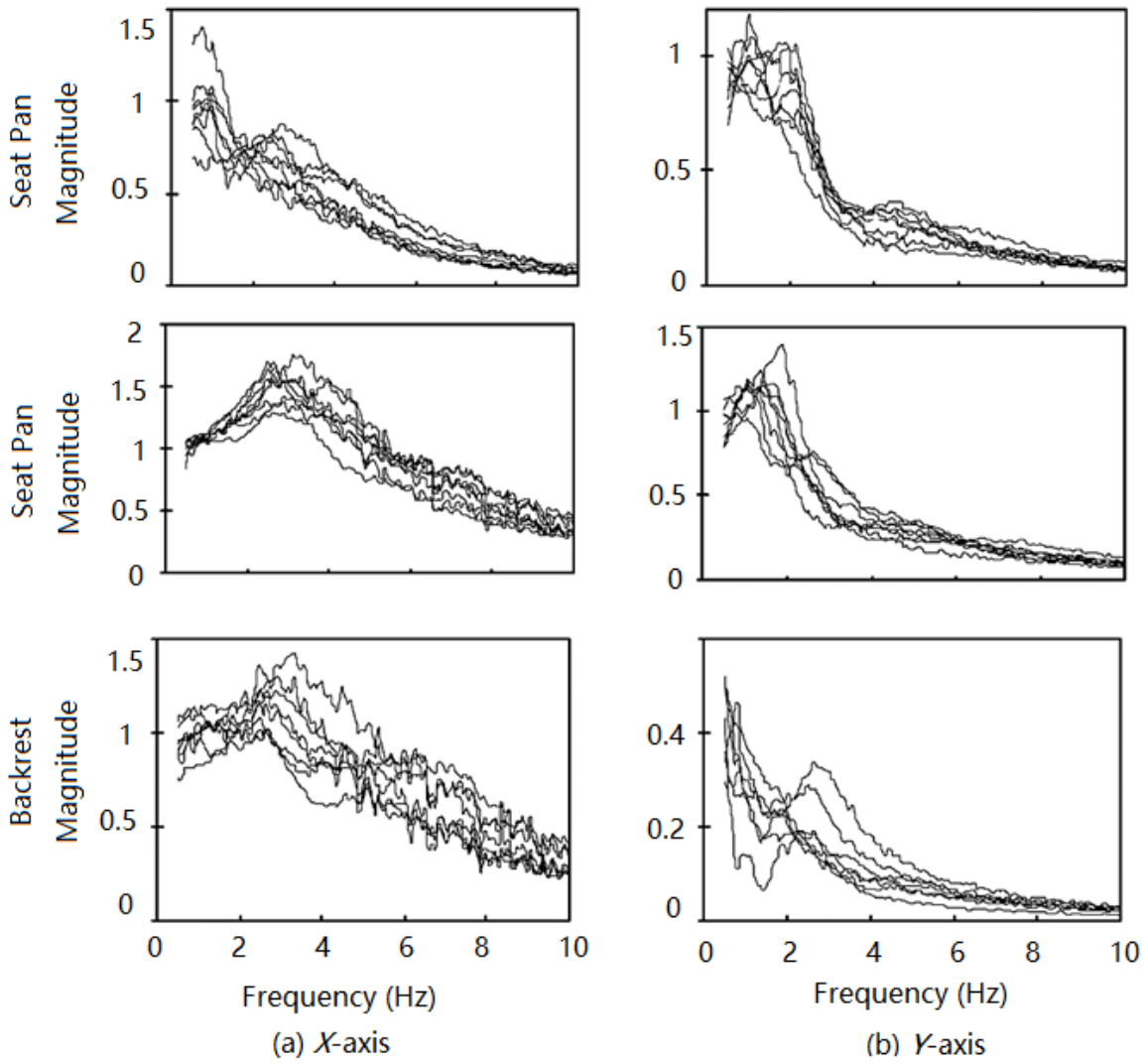

Figure 2.2 Comparison of the normalized fore-aft and lateral apparent mass measured at the seat pan and backrest of eight subjects without backrest (first row) and with inclined backrest (second and third row) (Mandapuram et al., 2005)

Apart from the in-line apparent mass of the human body that is calculated using the dynamic force measured in the same direction as the excitation, the so-called "cross-axis" apparent mass has also been widely studied under single-axial vertical or fore-aft excitation (Mansfield and Lundström, 1999; Nawayseh and Griffin, 2005; Mansfield and Maeda, 2006; Qiu and Griffin, 2012). They reveal the coupling of the biodynamic response of the human body in the x and z-axis. It is defined as the ratio of the force measured in an axis perpendicular to the axis of the excitation to the input acceleration. The modulus of the cross-axis vertical apparent mass under single-axial fore-aft direction excitation was found to be non-negligible, with the fundamental resonance frequency below 2 Hz and the second resonance frequency between 6 and 8 Hz without back support (Qiu and Griffin, 2010), or with only a fundamental resonance between 6 and 8 Hz when with the support of vertical backrest (Qiu and Griffin, 2012). Also, considerable cross-axis fore-aft apparent

mass was observed with a resonance at about 5 Hz under single-axial vertical excitation (Mansfield and Maeda, 2006), see Figure 2.3, regardless of the existence of backrest support.

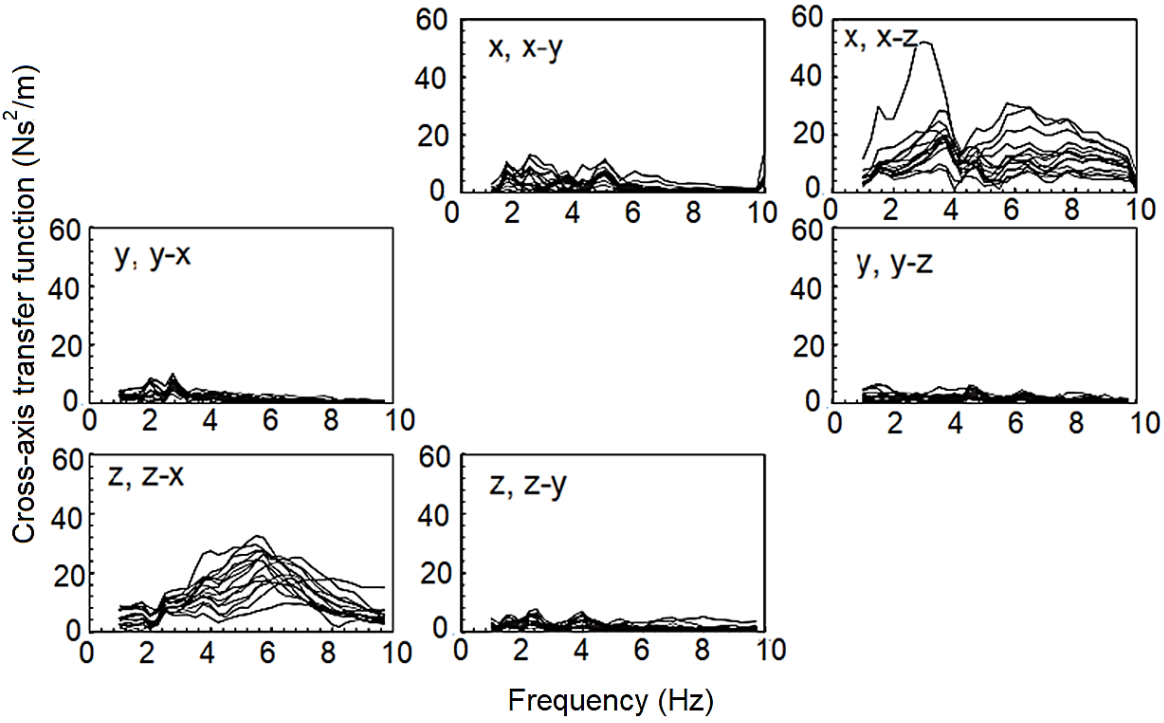

Figure 2.3 Cross-axis apparent mass modulus for 15 male subjects exposed to single-axial WBV with support of upright backrest. The labels refer to the direction of excitation and the nature of the cross-axis apparent mass (e.g., "y, z–x" refers to the cross-axis apparent mass between z vibration and x force under y-direction excitation) ((Mansfield and Maeda, 2006)

Rakheja et al. (2006) found that under single-axial vertical excitation, the cross-axis fore-aft apparent mass measured at the backrest and the in-line vertical apparent mass measured at the seat pan were associated due to the rotational motions of the upper body. On the other hand, the relationship between the cross-axis lateral apparent mass and that in the other directions is less significant (Nawayseh and Griffin, 2005; Mansfield and Maeda, 2006; Mandapuram et al., 2010).

2.2.2 The effect of in-line excitation magnitude on the apparent masses

The effect of the magnitude of the single-axial excitation on the apparent mass of the seated human body has been widely studied. It is reported that with the increase of vibration magnitude in one axis, the resonance frequency of in-line apparent mass generally tends to decrease, which has been observed in every translational axis, e.g., in x-axis by Qiu and Griffin (2012); in y-axis by Wu et al. (2021); and in z-axis by Mansfield et al. (2006). Figure 2.4, for example, shows the effect of increasing the vertical excitation magnitude (all the values of the excitation magnitudes in this thesis refer to the r.m.s. value of the corresponding magnitude, sic passim) on the median

normalized in-line vertical apparent mass. The decrease of the resonance frequency of the apparent mass due to the increase of the excitation magnitude is often referred to as the nonlinearity or the "softening" behaviour of the human body.

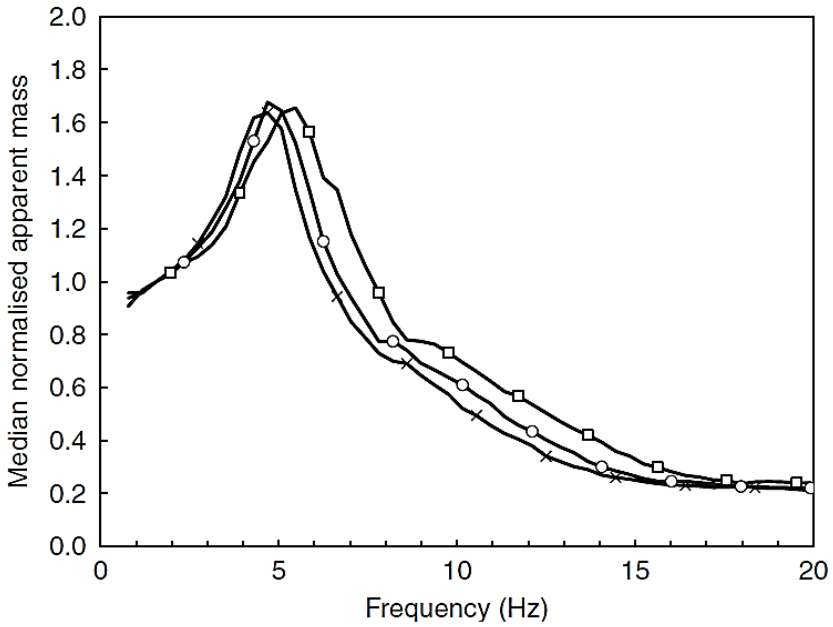

Figure 2.4 Median normalized vertical apparent masses of 12 subjects sitting with upright posture without backrest support: 0.5 ms^{-2} -□-; 1.0 ms^{-2} -○-; 1.5 ms^{-2} -×- (r.m.s.). (Mansfield et al., 2006)

2.2.3 The effect of backrest on the apparent masses

The existence of the support of an upright backrest could affect the resonance frequency of the horizontal apparent mass dramatically (Mandapuram et al., 2005; Mansfield and Maeda, 2007; Qiu and Griffin, 2010; Qiu and Griffin, 2012). The swaying motion of the upper body for compensating the vibration when the backrest is absent can be reduced with the support of an upright backrest. Besides, compared to the condition without back support, the contact between the upper body and the backrest introduces excitation to the human body in addition to the seat pan, and the backrest support also makes the upper torso of the human body stiffer (Qiu and Griffin, 2012).

Another influencing factor related to the backrest that affects the apparent mass of the seated human body is the inclination angle of the backrest. Toward and Griffin (2009) reported that under 1.0 ms^{-2} r.m.s. single-axial vertical excitation, the fundamental resonance frequency of the in-line vertical apparent mass at the seat pan tended to increase with the increase of the rigid backrest inclination angle from 0° to 25° (Figure 2.5). Similar observations have been reported by Zhang et al. (2021) and Liu and Qiu (2021), who measured the apparent masses under 0.5 ms^{-2} r.m.s. single-axial vertical excitation with the support of a rigid backrest or a backrest with foam at different

backrest inclination angles. They stated that the change of the resonance frequency of the apparent mass with the increase of the backrest inclination was possibly due to the change in the mass of the human body supported by the backrest. The stiffness or damping of the soft tissues of the human body may also have changed due to the change of backrest inclination angle (Liu and Qiu, 2021). Yang and Qiu (2015) measured the in-line vertical apparent mass and cross-axis fore-aft apparent mass under 1.0 ms^{-2} r.m.s. single-axial vertical excitation, and observed a decrease in the correlation between vertical in-line and fore-aft cross-axis apparent mass at the seat pan when the backrest inclination increased from 0° to 30°. The decrease of the correlation indicates that the biodynamic behaviour of the upper body is partly independent on that of the lower body.

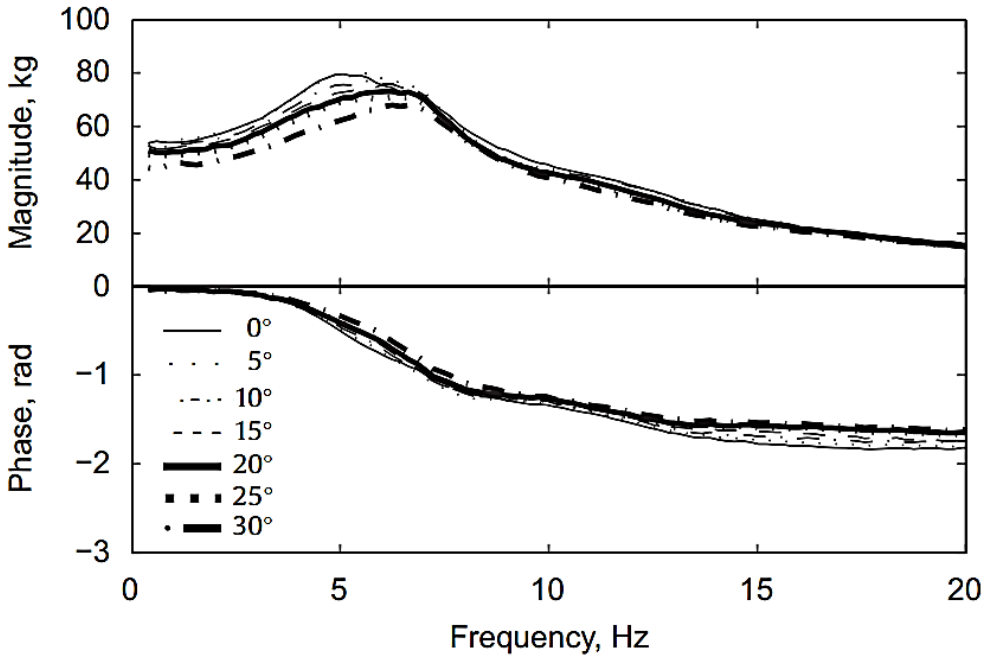

Figure 2.5 Median vertical apparent masses of 12 subjects measured on the seat pan (Toward and Griffin, 2009)

The effect of the backrest inclination on the apparent masses in the horizontal directions is less reported compared to that in the vertical direction. When the backrest was inclined by 12.5°, the resonance frequency of the in-line fore-aft apparent mass at the seat pan was found to be different compared to that when the backrest was upright under single-axial fore-aft excitation, whereas the lateral apparent mass was found to be less affected under single-axial lateral excitation (Mandapuram et al., 2005). The comparison of the horizontal apparent masses with a series of changes of the backrest inclination angles has not been reported.

2.2.4 Apparent masses under multi-axial vibration

The research on the biodynamic responses to multi-axial vibration is less well reported compared to that under single-axial vibration. Qiu and Griffin (2012) studied the in-line and cross-axis

apparent mass both at the seat pan and at the backrest in the vertical and fore-aft direction under dual-axis excitation in the x and z-axis. The magnitudes of vibration varied between four values (0, 0.25, 0.5 and 1.0 ms^{-2} r.m.s.) in either direction, and all the 15 combinations (4×4 but excluding the 0-magnitude condition) of the dual-axial excitation magnitudes were applied to the subjects. They observed softening behaviour of the human body in the x (or z) axis with the increase of both the excitation magnitude in the x (or z) axis and that in the z (or x) axis, and the effect of the former is more obvious than the latter. The higher the excitation magnitude in the x (or z) axis was, the less difference the excitation magnitude in the z (or x) axis made on the in-line fore-aft (or vertical) apparent mass. These results suggested the dominant effect of the in-line excitation magnitude over that of the cross-axis excitation. Furthermore, they also found that the support of upright backrest reduced the moduli associated with the fundamental resonances of the in-line and cross-axis apparent mass compared to that without backrest, under both single and dual-axial excitation.

Mansfield and Maeda (2007) compared the in-line apparent mass of the human body measured at the seat pan under single-axial excitation with those measured under dual- and tri-axial excitation. They found that the resonance frequency of the apparent mass in one axis decreased slightly when the excitation magnitude in other directions increased. However, only the apparent masses at the seat pan were measured. Mandapuram et al. (2012) measured the apparent masses in three translational directions, at the backrest and the seat pan under tri-axial vibration. Similar to the observation reported by Mansfield and Maeda (2007), the decrease of the resonance frequency of the apparent mass in one axis was found when the excitation magnitude in the perpendicular axis increased. However, the maximum overall magnitude of vibration was 0.7 ms^{-2} r.m.s. for the tri-axial vibration in that study. How the human body behaves under excitations with higher magnitudes remains to be investigated. Furthermore, the magnitude of excitation in each axis varied between two values in these two studies, while an investigation under a series of changes in the excitation magnitudes may be needed to draw a more comprehensive picture of the tendency of the nonlinearity.

Wu et al. (2021) reported the effect of the magnitudes of excitation on the biodynamic response under combined lateral, vertical and roll excitation with three magnitudes in each direction, and found that similar to the observations with dual-axis excitation made by Qiu and Griffin (2012), the effect of the excitation magnitude in one axis on the in-line apparent mass was affected by the excitation magnitude in the other directions.

2.2.5 Other influencing factors of the apparent mass

Apart from the excitation magnitude and the support of the backrest, other factors may affect the apparent mass of the seated human body. The inter-subject variabilities and the postures also play an important role in the biodynamic response to the WBV. Inter-subject variabilities include gender, weight, age, body mass index (BMI), and so on (Phate et al., 2019; Rakheja et al., 2020a). For example, the experiment conducted by Toward and Griffin (2011) showed that the subject with a larger body mass tended to possess an apparent mass with larger modulus, especially for that associated with the resonance frequency.

The posture of seated occupant is another one of the important factors, which can affect the apparent mass in three ways. The first is by affecting the mass distribution of the body and the body mass supported by the seat. The second is by affecting the biodynamic stiffness or damping of the human body via muscle activity (Huang and Griffin, 2006; Yang, 2016). The third is by introducing additional excitation into the human body from the supporting surface of the human body, such as when the occupant is holding a steering wheel. Studies on various upper body postures (which is usually related to the existence and inclination of backrest) and lower body postures (e.g., different thigh postures) have been reported. Nawayseh and Griffin (2003) observed a decrease in the in-line vertical and cross-axis fore-aft apparent mass under single-axial vertical excitation when the lower body posture changed by reducing the contact between the thigh and the seat pan, see Figure 2.6. Liu (2017) suggested that when adopting postures with different thigh contact, the apparent masses at different body segments would dominate the overall apparent mass.

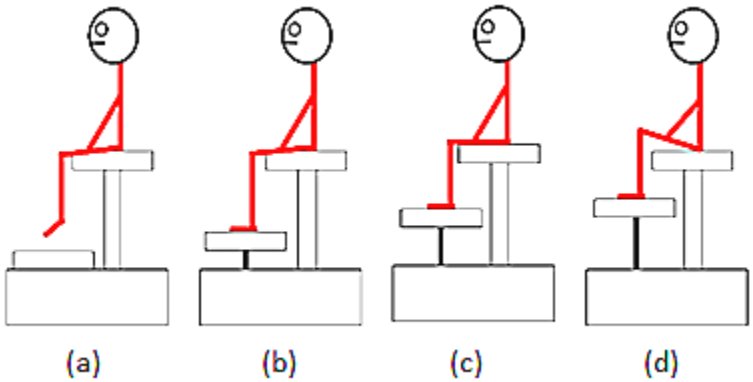

Figure 2.6 Schematic diagrams showing four postures: (a) feet hanging; (b) maximum thigh contact; (c) average thigh contact; (d) minimum thigh contact (Nawayseh and Griffin, 2003)

These previous studies show the non-negligible effect of inter-subject variability and posture on the apparent mass. Thus, in the experimental studies on the effect of the other influencing factors such as the excitation magnitude, it is necessary to test plenty of subjects with different statures and

weights to obtain solid and representative findings, and the posture of the subjects need to be restricted to reduce the effect of posture on the biodynamic response.

2.3 Seating dynamics

The vehicle seats supporting the occupants are not ideally rigid. The dynamic characteristics of the seat and the interaction between the seat and occupant would affect the dynamic behaviour of the coupled seat and human body, or the so-called seating dynamics. Hence, apart from the biodynamic response to vibration, the dynamic properties of the seat also need to be investigated. The seat transmissibility has been frequently used as an indicator of the seating dynamics. It is defined as the ratio of the response amplitude of a seat-occupant system to the input acceleration, usually expressed as a function of the frequency. In practise, the seat transmissibility is usually calculated using the cross-spectra of the acceleration at seat-occupant interface and the acceleration at seat base, and the PSD of the acceleration at seat base. When the human body is supported by the seat pan and backrest, the seat transmissibilities at both the seat pan and the backrest reveal the characteristics of the seating dynamics.

For the suspension seats, the seat transmissibility can be measured with inert masses loaded on the seat, with dummies or with a human subject seated in the seat, depending on the objective of the study. The measurement of the transmissibilities with inert masses or dummies enables the dynamic properties of the seat to be better studied without interaction with the biodynamic behaviour of the human body. The preload on the suspension seat is required because the seat transmissibility measured without any preload would be not comparable with that measured with a seated occupant, as the lock-up of the suspension mechanism due to friction (Qiu, 2017) may not be well overcome without the preload.

The transmissibility of a seat with the seated occupant is affected by many influencing factors, including the dynamic characteristics of the seat components (e.g., the suspension mechanism and seat cushion), the inter-subject characteristics of the seated occupant, the magnitude of the excitation, and the existence or inclination of the backrest.

2.3.1 Dynamic characteristics of the seat components

A modern vehicle seat normally consists of seat pan and backrest, both of which included the seat frame and seat cushion filled with polyurethane foam. Many heavy vehicles are equipped with the suspension seats. A suspension seat comprises of a suspension mechanism in addition to the seat pan and backrest, which is used for the attenuation of the vertical vibration. Most of the suspension seats currently used in the heavy vehicles have passive suspension mechanisms consisting of

dampers and springs. The spring in the suspension mechanism may be either a coil or air spring. Figure 2.7 shows the structure of a typical passive seat suspension mechanism which consists of coil springs and damper along with the cross-arm linkages.

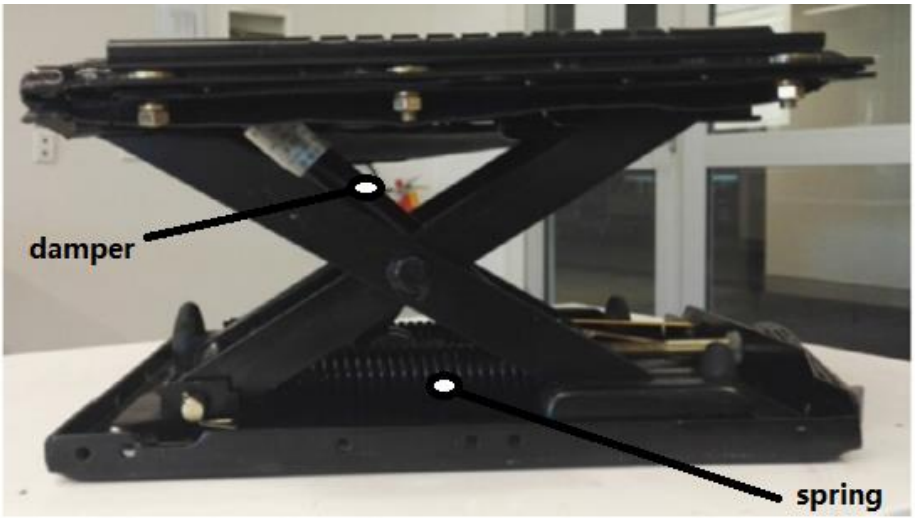

Figure 2.7 Suspension seat structure (Ning et al., 2018)

The stiffness and damping of the seat cushion and the suspension mechanism play an important role in determining the dynamic properties of the whole seat. Many studies have been carried out to study the dynamic characteristics of the seat components. Zhang (2014) measured the vertical dynamic stiffness of the polyurethane foam block and that of a car seat cushion (which included the same type of foam as the block) under vertical excitation, and found that they were affected by the excitation magnitude and the preload applied. With the increase of the excitation magnitude, the dynamic stiffness decreased, while with the increase of the preload, it increased. Nonlinear elastic and viscoelastic behaviour of the foam was also revealed by the large hysteresis observed in the quasi-static load-deflection curve. Krumm et al. (2020) found that compared to the car seat with standard foam cushion, a car seat with warp knitted spacer fabric cushions amplified the seat transmissibility measured at the seat pan.

Shahzad and Qiu (2012) measured the quasi-static load-deflection curve of the coil spring and damper of a suspension mechanism, and found that the spring exhibited a bi-linear quasi-static load-deflection relationship with little hysteresis, while the hysteresis of damper's load-deflection curve was greater. Qiu (2017) measured the vertical transmissibility of the suspension mechanism using rigid mass as preload, and found that under a low-level excitation magnitude of 0.25 ms^{-2} r.m.s., the suspension transmissibility was close to 1 in the low frequency range, possibly due to the fact that the suspension mechanism was locked up by the friction. When the excitation magnitude increased, the suspension transmissibility exhibited obvious nonlinear softening behaviour (see Figure 2.8).

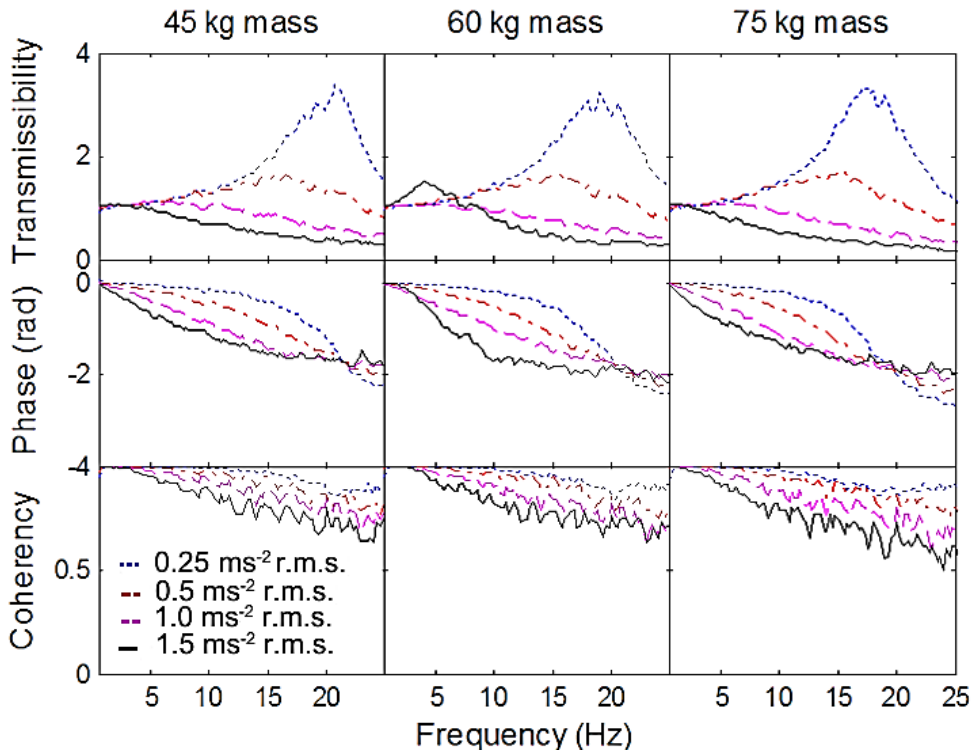

Figure 2.8 Transmissibility modulus, phase and coherency of suspension mechanism under different excitation magnitudes (Qiu, 2017)

2.3.2 Seat transmissibility under single-axial vibration

The modulus and phase of the vertical transmissibility of a car seat with the seated subject and the corresponding coherence are shown in Figure 2.9 (Griffin, 1990). The modulus of the transmissibility was greater than 1 at low frequency range below 10 Hz with a fundamental resonance at around 4 Hz, while at higher frequency range, the transmissibility decreased. Similar characteristics of the transmissibility of the car seats have also been reported in other previous studies under single-axial vertical excitation reported by Toward and Griffin (2011) and Tufano and Griffin (2013).

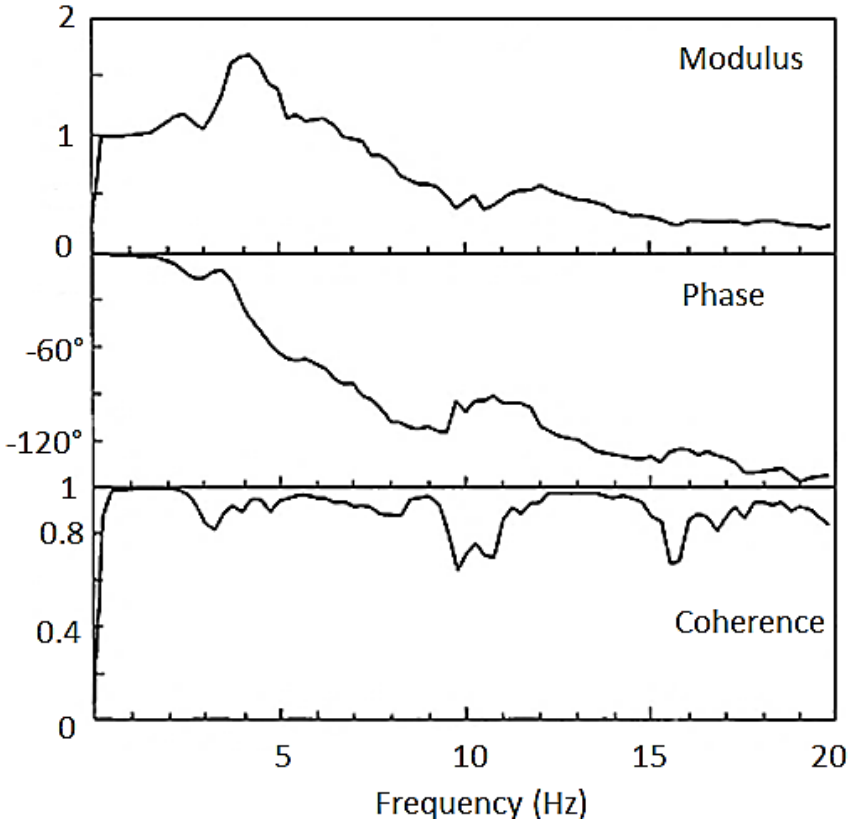

Figure 2.9 Seat vertical transmissibility and coherence (Griffin, 1990)

Qiu (2017) measured the vertical transmissibilities of the complete suspension seat with loaded inert masses and the seated subject under single-axial vertical excitation. The vertical transmissibility of the complete suspension seat with seated occupant exhibited three resonances below 6 Hz, between 7 and 15 Hz, and between 15 and 22 Hz, respectively. It was suggested that the lock-up effect found on the suspension mechanism also affected the transmissibility of the complete seat when the excitation magnitude was at a low level (e.g., below 0.25 ms^{-2} r.m.s.), as the seat transmissibility was close to 1 at low frequencies. Under vertical excitation with greater magnitude, the friction was overcome and the suspension mechanism could move more properly.

Qiu and Griffin (2003) measured the fore-aft transmissibility of a car seat at the backrest with seated subject under single-axial fore-aft excitation and found three resonances at around 5 Hz, 28 Hz and 48 Hz, respectively, which are shown in Figure 2.10. Zhang (2014) measured the fore-aft transmissibility of a car seat at the seat pan and backrest up to 40 Hz with manikin and participants under single-axial fore-aft excitation. The fore-aft transmissibility of seat at the seat pan under single-axial fore-aft excitation was found to be close to 1 at low frequencies. A distinctive fundamental resonance of the transmissibility at the seat pan was found at about 20 Hz with manikin while with seated human body, the fundamental resonance was at about 4 Hz, and another resonance possibly existed at over 40 Hz. The reported fore-aft transmissibility at the backrest was similar to that measured by Qiu and Griffin (2003).

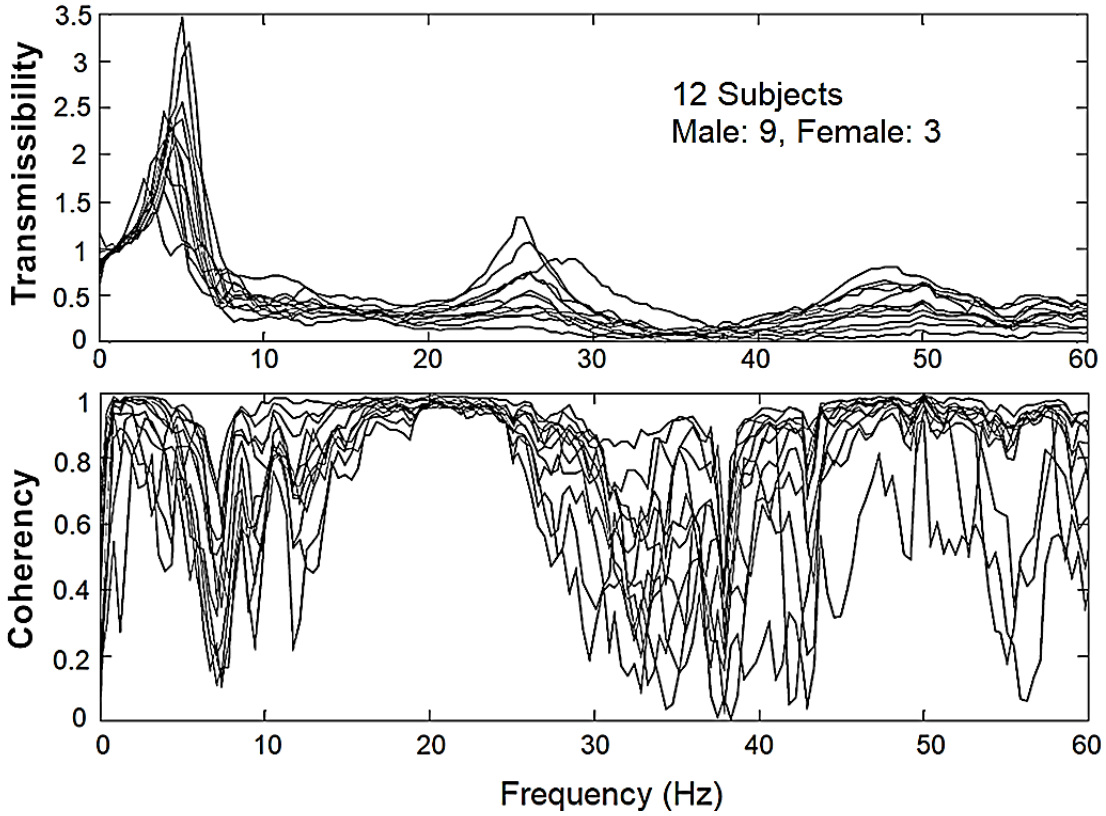

Figure 2.10 Transmissibility and coherence of the backrest in fore-aft direction (Qiu & Griffin, 2003)

Ittianuwat et al. (2014) measured the in-line lateral transmissibility of a car seat at various locations on the seat frame without seated subject under single-axial lateral excitation, and found a fundamental resonance located between 15 and 20 Hz. Gong and Griffin (2018) reported that a resonance of the lateral transmissibility of a train seat existed at around 25 Hz when the subject was seated. Wu and Qiu (2021) measured in a laboratory study the lateral transmissibility of a train seat at seat pan and backrest with and without seated subject, and found a fundamental resonance at about 15 Hz for both transmissibilities at the seat pan and that at the backrest, no matter whether the subject was seated or not. The resonance frequencies of the seat transmissibilities varied among different seats in these studies depending on the seat structure.

2.3.3 The effect of the excitation magnitude on the seat transmissibility

The nonlinearity of the dynamic properties of the seat cushion or the suspension mechanism subject to the excitation magnitude has been reported in the previous studies, which suggests that the dynamic behaviour of the complete seat consisting of these components may also show nonlinearity. Many experimental studies measuring the transmissibility of the complete seat under different excitation magnitudes were reported.

The in-line vertical or fore-aft transmissibilities measured at the seat pan and backrest of a car seat exhibited a decrease of the fundamental resonance frequency when the magnitude of vertical or

fore-aft vibration increased (Zhang, 2014), see Figure 2.11. Such a softening dynamic behaviour of the seat was observed both when the seat was loaded with a manikin and with a seated participant, which indicates that the nonlinear dynamic behaviour of the seat attributed to the nonlinearity of the seat-occupant system in addition to that of the seated human body.

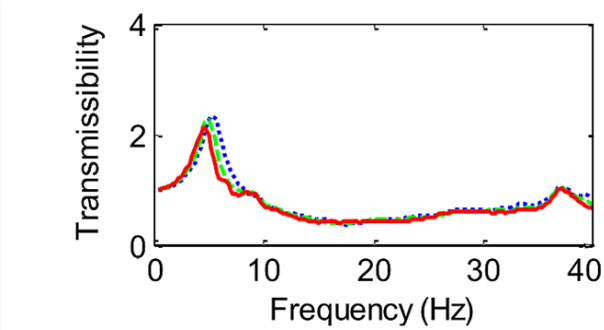

Figure 2.11 Median vertical seat transmissibility at the seat pan measured at different magnitudes (0.4 ms^{-2}, 0.8 ms^{-2}, 1.2 ms^{-2} r.m.s.) of the single-axial vertical excitation with seated subjects (Zhang, 2014)

Tufano and Griffin (2013) measured the vertical apparent mass of the seated subjects and the seat transmissibility on a rigid seat with a foam block at the seat pan under single-axial vertical random excitation, and found that the change of the resonance frequency of the seat transmissibility was more dependent on the nonlinearity of the seated human body than that of the foam. These conclusions are applicable for car seats with seat frame and seat cushion. D'Amore and Qiu (2021) found that when the subjects were supported by a backrest inclined by a relatively large angle and adopted more relaxed sitting postures (which is supposed by the authors to be a common situation in the future autonomous cars), the magnitude of vertical excitation could still affect the seat transmissibility.

For a suspension seat, the nonlinearity of the dynamic behaviour of the suspension mechanism also plays an important role in the nonlinearity of the whole seat-occupant system (Qiu, 2017). The resonance frequencies of the vertical transmissibility of the suspension seat with subjects were found to decrease as the magnitude of vertical excitation increased (Qiu, 2017).

2.3.4 The effect of the backrest support on the seat transmissibility

Compared to the condition without backrest support, the occupant's contact with an upright backrest led to an increase of the resonance frequency and the associated modulus of the vertical transmissibility at the seat pan of a car seat under single-axial vibration (Corbridge et al, 1989). The inclination of the backrest led to a further increase of the resonance frequency and the associated modulus of the vertical transmissibility under single-axial vibration compared to that measured

with an upright backrest (Houghton, 2003). In terms of the seat transmissibility in the horizontal directions, Jalil and Griffin (2007) found that the increase of the inclination angle of the backrest led to an increase of the resonance frequency of the fore-aft seat transmissibility measured at the backrest of a car seat under single-axial fore-aft excitation (Figure 2.12). This "stiffening" phenomenon of the seat-occupant system due to the increase of backrest inclination may be related to the similar tendency of the apparent mass observed when the backrest inclination increased (Toward and Griffin, 2009; Yang and Qiu, 2015).

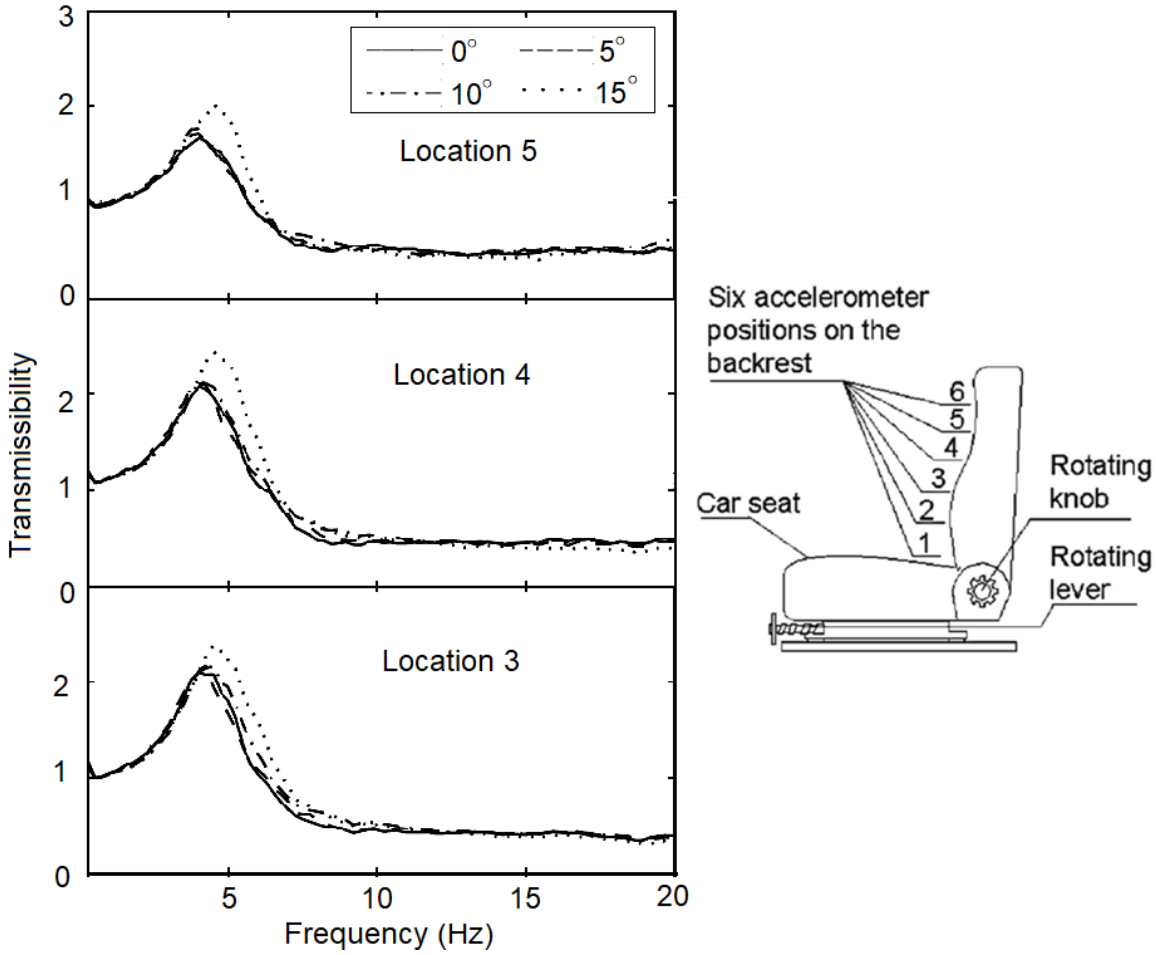

Figure 2.12 Median fore-aft transmissibilities measured at different locations on the backrest with seated subject under single-axial fore-aft vibration: effect of the backrest inclination angle (Jalil and Griffin, 2007a)

2.3.5 Seat transmissibility under multi-axial vibration

The seat transmissibility under multi- axial vibration has been less well reported compared to those under single-axial vibration, and most of them were measured during field studies. Qiu and Griffin (2004) measured the tri-axial translational accelerations at four corners of seat base as the input excitation and those at the backrest of a car seat as the output in a field study. The transfer function and coherence between inputs and outputs were derived using multi-input-single-output (MISO)

method. It was found and both the in-line and cross-axis vertical and fore-aft outputs at the seat pan had considerable correlation with the vertical and fore-aft inputs, while the outputs in the directions other than the lateral direction were much less correlated with the lateral inputs.

Kim et al. (2018) studied the lateral and vertical seat effective amplitude transmissibilities (SEAT-values) of two types of suspension seats exposed to the reproduced multi-axial vibration during a field study, by calculating the ratio of r.m.s acceleration at the seat base to that at the seat pan. It is found that the SEAT value in the horizontal direction measured on a seat with horizontal suspension mechanism was smaller than that measured on a seat with only vertical suspension mechanism. They chose the SEAT-values for the comparison between the dynamic behaviour of the two seats under multi-axis excitation, which is only a rough representation of the overall performance of the seat in terms of the vibration attenuation, while the frequency response of the seat transmissibility under tri-axial vibration was not reported. A laboratory study on the effect of the increased excitation magnitude on the seat transmissibilities under tri-axial vibration remains to be carried out.

2.4 Mathematical models of the seated human body

Apart from the experimental studies, the biodynamic response of the human body and the seating dynamics can also be studied using mathematical models. The computational simulation with the developed models is less time consuming than carrying out experimental studies, and it also enables the dynamic properties of the human body and seat-occupant system to be investigated virtually under the test conditions which are hard to be done via experimental study due to the limitation of test apparatus or the tolerance of the human body.

In general, most of the mathematical models proposed in the previous literature for the study of the human body exposed to the WBV can be categorized into three types: lumped parameter models (LPMs), multi-body models and finite element (FE) models. In the context of biodynamic modelling, the human body is often represented by lumped blocks with only mass and/or moment of inertia as parameter in the LPMs, and the forces are represented by spring- and damping forces. This type of model is widely developed due to the convenience in development and calibration, yet it can only capture the characteristics of the whole system while the dynamic behaviour of the parts of the system cannot be studied in detail. Multi-body models comprise rigid bodies with one or multiple degrees-of-freedom (DoFs) that are usually more anatomically or geometrically representative than lumped masses, and the bodies are connected with joints. They are beneficial for predicting the motions of each rigid body in the whole system. The FE models comprise numerous elements connected with nodes. They provide finer representation of the geometry of

the system, and can offer more precise predictions on the motion and internal force of a part of the system, but the computational cost is usually high.

2.4.1 Lumped parameter models (LPMs)

A lumped parameter model with two-DoF was developed by Wei and Griffin (1998), which is shown in Figure 2.13. The human body was represented by three masses in this phenomenological model, which were not representing any of the anatomical body segments. It was capable of predicting the in-line vertical apparent mass at the seat pan when the human body is exposed to single-axial vertical vibration.

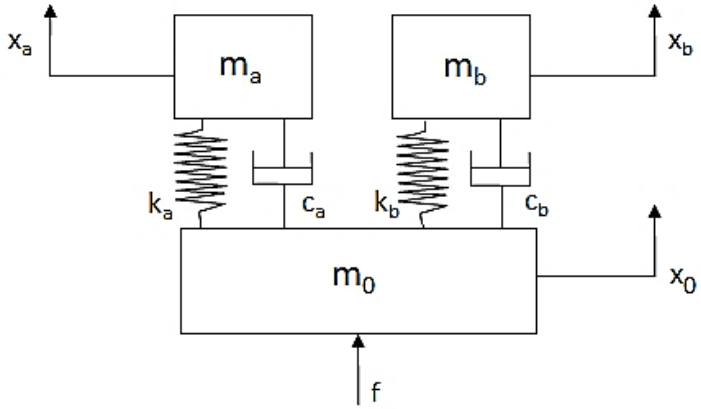

Figure 2.13 Schematic diagram of two degree-of-freedom human body model (Wei and Griffin, 1998)

Kumar and Saran (2019) developed a 6-DoF lumped parameter model to study the vertical apparent mass and the seat-to-head-transmissibility, in which the masses of the realistic body segments were roughly represented.

Nawayseh and Griffin (2009) developed a three-DoF lumped parameter model taking the vertical, fore-aft and pitch motions into consideration (Figure 2.14). The rotational degree of freedom enables the model to capture the coupling of the body motion between the vertical and fore-aft directions. The model achieved good agreement with the measured in-line vertical apparent mass and the cross-axis fore-aft apparent mass at the same time under single-axial vertical vibration.

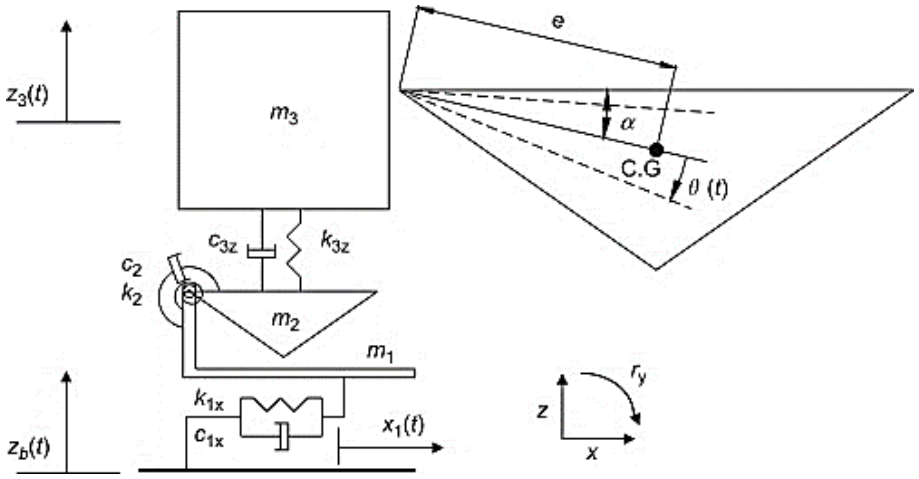

Figure 2.14 Schematic diagram of the human body model by Nawayseh and Griffin (2009)

Qiu and Griffin (2011) developed a lumped parameter human body model to predict the in-line fore-aft apparent mass of human body exposed to single-axial fore-aft vibration (Figure 2.15). The seated human body was represented by two masses at the upper- and lower part, respectively, and both parts were connected with torsion spring and damper which allowed the model to have a rotational DoF to simulate the pitch motion of the upper body. This model was also capable of predicting the cross-axis vertical apparent mass subject to fore-aft vibration.

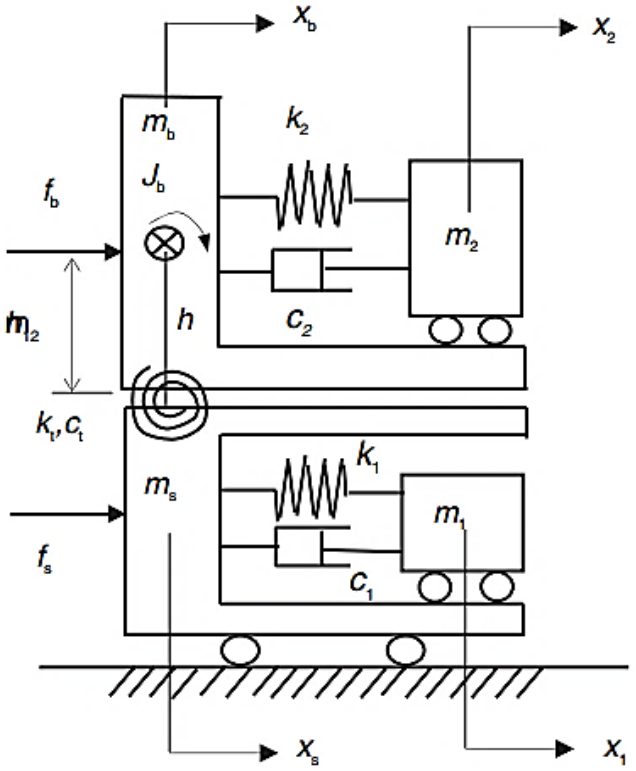

Figure 2.15 Schematic diagram of the human body model by Qiu and Griffin (2011)

The biodynamic modelling of human body exposed to tri-axial vibration using LPMs has been rarely reported. Although the vertical and fore-aft motion of the human body is partly correlated, and can

be modelled inside the mid-sagittal plane, the prediction of the biodynamic response in the additional lateral direction requires a three-dimensional model to be developed. Marzbanrad et al. (2016) developed a 15-DoF model of the human body to study the apparent masses and the seat-to-head transmissibility in the x, y, and z-axis. The human body segments were represented by 5 masses with 3 DoFs each and the forces between the masses were modelled using 3×3 stiffness and damping matrices. The calibrated model was able to achieve good agreement with the measured apparent masses at the seat pan and the seat-to-head transmissibilities. A prediction of the biodynamic response at the backrest using this model was not reported.

2.4.2 Multi-body models

Zheng et al. (2011) developed a seven-DoF multi-body model (Figure 2.16) to predict the in-line vertical and cross-axis fore-aft apparent mass of the human body under single-axial vertical vibration. The rigid bodies represented the upper body, middle body, pelvis, thighs, and legs, respectively. The DoFs included five rotational (around the x-axis) DoFs for the 5 rigid bodies, and two additional translational (in the x and z-axis) DoFs at the rigid body representing the pelvis. This multi-body model was capable of predicting both the vertical in-line and fore-aft cross-axis apparent mass of human body measured at the seat pan and the backrest when exposed to single-axial vertical vibration. By analysing the parameter sensitivity of the model, they found that the stiffness of tissue beneath pelvis might have affected the in-line vertical and cross-axis fore-aft apparent masses.

Liu and Qiu (2020) developed an 8-DoF multi-body model with a structure similar to that developed by Zheng et al. (2011), while excluding the backrest support and adding a rigid body representing the viscera. With an analysis of the parameter sensitivity using the model they proposed, they found that the simulated vertical apparent mass of the human body was most sensitive to the stiffness and damping representing the dynamic properties of the soft tissues beneath the ischial tuberosities and thighs and the viscera.

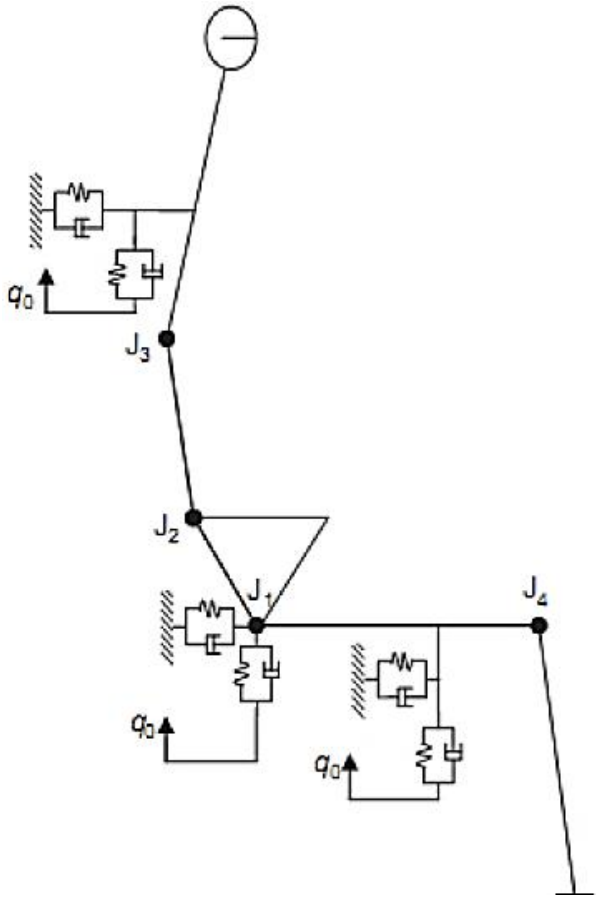

Figure 2.16 Schematic diagram of the 7-DoF multi-body model (Zheng et al., 2011)

Zhang et al. (2015) developed a 17-DoF multi-body human model (Figure 2.17). The rigid bodies represented the head, torso, viscera, pelvis, thighs, legs and feet of the human body, respectively. Each rigid body in this model had two DOFs in the z-axis and around x-axis except the one representing the viscera, and they were connected with each other using both translational and rotational springs and dampers. This model was used to connect with a vehicle model equipped with seats for the study of the WBV exposure instead of predicting the biodynamic responses of the seated human body.

Desai et al. (2018) developed a 20-DoF multi-body human model based on the model proposed by Zhang et al. (2015) by using two rigid bodies to represent the upper torso of the human body instead of one, and calibrating the model using the apparent masses measured in the laboratory experiments focusing on the study of the biodynamic response. That model can be used to predict the biodynamic response of the human body under dual-axial vibration in both vertical and fore-aft direction. Desai et al. (2021b) further compared the effectiveness of that model with some other LPMs in predicting the apparent masses under single-axial vibration.

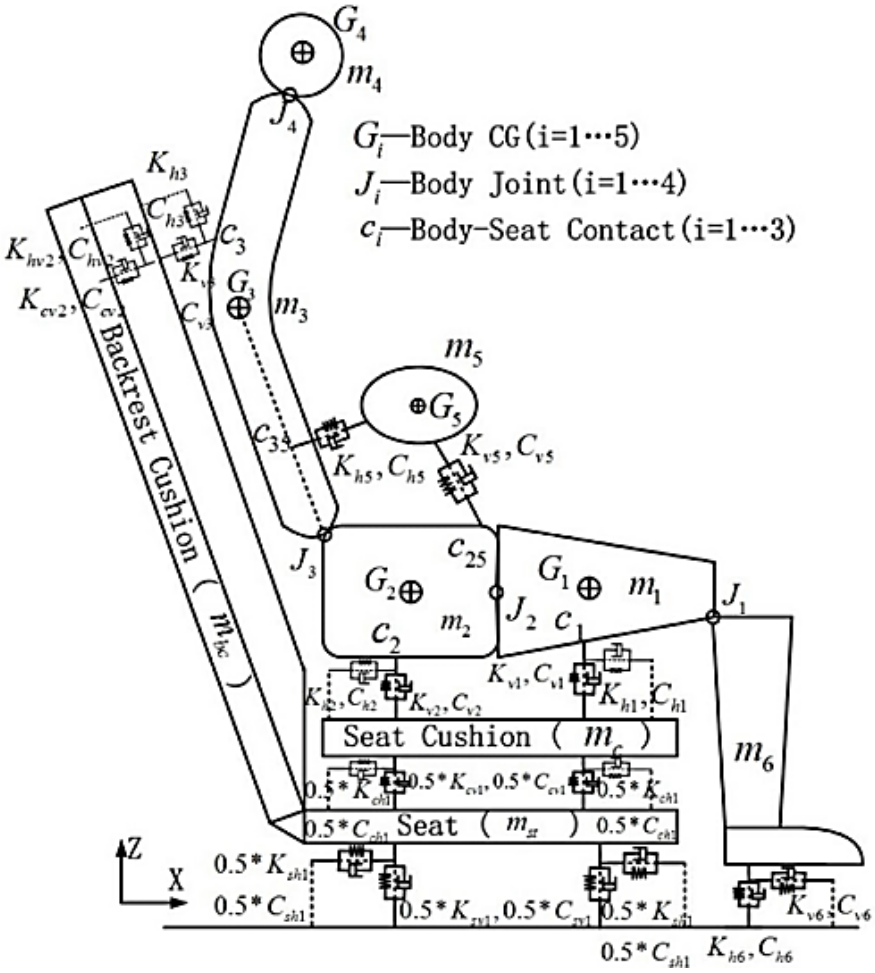

Figure 2.17 Schematic diagram of the 17-DoF multi-body model (Zhang et al., 2015)

Wu and Qiu (2020) developed a multi-body biodynamic model of the seated human body exposed to combined lateral, vertical and roll vibration. The model consisted of six rigid bodies representing the head and neck, upper torso, abdomen, pelvis, and thighs, respectively. The model was capable of predicting the apparent masses at the seat pan and backrest in the lateral and vertical direction.

It is reported in a systematic literature review that most of the existing multi-body biodynamic models are two-dimensional and are developed in the sagittal plane subject to in-plane excitations, such as the vertical, fore-and-aft or pitch excitation (Rakheja et al., 2020b). A biodynamic model of the human body capable of predicting the biodynamic response in three translational directions under tri-axial translational vibration, has not been reported.

2.4.3 Finite element (FE) models

The FE modelling approach has also been made to study the biodynamic responses of the human body to WBV. Zheng (2012) and Liu et al. (2015) developed finite element models of the human body to study the biodynamic response to vertical vibration, both paying close attention to the modelling of soft tissue and the bone structures at the pelvis and thighs. Figure 2.18 shows the

model developed by Liu et al. (2015) consisting of six body segments: head-neck, upper torso, lower torso, arms, pelvis-thighs and legs-feet. All the body segments were modelled as rigid bodies with flexible elements that were used to represent the soft tissues of the buttocks and thighs. The simulation result (Figure 2.18, lower part) indicates that this model can well predict the in-line vertical apparent mass and cross-axis fore-aft apparent mass.

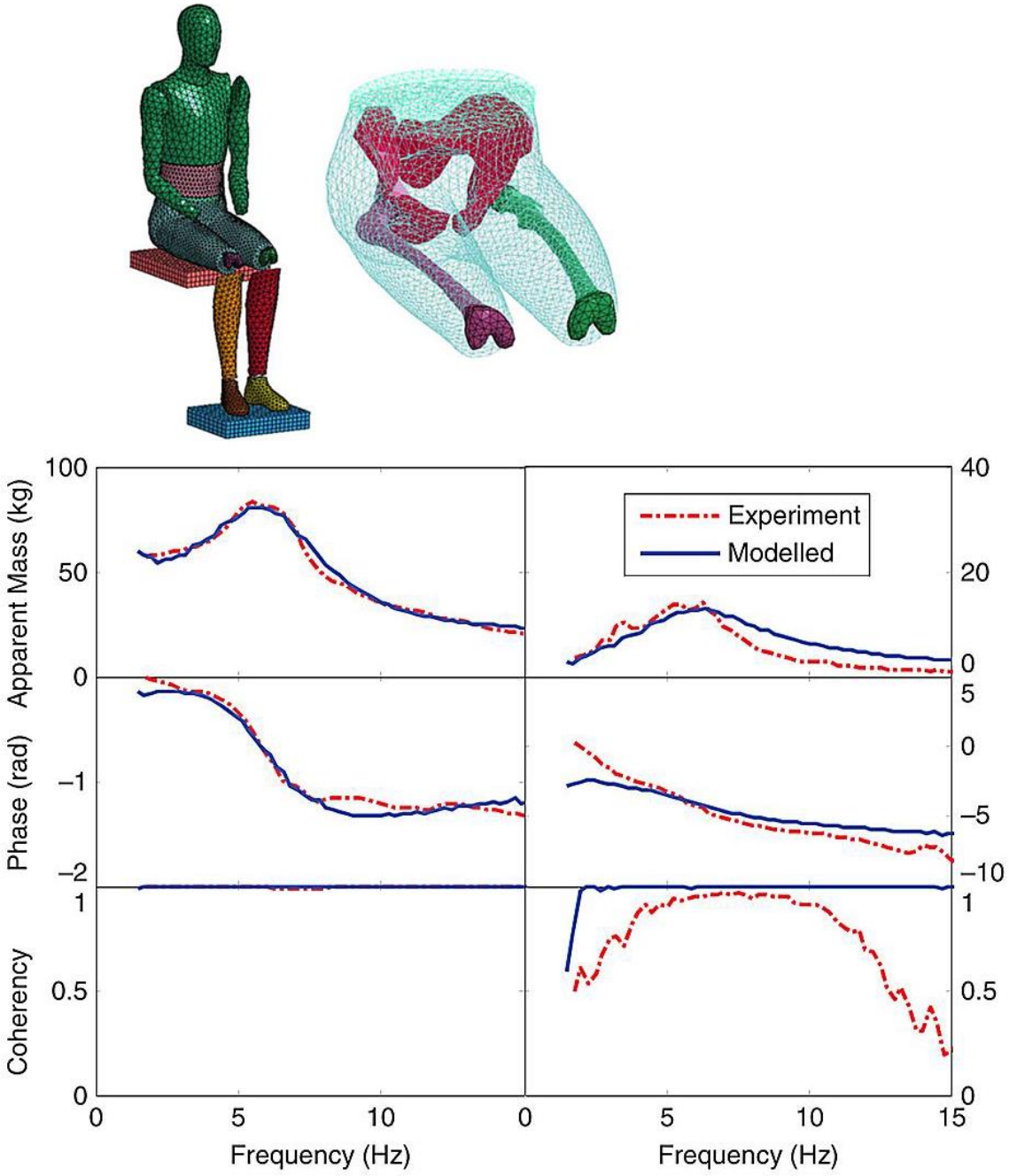

Figure 2.18 FE model of the seated human body and detailed presenting of pelvis and thighs modelling and comparison of measured ( ) and simulated ( ) apparent mass (left: vertical apparent mass; right: cross-axis fore-and-aft apparent mass). (Liu et al., 2015)

Dong et al. (2020) developed an FE model of the seated human body with special care taken on the modelling of the lumbar spine, which could be used to analyse the modes and the dynamic

responses of the lumbar spine under vertical vibration. An FE model developed by Gao et al. (2021) was capable of representing the vertical in-line and fore-and-aft cross-axis apparent mass of the human body without backrest under vertical excitation as well as the local transmissibility at the first thoracic spine.

2.5 Mathematical models of the vehicle seat and the seat-occupant system

A seat-occupant model that can reasonably predict the seat transmissibility requires that both the seat model and human body model be validated. Wei and Griffin (1998) developed a lumped parameter model of the seat-occupant system to predict the vertical transmissibility of a car seat. The seat cushion was modelled using stiffness and damping that were calibrated using the dynamic stiffness of the cushion measured using the indenter rig, and the parameters of the human body submodel were calibrated using the measured vertical apparent mass of the human body. The seat transmissibility predicted using this seat-occupant model achieved good agreement of the measured counterpart.

Gunston et al. (2004) developed a linear lumped parameter model (Figure 2.19, left) and a nonlinear “Bouc-Wen” model representing a suspension seat (Figure 2.19, right). The linear model consisted of various parameters of the suspension mechanism components, whose values were determined by the direct measurement, such as the stiffness and damping of the spring and damper. The nonlinear phenomenological Bouc-Wen model on the right was developed by using a combination of linear spring, linear damper and the nonlinear “Bouc-Wen force” to represent the suspension mechanism. Both models achieved good agreement of the vibration dose value (VDV) measured at the seat pan. The linear LPM proposed in this study was only used to predict the WBV exposure expressed as VDV, while the prediction of seat transmissibility was not reported. It was concluded that the linear lumped parameter model was beneficial for estimating the effect of each specific parameter of the seat component, while the nonlinear “Bouc-Wen model” was particularly suited for the study on the overall behaviour of the seat-occupant system.

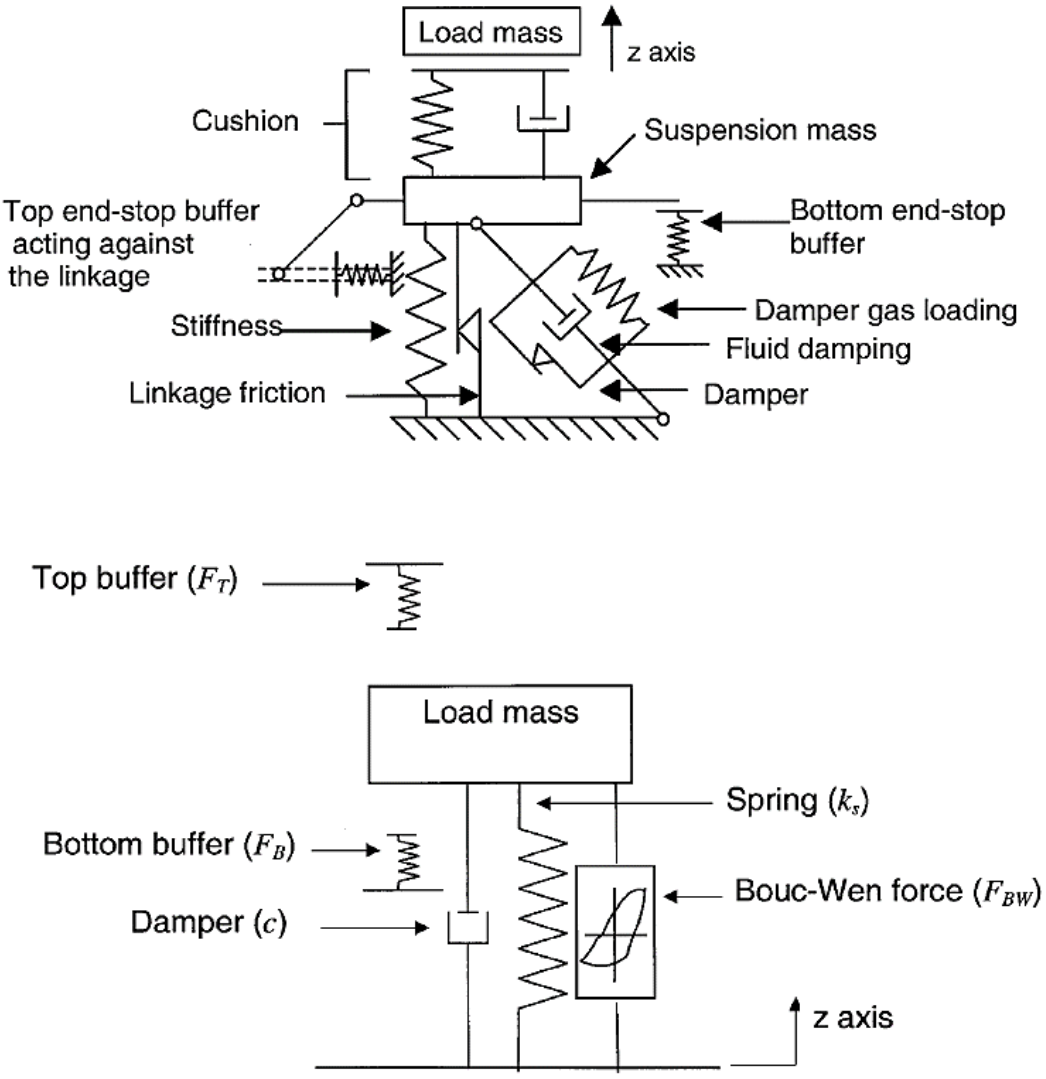

Figure 2.19 Schematic diagram of the component model (Top) and the Bouc-Wen model (Bottom) (Gunston et al., 2004)

Qiu and Griffin (2011) developed a lumped parameter seat-occupant model to study the fore-aft transmissibility at the backrest of a car seat (Figure 2.20). The human body in this model was the same as that shown in Figure 2.15. The backrest was divided into the upper and lower part connected with torsion spring and damper, and the two parts were connected with the upper and lower part of the human body model, respectively. After the calibration of human body model using the measured fore-aft apparent mass under single-axial fore-aft vibration, the parameters of human body model were determined. Then the parameters of the seat (including the contact stiffness and damping between the seat and the human body) were calibrated using the measured fore-aft transmissibility at the backrest. This seat-occupant model was capable of giving satisfactory prediction of the fore-aft transmissibility at the backrest.

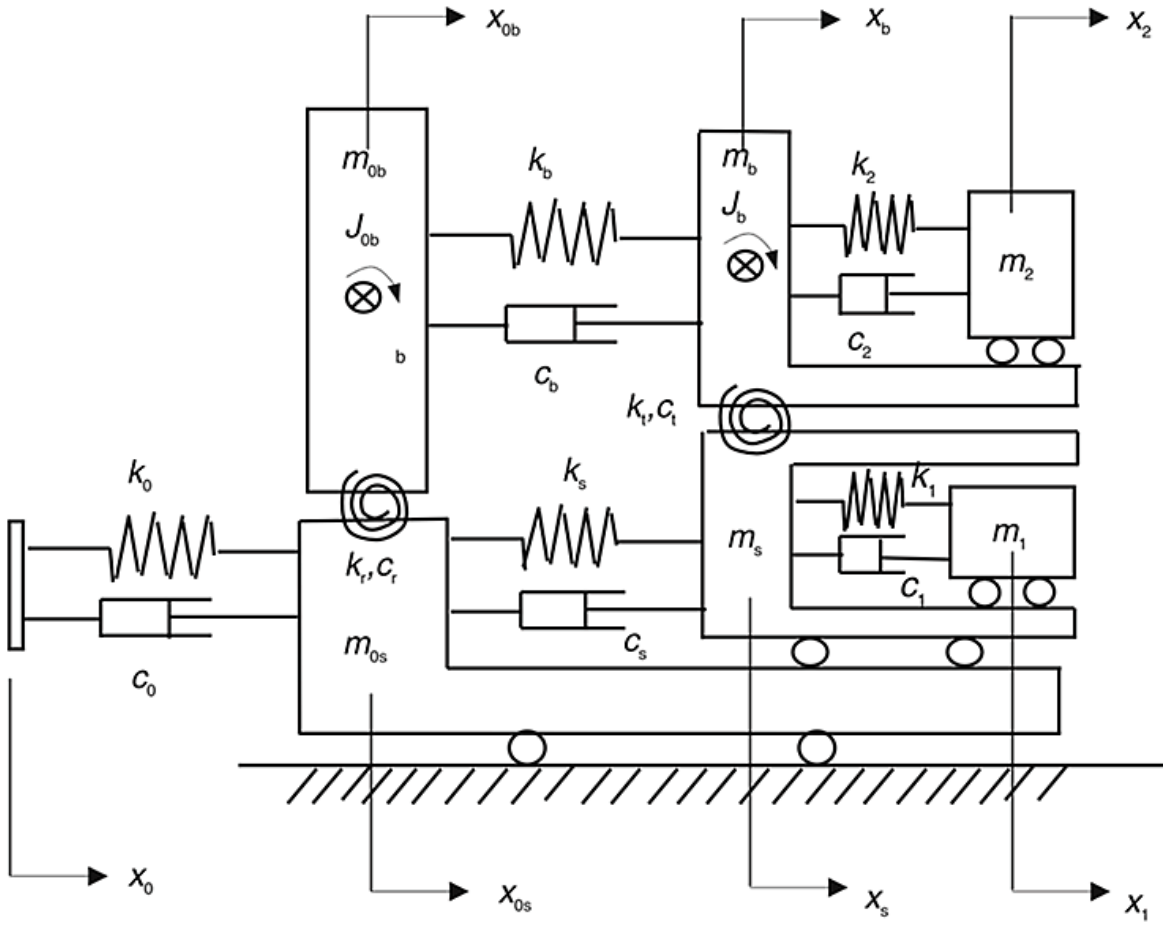

Figure 2.20 Schematic diagram of the seat-occupant model by Qiu and Griffin (2011)

Qiu (2012) developed a LPM of the suspension-seat-occupant system including the seat submodel and the human body submodel, following a systematic procedure by calibrating each submodel and the complete seat model step by step. The modelling procedure was:

1) The suspension mechanism model was developed and calibrated using the measured transmissibility of the suspension mechanism, and the values of the parameters of the suspension mechanism model were determined;

2) The cushion model was connected to the calibrated suspension mechanism model and the newly introduced parameters of the combined seat model were determined using the measured vertical transmissibility of the complete seat with loaded rigid mass, while keeping the determined values of the parameters in step 1) unchanged;

3) The human body submodel was developed and calibrated with the measured vertical apparent mass of the human body to determine the values of the human body model parameters;

4) Finally, the seat submodel and human body submodel were directly connected and the seat-occupant model was developed, which was capable of predicting the seat transmissibility without having to adjust the values of the determined parameters much.

Zhang (2014) developed a FE seat model consisting of the seat pan and backrest, and connected it with an FE model of human body. The parameters of the seat cushion were calibrated using the dynamic stiffness measured using the indenter rig. Then the complete seat model consisting of cushion and seat frame was calibrated using the vertical seat transmissibility measured when the seat was loaded with a manikin. The simulated seat transmissibility using the developed model achieved reasonable agreement with the measured counterpart.

Adam et al. (2019b) proposed a 3-DoF LPM of the suspension seat with seated occupant, in which the forces between the suspension mechanism, the seat cushion and the human body were represented by three pairs of spring and damping forces. Such a simple model was capable of predicting the vertical seat transmissibility. A parameter sensitivity analysis was carried out, and it was found that for that model, the transmissibility was most sensitive to the stiffness and damping of the suspension mechanism and the mass of the seated human body.

Wu and Qiu (2021) developed a three-dimensional multi-body train-seat-and-occupant model that was capable of achieving good agreement with the measured seat transmissibilities at the seat pan and backrest in the y- and z-axis under combined lateral, vertical and roll vibration (Figure 2.21). The seat submodel and the human body submodel were developed and calibrated separately before being connected. The contact between the seat and the human body was modelled using springs and dampers, and the corresponding stiffness and damping were adjusted after the two submodels were coupled. The model was further used to carry out modal analysis of the seat-occupant system.

Singh et al. (2021) developed an FE model of the seated human body coupled with a suspension seat on a farm tractor and concluded using that model that the factors including the seat cushion material and suspension mechanism affected the seat transmissibility. However, the verification of the model they developed via the comparison between the measured and simulated results was not presented.

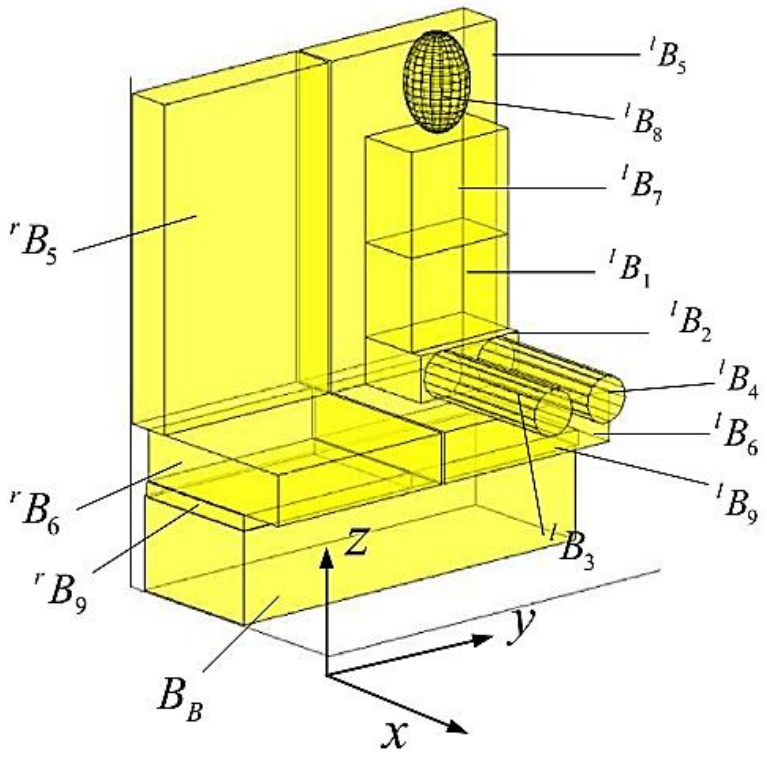

Figure 2.21 The seat-occupant model by Wu and Qiu (2021)

2.6 Discussion

2.6.1 Experimental study on the apparent masses of the seated human body

The effect of two influencing factors, the excitation magnitude and backrest inclination angle, on the apparent masses of the human body in the fore-aft, lateral and vertical directions at the seat pan and backrest has been studied in the past under limited conditions.

The previous studies on the effect of backrest inclination angle on the apparent mass have been limited to single-axial vibration (Mandapuram et al., 2005; Toward and Griffin, 2009; Yang and Qiu, 2015; Liu and Qiu, 2021), and most of them were carried out with a fixed magnitude of excitation. In real situations, however, the occupants on vehicle seats are exposed to multi-axial WBV with different magnitudes, and often with an inclined backrest. How would the biodynamic behaviour change in response to the varied backrest inclination angle under single and multi-axial vibration with a series of different excitation magnitudes still remains to be studied.

The apparent masses under tri-axial vibration were studied with limited number of excitation magnitudes previously (Mansfield and Maeda, 2007; Mandapuram et al., 2012). How will the apparent mass of the seated human body at the seat pan or backrest in the three translational directions be affected by a series of changes in the excitation magnitude in the in-line and cross-axis directions has not been reported. Whether there is interactive effect or the co-effect between

the excitation magnitudes and backrest inclination angle on the apparent mass of the seated human body, still remains to be investigated.

When exposed to multi-axial WBV, the seated human body can be regarded as a multi-input and multi-output system. It is expected that the relationship between each input and each output can be more precisely studied using multi-input-single-output method by eliminating the error caused by the potential correlation between the inputs. It also enables the comparison of the contribution of the multiple inputs (excitation in different axes) to the output (the apparent mass measured at the seat pan and backrest in different directions), which has been rarely adopted in the investigation of biodynamic response under multi-axial excitation.

2.6.2 Experimental study on the transmissibilities of the suspension seat

Some experimental studies on the influencing factors of the seat transmissibility have been carried out in the past, such as the magnitude of the single-axial vertical or fore-aft excitation and the backrest inclination angle. Suspension seats are usually designed to attenuate vertical vibration with a high-level magnitude above the resonance frequency of the seat-occupant system, and exhibit dramatic softening behaviour. The transmissibility of the suspension seat with the seated subject depends on not only the biodynamic response of the human body but also the dynamic properties of the seat. However, the transmissibility of a suspension seat in a tri-axial vibrational environment, instead of under single-axial vertical vibration, has been even less well discussed, although the suspension seats are widely used in the heavy vehicles where the effect of vibration in fore-aft and lateral directions on the ride comfort cannot be ignored in the reality. This requires the study of how the transmission of the vibration in the horizontal directions is affected by the dynamic properties of the seat and the seated human body.

Although some previous studies have reported the effect of the backrest inclination on the seat transmissibility, most of them were carried out under a certain excitation magnitude and focused on the transmissibilities in the directions on the sagittal plane of the seat-occupant system, e.g., under only single-axial excitation with a fixed vibration magnitude (Jalil and Griffin, 2007). How will the seat transmissibility change with a series of changes of the excitation magnitude and the backrest inclination angle still remains to be studied. Furthermore, whether interactive effect exists between these influencing factors is of interest.

The study of the seat transmissibility under tri-axial vibration, together with the study of the apparent mass, will also provide essential data for the development of seat-occupant model for studying the seating dynamics in the tri-axial vibrational environment, and assist the seat design accordingly to improve the ride comfort.

2.6.3 Dynamic modelling of the seated human body and the suspension-seat-occupant system

Various mathematical models have been developed for studying the biodynamic response of the seated human body to WBV and the seating dynamics of the seat-occupant system, including lumped parameter models, multi-body models and FE models. Most of the models of the human body were limited to capturing the dynamic behaviour of the human body in single-axial vibration, while the representation of the out-of-plane motion in the lateral directions is often not considered. It is required that a model of the seated human body be developed to reflect the biodynamics of human body exposed to tri-axial vibration, to study the relationship between the body modes and the resonances of the apparent masses in three translational directions.

Although a few seat models have been developed for predicting the transmissibility of the suspension seat exposed to single-axial vibration, a model of the suspension-seat-occupant system, which is capable of giving satisfactory prediction of the seat transmissibility at the seat pan and the backrest under tri-axial translational vibration, still remains to be developed. A seat-occupant model validated with experimental data would be beneficial to the optimal design of seat dynamic performance and improvement of ride comfort.

2.7 Research questions and objectives

Inspired by the above literature review and discussions, the following research questions are formed:

1) How will the backrest inclination angle affect the apparent masses at the seat pan and backrest of the seated human body under single-axial excitation of different magnitudes and is there any interactive effect between the backrest inclination angle and the excitation magnitude?
2) For the apparent mass of the seated human body exposed to tri-axial vibration in the fore-aft, lateral or vertical direction, how does the vibration magnitude in that axis interact with the excitation magnitude in the other two additional axes at different backrest inclination angles?
3) How can the transmissibility of the suspension seat in the fore-aft, lateral or vertical direction under tri-axial excitation be affected by the excitation magnitude in that axis and in the other two axes, combined with the effect of the backrest inclination angle?
4) Can a seated human body model be developed to characterize the in-line apparent masses of the human body in all three translational directions at the seat pan and backrest under tri-axial translational vibration with upright and inclined backrest?

5) How can a combined suspension seat-occupant model with tri-axial excitation be developed to predict the transmissibilities at the seat pan and backrest in the fore-aft, lateral and vertical directions?

The objective of this thesis is to answer these research questions, by investigating the effect of the influencing factors (the excitation magnitude in one axis and that in the other two additional axes, and the backrest support) on the apparent masses and the transmissibilities of suspension seat under tri-axial translational vibration. Additionally, how the characteristics of the biodynamic responses and transmissibilities of the suspension seat under tri-axial translational vibration could be reproduced by the dynamic models will be studied.

Chapter 3 THE APPARENT MASS OF THE SEATED HUMAN BODY EXPOSED TO SINGLE-AXIS VIBRATION: THE EFFECT OF THE BACKREST INCLINATION COMBINED WITH DIFFERENT EXCITATION MAGNITUDES

3.1 Introduction

A comprehensive understanding of the characteristics and influencing factors of the biodynamic response of the seated human body to WBV is beneficial to the improvement of the ride comfort. Two of the important influencing factors are the inclination of the backrest and the excitation magnitude. It has been found that the vertical apparent masses at both the seat pan and backrest were affected by the change of the backrest inclination angle (Yang and Qiu, 2015; Liu and Qiu, 2021) due to the increased interaction between the seat and upper body and the altered posture. Differences between the apparent masses in the horizontal directions with an upright backrest and with a backrest inclined by 12.5° have also been reported (Mandapuram et al., 2005). The increase of the excitation magnitude in one axis generally leads to the nonlinear behaviour of the human body, reflected by the decrease of resonance frequency of the apparent mass in the same direction (Mansfield et al., 2006; Qiu and Griffin, 2012; Wu et al., 2021).

However, most of the previous studies on the effect of the backrest inclination were limited to the condition where the excitation magnitude was fixed at only one level. It is of interest to know how the effect of backrest inclination on the apparent mass would change with different magnitudes of excitation. Despite the reported effect of backrest inclination angle on the apparent mass, most of the existing studies on the effect of the excitation magnitude on the apparent masses have been carried out without backrest or with an upright backrest. How the effect of the excitation magnitude on the apparent mass would be further affected by the backrest inclination is still unknown.

In this chapter, an experimental study was carried out measuring the apparent masses of the seated human body in the x, y and z-axis at the seat pan and backrest to investigate the effect of the backrest inclination angles combined with different magnitudes of single-axial excitation on the apparent masses. It is hypothesized that with the increased backrest inclination angle, the resonance frequency or the associated modulus of the apparent mass would be affected, which

would be observed under all the excitation magnitudes. It is further hypothesized that with different backrest inclination angles, the nonlinearity of the seated human body due to the increase of excitation magnitude would always be observed, while the degree of the nonlinearity would be different.

3.2 Experimental method

For the experimental studies on the apparent mass, it is assumed that with the rigid seat, the vibration inputs to the human body at the seat pan and backrest are identical to the motion at the seat base. Additionally, the effect of the constrain of the seat belt on the results are ignored.

3.2.1 Apparatus

The experimental study was approved by the Faculty of Engineering and Physical Sciences Ethics Committee at the University of Southampton. The experiment was carried out using the 6-axis motion simulator in the Institute of Sound and Vibration Research. A rigid seat with a seat pan and a backrest was mounted at the centre of the simulator (Figure 3.1). The backrest's backwards inclination angle can be adjusted between 0 and 80°with respect to the upright position.

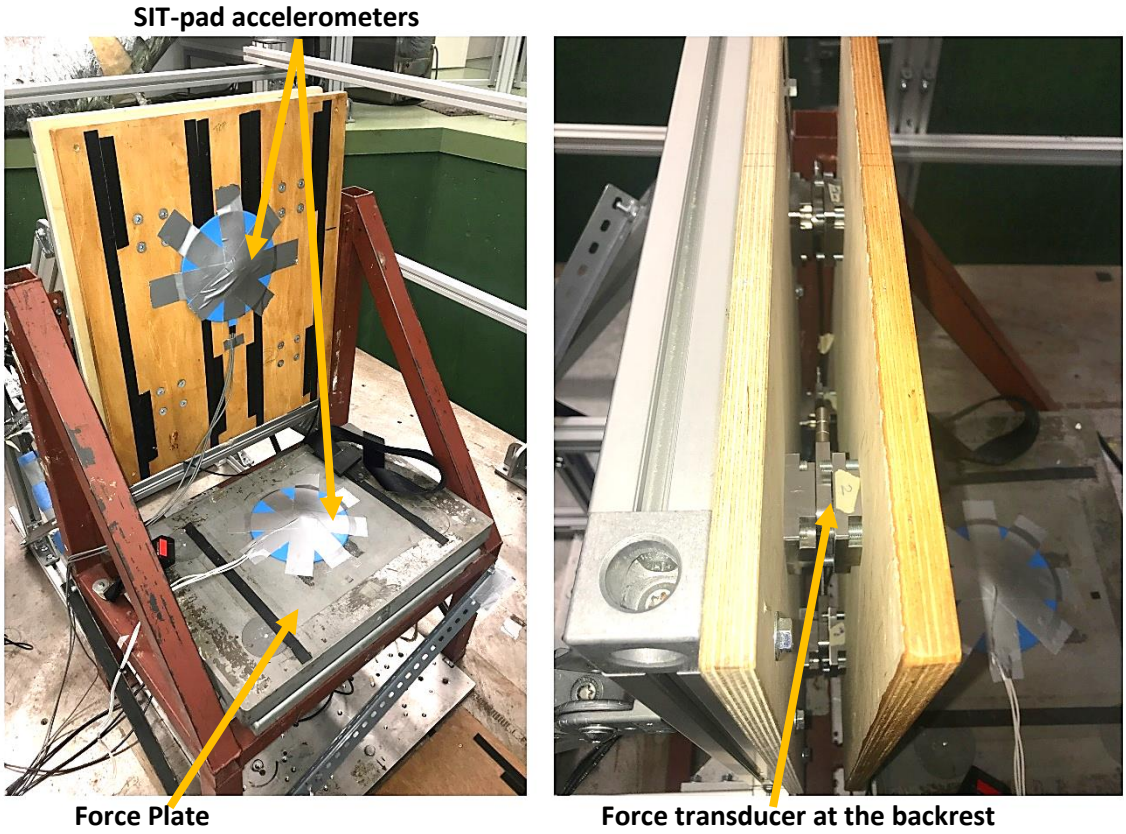

Figure 3.1 The rigid seat, with force plate at the seat pan, force transducers at the backrest and SIT-pads used in the experiment

To measure the tri-axial dynamic forces at the interface between the seat pan and subject, a Kistler 9281 B force plate with tri-axial force transducers located at the four corners was fixed on the seat pan. The tri-axial forces at the interface between the backrest and subject were measured using four tri-axial force transducers (Kistler 9602, with charge amplifier integrated), which were fixed at the four corners of the backrest. Three Kistler 5001 charge amplifiers were used to amplify the signals from the force plate. To measure the acceleration at the interface between the seat and subject, two tri-axial SIT-pads were fixed at the force plate and the backrest, respectively. The SIT-pad at the seat pan was positioned at the centre of the seat pan under the ischial tuberosity of the seated subjects, and the SIT-pad at the backrest was located at the centre of the backrest, 43cm above the seat pan surface. The measured data was recorded and processed using HVLab data acquisition system with a sampling rate of 512 samples per second and with an anti-aliasing filter set at 50 Hz.

3.2.2 Subjects

Twelve male subjects aged between 22 and 43 years old (with a mean age of 28.8 years old) participated in this experiment. The stature of the subjects ranged from 1.70 to 1.85 m (with a mean stature of 1.78 m) and the weights of the subjects ranged from 57.3 to 93.5 kg (with a mean weight of 75.3 kg). During the experiment, the subjects were asked to sit in an upright relaxed posture against the backrest when the backrest is upright, or sit in a relaxed posture against the backrest when the backrest was inclined. They were secured with the seat belt and were asked to rest their hands on the lap and rest their feet on the footrest, so as to maintain an average thigh contact with the force plate (Figure 3.2).

Figure 3.2 The postures of the subject sitting in the seat with different backrest inclination angles (from left to right: 0°, 10°, and 20°)

3.2.3 Stimuli and backrest inclination

Nine single-axial broad-band random excitations over a frequency range between 0.5 and 40 Hz were used, with a duration of 60 seconds each. The nine excitations include three single-axial fore-aft excitations, three single-axial lateral excitations and three single-axial vertical excitations. The excitation magnitudes in each axis varied between three levels: 0.25, 0.5 and 1.0 ms^{-2} r.m.s. The nine vibration signals were generated independently and was mutually uncorrelated.

During the experiment, each subject was exposed to the nine excitations three times, each time with the backrest support at a different inclination angle: 1) 0° (upright), 2) 10° backwards, and 3) 20° backwards (Figure 3.2). Hence, the total number of the combinations of the experiment conditions is 27. The order of these combinations was randomized for each subject.

3.2.4 Data analysis

In this experimental study, the force transducers and SIT-pads at the backrest were mounted in such a way that they measured the forces and accelerations in the axes perpendicular (z-axis of the backrest coordinate system) and parallel to the backrest surface (x and y-axis of the backrest coordinate system). When the backrest was inclined, the surface of the backrest was not perpendicular to the seat pan and floor, making the x and z-axis of the backrest coordinate system different from those of the coordinate system of the floor, while the directions of the unit vectors of the seat pan coordinate system are always the same as those of the floor coordinate system (Figure 3.3).

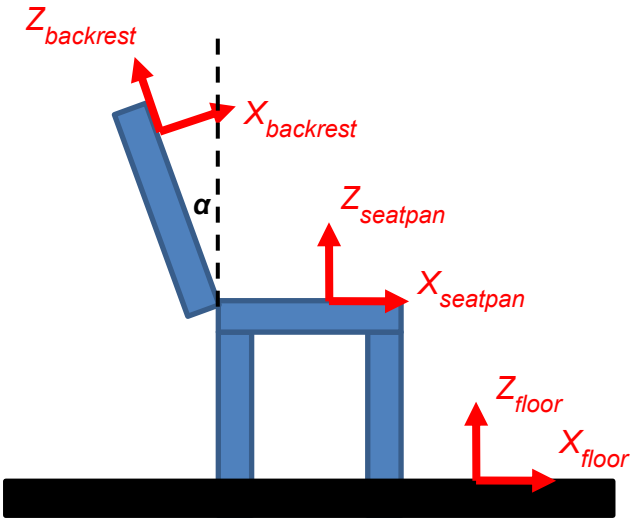

Figure 3.3 The x- and z-axis of the backrest coordinate system ($Z_{backrest}$ and $X_{backrest}$), seat pan coordinate system ($Z_{seatpan}$ and $X_{seatpan}$) and floor coordinate system (Z_{floor} and X_{floor}) when the backrest was inclined by an angle of α

In this study, when the backrest was inclined, the forces and acceleration measured in the x and z-axis of the backrest coordinate system were projected to the x and z-axis in the coordinate system of the floor to calculate the apparent mass at the backrest. Here, the accelerations and the forces at the seat pan or backrest are denoted as a_{ij} and F_{jk}^{c}, respectively. The subscript *i*=*s*, *b* represents the position of the measured force (seat pan and backrest, respectively), the subscripts *j, k*=*x*, *y* and *z*, represent the direction of the measured acceleration and force (fore-aft, lateral and vertical direction, respectively) and the superscript *c*=*s, b* represents the coordinate system in which the force was described (seat pan and backrest, respectively).

The vectors of the tri-axial forces in at the backrest expressed in the seat pan coordinate system $\mathbf{F}_{\boldsymbol{b}}^{\boldsymbol{s}}$, and the backrest coordinate system $\mathbf{F}_{\boldsymbol{b}}^{\boldsymbol{b}}$, are expressed as follows:

$$\mathbf{F}_{\boldsymbol{b}}^{\boldsymbol{s}} = \begin{bmatrix} F_{bx}^{s} & F_{by}^{s} & F_{bz}^{s} \end{bmatrix} \tag{3.1}$$

$$\mathbf{F}_{\boldsymbol{b}}^{\boldsymbol{b}} = \begin{bmatrix} F_{bx}^{b} & F_{by}^{b} & F_{bz}^{b} \end{bmatrix} \tag{3.2}$$

When the angle of backrest inclination was α, the forces measured at the backrest in the x and z-axis of the backrest coordinate system were transformed to the seat pan coordinate system:

$$\mathbf{F}_{\boldsymbol{b}}^{\boldsymbol{s}} = \mathbf{F}_{\boldsymbol{b}}^{\boldsymbol{b}}\mathbf{T} \tag{3.3}$$

Where **T** represents the transformation matrix for the experimental study:

$$\mathbf{T} = \begin{bmatrix} cos\alpha & 0 & -sin\alpha \\ 0 & 1 & 0 \\ sin\alpha & 0 & cos\alpha \end{bmatrix} \tag{3.4}$$

The acceleration measured at the backrest was transformed using the same method.

Mass cancellation was performed before the calculation of the apparent mass at the seat pan in the time domain to eliminate the inertia force due to the motion of the force plate and SIT-pad on top of the force transducers, by subtracting from the measured force the product of the measured acceleration at the seat pan and the mass of the top plate and SIT-pad. Similarly, mass cancellation was done on the force measured at the backrest to eliminate the inertia force due to the motion of the force transducers, the backrest structure and SIT-pad at the backrest.

Under single-axial vibration, the in-line and the cross-axis apparent masses at the seat pan and backrest were calculated using a single-input-single-output (SISO) method. For example, under the single-axial vertical vibration, if a_{iz} represents the measured vertical acceleration and F_{ij}^{s} represents the force in the x, y or z-axis in the seat pan coordinate system (*i* represents the position, and *j* represents the direction of the apparent mass), then the in-line (and cross-axis) apparent masses and the corresponding coherence could be calculated as follows:

$$AM_{izj} = \frac{G_{a_{iz}F_{ij}^s}}{G_{a_{iz}}} \tag{3.5}$$

$$\gamma_{ijk}^2 = \frac{\left|G_{a_{ij}F_{ik}^s}\right|^2}{G_{a_{ij}}G_{F_{ik}^s}} \tag{3.6}$$

Where $G_{a_{iz}F_{ij}^s}$ represents the cross-spectra between a_{iz} and F_{ij}^s; while $G_{a_{iz}}$ and $G_{F_{ij}^s}$ represent the auto-spectra of a_{iz} and F_{ij}^s, respectively. If *j*=*z*, then the calculated apparent mass AM_{bzz} or AM_{szz} was the in-line vertical apparent mass, and if *j*=*x* or *y*, it was a cross-axis fore-aft apparent mass. The apparent masses under single-axial fore-aft and lateral vibration were also calculated similarly.

In this study, the change of the biodynamic response due to the change of the excitation magnitude, and that due to the change of the backrest inclination angle, were quantified by the change of the resonance frequency and the associated modulus of the apparent mass, including: 1) the ratio of the resonance frequencies of the apparent masses R_{nl}; 2) the relative percentage change of the associated moduli, *PC*. The greater the value of R_{nl} or *PC* is, the greater the degree of the nonlinearity of the biodynamic response will be. In the studies presented in this and the following chapters, only the extent of the change due to the increased excitation magnitude was referred to as the "degree of the nonlinearity".

For the change of an apparent mass due to the increase of backrest inclination under a certain excitation magnitude, the two indices, R_{nl_br} and PC_{br}, were defined as follows:

$$R_{nl\_br} = \frac{f_{upright}}{f_{20^\circ}} \tag{3.7}$$

$$PC_{br} = \frac{(AM_{upright} - AM_{20^\circ})}{AM_{upright}} \times 100\% \tag{3.8}$$

Where the abbreviation "*br*" in the subscripts of R_{nl} and *PC* indicates that these indices are quantifying the degree of nonlinearity due to the changing **b**ack**r**est inclination angle; f_{upright} and f_{20° are the fundamental resonance frequency of the apparent mass measured with upright backrest and with a backrest inclined by 20°, respectively; AM_{upright} and AM_{20° are the modulus associated with the fundamental resonance frequency measured with upright backrest and with a backrest inclined by 20°, respectively. Similarly, the indices quantifying the degree of nonlinearity due to the changing excitation magnitude, R_{nl_ilm} and PC_{ilm}, are defined as follows:

$$R_{nl\_ilm} = \frac{f_{0.25}}{f_{1.0}} \tag{3.9}$$

$$PC_{ilm} = \frac{(AM_{0.25} - AM_{1.0})}{AM_{0.25}} \times 100\% \tag{3.10}$$

Where the abbreviation "*ilm*" in the subscripts indicates the indices quantifying the degree of nonlinearity due to the changing **i**n-**l**ine excitation **m**agnitude; $f_{0.25}$ and $f_{1.0}$ are the fundamental resonance frequency of apparent mass measured under the excitation magnitude of 0.25 and 1.0 ms^{-2} r.m.s., respectively, $AM_{0.25}$ and $AM_{1.0}$ are the modulus associated with the fundamental resonance frequency measured under excitation magnitude of 0.25 and 1.0 ms^{-2} r.m.s., respectively.

The Friedman two-way analysis of variance was applied to test the effect of the three different vibration magnitudes and the three different angles of the backrest inclination on the resonance frequency and the associated modulus of the apparent mass, and the degree of nonlinearity of the biodynamic response among the twelve subjects. The null hypothesis of the test is that there is no significant difference between the data sets measured with changing values of an influencing factor, i.e., the factor did not have a significant effect. If the value of p is smaller than 0.05, then the null hypothesis is rejected, and the likelihood of incorrectly rejecting it is small.

3.3 Results

Inter-subject variabilities due to different ages, body sizes, or weights can be found in the apparent masses. However, the moduli of the apparent masses measured with different subjects share some general commonalities which could be revealed by the median apparent mass. For example, Figure 3.4 shows the in-line vertical apparent masses of 12 subjects and the median vertical apparent mass measured at the seat pan with the support of the upright backrest under 0.5 ms^{-2} r.m.s. single-axial vertical excitation. Despite the inter-subject variability shown by the curves with different colours, the in-line vertical apparent masses of all the subjects generally exhibit a fundamental resonance between 4.5 and 6.5 Hz. The resonance frequency of the median in-line vertical apparent mass of the twelve subjects is within this frequency range (at 5.5 Hz). Such a capability of representing the similarities of the apparent masses over different subjects can be found in the median apparent masses in other directions, and the general effect of the influencing factors on the subjects can also be shown.

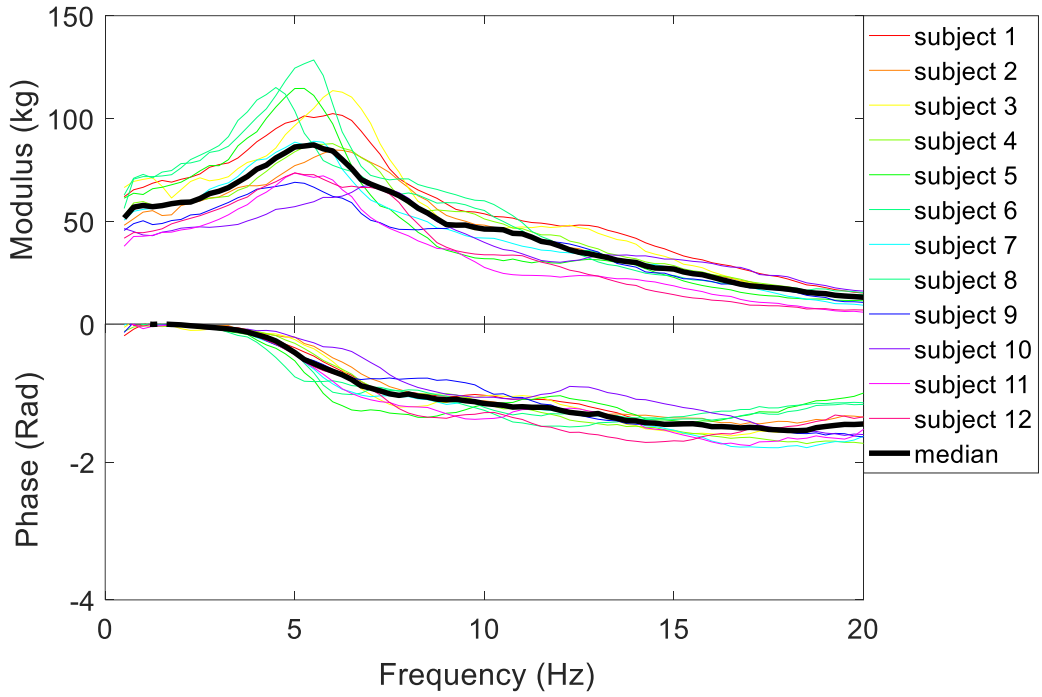

Figure 3.4 The in-line vertical apparent masses of 12 subjects and the median vertical apparent mass (bold black curve), measured at the seat pan with the support of an upright backrest and under single-axial vertical excitation with a magnitude of 0.5 ms^{-2} r.m.s.

The median apparent masses will be used to demonstrate the general characteristics of the biodynamic response of the subjects in the following sections.

3.3.1 In-line fore-aft apparent masses under single-axial fore-aft excitation

The in-line fore-aft apparent mass generally exhibited a fundamental resonance between 4 and 6 Hz at both the seat pan and at the backrest, while a second resonance can be found in the vicinity of 8 Hz for the apparent mass at the backrest when the backrest was inclined, see Figure 3.5.

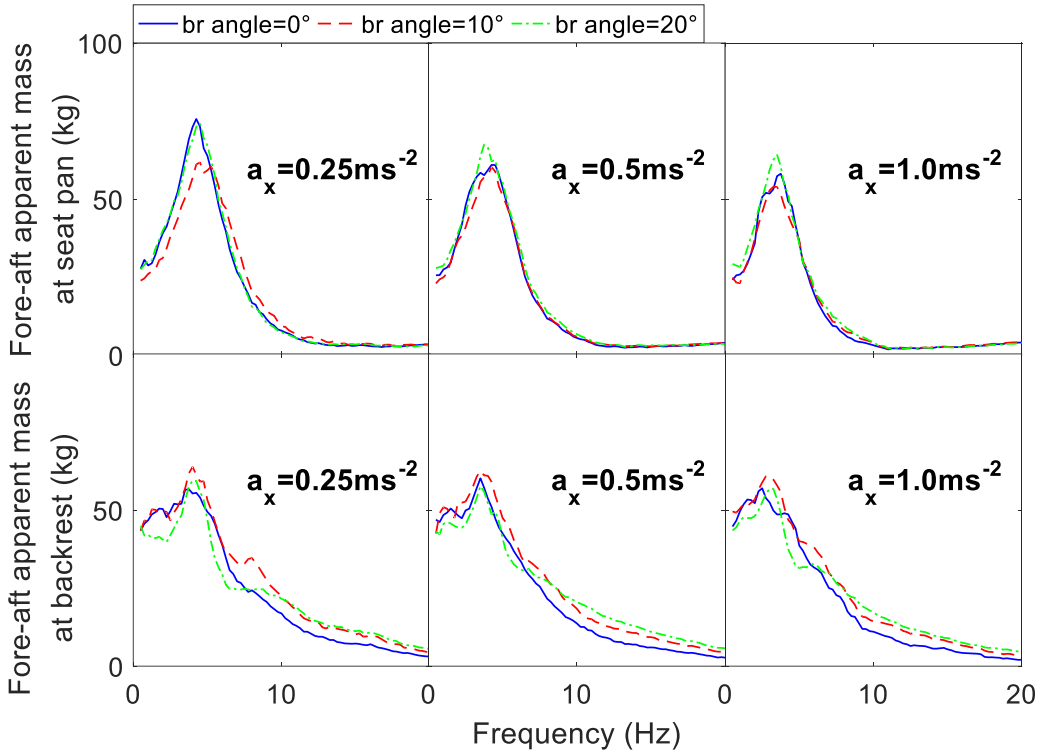

Figure 3.5 Median in-line fore-aft apparent mass at the seat pan and backrest: the effect of backrest inclination angle (abbreviated as "br angle")

3.3.1.1 The effect of the backrest inclination at different excitation magnitudes

With a series of the increase of the backrest inclination angle from 0° to 10° and then to 20°, the fundamental resonance frequency of the in-line fore-aft apparent mass at the seat pan and backrest hardly changed (Figure 3.5). The modulus associated with the fundamental resonance frequency of the apparent mass at the seat pan first decreased when the backrest inclination angle increased from 0° to 10° and then increased when the angle further increased from 10° to 20°, while that at the backrest first increased and then decreased. These phenomena can be found under all excitation magnitudes. Furthermore, when the backrest inclination angle increased, the percentage change of the modulus associated with the resonance of the in-line fore-aft apparent masses at the backrest due to the change of the excitation magnitude (PC_{ilm}) tended to increase significantly, which is shown in Table 3.1 ("*" highlights cases where $0.01<p<0.05$ and "**" highlights cases where $p<0.01$, and "ns" highlights the cases where $p>0.05$, sic passim), while the effect of backrest inclination on the PC_{ilm} or R_{nl_ilm} of the fore-aft apparent mass at the seat pan was not significant ($p>0.05$).

Table 3.1 The median values of the R_{nl_ilm} and PC_{ilm} of the fore-aft apparent masses of 12 subjects under single-axial fore-aft vibration, and statistical significance (*p*-value, Friedman) of the effect of backrest inclination angles on them

Quantities indicating the degree of the nonlinearity	**Median value of the quantities at different backrest inclination angles**			***p*-value**
	0°	**10°**	**20°**	
R_{nl_ilm} of in-line fore-aft apparent mass at seat pan	*1.23*	*1.39*	*1.31*	ns
R_{nl_ilm} of in-line fore-aft apparent mass at backrest	*1.25*	*1.37*	*1.25*	ns
PC_{ilm} of in-line fore-aft apparent mass at seat pan	*15.98%*	*16.59%*	*13.32%*	ns
PC_{ilm} of in-line fore-aft apparent mass at backrest	*-3.70%*	*6.51%*	*9.40%*	*

3.3.1.2 The effect of the excitation magnitude

Figure 3.6 shows that the nonlinearity reflected by the change of resonance frequency of the in-line fore-aft apparent mass with the increased fore-aft excitation magnitude can be found with both upright and inclined backrest (p<0.01). The moduli associated with both the fundamental resonance frequency of the in-line fore-aft apparent mass at the seat pan and that at the backrest generally tended to decrease with the increase of the excitation magnitude under most backrest conditions (p<0.01 for 5 out of 6 cases). Additionally, the increase of the fore-aft excitation magnitude significantly led to an increase of the PC_{br} of the in-line fore-aft apparent masses at the backrest due to the change of the backrest inclination angle (p<0.05, Table 3.2).

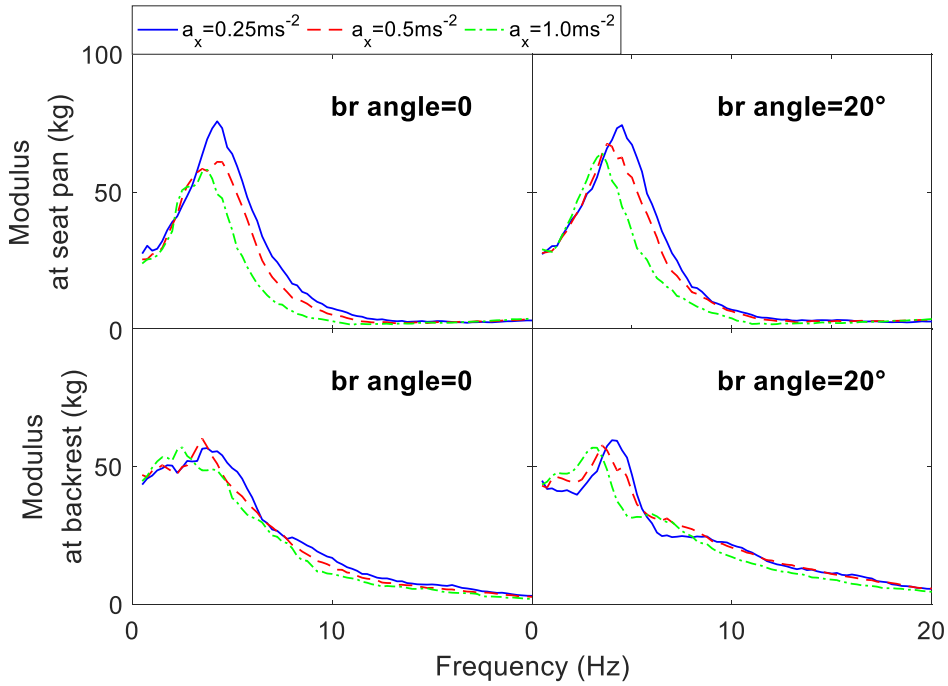

Figure 3.6 Median in-line fore-aft apparent mass at the seat pan and backrest: the effect of the magnitude of fore-aft excitation

Table 3.2 The median values of the R_{nl_br} and PC_{br} of the fore-aft apparent masses of 12 subjects under single-axial fore-aft vibration, and statistical significance (*p*-value, Friedman) of the effect of fore-aft excitation magnitude on them

Quantities indicating the degree of the nonlinearity	**Median value of the quantities at different fore-aft excitation magnitudes (r.m.s.)**			***p*-value**
	0.25 ms^{-2}	**0.5 ms^{-2}**	**1.0 ms^{-2}**	
R_{nl_br} of in-line fore-aft apparent mass at seat pan	*1.00*	*1.00*	*1.12*	ns
R_{nl_br} of in-line fore-aft apparent mass at backrest	*1.00*	*0.97*	*1.00*	ns
PC_{br} of in-line fore-aft apparent mass at seat pan	*-7.40%*	*-5.04%*	*-7.19%*	ns
PC_{br} of in-line fore-aft apparent mass at backrest	*7.48%*	*9.49%*	*16.83%*	*

3.3.2 In-line lateral apparent masses under single-axial lateral excitation

The modulus of the lateral apparent mass at the seat pan and backrest above 10 Hz was relatively small, so only the apparent masses up to 10 Hz are shown in this section for clarity. In general, the in-line lateral apparent mass at the seat pan exhibited one distinctive resonance between 1.5 and

2.5 Hz, which was regarded as the fundamental resonance, although a local peak at around 0.75 Hz with a relatively smaller modulus could be found in some cases (Figure 3.7). The fundamental resonance of the apparent mass at the backrest existed at 0.75 Hz when the lateral excitation magnitude was 0.25 ms^{-2} r.m.s. (Figure 3.7). Such a resonance was not clearly identifiable under 0.5 or 1.0 ms^{-2} r.m.s. vibration, presumed to be located at or below 0.5 Hz in these cases. Hence, the effect of the excitation magnitude and backrest inclination on the resonance of the lateral apparent mass at the backrest was examined using the modulus at 0.75 Hz instead. A second resonance of the apparent mass at the backrest can be found at around 2.5 Hz but was not identifiable not when the backrest was inclined by 20°.

3.3.2.1 The effect of the inclination angle of the backrest

Figure 3.7 shows that the increase of the backrest inclination angle generally led to an increase of the modulus associated with the resonance frequency of the in-line lateral apparent mass (p<0.05 only when the excitation magnitude was 0.25 ms^{-2} r.m.s.), while the effect on the resonance frequency was small. When the backrest inclination angle increased, the modulus of the in-line lateral apparent mass at the backrest between 3 and 10 Hz tended to decrease, while the effect of the backrest inclination on the modulus at 0.75 Hz was only significant under 0.25 or 0.5 ms^{-2} r.m.s. lateral excitation (p<0.05). The effect of the backrest inclination on the R_{nl_ilm} and PC_{ilm} of the lateral apparent mass at the seat pan was not significant (p>0.05, Table 3.3).

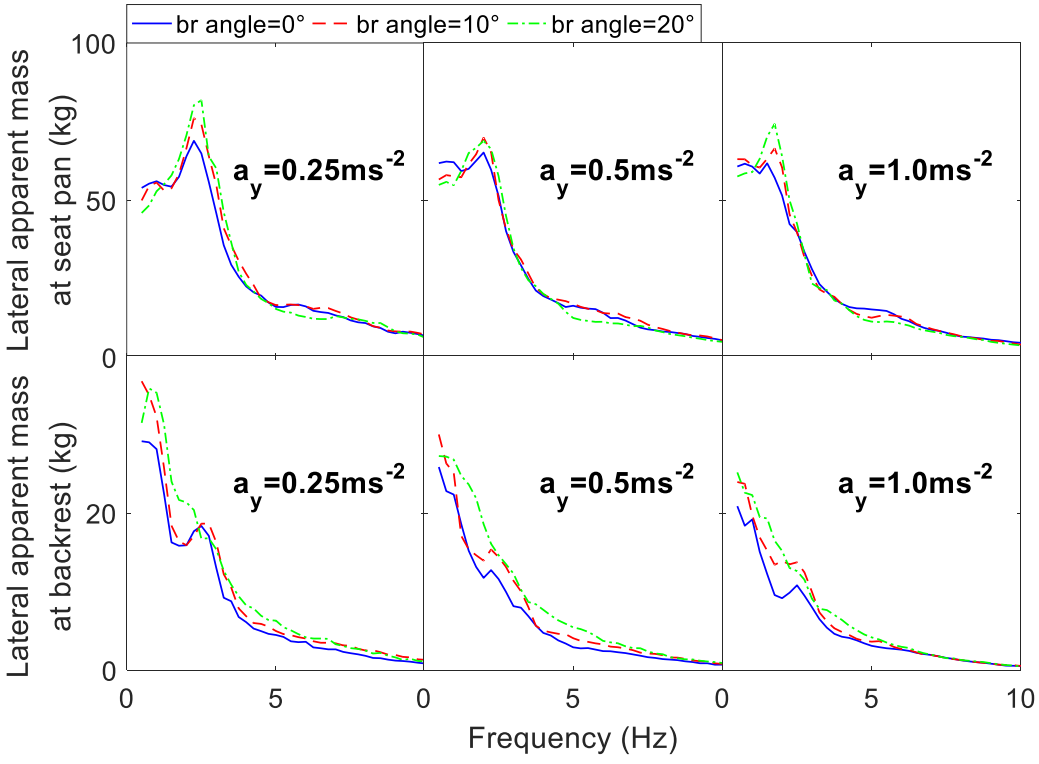

Figure 3.7 Median in-line lateral apparent mass at the seat pan and backrest: the effect of backrest inclination angle

Table 3.3 The median values of the R_{nl_ilm} and PC_{ilm} of the lateral apparent masses of 12 subjects under single-axial lateral vibration, and statistical significance (p-value, Friedman) of the effect of backrest inclination angles on them

Quantities indicating the degree of the nonlinearity	Median value of the quantities at different backrest inclination angles			p-value
	0°	10°	20°	
R_{nl_ilm} of in-line lateral apparent mass at seat pan	*1.55*	*1.46*	*1.48*	ns
PC_{ilm} of in-line lateral apparent mass at seat pan	*2.88%*	*9.52%*	*7.75%*	ns

3.3.2.2 The effect of the excitation magnitude

With the increased lateral excitation magnitude, the resonance frequency of the lateral apparent mass at the seat pan decreased significantly both with upright and inclined backrest (p<0.01, Figure 3.8). The effect of the lateral excitation magnitude on the modulus associated with the fundamental resonance frequency of the lateral apparent mass at the seat pan was significant when the backrest was inclined (p<0.05). When the lateral excitation magnitude increased, the modulus of the lateral apparent mass at the backrest at 0.75 Hz decreased significantly under all conditions (p<0.01; Figure 3.8). The R_{nl_br} and PC_{br} of the lateral apparent mass at the seat pan tended to decrease with the increase of the lateral excitation magnitude, although only the effect of the excitation magnitude on the PC_{br} was significant (p<0.05; Table 3.4).

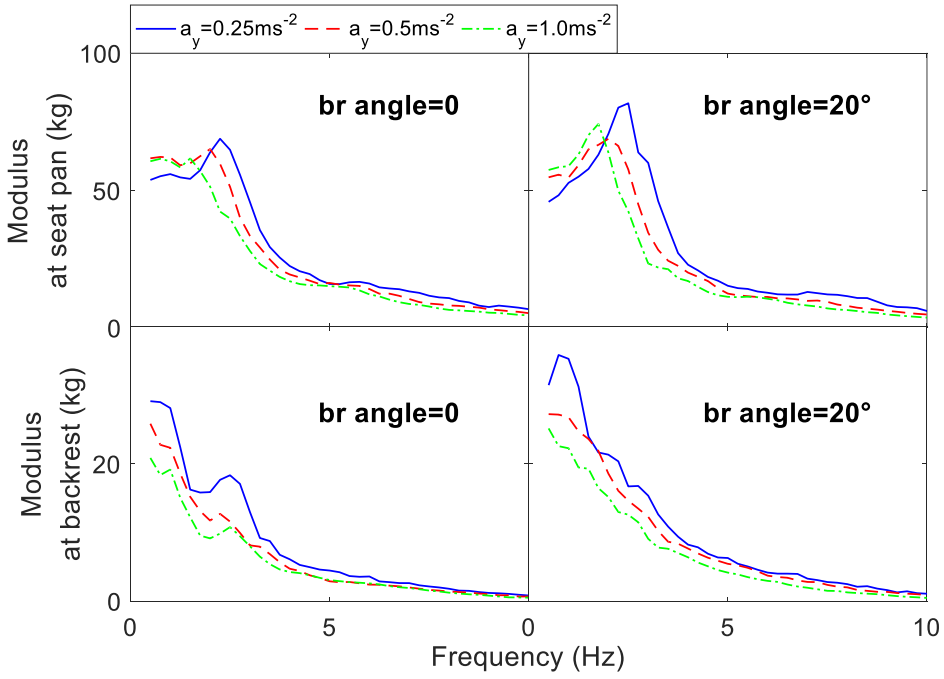

Figure 3.8 Median in-line lateral apparent mass at the seat pan and backrest: the effect of the magnitude of lateral excitation

Table 3.4 The median values of the R_{nl_br} and PC_{br} of the lateral apparent masses of 12 subjects under single-axial lateral vibration, and statistical significance (p-value, Friedman) of the effect of lateral excitation magnitude on them

Quantities indicating the degree of the nonlinearity	Median value of the quantities at different lateral excitation magnitudes (r.m.s.)			p-value
	0.25 ms^{-2}	0.5 ms^{-2}	1.0 ms^{-2}	
R_{nl_br} of in-line lateral apparent mass at seat pan	*1.00*	*0.94*	*0.92*	ns
PC_{br} of in-line lateral apparent mass at seat pan	*-24.11%*	*-15.30%*	*-8.49%*	*

3.3.3 In-line vertical apparent masses under single-axial vertical excitation

The in-line vertical apparent mass at the seat pan exhibited a distinctive principal resonance between 4.5 and 7.5 Hz. The in-line vertical apparent mass at the backrest generally had one principal resonance in the frequency range between 4 and 8 Hz (Figure 3.9).

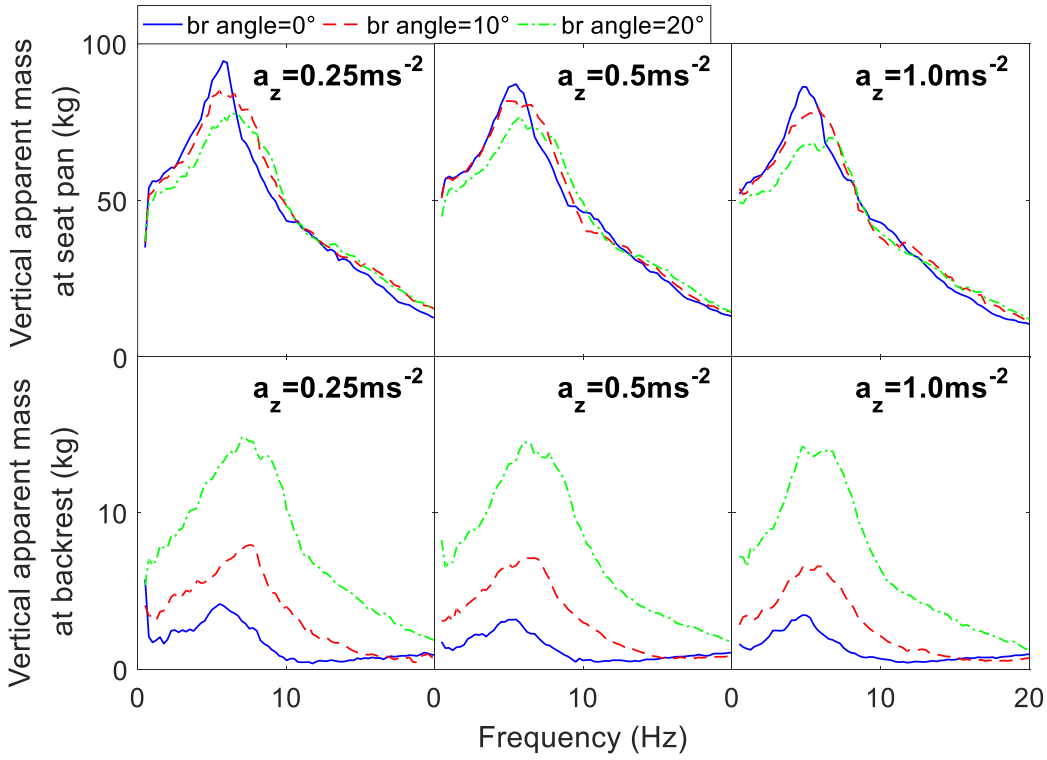

Figure 3.9 Median in-line vertical apparent mass at the seat pan and backrest: the effect of backrest inclination angle

3.3.3.1 The effect of the inclination angle of the backrest

The fundamental resonance frequencies of the apparent masses at both the seat pan (p>0.05) and backrest (p<0.05) increased when the inclination angle increased (Figure 3.9). With the increase of

the backrest inclination angle, the modulus associated with the resonance frequency of the vertical apparent mass at the seat pan decreased (p<0.01), while that at the backrest increased (p<0.01). Such an effect of the backrest inclination angle was observed under all excitation magnitudes.

The R_{nl_ilm} and PC_{ilm} of the vertical apparent mass at the seat pan increased with the increase of backrest inclination angle, yet the effects of backrest inclination on the quantities of the nonlinearity at both the seat pan and backrest were insignificant (p>0.05; Table 3.5).

Table 3.5 The median values of the R_{nl_ilm} and PC_{ilm} of the vertical apparent masses of 12 subjects under single-axial vertical vibration, and statistical significance (p-value, Friedman) of the effect of backrest inclination angles on them

Quantities indicating the degree of the nonlinearity	**Median value of the quantities at different backrest inclination angles**			***p*-value**
	0°	**10°**	**20°**	
R_{nl_ilm} of in-line vertical apparent mass at seat pan	*1.14*	*1.16*	*1.19*	ns
R_{nl_ilm} of in-line vertical apparent mass at backrest	*1.21*	*1.18*	*1.19*	ns
PC_{ilm} of in-line vertical apparent mass at seat pan	*-1.76%*	*3.62%*	*6.27%*	ns
PC_{ilm} of in-line vertical apparent mass at backrest	*15.45%*	*13.47%*	*4.79%*	ns

3.3.3.2 The effect of the excitation magnitude

The increase of vertical excitation magnitude led to a decrease of the fundamental resonance frequency of the vertical apparent masses at the seat pan and backrest (Figure 3.10). Such an effect on the apparent mass at the seat pan was significant (p<0.05) when the backrest was upright or inclined by 10° but was insignificant (p>0.05) when the backrest inclination angle was 20°. For the resonance frequency of the apparent mass at the backrest, the effect of the excitation magnitude was significant (p<0.05) with all backrest inclination angles. The moduli associated with the resonance frequency of the apparent mass, both at the seat pan and backrest, tended to decrease when the magnitude of excitation increased (Figure 3.10). Such an effect was significant (p<0.05) when the angle of backrest inclination was 0 or 20°. Furthermore, the increase of the vertical excitation magnitude affected the PC_{br} significantly (p<0.05; Table 3.6).

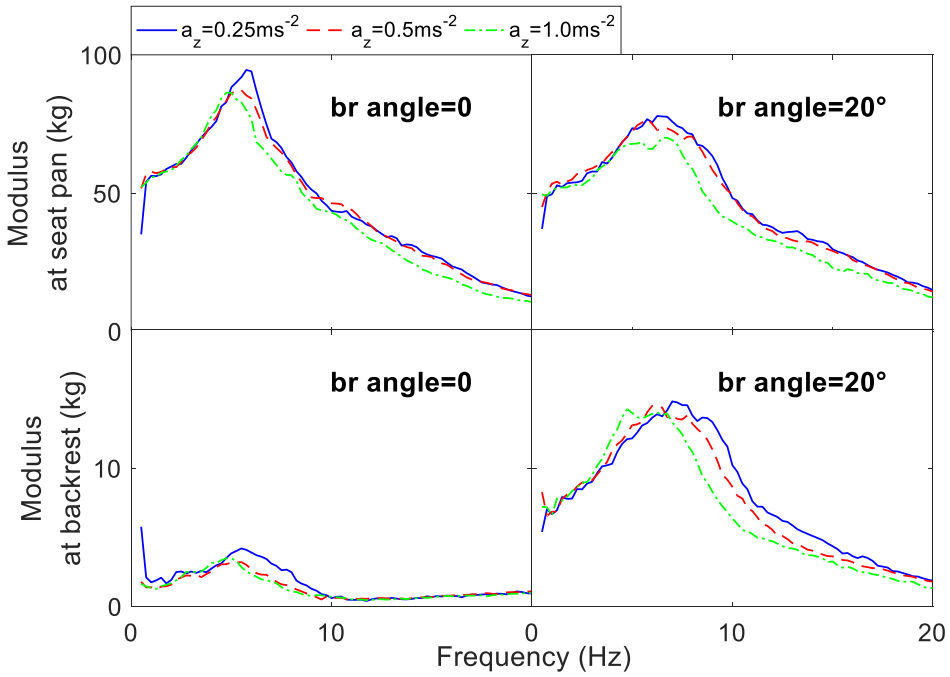

Figure 3.10 Median in-line vertical apparent mass at the seat pan and backrest: the effect of the magnitude of vertical excitation

Table 3.6 The median values of the R_{nl_br} and PC_{br} of the fore-aft apparent masses of 12 subjects under single-axial vertical vibration, and statistical significance (*p*-value, Friedman) of the effect of fore-aft excitation magnitude on them

Quantities indicating the degree of the nonlinearity	**Median value of the quantities at different vertical excitation magnitudes (r.m.s.)**			***p*-value**
	0.25 ms^{-2}	**0.5 ms^{-2}**	**1.0 ms^{-2}**	
R_{nl_br} of in-line vertical apparent mass at seat pan	*0.75*	*0.75*	*0.82*	ns
R_{nl_br} of in-line vertical apparent mass at backrest	*0.89*	*0.92*	*0.94*	ns
PC_{br} of in-line vertical apparent mass at seat pan	*-213.89%*	*-327.41%*	*-276.09%*	ns
PC_{br} of in-line vertical apparent mass at backrest	*14.12%*	*12.96%*	*16.69%*	*

3.4 Discussion

3.4.1 The effect of the backrest inclination angle

In the lateral and vertical direction, the change of the apparent masses generally followed the similar trend when the backrest inclination angle increased from 0° to 20°. However, the changes

of the fore-aft apparent masses were found to be inconsistent when the inclination angle increased from 0° to 10° and then to 20°.

3.4.1.1 The effect of the backrest inclination angle on the in-line fore-aft apparent masses: an increase from 0° to 10° vs an increase from 10° to 20°

The modulus of the in-line fore-aft apparent mass at the seat pan associated with the resonance frequency decreased, and the modulus associated with the resonance frequency around 6 Hz of the in-line fore-aft apparent mass at the backrest increased, when the backrest inclination angle increased from 0° to 10°. These phenomena are similar to those reported by Mandapuram et al. (2005) when the backrest angle increased from 0° to 12.5°. These results were possibly due to the increase of the body mass supported by the backrest and the decrease of that at the seat pan. The change of the resonance frequency of the in-line fore-aft apparent mass at the seat pan was less obvious in the current study compared to that reported by Mandapuram et al. (2005). Such a difference may be explained by the fact that in the study by Mandapuram et al. (2005) the participants adopted an erect posture with the support of an upright backrest but then sat with relaxed posture when the backrest was inclined by 12.5°. The stiffness of the human body would be greater with the erect posture than with the relaxed posture, which led to a more obvious decrease of the resonance frequency when the posture was changed from erect to relaxed.

The phase of the in-line fore-aft apparent mass at the seat pan in the current study is shown in Figure 3.11, to better show the change of the biodynamic response in the vicinity of the resonance frequency in addition to the modulus (Figure 3.5). The slope of the phase curve decreased marginally when the backrest inclination angle increased from 0° (—) to 10° (– –), which indicates that in the current study, the damping ratio of the human body and the seat system slightly increased.

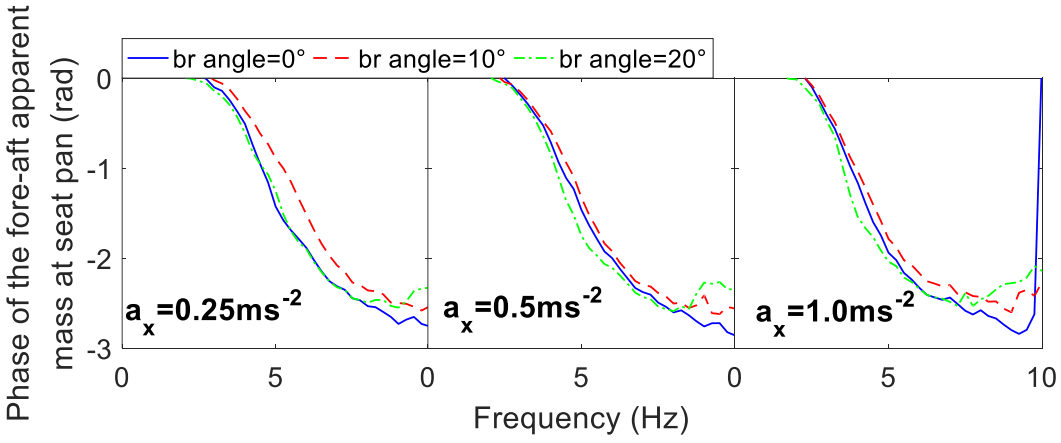

Figure 3.11 Median phase of the in-line fore-aft apparent mass at the seat pan under single-axial fore-aft vibration: the effect of backrest inclination angle

On the other hand, when the backrest inclination angle further increased from 10° ( ) to 20° ( ), the slope of the phase of the apparent mass at the seat pan increased marginally (Figure 3.11), indicating that the damping ratio of the human body and the seat pan system decreased.

For the apparent mass at the backrest, Figure 3.5 shows that the modulus associated with the resonance frequency decreased with the increased inclination angle from 10° to 20°, despite more body mass supported by the backrest, which may suggest an increase of the damping ratio of the upper body and backrest system. Similar changes were found under all excitation magnitudes, which were in contrast with those when the backrest inclination angle increased from 0° to 10°. Considering the tendency of the sliding of the upper body against the backrest under fore-aft excitation when the backrest was inclined by an angle of as large as 20°, such a phenomenon may indicate that the effective damping of the upper body and backrest system would increase to maintain the posture and the contact with the backrest.

In general, the changes of the fore-aft apparent masses at the backrest and seat pan show that the increase of the backrest inclination angle not only affected the apparent mass by means of altering the distribution of the body mass but also by affecting the damping of the human body and seat system.

3.4.1.2 The effect of the backrest inclination angle on the in-line lateral apparent masses

When the backrest inclination angle was 20°, the resonance of the in-line lateral apparent mass at the backrest near 2.5 Hz was less evident than that when the backrest was the upright or inclined by 10° under all excitation magnitudes, which may indicate a changed effective damping of the upper body and seat system.

When the backrest inclination angle changed from 0° to 10°, the modulus of the in-line lateral apparent mass at the backrest between 1 and 10 Hz increased, which is similar to the observation reported by Mandapuram et al. (2012). In the current study, it further increased when the inclination angle of the backrest increased from 10° to 20°. The result indicated that with a series of increase of the backrest inclination angle, the interaction between the human body and the backrest increased, and since the backrest served as a source of excitation, the modulus of the in-line lateral apparent mass of the human body tended to increase.

3.4.1.3 The effect of the backrest inclination angle on the in-line vertical apparent masses

Under the single-axial vertical vibration, the modulus associated with the resonance frequency of the vertical apparent mass at the backrest significantly increased while that at the seat pan

decreased when the backrest inclination angle increased, as a result of increased mass supported by the backrest. It was also found that the resonance frequencies of the in-line vertical apparent mass at both the seat pan and backrest tended to increase with the increase of the angle of the backrest inclination. These results are consistent with the results of previous studies (Toward and Griffin, 2009; Yang and Qiu, 2015; Liu and Qiu, 2021; Zhang et al., 2021) with one fixed excitation magnitude. In the current study, the effect of the backrest inclination angle on the in-line vertical apparent mass was also found under all three excitation magnitudes.

3.4.2 The effect of the excitation magnitude

Under single-axial fore-aft or lateral vibration, with the increase of the excitation magnitude, the fundamental resonance frequencies and the associated moduli of the in-line apparent masses at the seat pan and backrest in the same axis decreased when the backrest was upright. It is in agreement with previous studies (Mandapuram et al., 2005; Nawayseh and Griffin, 2005; Jalil and Griffin, 2008; Qiu and Griffin, 2012). In the current study, when the backrest was inclined by 10° (which is comparable with that reported by Mandapuram et al. (2005) with an inclination of 12.5°) and 20°, they also tended to decrease with the increased excitation magnitude.

Similarly, the resonance frequencies of the in-line vertical apparent mass measured at the seat pan tended to decrease significantly with the increase of the vertical excitation magnitude when the backrest was upright. This is consistent with the results reported by Qiu and Griffin (2012), which was also observed when the backrest was inclined by 10° and 20° in the current study.

In general, the nonlinearity of the biodynamic response due to the increase of the excitation magnitude in three translational axes should be considered both when the backrest was upright and when it was inclined by different angles.

3.4.3 Interactive effect between the excitation magnitude and the backrest inclination angle

3.4.3.1 The effect of backrest inclination angle on the degree of nonlinearity due to the change of the excitation magnitude

It was found in the current study that with the increase of the backrest inclination angle, the PC_{ilm} of the modulus of the in-line fore-aft apparent mass at the backrest associated with the resonance frequency tended to increase (p<0.05, Table 3.1), i.e., the extent of the effect of the fore-aft excitation magnitude could be further affected by the backrest inclination angle. This may be attributed to the increased interaction between the human body and the backrest when the

backrest was inclined compared to that when the backrest was upright. With such an increased interaction, the excitation magnitude could better act on the apparent mass of the upper body, as the upper body was exposed to the vibration transmitted from the backrest.

The change of the other indicators that represent the degree of the nonlinearity subject to the increased excitation magnitude (PC_{ilm} and R_{nl_ilm}) in the horizontal directions did not follow the same trend when the backrest inclination angle increased from 0° to 10° and then to 20°. This may be related to the fact that the change of the fore-aft apparent mass when the backrest inclination angle changed from 0° to 10° was quite different from that when the backrest inclination angle changed from 10° to 20° (Section 3.4.1.1). For the horizontal biodynamic response, the mechanism leading to the different biodynamic response (such as muscle activities) between different inclination angles may need to be investigated in the future.

For the in-line vertical apparent mass, when the inclination angle of the backrest increased, the median values of PC_{ilm} and R_{nl_ilm} of that at the seat pan increased, and the PC_{ilm} of that at the backrest decreased. However, the effect of backrest inclination on neither of them was significant. Nevertheless, the PC_{ilm} and R_{nl_ilm} of each individual subject indeed varied with increased backrest inclination angles despite showing no general trend. This may suggest that other factors, such as the inter-subject variabilities, affect the interaction between the backrest inclination angle and the excitation magnitude.

3.4.3.2 The effect of excitation magnitude on the change of the apparent mass due to the change of the backrest inclination angle

The value of the PC_{br} of the fore-aft apparent mass at the backrest increased significantly with the increase of fore-aft excitation magnitude (Table 3.2). This could be explained that due to the increased effect of the excitation magnitude when the backrest was inclined (Section 3.4.3.1), the modulus associated with the resonance frequency measured under 1.0 ms^{-2} r.m.s. excitation with a backrest inclination angle of 20° was much smaller than that measured under 0.25 ms^{-2} r.m.s. excitation with the same backrest inclination angle; while with an upright backrest, the difference between the modulus measured with different excitation magnitudes was smaller. Because of this, the modulus associated with the resonance frequency measured under 1.0 ms^{-2} r.m.s. excitation with the backrest inclined by 20° was also much smaller than that measured under 1.0 ms^{-2} r.m.s. excitation with an upright backrest, so the PC_{br} at an excitation of 1.0 ms^{-2} r.m.s. was higher.

Figure 3.12 further explains such a phenomenon more intuitively with the normalised moduli associated with the fundamental resonance frequency of the fore-aft apparent mass at the backrest under 0.25 and 1.0 ms^{-2} r.m.s. excitations and backrest inclination angles of 0° and 20°. The

normalisation was carried out by dividing each modulus with the modulus measured under 0.25 ms^{-2} fore-aft and with the support of upright backrest. From Figure 3.12, the increase of PC_{br} when the excitation magnitude increased from 0.25 to 1.0 ms^{-2} r.m.s. excitation can be found.

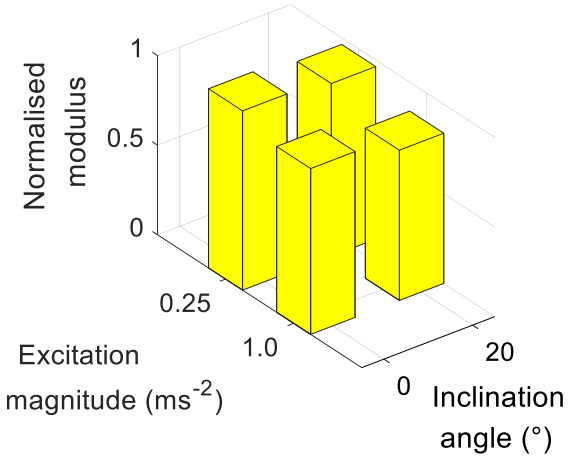

Figure 3.12 Bar chart of the normalised modulus of the fore-aft apparent mass at the backrest associated with the resonance frequency under different conditions

On the other hand, the value of the PC_{br} of the lateral apparent mass at the seat pan decreased significantly with the increase of lateral excitation magnitude (Table 3.4), which may be explained from a reversed perspective: due to the increased body mass supported by the backrest and the increased interaction with the backrest, the effect of excitation magnitude on the apparent mass at the backrest increased, while that on the change of apparent mass at the seat pan became smaller.

The PC_{br} of the vertical apparent mass at the backrest was significantly affected by the vertical excitation magnitude, while the effect of that on the PC_{br} and R_{nl_br} of the vertical apparent masses at the seat pan were insignificant (Table 3.6). This can be explained that with the increased backrest inclination angle, the modulus of vertical apparent mass at the backrest dramatically increased compared to that at the seat pan as a result of the increased body mass supported by the backrest (Figure 3.9), so the effect of the excitation magnitude on the PC_{br} at the backrest was more significant than that at the seat pan.

3.5 Conclusions

In the current study, the apparent masses at the seat pan and backrest were measured under single-axial fore-aft, lateral and vertical excitation with various magnitudes and backrest inclination angles. The results showed that the nonlinearity of the human body due to the increase of the excitation magnitude, revealed by the decrease of the resonance frequencies of the in-line apparent masses

in all the three translational directions, existed not only when the backrest was upright but also when it was inclined by 10° or 20°.

The angle of backrest inclination also affected the apparent mass measured at the seat pan and backrest in the three translational directions, which could be observed under various excitation magnitudes. With the increased backrest inclination angle, the human-body-and-backrest interaction increased. This led to the increase of the moduli associated with the resonance frequencies of the in-line lateral apparent masses at the seat pan and backrest, and the modulus associated with the resonance frequency of the in-line vertical apparent masses at the backrest. Meanwhile, the modulus associated with the resonance frequency of the in-line vertical apparent masses at the seat pan tended to decrease. The change of the fore-aft apparent masses did follow the same trend with a series of changes of the backrest inclination angle, and clear changes of the moduli took place when the backrest was inclined by 20° compared to that by 10°. This reveals the effect of the backrest inclination angle on the effective damping of the seat and human body system.

The results of the current experimental study also show that interaction existed between the excitation magnitude and the backrest inclination angle. The degree of nonlinearity at the backrest due to the increased fore-aft and lateral excitation magnitude was significantly affected by the backrest inclination. Hence, when the dynamic performance of a vehicle seat is to be optimized for promoting the ride comfort, the effects of both the excitation magnitude and the inclination of backrest on the nonlinear response of the human body need to be taken into consideration.

Chapter 4 THE APPARENT MASS OF THE SEATED HUMAN BODY EXPOSED TO TRI-AXIAL TRANSLATIONAL VIBRATION: THE EFFECT OF THE EXCITATION MAGNITUDE AND THE BACKREST INCLINATION ANGLES

4.1 Introduction

In real life, an occupant seated in the vehicles is exposed to the Whole-Body Vibration (WBV) arising in multiple directions simultaneously, causing ride discomfort. Under dual-axial vibration, it has been found that the resonance frequency of the apparent mass in either vertical or fore-aft direction is affected by the excitation magnitude in the both x and z-axis (Qiu and Griffin, 2010; Qiu and Griffin, 2012; Zheng et al., 2012; Zheng et al., 2019). The apparent mass of the human body under tri-axial vibration has also been found to be different from that under single-axial vibration (Mansfield and Maeda, 2007; Mandapuram et al., 2012) by introducing additional excitation in the other two directions with a limited number of magnitudes. However, under tri-axial translational vibration, how the apparent mass of the seated human body in a certain direction is affected by a series of changes of the in-line and cross-axis excitation magnitude, and whether interactive effect exists between the excitation magnitudes in different directions, have rarely been reported.

The occupant seated in the vehicle seat is often supported by an inclined backrest in real life. The backrest inclination has been found to affect the apparent masses under single-axial vibration, as discussed in Chapter 3. Nevertheless, how does the backrest inclination affect the apparent mass of the seated human body under tri-axial translational vibration, especially combined with a series of changes of the excitation magnitude in different axes, has not been reported.

In this chapter, an experimental study was conducted by measuring the apparent masses in the x, y and z-axis at the seat pan and backrest under tri-axial excitation to investigate how would they be affected by the excitation magnitudes in the same direction and in the other two axes, as well as the backrest inclination angle. It was hypothesised that the resonance frequency of the apparent mass in each one of the axes would decrease with both the increased excitation magnitude in the same axis and that in the other two axes. It was also hypothesised that the change of the apparent mass due to the increase of excitation magnitude in the same axis would become smaller when the excitation magnitude in the other two directions increased, and vice versa. Additionally, it was

hypothesised that the effect of the backrest inclination angle on the apparent mass under tri-axial translational vibration would be similar to that under single-axial vibration, and it would interact with the effect of the mangitudes of the tri-axial excitation.

4.2 Experimental method

The assumptions for the experimental study introduced in this chapter are the same as those mentioned in Chapter 3.

4.2.1 Apparatus and subjects

The experimental set up and the subjects participating in this study were the same as those of the study presented in Chapter 3.

4.2.2 Stimuli and backrest inclination

In this experiment, 14 tri-axial random excitations were used. The magnitudes of the tri-axial excitations are shown in Table 4.1 together with the 9 single-axial excitations used in Chapter 3.

Table 4.1 The matrices of the single- and tri-axial excitations

Study on the in-line fore-aft apparent mass		**The excitation magnitude in x-axis (ms^{-2} r.m.s.)**		
		0.25	**0.50**	**1.00**
The excitation magnitude in y and z-axis (ms^{-2} r.m.s.)	**0.00**	a_x	a_x	a_x
	0.50	$a_x+a_y+a_z$	$a_x+a_y+a_z$	$a_x+a_y+a_z$
	1.00	$a_x+a_y+a_z$	$a_x+a_y+a_z$	$a_x+a_y+a_z$
Study on the in-line lateral apparent mass		**The excitation magnitude in y-axis (ms^{-2} r.m.s.)**		
		0.25	**0.50**	**1.00**
The excitation magnitude in x and z-axis (ms^{-2} r.m.s.)	**0.00**	a_y	a_y	a_y
	0.50	$a_x+a_y+a_{z\,z}$	-	$a_x+a_y+a_z$
	1.00	$a_x+a_y+a_z$	$a_x+a_y+a_z$	-
Study on the in-line vertical apparent mass		**The excitation magnitude in z-axis (ms^{-2} r.m.s.)**		
		0.25	**0.50**	**1.00**
The excitation magnitude in x and y-axis (ms^{-2} r.m.s.)	**0.00**	a_z	a_z	a_z
	0.50	$a_x+a_y+a_z$	-	$a_x+a_y+a_z$
	1.00	$a_x+a_y+a_z$	$a_x+a_y+a_z$	-

In Table 4.1, the symbol "a" stands for the input acceleration, and the subscripts x, y and z represent the direction of the acceleration. The contents "a_x", "a_y" and "a_z" represent the single-axial fore-

aft, lateral and vertical excitations that was used in the experiment in Chapter 3 respectively, while "a_x+a_y+a_z" denotes a tri-axial excitation. The dashes ("-") indicate the tri-axial excitations with identical magnitude in all three axes (0.5 or 1.0 ms^{-2}), and these excitations were not repeated.

The 14 tri-axial excitations were sorted in three groups. In each group, the in-line apparent mass in one of the three translational directions (x, y, or z-axis) was studied, and the excitation in the same axis was referred to as the excitation in the "primary-axis", while the excitations in the other two axes were called the excitation in the "secondary-axes". For the apparent mass in each direction, the excitation magnitude in the "primary-axis" varied between 0.25, 0.5 and 1.0 ms^{-2} r.m.s. To study the effect of the excitation magnitude in the "secondary-axes", the apparent masses measured with single-axial excitations in Chapter 3 were also used to compare with the results measured with tri-axial excitations in this chapter, as shown in Table 4.1. Then the magnitudes of the excitation in the two "secondary-axes" were fixed at an identical level of either 0 (which means a single-axial excitation), 0.5 or 1.0 ms^{-2} r.m.s. For example, to study the effects of the excitation magnitude in the "primary-axis" and the "secondary-axes" on the in-line fore-aft apparent mass, the excitation magnitude in the x-axis ("primary-axis") varied between 0.25, 0.5 and 1.0 ms^{-2} r.m.s., while the magnitudes of excitation in the y and z-axis ("secondary-axes") were both at 0, 0.5 or 1.0 ms^{-2} r.m.s.

Each of the excitations lasted 60s over a frequency range between 0.5 and 40 Hz. For the 14 tri-axial excitations, the inputs in different axes were generated independently and they were mutually uncorrelated.

During the experiment, the subjects sat on the rigid seat with the support of the rigid backrest with three different inclination angles 0°, 10° and 20° backwards. Each subject was exposed to the 14 tri-axial stimuli three times, each time under the support of the backrest with one of the three inclination angles, making the total number of the combinations of the test conditions to be 42. The order of the test conditions for each subject was randomized.

4.2.3 Data analysis

The forces and accelerations measured by the force-transducers and accelerometers at the backrest in the fore-aft and vertical directions were transformed using Eqs. (3.1) to (3.4) when the backrest was inclined, so that the directions of the forces and accelerations after the transformation were consistent with those in the coordinate system of the floor.

The degree of the nonlinearity of the biodynamic response due to the increase of excitation magnitude in the "primary-axis" was quantified using R_{nl_ilm} and PC_{ilm}, which were defined in Eqs. (3.9) and (3.10). The degree of the nonlinearity of the biodynamic response due to the increase

of excitation magnitude in the "secondary-axes" was quantified using the indices R_{nl_sec} and PC_{sec} respectively, which were defined as follows, where the abbreviation "*sec*" in the subscripts represents the "**sec**ondary-axes":

$$R_{nl\_sec} = \frac{f_{\text{sec\_0}}}{f_{\text{sec\_1}}} \tag{4.1}$$

$$PC_{sec} = \frac{(AM_{\text{sec\_0}} - AM_{\text{sec\_1}})}{AM_{\text{sec\_0}}} \times 100\% \tag{4.2}$$

Where $f_{\text{sec\_0}}$ and $f_{\text{sec\_1}}$ are the fundamental resonance frequency of the apparent mass measured under excitation magnitude of 0 in the "secondary-axes" (i.e., under single-axial vibration) and under excitation magnitude of 1.0 ms^{-2} r.m.s. in the "secondary-axes", respectively; $AM_{\text{sec\_0}}$ and $AM_{\text{sec\_1}}$ are the modulus associated with the fundamental resonance frequency of the apparent mass measured when the excitation magnitude in the "secondary-axes" were 0 and 1.0 ms^{-2} r.m.s., respectively.

Friedman two-way analysis of variance was adopted to study among the 12 subjects the significance of the effects of the excitation magnitude in the "primary-axis", in the "secondary-axes", and the backrest inclination angle on the resonance frequency and the associated modulus of the tri-axial apparent mass. The effect of excitation magnitude in the "secondary-axes" and backrest inclination on the R_{nl_ilm} and PC_{ilm}, and the effect of excitation magnitude in the "primary-axis" on the R_{nl_sec} and PC_{sec} were also tested by Friedman two-way analysis of variance. The definition of the null hypothesis and *p*-value are the same as those in Chapter 3.

Under tri-axial excitation, if the acceleration measured at the seat pan and backrest in the three axes were mutually uncorrelated, then the apparent masses could be calculated using SISO method using Eq. (3.5). However, due to unavoidable crosstalk between the imposed motion produced by the vibrator, and the fact that the rigid seat was not ideally rigid in the reality, the excitations in the x, y and z-axis that were transmitted to the seated human body were not completely mutually uncorrelated. To estimate the apparent mass in either one of the three directions under tri-axial excitation more precisely, the components of an excitation correlated with the others should be eliminated. In this chapter, the seated human body was considered as a Multi-Input-Single-Output (MISO) system, and the apparent masses were calculated using a signal processing method based on the MISO system proposed by Bendat and Piersol (2011). The general principle of that method is to convert the original input and output system with partly correlated inputs into a new system with "conditioned" inputs that are uncorrelated with each other.

Assuming that q inputs in the order a_1, …, a_q (with their corresponding Fourier transforms $A_1(f)$…, $A_q(f)$) contribute to the output b in the original MISO system, see Figure 4.1:

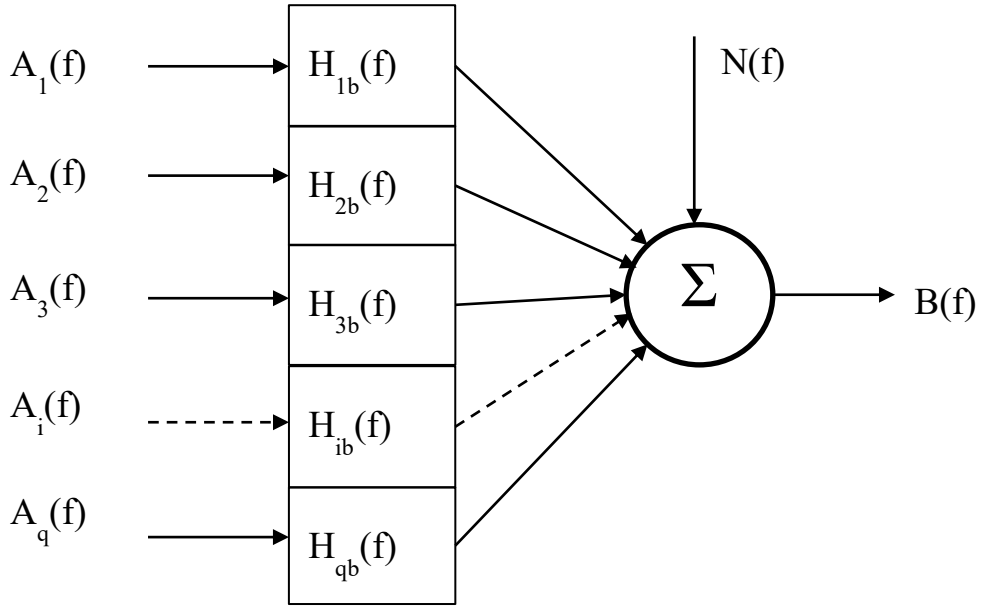

Figure 4.1 Multiple-Input system for original inputs (Bendat and Piersol, 2011)

In case these inputs are not mutually uncorrelated, the transfer functions between original inputs and the output H_{ib} (*i*=1, …, q) require converted calculation method by adjusting the original inputs. The converted MISO system is show in Figure 4.2:

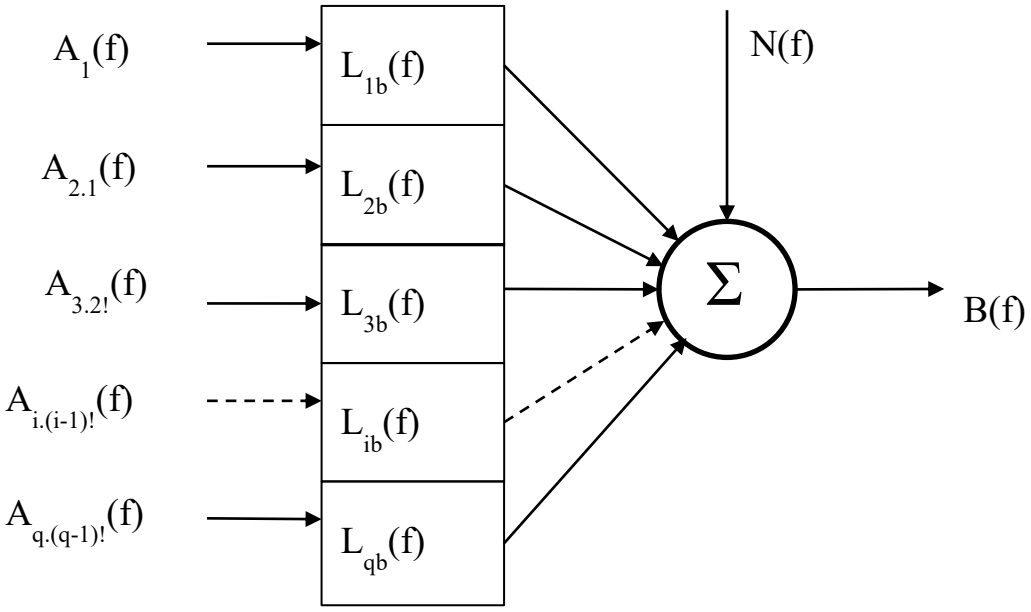

Figure 4.2 Multiple-Input system for conditioned inputs (Bendat and Piersol, 2011)

Where the terms $A_1(f)$, $A_{2.1}(f)$… $A_{i.(i-1)!}(f)$,… $A_{q.(q-1)!}(f)$ are the Fourier transforms of the conditioned inputs of the converted system., and for *i*=1, …,q, the subscript *i.(i-1)!* stands for the *i*th "conditioned" input, indicating that the linear effects of the inputs (a_1, a_2, …a_{i-1}) with higher orders have been eliminated from the input a_i, so that all the conditioned inputs are mutually uncorrelated. Then the transfer functions between conditioned inputs L_{rj}, the transfer functions between the conditioned

inputs and the output L_{ib} and the conditioned auto and cross spectral density function can be calculated as follows:

$$L_{rj} = G_{rj.(r-1)!}/G_{rr.(r-1)!} \qquad r = 1, \dots, j-1; j = 1, \dots, q \tag{4.3}$$

$$G_{ij.r!} = G_{ij.(r-1)!} - L_{rj}G_{ir.(r-1)!} \qquad i > r, j > r, i \neq j \tag{4.4}$$

$$G_{jj.r!} = G_{jj.(r-1)!} - \left|L_{rj}\right|^2 G_{rr.(r-1)!} \qquad j > r \tag{4.5}$$

$$G_{ib.r!} = G_{ib.(r-1)!} - L_{rb}G_{ir.(r-1)!} \qquad i > r \tag{4.6}$$

$$L_{ib} = G_{ib.(i-1)!}/G_{ii.(i-1)!} \qquad i = 1, \dots, q \tag{4.7}$$

Finally, the transfer functions between original inputs and the output H_{iy} can be obtained as:

$$H_{qb} = L_{qb} \tag{4.8}$$

$$H_{ib} = L_{ib} - \sum_{j=i+1}^{q} L_{ij}H_{jb} \qquad i = (q-1), \dots, 1 \tag{4.9}$$

Additionally, the partial coherence between each conditioned input and the output $\gamma^2_{ib.(i-1)!}$, and the multiple coherence function between all the conditioned inputs and the output $\gamma^2_{b:q!}$ can be derived as follows:

$$\gamma^2_{ib.(i-1)!} = \left|G_{ib.(i-1)!}\right|^2/(G_{ii.(i-1)!}G_{bb.(i-1)!}) \quad i = 1, \dots, q \tag{4.10}$$

$$\gamma^2_{b:q!} = \sum_{i=1}^{k} \gamma^2_{iy.(i-1)!} \qquad i = 1, \dots, q \tag{4.11}$$

The partial and multiple coherence functions can provide information on the relative contribution of the different inputs to the output.

4.3 Results

4.3.1 In-line fore-aft apparent masses under tri-axial vibration

4.3.1.1 The effect of the excitation magnitude in the "primary-axis" (x-axis)

Figure 4.3 shows the effect of the magnitude of fore-aft excitation on the in-line fore-aft apparent masses at the seat pan and backrest. Under tri-axial vibration, the increase of the excitation magnitude in the x-axis led to a decrease of the fundamental resonance frequency of the in-line fore-aft apparent mass at the backrest (p<0.05 for 4 out of 6 tri-axial excitation conditions), similar to that under the single-axial vibration. The change in the modulus associated with the resonance

of the apparent mass at the backrest was not significant under most of the conditions (p>0.05 for 5 out of 6 conditions). For the fore-aft apparent mass at the seat pan, the fundamental resonance frequency (p<0.05 for 4 out of 6 conditions) and the associated modulus (p<0.05 for all 6 conditions) tended to decrease with the increase of the fore-aft excitation magnitude under tri-axial excitation (Figure 4.3).

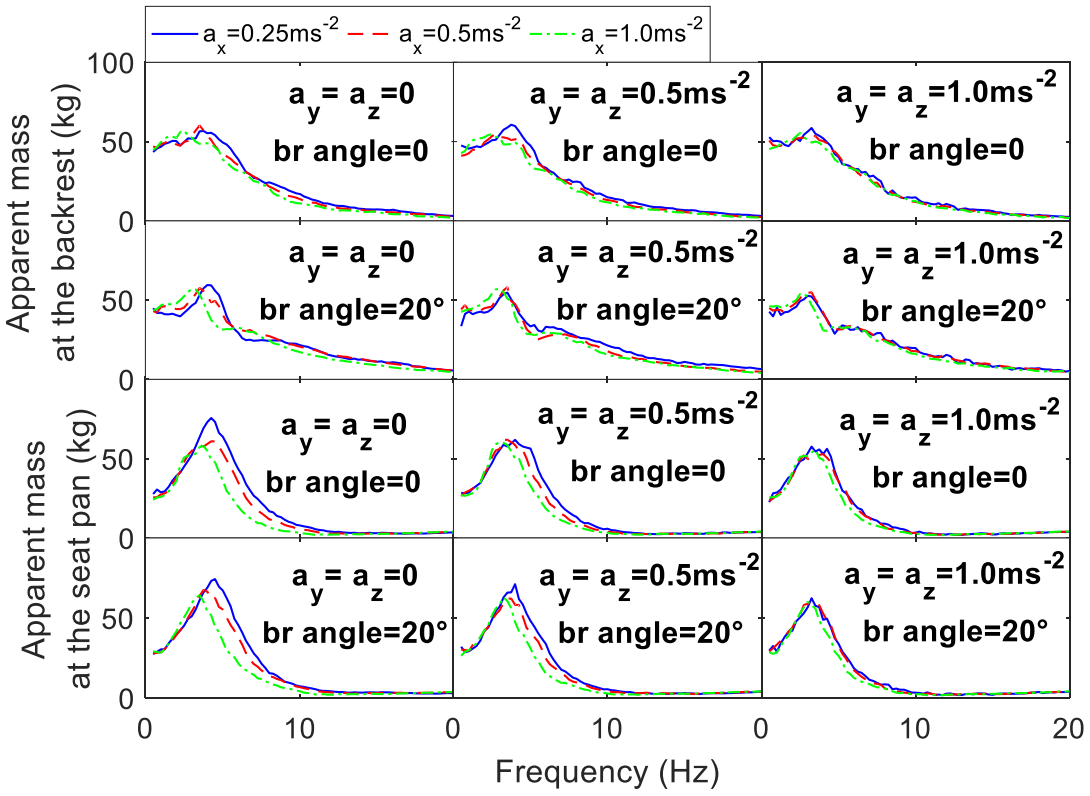

Figure 4.3 Median in-line fore-aft apparent mass at the seat pan and backrest under different excitation magnitudes in y and z-axis (0, 0.5 or 1.0 ms^{-2} r.m.s.) and different backrest inclination angles (0 or 20°): the effect of the fore-aft excitation magnitude

4.3.1.2 The effect of the excitation magnitude in "secondary-axes" (y and z-axis)

The increased excitation magnitude in the "secondary-axes" (y and z-axis) led to a decrease of the resonance frequency of the in-line fore-aft apparent mass at the backrest (p<0.05 for 8 out of 9 single and tri-axial excitation conditions), which is more noticeable when the backrest was inclined than when it was upright (Figure 4.4), especially when the fore-aft excitation magnitude was 0.25 ms^{-2} r.m.s. Similarly, the resonance frequency of the in-line fore-aft apparent mass at the seat pan tended to decrease with the increased excitation magnitude in the "secondary-axes" (p<0.05 for 8 out of 9 conditions).

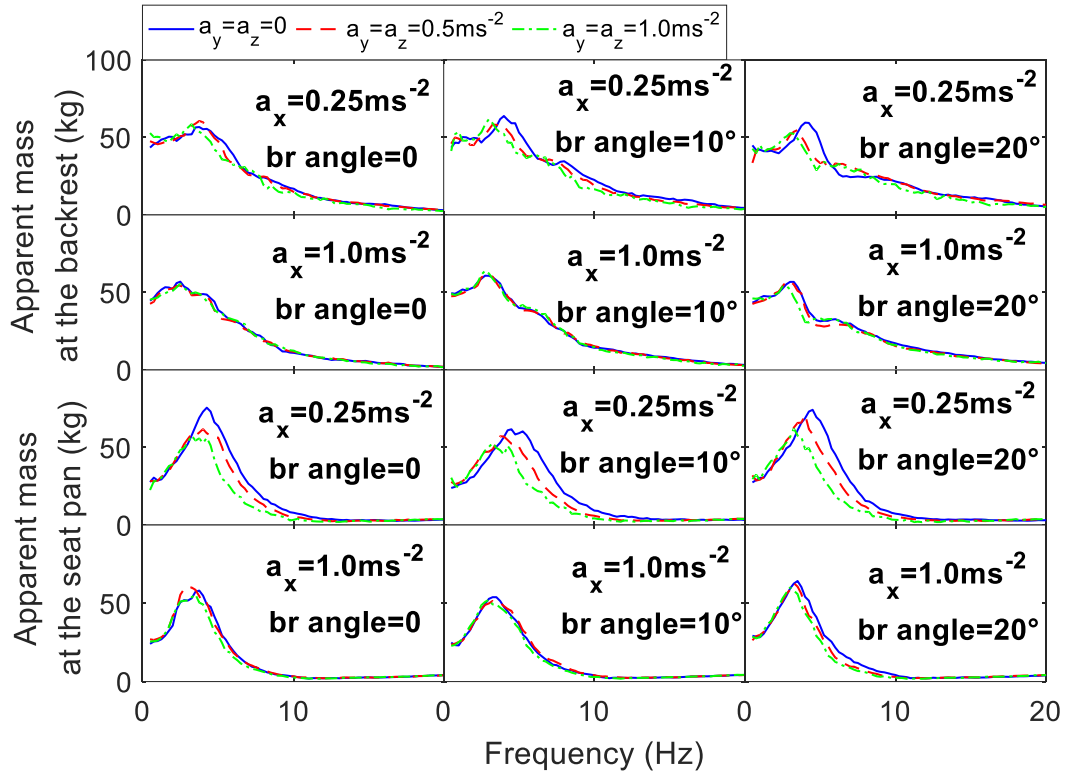

Figure 4.4 Median in-line fore-aft apparent mass at the seat pan backrest under different x-axis excitations (0.25 and 1.0 ms^{-2} r.m.s.) and different backrest inclination angles (0, 10° or 20°): the effect of the excitation magnitude in y and z-axis

4.3.1.3 The effect of the inclination of backrest and interactive effects among the factors

The effect of the backrest inclination angle on the in-line fore-aft apparent mass at the seat pan and backrest under tri-axial vibration was similar to that under single-axial fore-aft excitation.

Interaction was found between the excitation magnitudes in the "primary-axis" and "secondary-axes", which are shown in Table 4.2 and Table 4.3. The values of R_{nl_ilm} of the fore-aft apparent mass at the seat pan (p<0.05 under all 3 backrest conditions) and backrest (p<0.05 when the backrest was upright and inclined by 10°) decreased with the increased excitation magnitude in the "secondary-axes". On the other hand, the R_{nl_sec} of the fore-aft apparent mass at the seat pan (p<0.05 when the backrest was inclined by 10°and 20°) and backrest (p<0.05 under all 3 backrest conditions) decreased with the increase of excitation magnitude in the "primary-axis".

Table 4.2 *p*-values of the effect of excitation magnitude in the "secondary-axes" on the indicators of the nonlinearity in the fore-aft direction due to the excitation magnitude in the "primary-axis"

Degree of the nonlinearity due to the excitation magnitude in the "primary-axis"	**Backrest inclination angle**		
	0°	**10°**	**20°**
R_{nl_ilm} of in-line fore-aft apparent mass at the seat pan	**	*	**
R_{nl_ilm} of in-line fore-aft apparent mass at the backrest	*	*	ns
PC_{ilm} of in-line fore-aft apparent mass at the seat pan	*	**	ns
PC_{ilm} of in-line fore-aft apparent mass at the backrest	ns	ns	*

Table 4.3 *p*-values of the effect of excitation magnitude in the "primary-axis" on the indicators of the nonlinearity in the fore-aft direction due to the excitation magnitude in the "secondary-axes"

Degree of the nonlinearity due to the excitation magnitude in the "secondary-axes"	**Backrest inclination angle**		
	0°	**10°**	**20°**
R_{nl_sec} of in-line fore-aft apparent mass at the seat pan	ns	**	**
R_{nl_sec} of in-line fore-aft apparent mass at the backrest	*	*	*
PC_{sec} of in-line fore-aft apparent mass at the seat pan	*	**	ns
PC_{sec} of in-line fore-aft apparent mass at the backrest	*	ns	ns

4.3.1.4 Multiple coherence

Figure 4.5 shows the coherences between the excitations and the fore-and-aft force at the seat pan and backrest under different conditions. The coherence was calculated using Eq. (3.6) under single-axial fore-aft excitation and using Eqs. (4.10) and (4.11) under tri-axial vibration. For the latter, the order of the input excitation was: x-axis (with the corresponding partial coherence γ^2_{1b}), z-axis (with the corresponding partial coherence $\gamma^2_{2b.1}$), and y-axis.

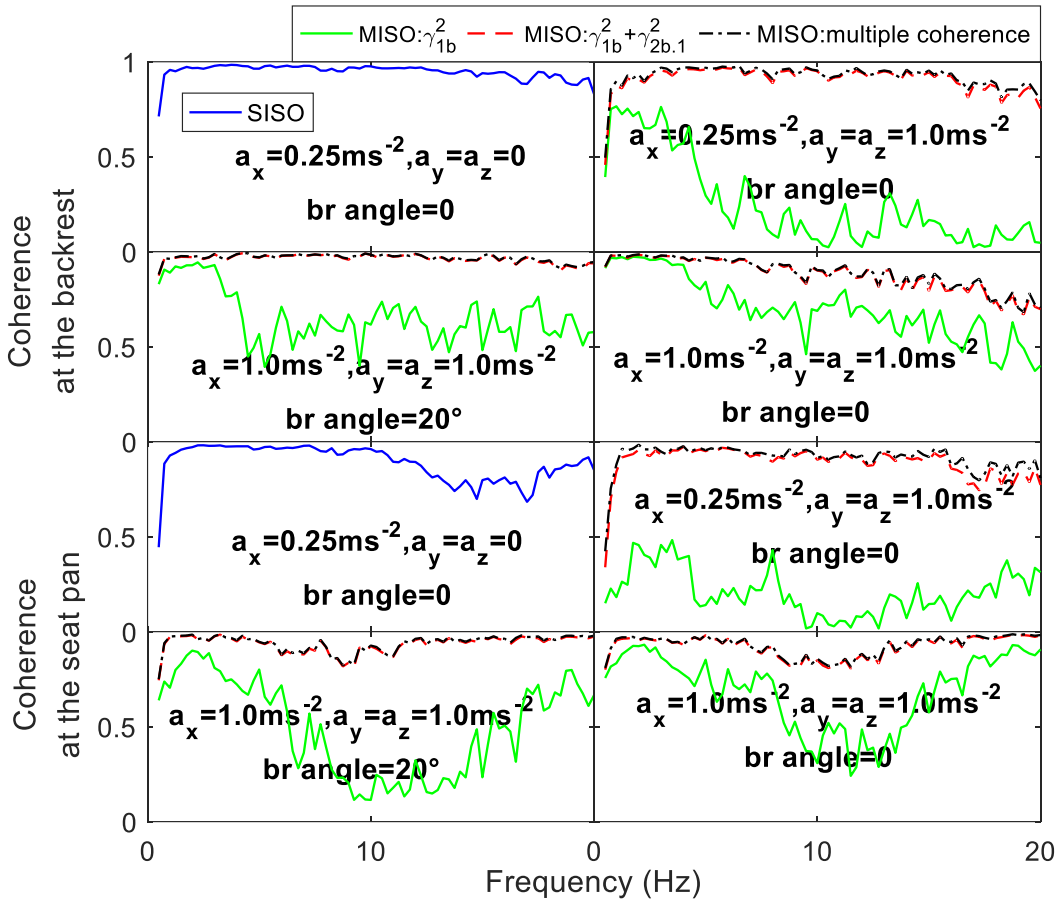

Figure 4.5 Coherence between the excitations and the fore-and-aft force at the seat pan and backrest calculated using SISO method under single-axial fore-aft vibration and those calculated using MISO method under tri-axial vibration

The coherence under single-axial fore-aft excitation (▬) was generally at a high level over the frequency range below 20°, while under tri-axial excitation, the partial coherence γ^2_{1b} between the fore-aft input and fore-aft force (▬) was lower. However, with additional partial coherence between the vertical input and fore-aft force, the sum of the coherence $\gamma^2_{1b}+\gamma^2_{2b.1}$ (▬) increased to a high level, while the further addition of the partial coherence only improved the multiple coherence (▬) marginally. Under tri-axial excitation, γ^2_{1b} tended to increase with the increase of the excitation magnitude in the "primary-axis". It also shows that when the backrest was inclined, the γ^2_{1b} at the seat pan and the backrest were slightly smaller compared to their counterpart with upright backrest.

4.3.2 In-line lateral apparent masses under tri-axial vibration

4.3.2.1 The effect of the excitation magnitude in the "primary-axis" (y-axis)

Under tri-axial vibration, the effect of the increase of the lateral excitation magnitude on the modulus of the in-line lateral apparent mass at the backrest at 0.75 Hz was significant under all tri-

axial excitations (p<0.01). For the in-line lateral apparent mass at the seat pan, the fundamental resonance frequency between 1.5 and 2.5 Hz tended to decrease with the increase of the lateral excitation magnitude under all conditions (Figure 4.6; p<0.05).

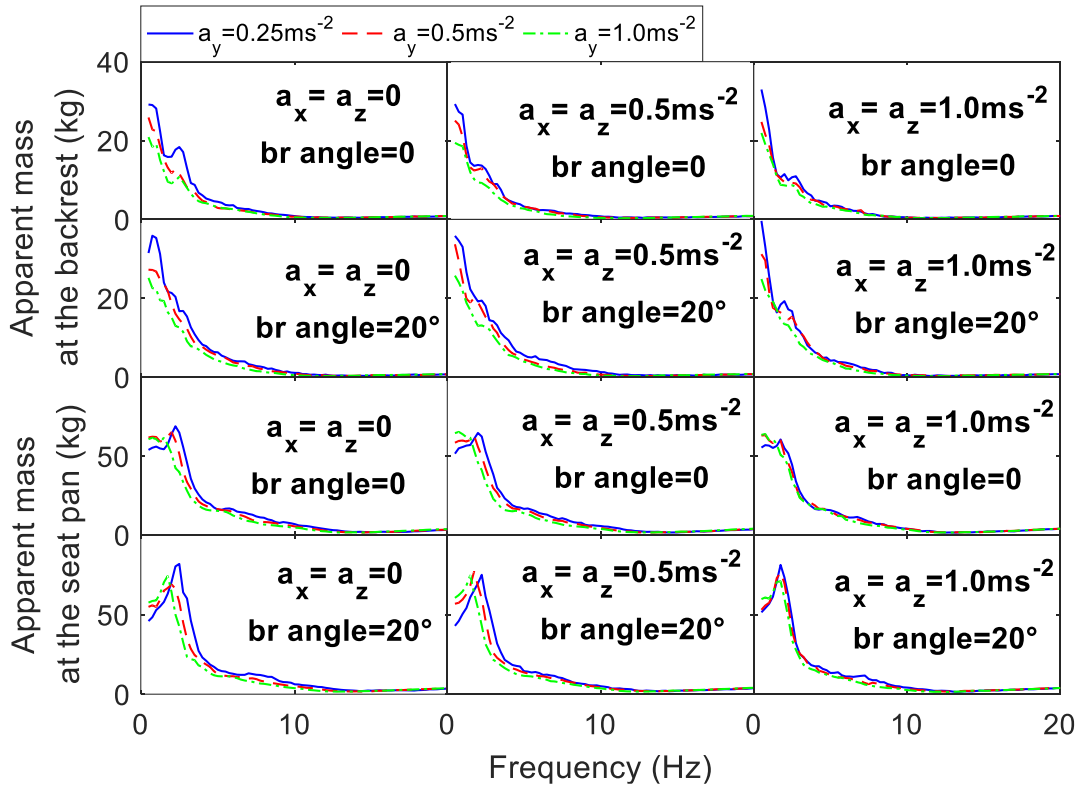

Figure 4.6 Median in-line lateral apparent mass at the seat pan and backrest under different excitation magnitudes in x and z-axis (0, 0.5 or 1.0 ms^{-2}) and different backrest inclination angles (0 or 20°): the effect of the lateral excitation magnitude

4.3.2.2 The effect of the excitation magnitude in "secondary-axes" (x and z-axis)

The increase of the excitation magnitude in the "secondary-axes" (x and z-axis) didn't have a significant effect on the modulus of in-line lateral apparent masses at the backrest at 0.75 Hz under all the conditions (p>0.05).

With the increase of the excitation magnitude in x and z-axis, the resonance frequency of the in-line lateral apparent mass at the seat pan tended to decrease, especially when the lateral excitation magnitude was 0.25 ms^{-2} r.m.s. (Figure 4.7). Such an effect was only significant when the lateral excitation magnitude was 0.25 and 0.5 ms^{-2} r.m.s. (p<0.05). The modulus associated with the resonance decreased with the increased excitation magnitude in x and z-axis when the backrest was upright or inclined by 10° (Figure 4.7), especially when the lateral excitation magnitude was at a low level of 0.25 ms^{-2} r.m.s. (p<0.05 for all 3 backrest conditions).

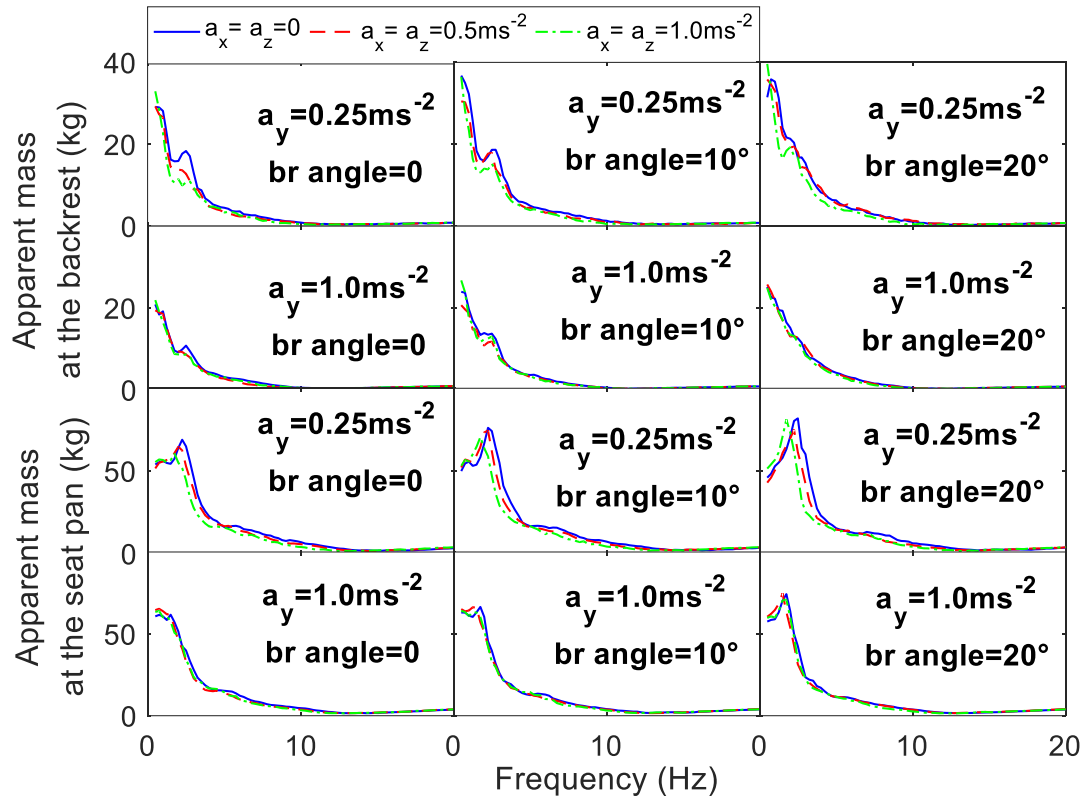

Figure 4.7 Median in-line lateral apparent mass at the seat pan and backrest under different y-axis excitations (0.25 and 1.0 ms^{-2} r.m.s.) and different backrest inclination angles (0, 10° or 20°): the effect of the excitation magnitude in x and z-axis

4.3.2.3 The effect of the inclination of backrest and interactive effects among the factors

Under tri-axial excitation, the effect of the increase of the backrest inclination angle on the modulus of the in-line lateral apparent mass at the backrest at 0.75 Hz was significant under all excitations (p<0.05), and also led to an increase of the modulus associated with the resonance frequency of the in-line lateral apparent mass at the seat pan, similar to that under single-axial lateral excitation.

Under single-axial lateral excitation, the effect of the increase of the backrest inclination angle on the modulus associated with the resonance frequency of the in-line lateral apparent mass at the seat pan was not significant for most cases (p<0.05 for only 1 out of 3 cases), while when the excitation magnitude in the x and z-axis was 0.5 or 1.0 ms^{-2} r.m.s., such an increase was significant for 5 out of 6 cases.

The effect of the increase of the excitation magnitude in the "secondary-axes" on the R_{nl_ilm} of the lateral apparent mass at the seat pan was not significant (p>0.05) with upright backrest, but became significant (p<0.05) when the backrest was inclined by 20° (Table 4.4). On the other hand, the effect of the excitation magnitude in "primary-axis" on the R_{nl_sec} of the that apparent mass was significant (p<0.05) both when the backrest was upright and when it was inclined by 20°, see Table 4.5.

Table 4.4 *p*-values of the effect of excitation magnitude in the "secondary-axes" on the indicators of the nonlinearity in the lateral direction due to the excitation magnitude in the "primary-axis"

Degree of the nonlinearity due to the excitation magnitude in the "primary-axis"	**Backrest inclination angle**		
	0°	**10°**	**20°**
R_{nl_ilm} of in-line lateral apparent mass at the seat pan	ns	ns	*
PC_{ilm} of in-line lateral apparent mass at the seat pan	ns	ns	ns

Table 4.5 *p*-values of the effect of excitation magnitude in the "primary-axis" on the indicators of the nonlinearity in the lateral direction due to the excitation magnitude in the "secondary-axes"

Degree of the nonlinearity due to the excitation magnitude in the "secondary-axes"	**Backrest inclination angle**		
	0°	**10°**	**20°**
R_{nl_sec} of in-line lateral apparent mass at the seat pan	**	ns	**
PC_{sec} of in-line lateral apparent mass at the seat pan	ns	ns	ns

4.3.2.4 Multiple coherence

For the lateral forces measured under tri-axial excitation, the order of the input excitations was: y-axis, x-axis, and z-axis. Figure 4.8 shows that under tri-axial excitation, the partial coherence γ^2_{1b} between the lateral input and lateral force at the backrest (—) was much lower compared to that under single-axial lateral excitation (—). The input in the x and z-axis both played a non-negligible role in the multiple coherence (— ▪) related to the lateral force at the backrest. On the other hand, their contribution to the multiple coherence of the lateral force at the seat pan was smaller.

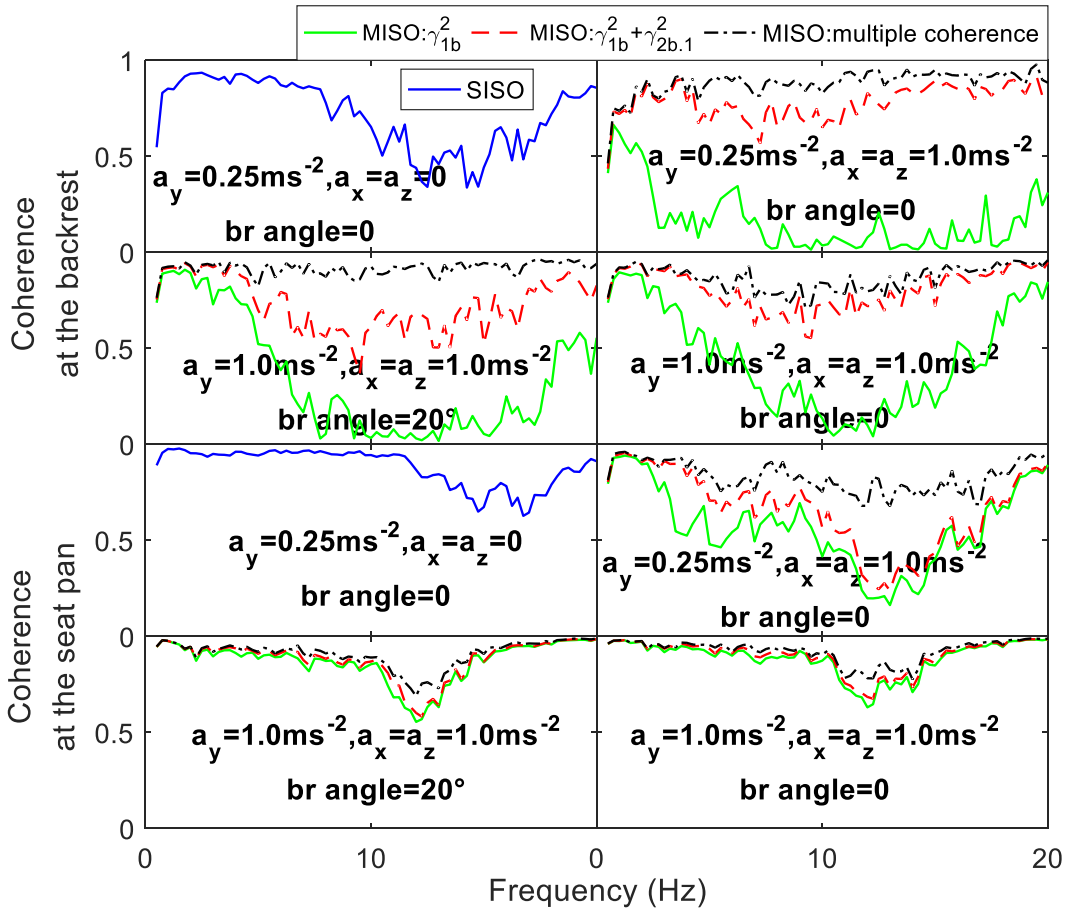

Figure 4.8 Coherence between the excitations and the lateral force at the seat pan and backrest calculated using SISO method under single-axial lateral vibration and those calculated using MISO method under tri-axial vibration

The addition of the excitation in the "secondary-axes" generally led to a decrease of the partial coherence γ^2_{1b}, which increased with the increase of the excitation magnitude in the "primary-axis" under tri-axial excitation. The effect of the backrest inclination angle on the partial and multiple coherences was small.

4.3.3 In-line vertical apparent masses under tri-axial vibration

4.3.3.1 The effect of the excitation magnitude in the "primary-axis" (z-axis)

Under tri-axial excitation, multiple local peaks existed in the modulus in the vicinity of the resonances of the in-line vertical apparent masses at the backrest and the seat pan (Figure 4.9), and the effect of the increase of the vertical excitation magnitude on the frequency of the fundamental resonance of the in-line vertical apparent mass at the backrest was relatively small.

The resonance frequency of the in-line vertical apparent mass at the seat pan tended to decrease with the increase of the vertical excitation magnitude when the excitation magnitude in the x and

y-axis was 0.5 ms^{-2} r.m.s. or when the backrest was inclined (p<0.01). The effect of the vertical excitation magnitude under tri-axial vibration was not identifiable when the excitation magnitude in the x and y-axis was 1.0 ms^{-2} r.m.s. (p>0.05 for 2 out of 3 backrest inclination angles).

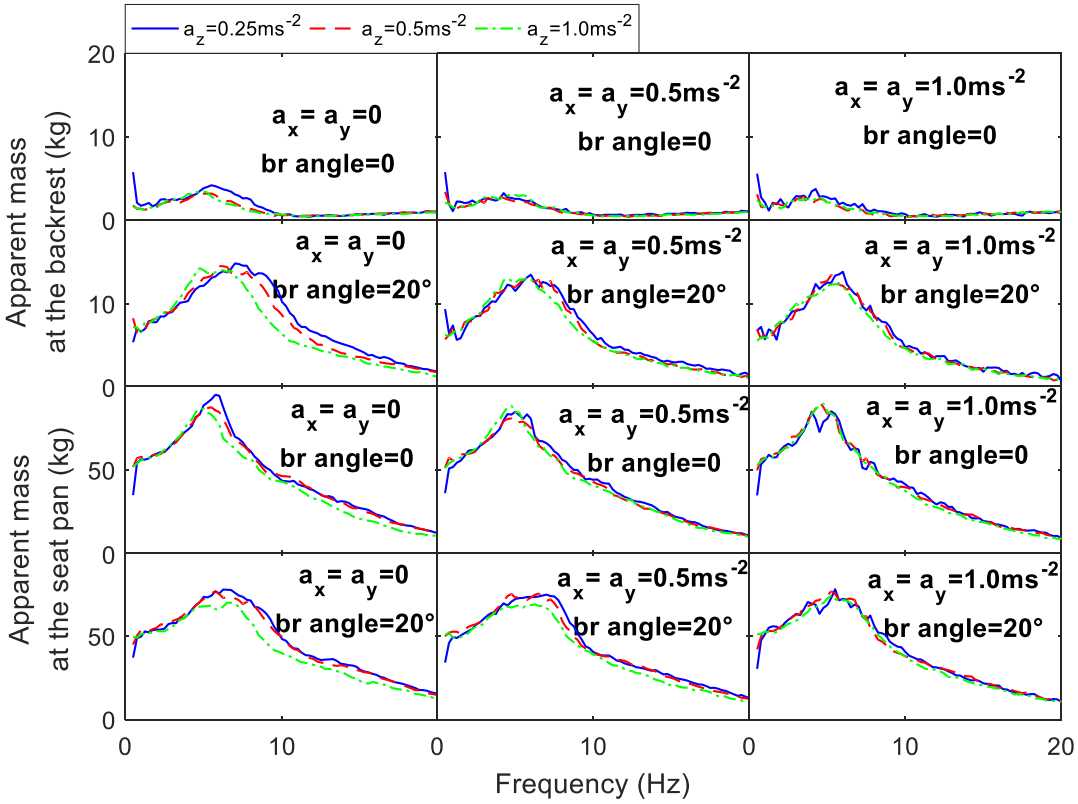

Figure 4.9 Median in-line vertical apparent mass at the seat pan and backrest under different levels of excitation magnitudes in x and y-axis (0, 0.5 or 1.0 ms^{-2} r.m.s.) and different backrest inclination angles (0 or 20°): the effect of the vertical excitation magnitude

4.3.3.2 The effect of the excitation magnitude in "secondary-axes" (x and y-axis)

Figure 4.10 shows that, when the magnitude of the vertical excitation was 0.25 ms^{-2} r.m.s., the fundamental resonance frequency of the vertical apparent mass at the backrest tended to decrease with the increase of the magnitude of the excitations in the "secondary-axes" (x and y-axis). With a vertical excitation of 1.0 ms^{-2} r.m.s., the decrease of the fundamental resonance frequency was not clear, while the effect of the excitation magnitude in "secondary-axes" on such a frequency was significant under all 9 conditions (p<0.01). For the in-line vertical apparent mass at the seat pan, when the vertical excitation magnitude was 0.25 or 0.5 ms^{-2} r.m.s., the resonance frequency decreased slightly with the increase of the magnitude of the excitations in the "secondary-axes" (Figure 4.10), although not significant when the backrest was inclined by 20° (p>0.05). When the vertical excitation magnitude was 1.0 ms^{-2} r.m.s., the change of the resonance frequency due to the change of the magnitude of the excitations in the "secondary-axes" was very small but significant (p<0.05).

The effect of the excitation magnitude in the "secondary-axes" on the modulus associated with the resonance frequency was generally insignificant for that at the backrest (p>0.05 for 7 out of 9 cases) and the seat pan (p>0.05 for 8 out of 9 cases).

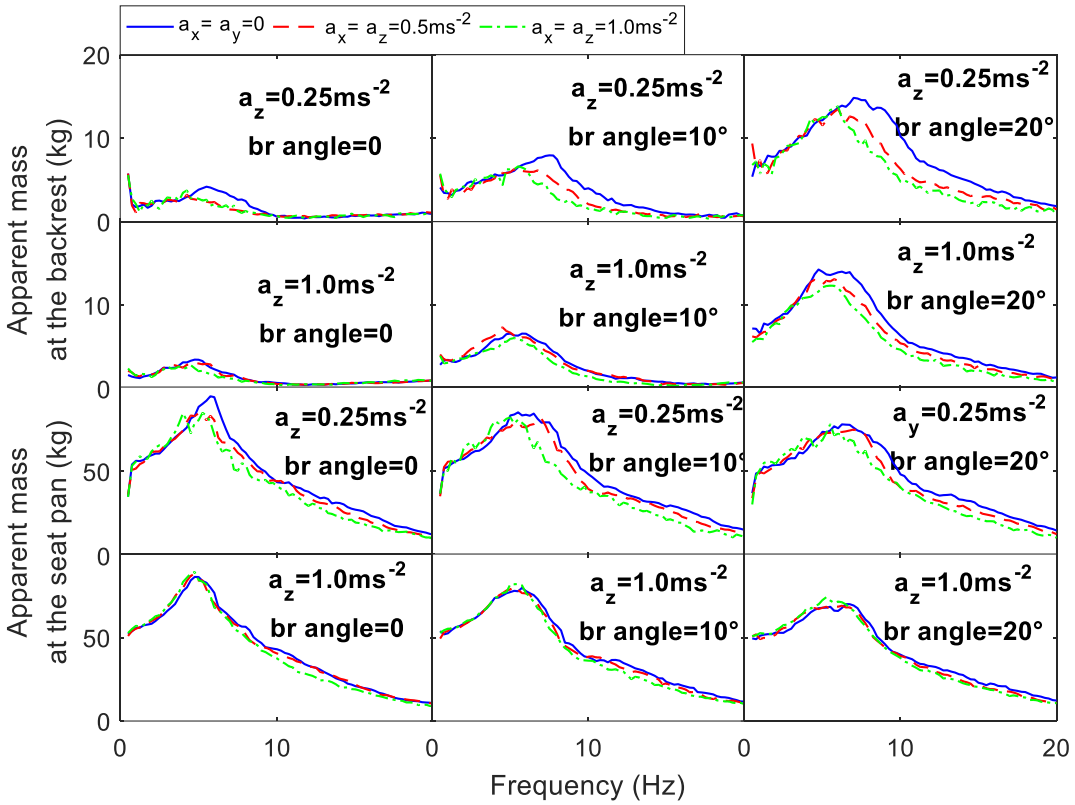

Figure 4.10 Median in-line vertical apparent mass at the sear pan backrest under different z-axis excitations (0.25 and 1.0 ms^{-2}) and different backrest inclination angles (0, 10° or 20°): the effect of the magnitudes of x- and y-axis excitation

4.3.3.3 The effect of the inclination of backrest and interactive effects among the factors

With the increased backrest inclination angle, the change of the in-line vertical apparent mass at the backrest under tri-axial vibration in general followed the same trend as that under single-axial vertical excitation: the resonance frequency tended to increase and the associated modulus tended to increase (p<0.05). With the increased backrest inclination angle, the modulus associated with the fundamental resonance of the in-line vertical apparent mass at the seat pan tended to decrease under tri-axial vibration (p<0.01), similar to the observations under single-axial vertical excitation.

Interactive effect existed between the magnitude of excitation in the "primary-axis" and that in the "secondary-axes", which is shown in Table 4.6 and Table 4.7. The R_{nl_ilm} of the vertical apparent mass at the backrest was significantly affected by the excitation magnitude in the "secondary-axes" (p<0.05) at all 3 backrest inclination angles, which tended to decrease with the increased excitation magnitude of in the "secondary-axes" when the backrest was inclined. The effect of excitation

magnitudes in the "secondary-axes" on the PC_{ilm} of the vertical apparent mass at the backrest was significant when the backrest was upright or inclined by 10°.

Table 4.6 *p*-values of the effect of excitation magnitude in the "secondary-axes" on the indicators of the nonlinearity in the vertical direction due to the excitation magnitude in the "primary-axis"

Degree of the nonlinearity due to the excitation magnitude in the "primary-axis"	**Backrest inclination angle**		
	0°	**10°**	**20°**
R_{nl_ilm} of in-line vertical apparent mass at the seat pan	ns	*	ns
R_{nl_ilm} of in-line vertical apparent mass at the backrest	*	*	*
PC_{ilm} of in-line vertical apparent mass at the seat pan	ns	ns	ns
PC_{ilm} of in-line vertical apparent mass at the backrest	*	*	ns

The increase of the excitation magnitude in the "primary-axis" generally led to a decrease of the R_{nl_sec} of the vertical apparent mass at both the seat pan and backrest, and such an effect was significant for that at the backrest when the backrest was inclined (Table 4.7, $p<0.05$). Its effect on the PC_{sec} due to the increased excitation magnitude in the "secondary-axes" was not significant under all conditions.

Table 4.7 *p*-values of the effect of excitation magnitude in the "primary-axis" on the indicators of the nonlinearity in the vertical direction due to the excitation magnitude in the "secondary-axes"

Degree of the nonlinearity due to the excitation magnitude in the "secondary-axes"	**Backrest inclination angle**		
	0°	**10°**	**20°**
R_{nl_sec} of in-line vertical apparent mass at the seat pan	ns	**	ns
R_{nl_sec} of in-line vertical apparent mass at the backrest	ns	**	**
PC_{sec} of in-line vertical apparent mass at the seat pan	ns	ns	ns
PC_{sec} of in-line vertical apparent mass at the backrest	ns	ns	ns

The effect of the backrest inclination on the R_{nl_ilm} or PC_{ilm} of the vertical apparent masses was not significant under single-axial vertical excitation, but under tri-axial excitation, it was significant for the R_{nl_ilm} of the vertical apparent mass at the backrest with 0.5 ms^{-2} excitation in the "secondary-axes", and for the R_{nl_ilm} at the seat pan with 1.0 ms^{-2} excitation in the "secondary-axes".

4.3.3.4 Multiple coherence

For the vertical response, the order of the input excitations is: z-axis, x-axis, and y-axis. Figure 4.11 shows that under tri-axial excitation, the partial coherence γ^2_{1b} between the vertical input and vertical force at the backrest ( ) was much lower compared to that under single-axial vertical excitation ( ). The addition of partial coherence $\gamma^2_{2b.1}$ due to the input in the x-axis led to dramatic increase of the summed-up coherence ( ). The contribution of the additional lateral input to the multiple coherence of the vertical apparent mass at the seat pan was smaller ( ). For the vertical apparent mass at the seat pan, the partial coherence γ^2_{1b} was low when the excitation magnitude in the "secondary-axes" (1.0 ms^{-2}) were much greater than that in the "primary-axis" (0.25 ms^{-2}), but when the excitation magnitude in the "primary-axis" was 1.0 ms^{-2}, that partial coherence was at a high level even under tri-axial excitation.

The effect of the backrest inclination angle on the partial and multiple coherences was small.

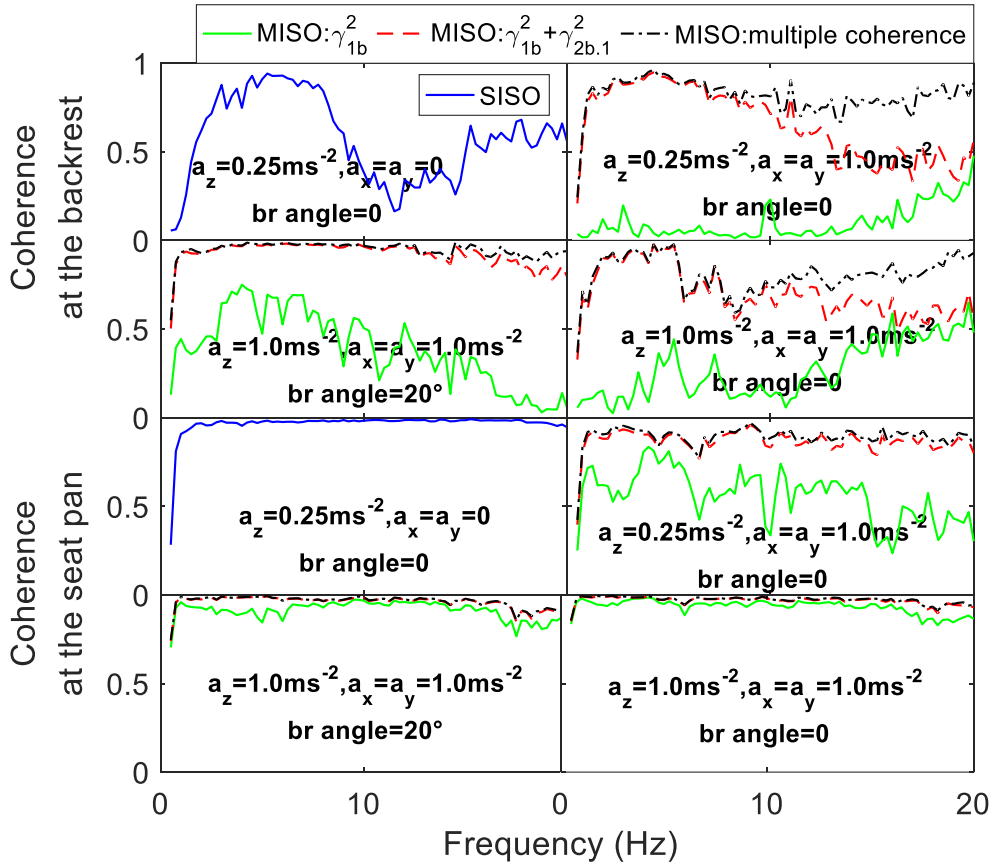

Figure 4.11 Coherence between the excitations and the vertical force at the seat pan and backrest calculated using SISO method under single-axial vertical vibration and those calculated using MISO method under tri-axial vibration

4.4 Discussion

4.4.1 The effect of the excitation magnitude in the "primary-axis" under tri-axial vibration

Under tri-axial vibration, the increase of the excitation magnitude in the "primary-axis" generally led to the decrease of the resonance frequency of the apparent mass in the same direction. This was found in all three translational directions with both upright and inclined backrest. It is consistent with the results reported in previous studies considering dual (Qiu and Griffin, 2012; Zheng et al., 2019) and tri-axial translational vibrations (Mansfield and Maeda, 2007; Mandapuram et al., 2012), and the latter was limited to the conditions with an upright backrest and a smaller number of excitation magnitudes. Such an effect of the excitation magnitude in the "primary-axis" has also been reported by an existing study considering combined vertical, lateral and roll excitation (Wu et al., 2021).

The partial coherence between the force in each axis and the corresponding input in the same axis tended to become lower under tri-axial excitation compared to that under single-axial excitation. This can be explained that under tri-axial excitation, the part of the in-line input correlated with the excitation in the "secondary-axes" was eliminated using the MISO method, leading to a lower partial coherence compared to that under single-axial excitation.

When the excitation magnitude in the "primary-axis" increased, such a partial coherence tended to increase. The further increase of excitation magnitude in the "primary-axis" could lead to an increase of the signal-to-noise ratio, if the excitation in the "secondary-axes" is regarded as "noise".

4.4.2 The effect of the excitation magnitude in the "secondary-axes" under tri-axial vibration

In the current study, the increase of the excitation magnitude in the two "secondary-axes" led to a decrease of the resonance frequencies of the in-line fore-aft apparent masses at the seat pan and the backrest under tri-axial vibration. This is consistent with the results reported by Mansfield and Maeda (2007), which was conducted only with an upright backrest and two excitation magnitude levels (0.4 and 0.8 ms^{-2} r.m.s.) in each of the three translational axes. The results from the current study show that the nonlinearity of the fore-aft biodynamic response due to the increase of the excitation magnitude in "secondary-axes" could also be recognized when the backrest was inclined and with a series of changes of the excitation magnitudes in the "primary-axis". Similarly, the resonance frequency of the vertical apparent mass was also affected by the excitation magnitudes in the "secondary-axes" with different backrest inclination angles.

It is worth mentioning that, compared to the results of the existing studies under combined fore-aft and vertical excitations (Qiu and Griffin, 2012; Zheng et al., 2019), the effect of the excitation magnitude in the "secondary-axes" on the lateral apparent masses with tri-axial excitation was also found in the current study, especially when the lateral excitation magnitude was at a low level. Although the coupling of the dynamic response of the seated human body was mainly found in the x and z-axis, and the lateral response was less correlated with those in the x and z-axis, such a result indicates that the effect of the excitation magnitude in the x and z-axis on the lateral response should not be ignored when the human body was exposed to tri-axial vibration.

When the vertical excitation magnitude was 0.25 ms^{-2} r.m.s. and when the excitation magnitudes in the x and y-axis were both 1.0 ms^{-2}, the in-line vertical apparent mass at the seat pan exhibited two peaks with the similar modulus between 3 and 8 Hz under tri-axial vibration, instead of one that was identified under single-axial vertical excitation (Figure 4.9). This was found on 8 out of 12 subjects, which may indicate that when the excitation magnitude in the "secondary-axes" was at a high level, the modes of the human body that were merged by the body damping may be activated by the excitation in the "secondary-axes".

4.4.3 The effect of the backrest inclination angle under tri-axial vibration

The effect of the backrest inclination angle on in-line fore-aft apparent mass, which has been observed with single-axial fore-aft excitation, can also be found under tri-axial excitations. When the backrest was upright, multiple local peaks in the vicinity of the fundamental resonance frequency of the in-line fore-aft apparent masses at the backrest with the similar associated moduli was found, while when the backrest was inclined by 20°, the fundamental resonance became more distinct (Figure 4.3 and Figure 4.4). The coherence in the vicinity of the resonance frequency was found not to increase with the increased backrest inclination angle, so this was not likely to be attributed to the effect of the noise. The change in the moduli associated with the resonance frequency may be explained that when the backrest changed from upright to inclined condition, the interaction between the human body and the backrest increased. That may have led to a change of the body damping, which made some modes of the human body inactivated. The effect of the backrest inclination angle on the in-line lateral apparent masses under tri-axial vibration was also similar to that observed with single-axial lateral excitation.

The effects of the backrest inclination angle on the lateral and vertical apparent masses under tri-axial excitations were similar to those under single-axial excitations (Chapter 3).

The effect of the increase of the backrest inclination angle on the multiple coherences was relatively small. Nevertheless, it could still be found in Figure 4.5 and Figure 4.11 that its effect on the multiple

coherences related to the force at the backrest was greater than that at the seat pan, which may be as a result of the increased of body mass supported by the backrest and the increased interaction between the upper human body and the backrest.

4.4.4 Interactive effect between the influencing factors

Interactive effect existed between two influencing factors: the excitation magnitude in the "primary-axis" and that in the "secondary-axes", on the nonlinearity of the seated human body exposed to the tri-axial translational excitation. Figure 4.3, Figure 4.4, Figure 4.6, Figure 4.7, Figure 4.9, and Figure 4.10 show that for the apparent mass in either x, y, or z-axis, the effect of one of these two factors tended to become smaller when the value of the other factor increased. Such a finding is an expansion of the findings made by Qiu and Griffin (2012) and Zheng et al. (2019) that interaction existed between the excitation magnitudes under dual-axial fore-aft and vertical excitation, into the tri-axial excitation conditions.

It can be found from Table 4.2 to Table 4.7 that the significant interactive effect between the excitation in different axes mostly existed on the fore-aft and vertical apparent masses, but rarely on the lateral apparent mass. This may be explained by the relatively strong coupling between the biodynamic response in the fore-aft and vertical direction, while that between the lateral response and those in other axes is smaller.

Noticeably, the increase of the excitation magnitude in the y and z-axis led to a significant decrease of R_{nl_ilm} of the in-line fore-aft apparent mass at the seat pan (p<0.01) in the current study. On the other hand, it was reported that under dual-axis fore-aft and vertical excitation, the change of the resonance frequency of the in-line fore-aft apparent mass at the seat pan was hardly affected when the vertical excitation magnitude increased (Qiu and Griffin, 2012; Zheng et al., 2019). The difference between the results of the current and previous studies may be attributed to the additional lateral excitation under the tri-axial vibration, which was not present in the study by Qiu and Griffin (2012). Although the correlation between the lateral excitation and fore-aft response was low (Figure 4.5), its contribution to the overall magnitude of the excitation in three axes that affected the overall biodynamic response may still be not negligible.

Furthermore, the effect of the excitation magnitude in the "primary-axis" on the degree of nonlinearity of the biodynamic response also varied among different backrest inclination angles. The increase of the backrest inclination angle significantly led to: 1) an increase of the PC_{ilm} of the in-line lateral apparent mass measured at the seat pan when the excitation magnitude in the "secondary-axes" was 1.0 ms^{-2} r.m.s.; 2) a decrease of the PC_{ilm} of the in-line vertical apparent mass at the seat pan when the excitation magnitude in the "secondary-axes" were 1.0 ms^{-2} r.m.s. The

significant change of these *PC*s may indicate that the backrest inclination angle affected the damping of the seated human body that was related to the nonlinearity.

4.4.5 Relationship between the apparent masses and the overall excitation magnitude of tri-axial vibration

It was concluded in Section 4.4.4 that the interactive effects existed between the excitation magnitude in the "primary-axis" and that in the "secondary-axes" in affecting the apparent masses in the x, y and z-axis. A higher level of excitation magnitude in the "primary-axis" tended to suppress the effect of the excitation magnitude in the "secondary-axes" and vice versa. Such phenomenon provides further evidence for the conclusion made by Mansfield and Maeda (2007) that under tri-axial vibration, the resonance frequency of the apparent mass in any axis may be a function of the overall excitation magnitude in all the translational axes. The response of the human body to WBV with a high-level overall magnitude may have less potential for the further adjustment, then the effect of the increased excitation magnitude in any direction on the biodynamic response tended to be smaller. It is of interest to know how the overall excitation magnitude is related to the fundamental resonance frequency of the apparent mass, and which of the excitation magnitudes in the "primary-axis" or the "secondary-axes" played the more important role. To explore the different sensitivities of the human body to the WBV in different directions, the excitation magnitudes in different axes should be weighted for the calculation of the overall excitation magnitude.

For the apparent mass in the direction under investigation, the overall weighted magnitude of the tri-axial translational excitation $a_{overall}$ is defined in the current study based on that proposed by Wu et al. (2021), as follows:

$$a_{overall} = \sqrt{a_{ilm}^2 + 2 * (w_{sec} a_{sec})^2} \tag{4.11}$$

Where a_{ilm}, a_{sec}, and w_{sec} represent the r.m.s. values of the excitation magnitude in the "primary-axis" and the "secondary-axes", and the weighting factor for the "secondary-axes" excitations respectively, assuming that the weighting factor of the excitation in the "primary-axis" is 1. This way, the effect of the excitation magnitude in the "secondary-axes" relative to that in the "primary-axis" can be reflected by the value of w_{sec}. For example, if w_{sec}>1, then the excitation magnitude in the "secondary-axes" played more important role than that in the "primary-axis".

Assuming that the dependent variable, the resonance frequency res_i (i=x, y, z) of the apparent mass at the seat pan in the x, y or z-direction, is linearly correlated with the independent variable, the weighted overall magnitude of the excitation ($a_{overall}$):

$$res_i = E_1 a_{overall} + E_0 \quad (4.12)$$

Where E_1 and E_0 are correlation coefficient (i.e., the slope of the linear regression function) and the constant, respectively. The null hypothesis is that $E_1 = 0$, which is tested by the F-test of the overall significance of the regression model. When p<0.05, the null hypothesis is rejected.

Then, the weighting factor of the excitation in the "secondary-axes" w_{sec} can be determined by maximizing the mean value of the R^2 of the linear regression analysis carried out on the 12 subjects using the same optimization method for the model calibration (Chapter 6). The optimized relationship between the dependent and independent variables are shown in Table 4.8.

Table 4.8 The optimized relation between the resonance frequency of the apparent mass at the seat pan in x, y and z-direction and the weighted overall excitation magnitude with different backrest inclination angles

Direction of the apparent mass at the seat pan	Backrest inclination angle	Weighting factor w_{sec}	Mean correlation coefficient E_1	Mean constant E_0	Mean R^2	Mean p-value
x	0°	0.441	-1.066	4.874	0.551	ns
	10°	0.567	-1.038	4.919	0.591	ns
	20°	0.685	-1.017	4.547	0.639	*
y	0°	1.000	-0.644	2.143	0.472	ns
	10°	0.944	-0.760	2.520	0.708	**
	20°	0.928	-0.581	2.406	0.636	*
z	0°	1.068	-0.585	5.915	0.516	ns
	10°	0.901	-0.678	5.946	0.509	ns
	20°	0.913	-0.727	5.956	0.497	ns

Table 4.8 shows that the values of the weighting factors of the excitation magnitude in the "secondary-axes" w_{sec} are generally much greater than 0, indicating that the effect of the magnitude of the excitation in the "secondary-axes" on the apparent masses was non-negligible. It also shows that the values of w_{sec} for the lateral and vertical apparent masses are generally greater than those for the fore-aft apparent masses, indicating that the resonance frequency of the fore-aft apparent mass was less affected by the magnitude of the excitation in the "secondary-axes" compared to the lateral and vertical apparent mass. The value of w_{sec} is greater than 1 in only 1 out of 9 cases, indicating that in most cases, the magnitude of excitation in the "primary-axis" affected the apparent masses in the same direction more than that in the "secondary-axes", which is consistent with the previous studies under multi-axial excitations (Zheng et al., 2012; Zheng et al., 2019).

It is also noticed that the linear correlations between the resonance frequencies of the vertical apparent masses and the overall magnitude of excitation are not statistically significant (p>0.05), and the correlations related to the resonance frequencies of the horizontal apparent masses are only significant when the backrest was inclined. Besides, the values of the R^2 are only around 0.5 in some (5 out of 9) cases. In the future, a nonlinear regression model or a linear regression model including the cross-correlation terms may need to be established, so that the relationship between the resonance frequency and the overall excitation magnitude can be studied more completely.

4.4.6 MISO vs SISO method for the estimation of the apparent masses under tri-axial vibration

Figure 4.12 shows the comparison of the in-line vertical apparent masses and the corresponding partial coherences of a certain subject calculated using conventional SISO method (Eq. (3.5)) and MISO method (Eqs. (4.10) and (4.11)) under tri-axial excitation with different magnitudes. When the excitation magnitude in z-axis (i.e., "primary-axis") was greater than that in the x and y-axis (i.e., "secondary-axes"), the difference between the apparent masses calculated using both methods are very small (Figure 4.12, left). When the excitation magnitude in the "secondary-axes" was much greater than that in the "primary-axis", the error of the SISO estimation becomes relatively greater (Figure 4.12, right).

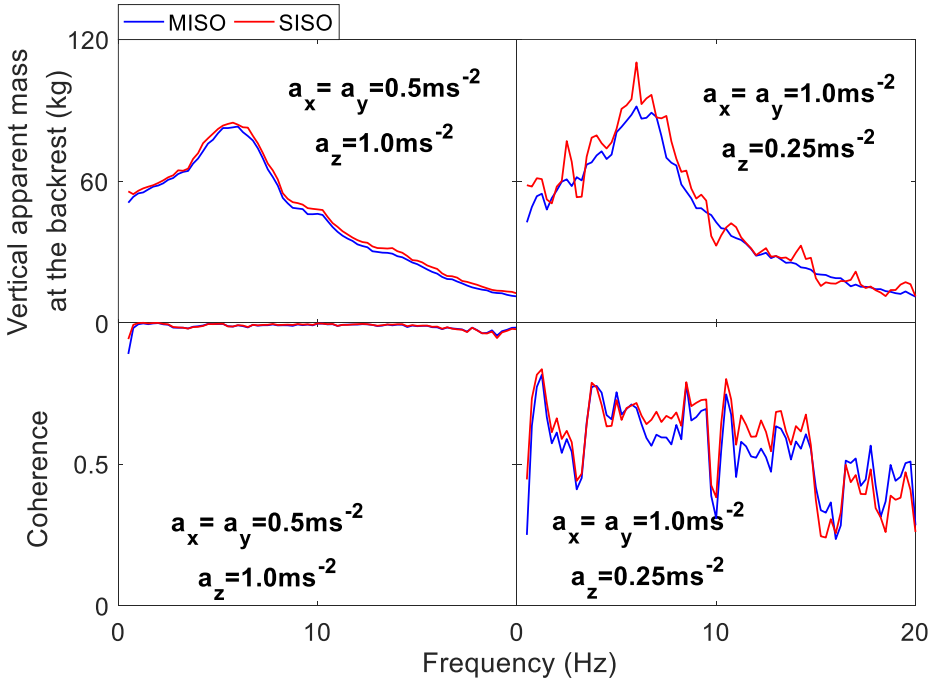

Figure 4.12 Comparison of the in-line vertical apparent masses and the corresponding coherences of a subject (1.77m, 67kg) at the seat pan estimated using MISO and SISO method under tri-axial vibration. Left: 0.5 ms^{-2} r.m.s. excitation in the x and y-axis, 1.0 ms^{-2} r.m.s. excitation in z-axis; right: 1.0 ms^{-2} r.m.s. excitation in the x and y-axis, 0.25 ms^{-2} r.m.s. excitation in z-axis

Hence, the MISO method is beneficial for the estimation of the apparent mass under multi-axial vibration with unavoidable mutual correlation between the excitation in different axes. When the excitation magnitude in the “secondary-axes” were at a high level, the effect of such a correlation on the accuracy of the apparent mass estimation should not be ignored, and a more accurate estimation could be made by adopting the MISO method.

4.5 Conclusions

In the current study, the in-line apparent masses in the fore-aft, lateral and vertical directions were measured under tri-axial vibrations with various magnitudes and with different backrest inclination angles. The results show that with different backrest inclination angles, the resonance frequency or the associated modulus of the in-line apparent mass in any one of the translational axes could be affected by the increase of the excitation magnitude in both the “primary-axis” and the corresponding “secondary-axes”. The multiple coherence between the excitation in “primary-axis” and the force in the same direction tended to increase with the increase of excitation magnitude in the “primary-axis”, and decrease with the increase of that in the “secondary-axes”.

Furthermore, interactive effects were found between the excitation magnitude in the “primary-axis” and that in the “secondary-axes” on the apparent masses in all three translational directions. When the excitation magnitudes in the “secondary-axes” were at a relatively high level, the effect of the excitation magnitudes in the “primary-axis” on the nonlinearity of the biodynamic response would be smaller, and vice versa. The results of the linear regression analysis indicated that the resonance frequencies of the horizontal apparent masses at the seat pan were linearly related to the weighted overall magnitude of tri-axial excitation when the backrest was inclined.

Under tri-axial vibration, the effect of the backrest inclination angle on the biodynamic response was similar compared to that with single-axial vibration. The backrest inclination could also have an impact on the effects of the excitation magnitude in the “primary-axis” or the corresponding “secondary-axes” on the changes of the apparent masses by affecting the effective damping of the human body and seat system.

The results from the current study reveals that under tri-axial vibration, the biodynamic response of the human body is affected by the excitation magnitude in all the three axes as well as the backrest inclination. Hence, when the dynamic characteristics of the seat-occupant system in a tri-axial vibrational environment are to be studied, the effects of the excitation magnitudes in all the directions and the backrest inclination angle need to be taken into consideration at the same time.

Chapter 5 THE TRANSMISSION OF TRI-AXIAL VIBRATION THROUGH THE SUSPENSION-SEAT-OCCUPANT SYSTEM: THE EFFECT OF THE EXCITATION MAGNITUDE AND THE BACKREST INCLINATION ANGLE

5.1 Introduction

Suspension seats are widely used in heavy vehicles to attenuate the vibration transmitted to the seated occupant. The performance of the suspension seat depends on the dynamic behaviour of the seat and the seated human body, both of which exhibit nonlinear behaviour with the change of the excitation magnitude. The resonance frequency of the transmissibility of suspension seats in the vertical direction has been found to decrease with the increased magnitude of single-axial vertical excitation when loaded with inert masses and with seated occupants (Qiu, 2017). The vibration in the horizontal directions also affects the ride comfort of the seated occupant, especially in heavy vehicles (Chaudhary et al., 2015; Rao et al., 2018; Johnson et al., 2019). However, many previous laboratory studies of the suspension seat transmissibility and dynamic modelling of the suspension seat have been limited to single-axial vertical excitation. How the seat-occupant system behaves under tri-axial vibration and how the transmissibility of the suspension seat in each direction is affected by the excitation magnitudes in different axes have not been reported.

It has been reported that the backrest inclination affected the apparent mass of the seated human body (Toward and Griffin, 2009; Yang and Qiu, 2015; Zhang et al., 2021) and the transmission of the fore-aft vibration to the backrest of a vehicle seat (Jalil and Griffin, 2007). The effect of the backrest inclination on the transmissibility of a suspension seat at the seat pan and backrest under tri-axial vibration remains to be explored.

In this chapter, the transmissibilities of the suspension mechanism, and those of the suspension seat with rigid masses and seated subjects in vertical, fore-and-aft, and lateral directions were measured in an experimental study with multi-axial translational vibration. How the vibration magnitude and the backrest inclination angle affected the transmissibilities were studied. It is hypothesised that under tri-axial vibration, the resonance of the seat transmissibilities in one direction would be affected by increase of the excitation magnitude in the same direction, and further affected by the additional excitations in the other two axes. It is further hypothesised that

the increase of the angle of backrest inclination would affect the seat transmissibility measured at the backrest, especially in the vertical and the fore-aft directions.

5.2 Experimental method

In this experimental study, it is assumed that the effect of the constrain of the seat belt on the results is small enough to be ignored.

5.2.1 Apparatus

This experimental study was approved by the Faculty of Engineering and Physical Sciences Ethics Committee at the University of Southampton. The experiment was carried out on the same 6-axis motion simulator as the one introduced in Chapters 3. A passive air-suspension seat to be tested was mounted at the centre of the simulator (Figure 5.1).

Figure 5.1 The suspension seat, the SIT-pads (blue) and single-axial accelerometers (circled) used in this study

Three single-axial Entran ECGS-DO10/V10 accelerometers were mounted at the seat base to measure the excitation in three translational directions. For the measurement of the transmissibilities of the suspension mechanism, another three accelerometers of the same type were mounted on the top plate of the suspension mechanism to measure the acceleration in three translational directions. For the measurement of the transmissibilities of the suspension seat (with loaded inert mass or with the seated subject), two tri-axial SIT-pads were fixed at the seat pan and the backrest, respectively, to measure the local acceleration in the x, y and z-axis. The SIT-pad at the seat pan was positioned at the centre of the seat pan under the ischial tuberosity of the seated

subjects, and the SIT-pad at the backrest was located at the centre of the backrest, 43cm above the seat pan surface when the backrest was upright.

The stroke of the suspension mechanism was 14 cm. Before each test started, the height of the suspension top plate was adjusted after the inert mass was loaded or the subject was seated, so that the static equilibrium position of the suspension top plate was located at the middle of the suspension travel. This was intended to avoid the contact between the suspension mechanism and the end-stop buffers at the top and bottom of the suspension mechanism, which could cause shock input to the seat pan that is beyond the scope of the current study. The measured data were recorded and processed using HVLab data acquisition system with a sampling rate of 512 samples per second and with an anti-aliasing filter set at 50 Hz.

5.2.2 Stimuli and backrest inclination

In this experiment, 23 excitations were introduced: 9 single-axial random excitations that were the same as those introduced in Chapter 3, and 14 tri-axial random excitations that were the same as those introduced in Chapter 4. Each of the excitations had a duration of 60 seconds over a frequency range between 0.5 and 40 Hz. The magnitudes of the single- and tri-axial excitations were the same as those shown in Table 4.1. Similar to the experimental study presented in Chapter 4, the excitations were sorted in three groups in the current study. In each group, the in-line seat transmissibility in one of the three translational axes was studied, and the excitation in the same axis was referred to as excitation in the “primary-axis”, while the excitation in the other two axes was called the excitation in the “secondary-axes”. All the excitation signals were generated independently.

For the measurement of seat transmissibility with subjects, the backrest inclination angles varied between 0°, 10° and 20°. Each subject was exposed to the 23 excitations three times, each time under the support of the backrest with one of the three inclination angles, making the total number of the excitations that a subject experienced throughout the experiment to be 69.

5.2.3 Inert masses and subjects

Prior to the tests with human subjects, inert masses were loaded on the suspension mechanism and the complete suspension seat to measure the transmissibilities of the suspension and the seat. First, the seat-pan-and-backrest assembly (with a total mass of 18.8 kg) was removed from the seat, leaving the suspension mechanism alone to be fixed on the simulator. Then the inert mass contained in a rigid box was secured on the top plate of the suspension mechanism (Figure 5.2). The mass of the inert mass varied between 45 kg, 60 kg and 75 kg. The mass of rigid box was 18.8 kg,

identical to the total mass of the seat-pan-and-backrest assembly. This makes the total mass supported by the suspension mechanism during the measurement of the suspension transmissibility the same as that during the measurement of the complete seat transmissibility. The suspension mechanism was applied with all the 23 excitations, and the transmissibilities of the suspension mechanism in three directions were measured.

After the experiment on the suspension mechanism, the seat-pan-and-backrest assembly were mounted back, and the same inert masses (45 kg, 60 kg or 75 kg) without the rigid box were secured on the seat pan of the complete seat (Figure 5.2). The transmissibilities of the suspension seat at the seat pan and backrest were then measured under all the 23 excitations. During the measurement on the suspension seat with loaded inert mass, the backrest was kept in the upright position.

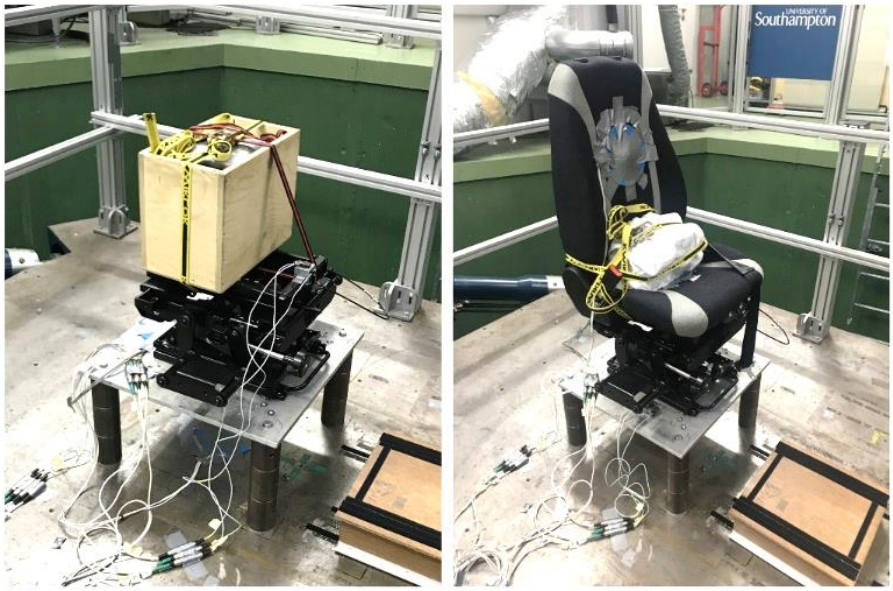

Figure 5.2 Suspension mechanism (left) and the complete seat (right) loaded with inert mass

After the experiment using the inert masses, twelve male subjects aged between 24 and 43 years old (with a mean age of 29.1 years old) participated in this experiment. The stature of the subjects ranged from 1.65 to 1.85 m (mean stature: 1.78 m) and the weights of them ranged from 56.2 to 96.6 kg (mean weight: 78.1 kg). Nine out of these twelve subjects also participated in the experimental studies introduced in Chapters 3 and 4. During this experiment, the subjects were secured with the seat belt, and they were asked to sit in a relaxed posture against the backrest when the backrest is upright or inclined. They were asked to rest their hands on the lap and rest their feet on the footrest (Figure 5.3).

For each inert mass and each subject, the order of the excitations was randomized.

Figure 5.3 One subject seated in the suspension seat with upright backrest

5.2.4 Data analysis

The accelerations measured by the SIT-pad at the backrest in the fore-aft and vertical directions were transformed in the same way as described in Eqs. (3.1) to (3.4) so that the accelerations after the transformation are in the same direction as the x or z-axis in the coordinate systems of the seat pan and the floor.

For the single-axial excitations, the in-line transmissibilities at the seat pan and backrest were calculated using the SISO method as that adopted in Chapter 3:

$$TR_{ij} = \frac{G_{a_j a_{ij}^s}}{G_{a_j}} \tag{5.1}$$

Where TR_{ij} stands for the transmissibility measured at the seat pan (when $i=s$) or the backrest (when $i=b$), a_j represents the input acceleration in a translational direction ($j=x$ or y or z), a_{ij}^s represents a measured acceleration at the seat pan or at the backrest after transformation to the seat pan coordinate system, $G_{a_j a_{ij}^s}$ represents the cross-spectra between a_j and a_{ij}^s, and G_{aj} represents the auto-spectra of a_j. Under tri-axial vibration, the MISO method described in Chapter 4 was used to calculate the seat transmissibilities in this study.

The seat effective amplitude transmissibility (SEAT) offers a general measure of the seat performance in terms of the attenuation of the vertical vibration over the whole spectrum of the vibration inputs. The SEAT value is defined as the ratio of the weighted root-mean square value of the vertical acceleration measured at the seat pan (a_{wseat}) to that measured at the seat base (a_{wfloor}) according to ISO 10326-1:2016 as follows:

$$SEAT = a_{w_{seat}}/a_{w_{floor}} \tag{5.2}$$

The degree of nonlinearity due to the changed excitation magnitude in the "primary-axis", reflected by the change of the transmissibility of the seat with seated subject, was quantified using R_{nl_ilmTR} and PC_{ilmTR}, which are defined as follows:

$$R_{nl\_ilmTR} = \frac{f_{TR0.25}}{f_{TR1.0}} \tag{5.3}$$

$$PC_{ilmTR} = \frac{(TR_{0.25} - TR_{1.0})}{TR_{0.25}} \times 100\% \tag{5.4}$$

Where the abbreviation "*TR*" in the subscripts indicates the change of the seat transmissibility; $f_{TR0.25}$ and $f_{TR1.0}$ are the fundamental resonance frequency of the seat transmissibility measured when the excitation magnitude in the "primary-axis" was 0.25 and 1.0 ms^{-2} r.m.s., respectively; $TR_{0.25}$ and $TR_{1.0}$ are the modulus associated with the fundamental resonance frequency of the seat transmissibility measured under excitation magnitude of 0.25 and 1.0 ms^{-2} r.m.s. in the "primary-axis", respectively.

Friedman two-way analysis of variance was adopted to study the significance of the effect of the excitation magnitudes or the angle of the backrest inclination on the seat transmissibilities among the 12 subjects. The definitions of null hypothesis and *p*-value are the same as in Chapter 3. Spearman's rank correlation coefficient was used to study the correlation between the resonances of the seat transmissibilities at the seat pan and backrest in each direction that were located in the same frequency range. The null hypothesis of the Spearman's rank correlation test was that there was zero correlation between them.

5.3 Results

5.3.1 Transmissibilities of the suspension mechanism with inert masses under tri-axial vibration

The in-line fore-aft transmissibility of the suspension mechanism exhibited a fundamental resonance in the vicinity of 7 Hz. When the 75 kg inert mass was loaded, a second resonance could be identified between 27 and 32 Hz (Figure 5.4). When the magnitude of single-axial fore-aft excitation was 0.25 ms^{-2} r.m.s., the transmissibility exhibited two peaks instead of one in the vicinity of 7 Hz. The fundamental resonance frequency was hardly affected by the magnitudes of excitation. The second resonance frequency tended to decrease with the increase of the fore-aft excitation magnitude.

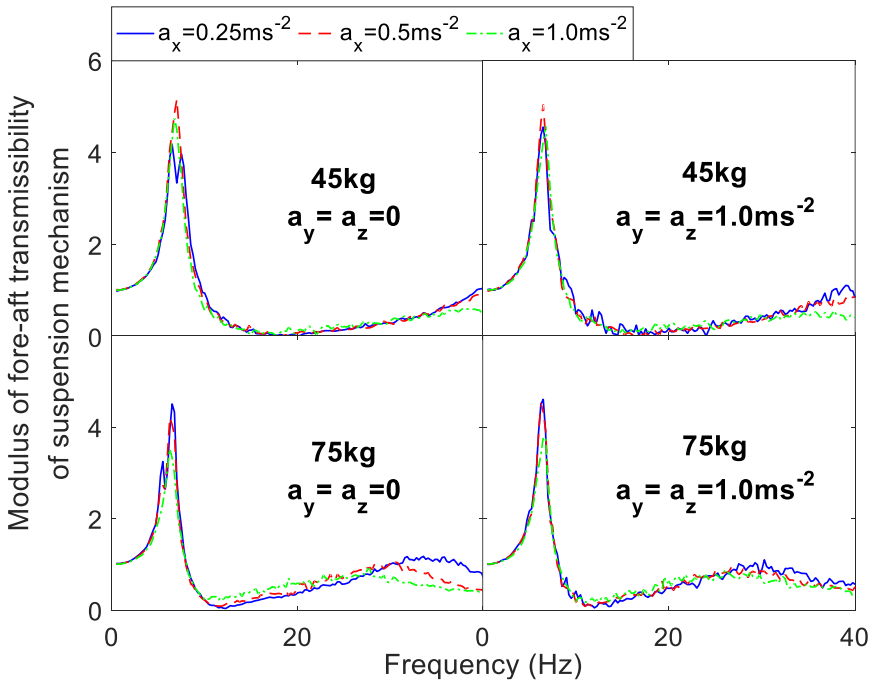

Figure 5.4 In-line fore-aft transmissibility of the suspension mechanism measured with inert masses under single- and tri-axial vibration: the effect of the fore-aft excitation magnitude

The in-line lateral transmissibility of the suspension mechanism exhibited two resonances below 40 Hz: the fundamental resonance between 5.25 and 6.5 Hz and the second resonance between 21 and 25 Hz. With the increase of the lateral excitation magnitude, both resonance frequencies tended to decrease, but the decrease was less evident when the excitation magnitude in x and z-axis were 1.0 ms^{-2} r.m.s. (Figure 5.5).

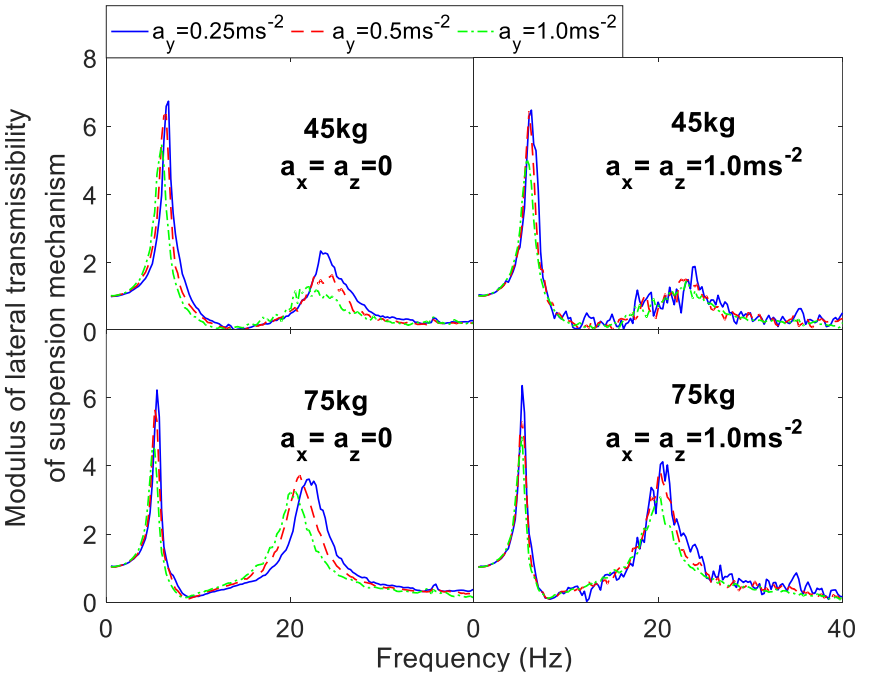

Figure 5.5 In-line lateral transmissibility of the suspension mechanism measured with inert masses under single- and tri-axial vibration: the effect of the lateral excitation magnitude

The in-line vertical transmissibility of the suspension mechanism exhibited one fundamental resonance between 2.25 and 12 Hz (Figure 5.6), which decreased dramatically with the increase of the vertical excitation magnitude, especially under single-axial vertical excitation. When the excitation magnitudes in x and y-axis were 1.0 ms^{-2} r.m.s., the decrease was smaller.

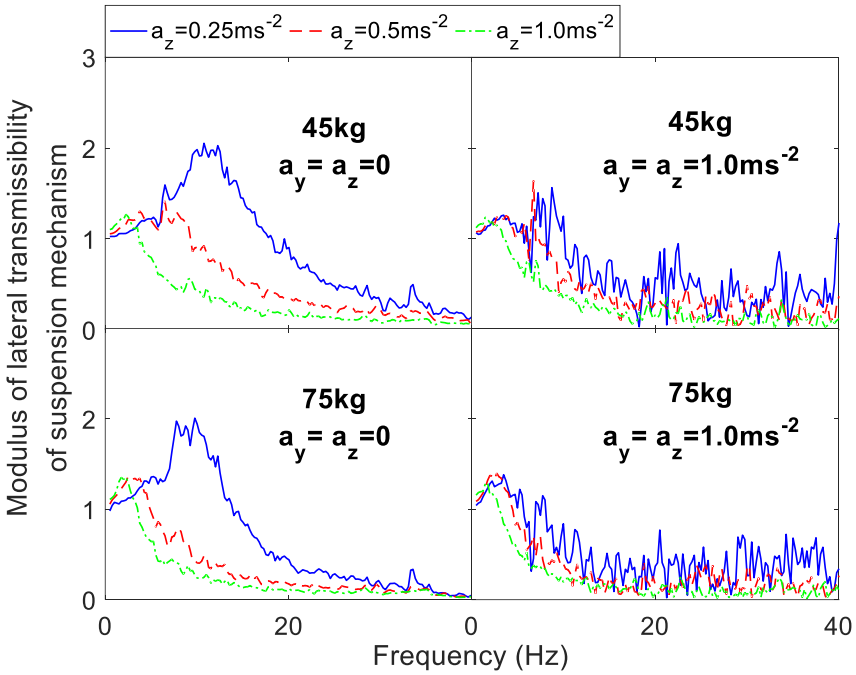

Figure 5.6 In-line vertical transmissibility of the suspension mechanism measured with three inert masses under single- and tri-axial vibration: the effect of the vertical excitation magnitude

5.3.2 Transmissibilities of the suspension seat with loaded inert masses under tri-axial vibration

5.3.2.1 Fore-aft transmissibility at the seat pan of the suspension seat with loaded inert masses

When the suspension seat was loaded with inert masses, the in-line fore-aft transmissibility at the seat pan exhibited a fundamental resonance between 3.5 and 4.75 Hz, a second resonance between 11 and 13 Hz and a third resonance between 18.5 and 23.75 Hz (Figure 5.7). With the increase of the fore-aft excitation magnitude, the frequencies of all three resonance frequencies tended to decrease, which was more obvious under single-axial fore-aft excitation than under tri-axial excitation.

With the increase of the excitation magnitude in the "secondary-axes" (y and z-axis), the fundamental resonance frequency of the in-line fore-aft transmissibility at the seat pan tended to decrease slightly (Figure 5.8, only the data up to 10 Hz is shown for clarity), especially when loaded

with the 75kg inert mass and when the vertical excitation magnitude was 0.25 ms^{-2}. When the vertical excitation magnitude was 1.0 ms^{-2} r.m.s., such an effect was much smaller.

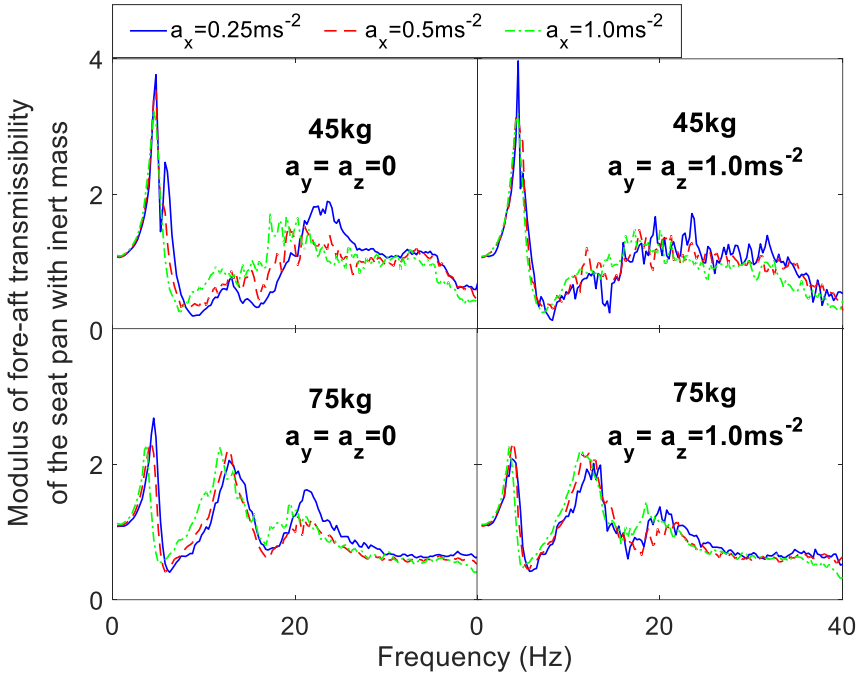

Figure 5.7 In-line fore-aft transmissibility at the seat pan measured with three inert masses under single- and tri-axial vibration: the effect of the fore-aft excitation magnitude

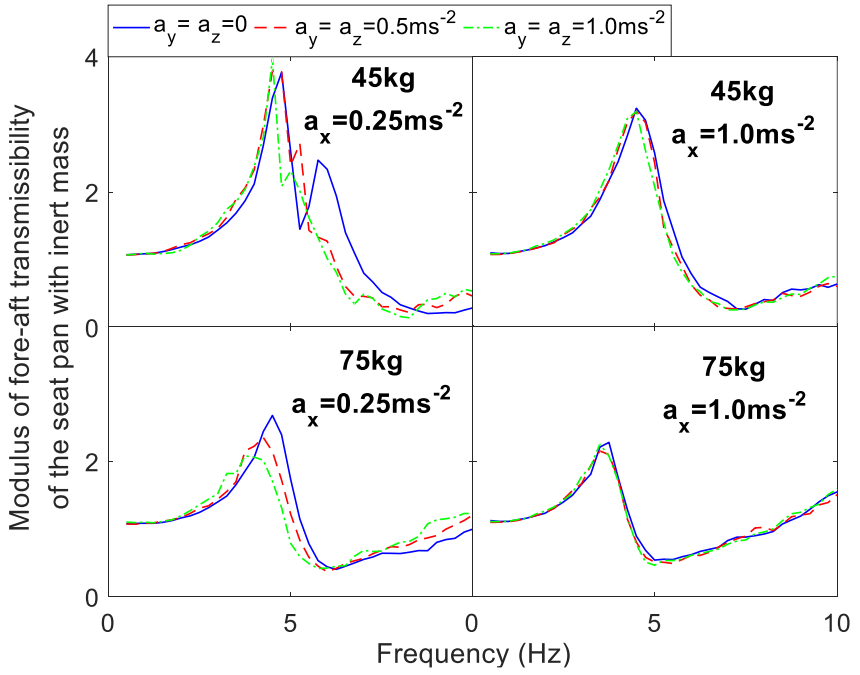

Figure 5.8 In-line fore-aft transmissibility at the seat pan measured with three inert masses under single- and tri-axial vibration: the effect of excitation magnitude in the “secondary-axes”

5.3.2.2 Lateral transmissibility at the seat pan of the suspension seat with loaded inert masses

The modulus of the in-line lateral transmissibility at the seat pan exhibited a fundamental resonance between 3.75 and 5.25 Hz, a second resonance between 15 and 15.25 Hz and a third resonance between 24.25 and 26.75 Hz when the seat was loaded with inert mass (Figure 5.9). With the increase of the lateral excitation magnitude, the moduli associated with all three resonance frequencies generally tended to decrease.

The excitation magnitude in the "secondary-axes" hardly affected the fundamental resonance of the in-line lateral transmissibility at the seat pan.

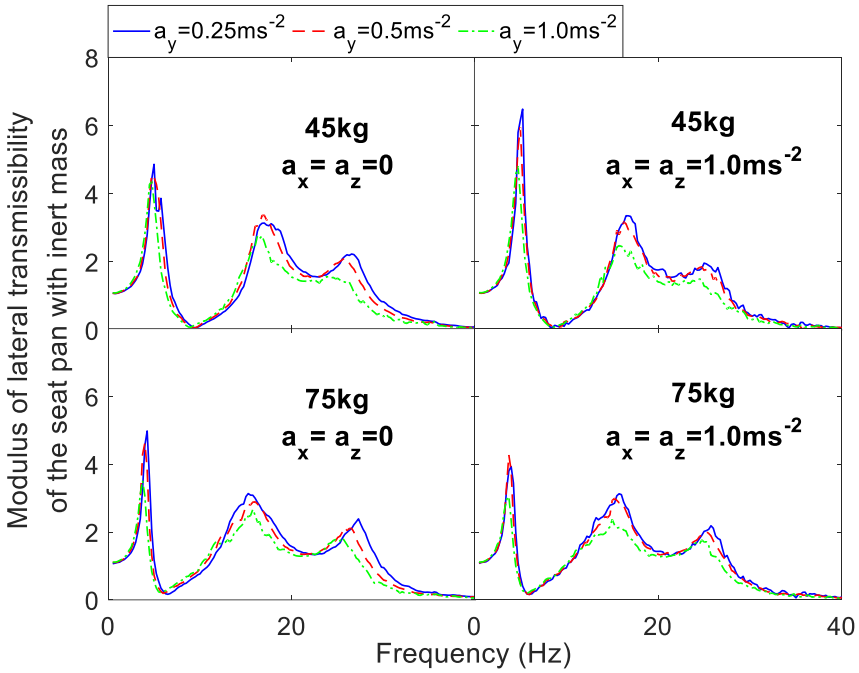

Figure 5.9 In-line lateral transmissibility at the seat pan measured with three inert masses under single- and tri-axial vibration: the effect of the magnitude of the lateral excitation

5.3.2.3 Vertical transmissibility at the seat pan of the suspension seat with loaded inert masses

When loaded with inert masses, the in-line vertical transmissibility at the seat pan generally exhibited a fundamental resonance between 2.25 and 9.75 Hz (Figure 5.10). With the increase of the vertical excitation magnitude, the fundamental resonance frequency and the associated modulus tended to decrease. Figure 5.11 shows that when the vertical excitation magnitude was 0.25 ms^{-2}, the increase of the excitation magnitude in the "secondary-axes" (x and y-axis) led to an obvious decrease of the resonance frequency of the in-line vertical transmissibility at the seat pan.

When the vertical excitation magnitude was 1.0 ms^{-2} r.m.s., the effect of the excitation magnitude in the "secondary-axes" was very small.

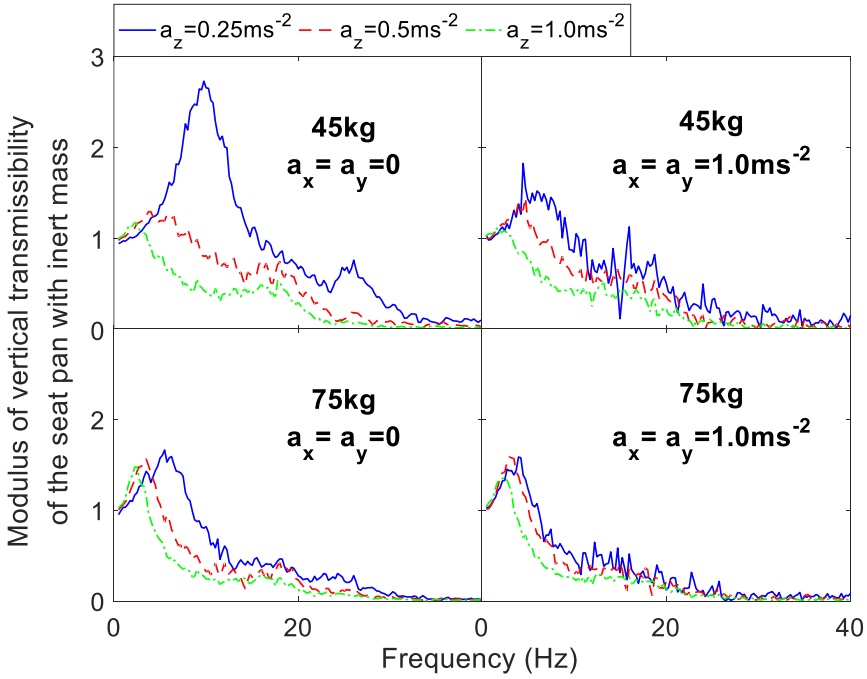

Figure 5.10 In-line vertical transmissibility at the seat pan measured with three inert masses under single- and tri-axial vibration: the effect of the magnitude of the vertical excitation

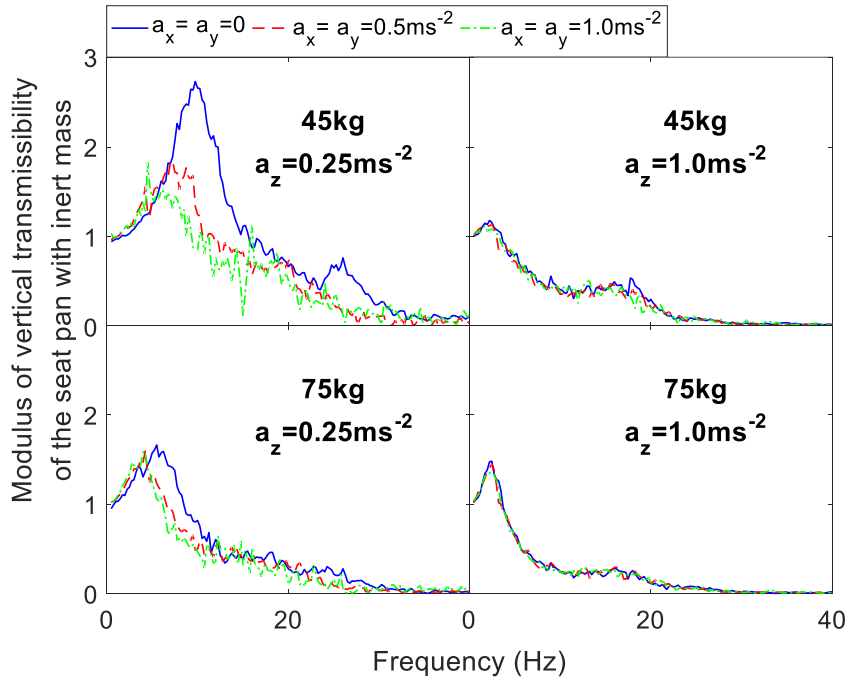

Figure 5.11 In-line vertical transmissibility at the seat pan measured with three inert masses under single- and tri-axial vibration: the effect of excitation magnitude in the "secondary-axes"

5.3.3 Transmissibility of the suspension seat with seated subject in the horizontal directions under tri-axial vibration

Figure 5.12 shows the horizontal transmissibilities at the seat pan and backrest of the suspension seat with the seated subjects under combined 0.5 ms^{-2} fore-aft, 0.5 ms^{-2} lateral and 0.5 ms^{-2} (r.m.s.) vertical excitation (the legend of this figure is the same as that of Figure 3.4). Despite the inter-subject variabilities, both the in-line fore-aft transmissibility at the backrest and at seat pan with seated subjects generally exhibited three resonances below 40 Hz, respectively: at around 3 Hz, between 12 and 20 Hz, and between 30 and 40 Hz. The in-line lateral transmissibilities at the seat pan and backrest generally exhibited three resonances at around 1.5 Hz, 10 Hz, and 22 Hz, respectively. The moduli associated with the fundamental resonance frequency of the lateral transmissibilities at the seat pan and backrest were much smaller compared to those at the second and third resonance frequencies.

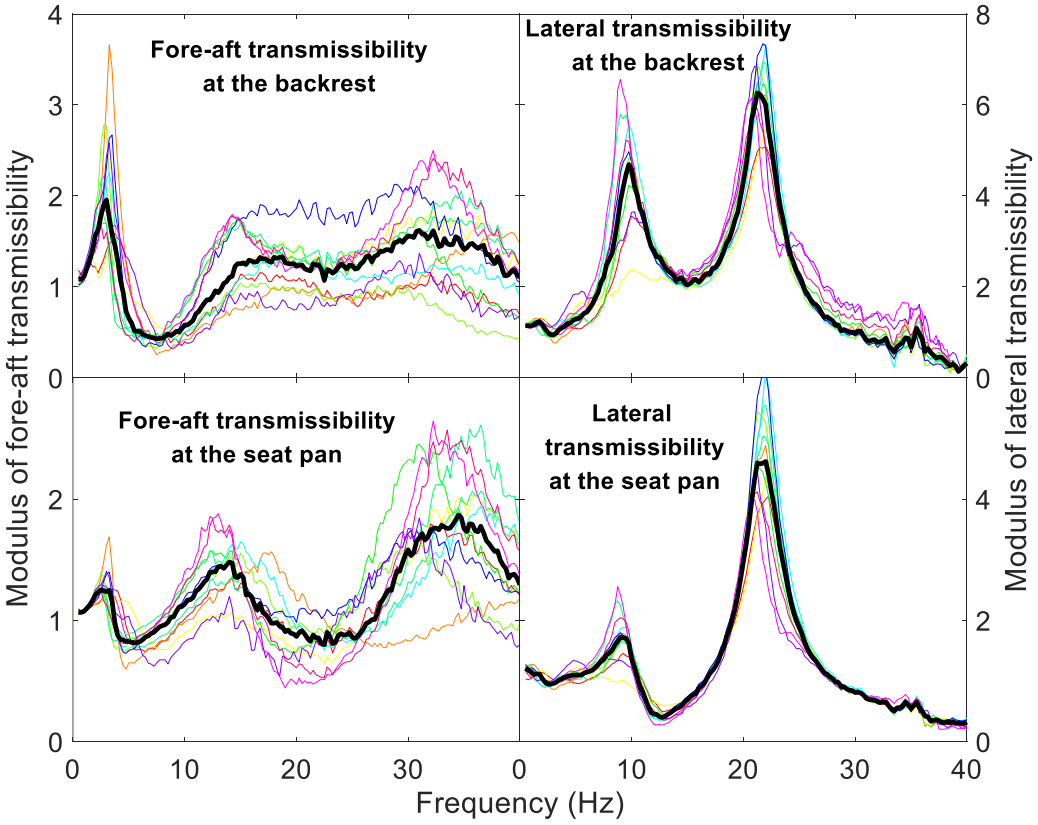

Figure 5.12 The seat transmissibilities in the horizontal directions with 12 subjects and the corresponding median transmissibilities (bold black curve) under tri-axial excitation with magnitude of 0.5 ms^{-2} r.m.s. in the x, y and z-axis. Left: fore-aft transmissibilities; right: lateral transmissibilities.

The median seat transmissibilities will be used to demonstrate the general characteristics of the tri-axial seating dynamics in the following sections, as they are capable of representing the general commonalities of the transmissibilities measured with different subjects. The transmissibilities with

the seated subject in the horizontal directions up to 20 Hz will be shown in the following figures to demonstrate the effect of the influencing factors more clearly.

5.3.3.1 Fore-aft transmissibilities of the suspension seat with seated subject under tri-axial vibration

With the increase of the fore-aft excitation magnitude, the frequency of the fundamental resonance of the fore-aft transmissibility at the backrest tended to decrease under both single-and tri-axial excitation (p<0.05 for 7 out of 9 test conditions), and under tri-axial excitation, the change of the fundamental resonance frequency became very small (Figure 5.13). The frequency of the second resonance also decreased with the increase of the fore-aft excitation magnitude.

For the transmissibility at the seat pan, the fundamental resonance frequency (p<0.05 for 8 out of 9 test conditions) tended to decrease with the increase of the fore-aft excitation magnitude, and when the seat-occupant system was exposed to tri-axial vibration, such decrease became less obvious. The decrease of the second resonance frequency with increased fore-aft excitation magnitude was only obvious under single-axial fore-aft excitation.

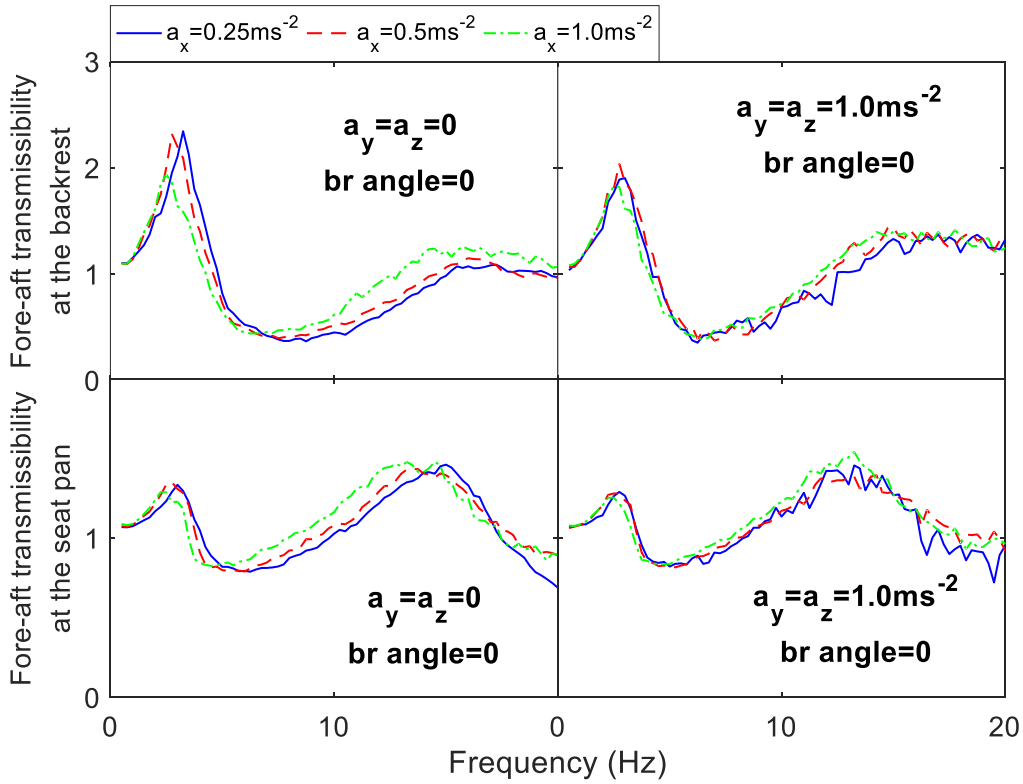

Figure 5.13 Median in-line fore-aft seat transmissibility measured with subjects under single-axial and tri-axial vibration: the effect of the fore-aft excitation magnitude

Figure 5.14 shows that, the increase of the excitation magnitude in the y and z-axis also led to a decrease of the fundamental resonance frequency and the associated modulus of the fore-aft

transmissibilities at the backrest and the seat pan (p<0.05 when the fore-aft excitation magnitude was 0.25 and 0.5 ms^{-2} r.m.s.). With the increased excitation magnitude in the y and z-axis, the modulus associated with the second resonance frequency of the transmissibility at the backrest tended to increase, and the second resonance frequency of that at the seat pan tended to decrease, which were only obvious when the fore-aft excitation magnitude was 0.25 ms^{-2} r.m.s.

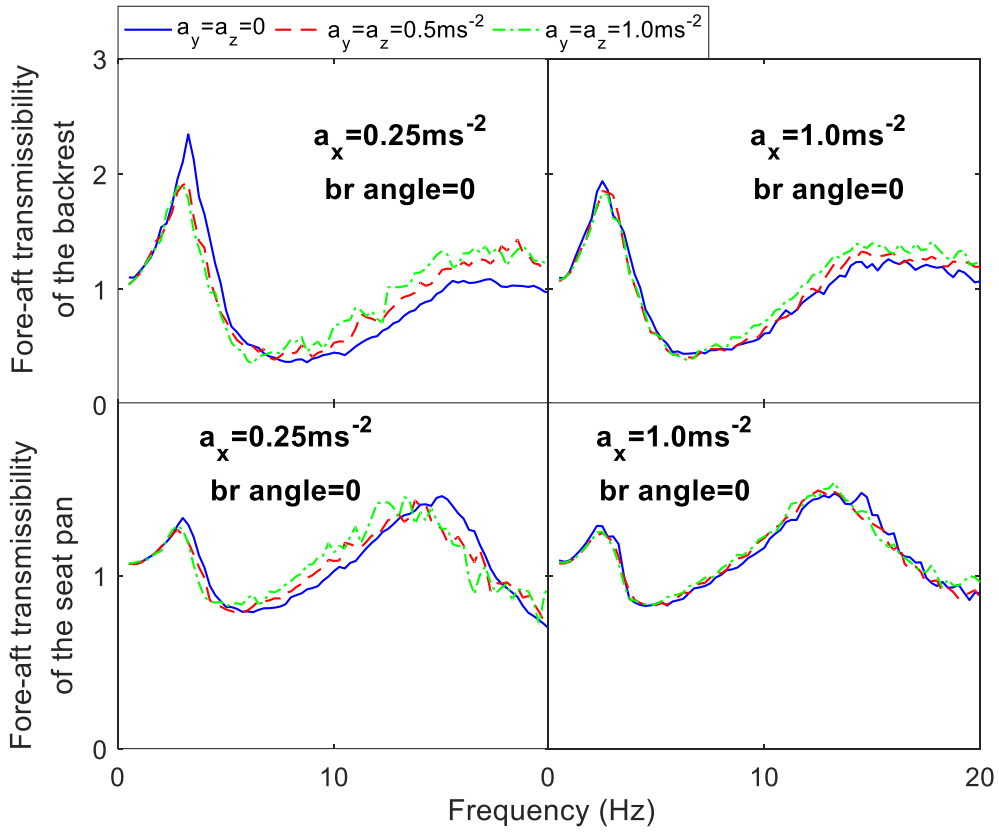

Figure 5.14 Median in-line fore-aft seat transmissibility measured with subjects under single-axial and tri-axial vibration: the effect of the excitation magnitude in the "secondary-axes"

The fundamental resonance frequencies of the transmissibilities at the backrest (p>0.05) and seat pan (p<0.05 when the excitation magnitude was 0.25 and 0.5 ms^{-2} r.m.s.) slightly increased with the increase of the backrest inclination angle under single-axial excitation (Figure 5.15). With tri-axial excitation, such an effect was not significant.

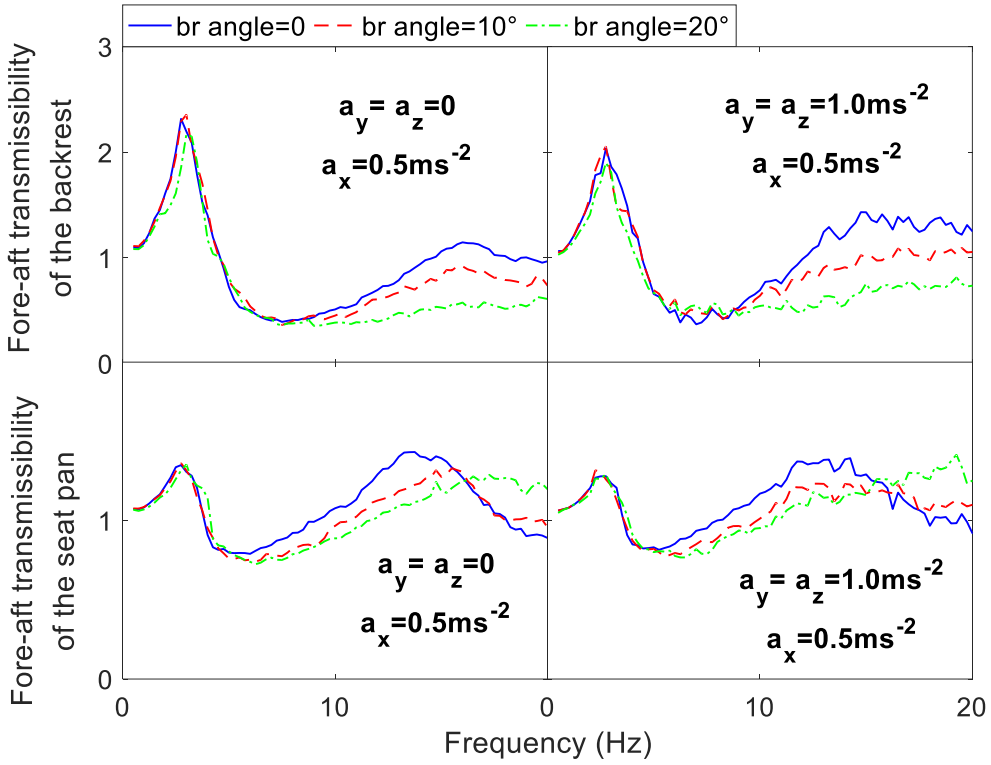

Figure 5.15 Median in-line fore-aft seat transmissibilities at the backrest and seat pan with subjects under single-axial and tri-axial vibration: the effect of the angle of backrest inclination

5.3.3.2 Lateral transmissibilities of the suspension seat with seated subject under tri-axial vibration

The fundamental resonances of the lateral transmissibilities at the seat pan and backrest were hardly affected by the excitation magnitudes or the backrest inclination angle.

Figure 5.16 shows that the second resonance frequency of the lateral transmissibility at the seat pan (p<0.05 when the excitation magnitude in x and z-axis were 0 or 0.5 ms^{-2} r.m.s.) and that at the backrest (p<0.01 under all conditions) both tended to decrease with the increase of the lateral excitation magnitude. When the excitation magnitude in x and z-axis were 1.0 ms^{-2} r.m.s., the changes of the resonance frequencies due to the increase of lateral excitation magnitude were very small.

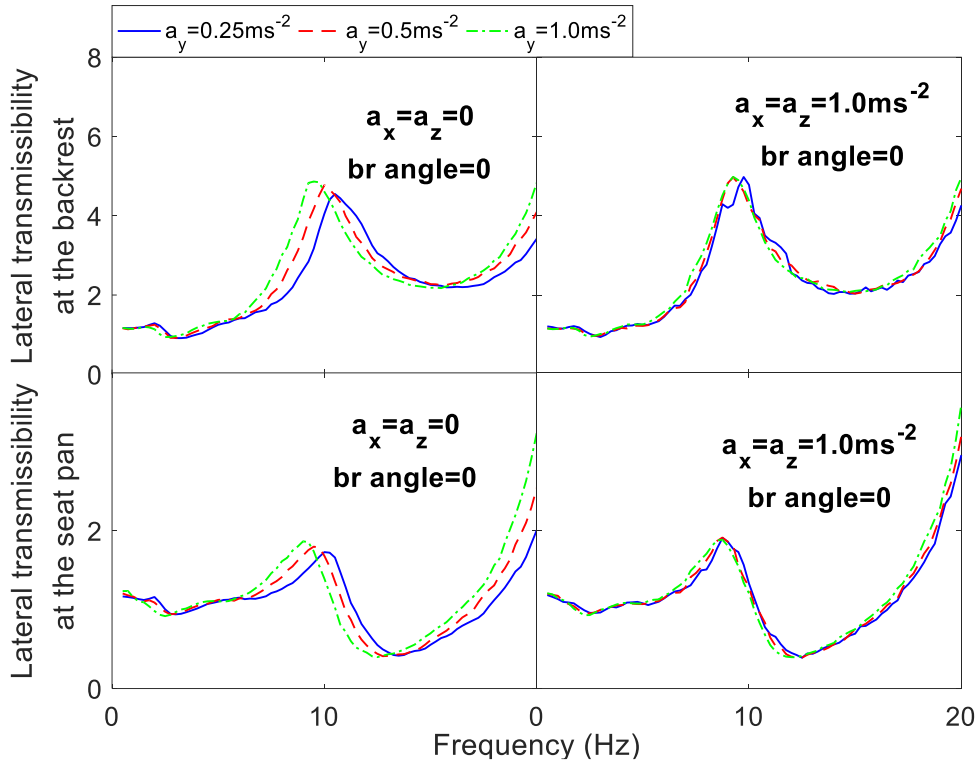

Figure 5.16 Median in-line lateral seat transmissibility measured with subjects under single-axial and tri-axial vibration: the effect of the lateral excitation magnitude

Figure 5.17 shows that the second resonance frequencies of the in-line lateral transmissibilities at the backrest (p<0.05 under all conditions) and the seat pan (p<0.05 for 8 out of 9 conditions) tended to decrease with the increase of the excitation magnitude in x and z-axis. However, when the lateral excitation magnitude was 1.0 ms^{-2} r.m.s., such a decrease was relatively small. The modulus associated with the second resonance at the seat pan also tended to increase with the increase of the magnitude of "secondary-axes" excitations (p<0.05 for 7 out of 9 conditions). Figure 5.18 shows that the moduli associated with the second resonances of the in-line lateral transmissibilities at the seat pan and backrest decreased with the increased backrest inclination angle (p<0.05).

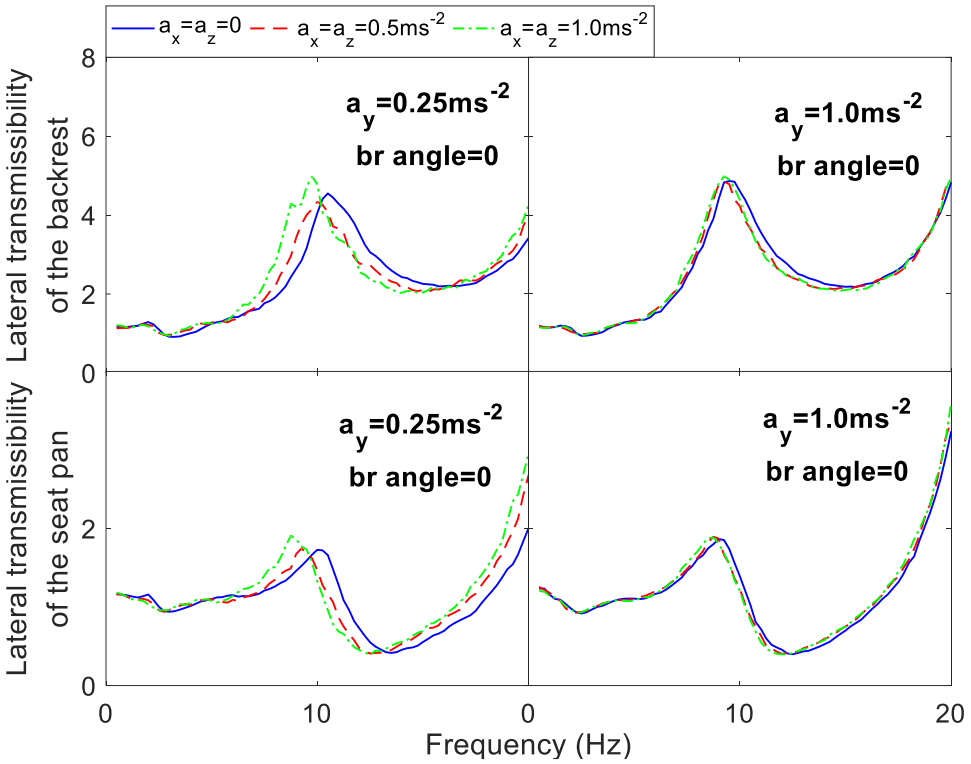

Figure 5.17 Median in-line lateral seat transmissibility measured with subjects under single-axial and tri-axial vibration: the effect of the excitation magnitude in the "secondary-axes"

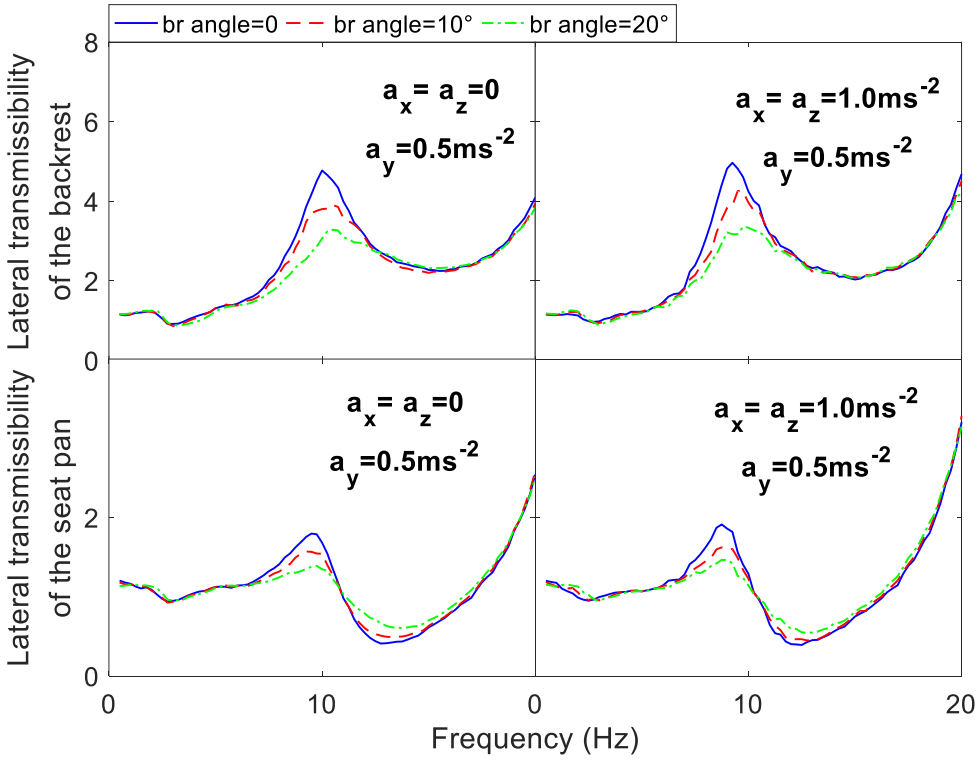

Figure 5.18 Median in-line lateral seat transmissibilities at the backrest and seat pan with subjects under single-axial and tri-axial vibration: the effect of the angle of backrest inclination

5.3.4 Vertical transmissibilities of the suspension seat with seated subject under tri-axial vibration

The in-line vertical transmissibility at the backrest of the suspension seat with seated subject generally exhibited a fundamental resonance between 2.25 and 3.75 Hz and a second resonance between 10 and 20 Hz when the vertical excitation was 0.25 ms^{-2} r.m.s. (Figure 5.19). The in-line vertical transmissibility at the seat pan of the suspension seat with seated subject generally exhibited a fundamental resonance between 2 and 5 Hz (Figure 5.19), and under single-axial vertical excitation, a second resonance existed in the vicinity of 20 Hz when the vertical excitation magnitude was 0.25 ms^{-2} r.m.s. The fundamental and second resonance frequencies of the vertical transmissibility at the backrest, and the fundamental resonance frequency of the in-line vertical transmissibility at the seat pan tended to decrease with the increase of the vertical excitation magnitude (p<0.01).

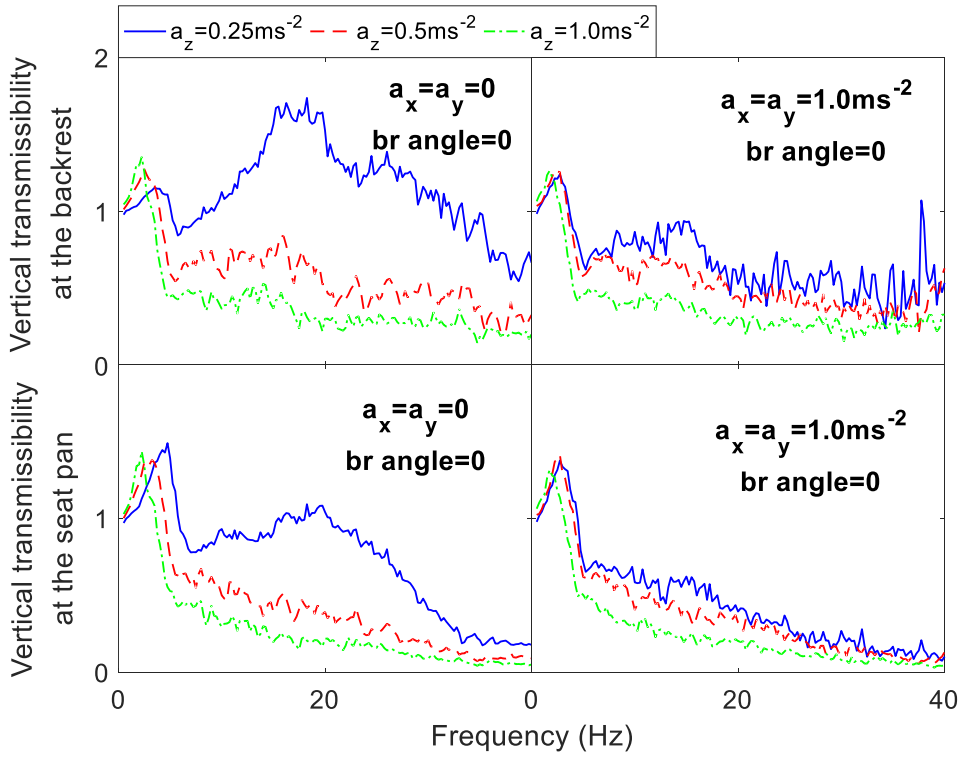

Figure 5.19 Median in-line vertical transmissibility of the suspension seat measured with subjects under single-axial and tri-axial vibration: the effect of the vertical excitation magnitude

For clarity, only the transmissibilities up to 20 Hz will be shown in the following figures to show the effect of the excitation magnitude in the "secondary-axes" (x and y-axis). Figure 5.20 shows that the fundamental resonance frequency of the vertical transmissibility at the backrest tended to decrease with the increase of the excitation magnitude in the "secondary-axes" under all conditions (p<0.05). When the vertical excitation magnitude was 0.25 ms^{-2} r.m.s., the modulus associated with

the second resonance frequency tended to decrease with the increase of the excitation magnitude in the "secondary-axes".

With the increase of the excitation magnitude in the x and y-axis, the fundamental resonance frequency of the in-line vertical transmissibility at the seat pan tended to decrease (p<0.01 for 6 out of 9 conditions). The 6 conditions in which such an effect was significant included those with upright backrest or when the vertical excitation magnitude was 0.25 ms^{-2} r.m.s. The modulus associated with the fundamental resonance of the vertical transmissibility at the seat pan decreased significantly under all conditions. When the vertical excitation magnitude was 1.0 ms^{-2} r.m.s., the effect of the excitation magnitude in the x and y-axis on the vertical transmissibilities at the seat pan and backrest became smaller compared to that under 0.25 ms^{-2} r.m.s. vertical excitation (Figure 5.20).

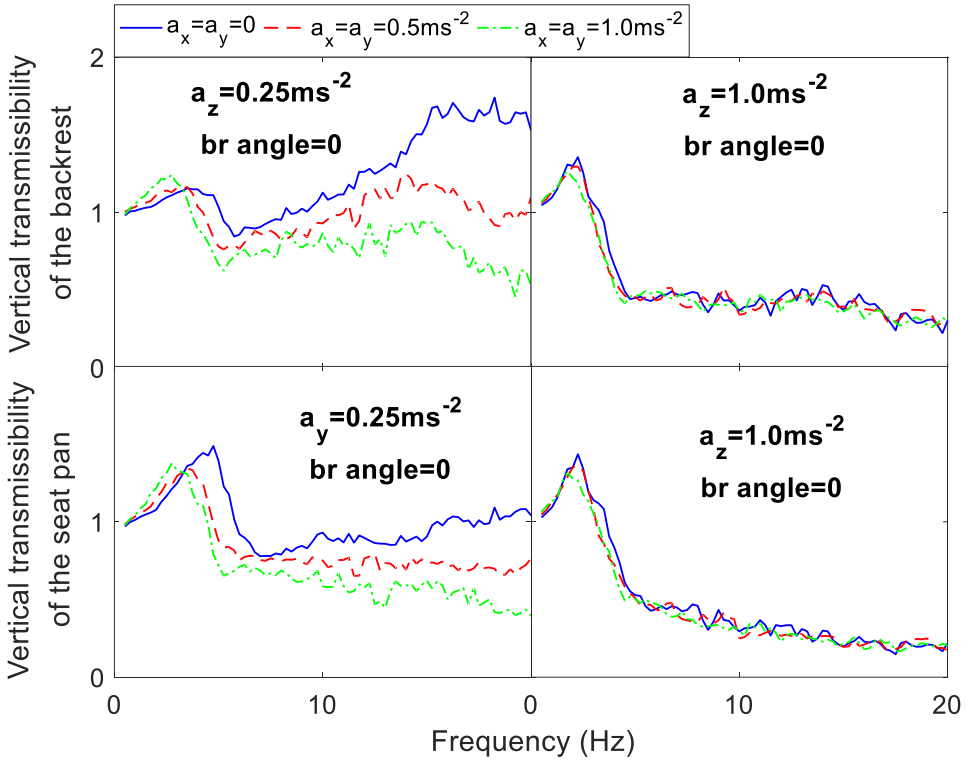

Figure 5.20 Median in-line vertical transmissibility at the backrest of the suspension seat measured with subjects under single-axial and tri-axial vibration: the effect of the magnitude of the excitation in the "secondary-axes" (x and y-axis)

The excitation magnitude in different axes also affected the SEAT value of the suspension seat in the vertical direction (Figure 5.21). With the increase of the vertical excitation magnitude, the SEAT value tended to become smaller. When the vertical excitation magnitude was 0.25 ms^{-2} r.m.s., the SEAT value measured with 1.0 ms^{-2} r.m.s. excitation in the "secondary-axes" was greater compared to that measured under single-axial vertical excitation. When the vertical excitation magnitude was 0.5 or 1.0 ms^{-2} r.m.s., the SEAT value tended to increase with the increase of the excitation

magnitude in the "secondary-axes". The effects of the excitation magnitude in the "primary-axis" and "secondary-axes" on the vertical SEAT value of the suspension seat were both significant under all conditions (p<0.01).

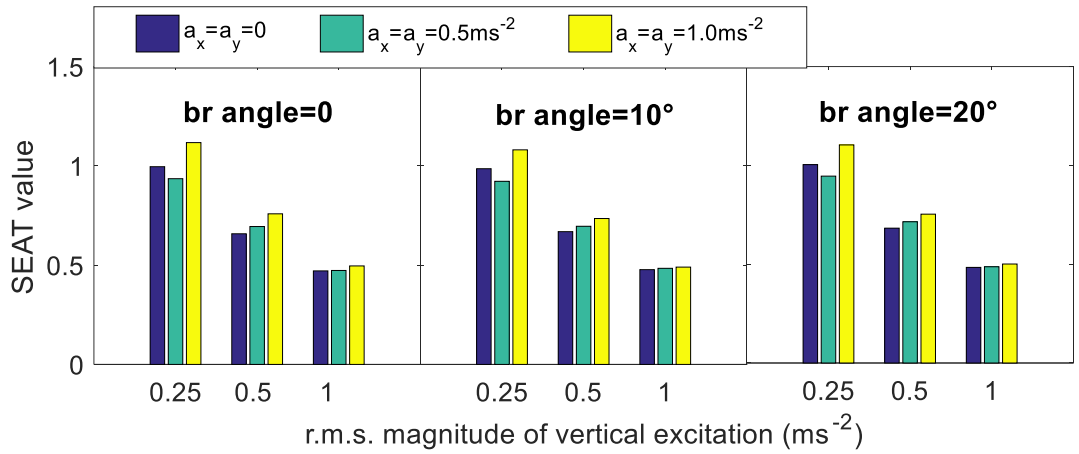

Figure 5.21 Median SEAT value measured with subjects under single-axial and tri-axial vibration: the effect of the excitation magnitude in the "secondary-axes" (x and y-axis)

The increase of the backrest inclination angle generally led to an increase of the modulus associated with the fundamental resonance of the in-line vertical transmissibility at the backrest under all excitations (p<0.01; Figure 5.22, only the transmissibilities up to 10 Hz are shown for clarity). The modulus associated with the fundamental resonance of the in-line vertical transmissibility at the seat pan also increased with the increase of the backrest inclination angle under 0.25 ms^{-2} r.m.s. single-axial vertical excitation (p<0.05). Under tri-axial excitations, the effect of the backrest inclination angle on the in-line vertical transmissibility at the seat pan was small.

Furthermore, the effect of backrest inclination angle on the vertical SEAT value was generally small and, in most cases, insignificant (p<0.05 only for 3 out of 9 excitations).

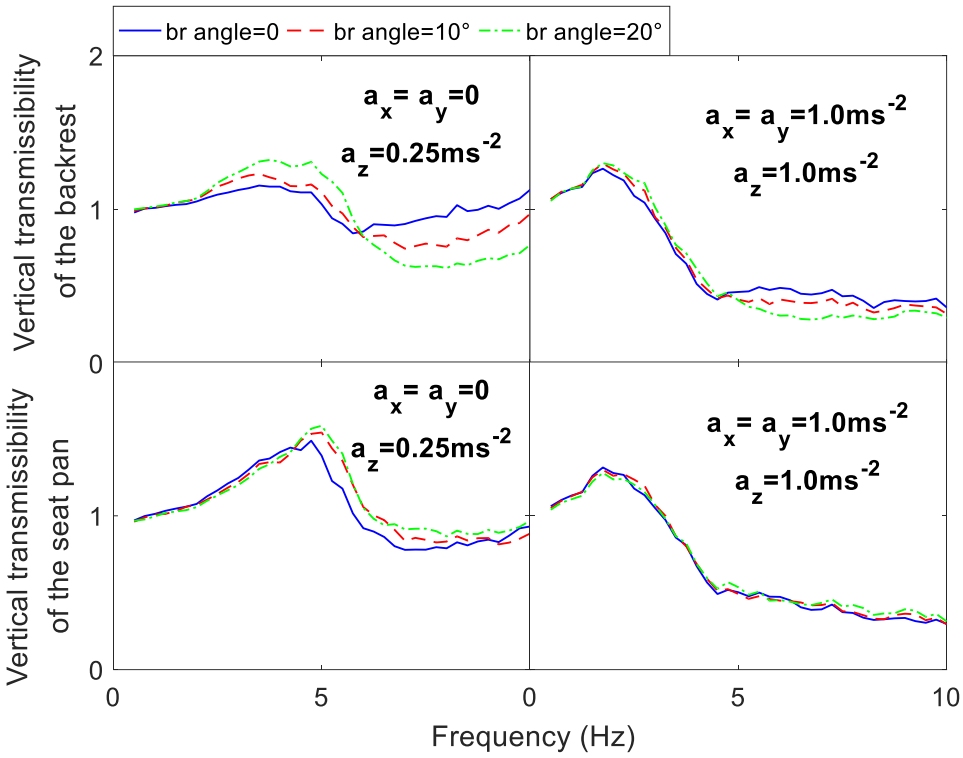

Figure 5.22 Median in-line vertical transmissibility of the suspension seat measured with subjects under single-axial and tri-axial vibration: the effect of the angle of backrest inclination

5.4 Discussion

5.4.1 The transmission of the vertical vibration through the suspension-seat-occupant system

The resonance frequency of the in-line vertical transmissibility of the suspension mechanism loaded with inert masses tended to decrease with the increase of the vertical excitation magnitude, which is consistent with the result reported by Qiu (2017). The in-line vertical transmissibility of the suspension seat pan with the loaded inert mass generally exhibited two resonances below 40 Hz, while the vertical transmissibility of the suspension mechanism only exhibited one resonance below 40 Hz. The existence of the second resonance may be related to the dynamic characteristic of the seat cushion. Both the in-line vertical transmissibilities at the seat pan and the backrest with the seated subject exhibited a fundamental resonance between 2 and 5 Hz, which is consistent with the results reported by Qiu (2017). As the human body is a highly-damped system, the modulus associated with fundamental resonance frequency of the seat transmissibility with the subject was lower compared to those with the loaded inert mass.

5.4.2 The transmission of horizontal vibration through the suspension-seat-occupant system

There have been no previous laboratory studies reporting the transmission of the horizontal vibration through the suspension-seat-occupant system via measuring the transmissibilities of the suspension mechanism and suspension seat in the horizontal directions. Figure 5.23 shows the comparison of the fore-aft and lateral transmissibilities measured on the suspension mechanism with inert mass (60 kg+18.8 kg=78.8 kg), the complete seat with inert mass (60 kg) and the complete seat with a seated subject (with a body mass of 78.6 kg). The subject was chosen for the comparison as the body mass supported by the seat pan was close to 60 kg (Qiu, 2012; Qiu, 2017). Thus, the total mass supported by the suspension mechanism in these three conditions are comparable. The seat transmissibilities shown in this figure are measured with upright backrest. It can be found in Figure 5.23 that the transmissibilities measured with the suspension mechanism, the seat with loaded inert mass and the seat with seated subjects were quite different from each other.

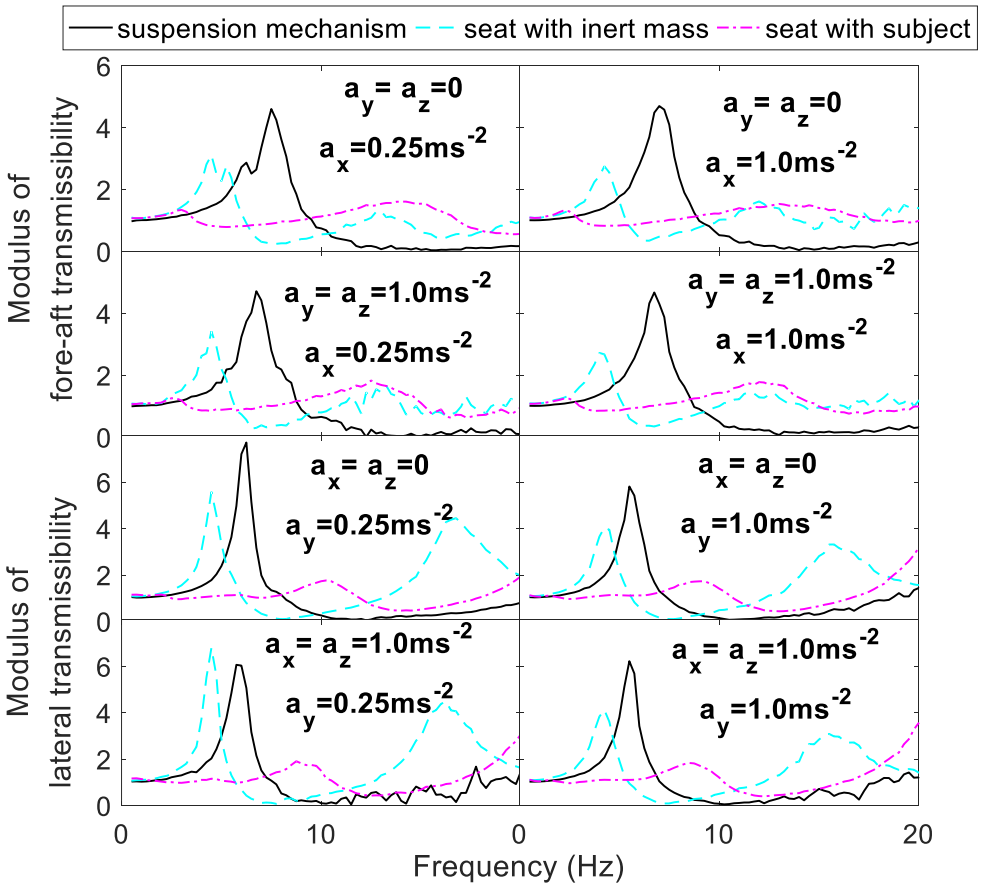

Figure 5.23 Comparison of the horizontal transmissibilities of the suspension mechanism with 78.8 kg inert mass, the transmissibility the suspension seat at the seat pan with 60 kg inert mass, and the transmissibility the suspension seat at the seat pan with 78.6 kg subject under single and tri-axial vibration

5.4.2.1 Transmission of the horizontal vibration through the suspension mechanism

The in-line fore-aft transmissibility of the suspension mechanism loaded with inert masses exhibited a fundamental resonance below 40 Hz (Figure 5.4), while the in-line lateral transmissibility of the suspension mechanism with loaded inert masses exhibited two resonances below 40 Hz under some of the test conditions (Figure 5.5). The fundamental resonance frequency of the fore-aft transmissibility of the suspension mechanism and that of the lateral transmissibility were similar, which may be related to a same vibration mode of the suspension mechanism. When the excitation magnitude in the fore-aft direction increased, the change of the fundamental resonance frequency of the fore-aft transmissibility of the suspension was small (Figures 5.4). Hence, the suspension mechanism can be regarded as a linear system in the fore-aft direction below 10 Hz.

5.4.2.2 Transmission of the horizontal vibration through the suspension seat with loaded inert mass

Figure 5.23 shows that the resonance frequencies of the horizontal transmissibilities of the suspension seat with inert masses ( ) are generally smaller compared to those of the suspension mechanism ( ). This may be due to the dynamic behaviour of the seat pan cushion. With the loaded inert mass, the in-line fore-aft transmissibility of the suspension seat at the seat pan exhibited two resonances below 20 Hz, while the fore-aft transmissibility of the suspension mechanism exhibited one fundamental resonance in the same region (Figure 5.23). Similarly, the in-line lateral transmissibility of the suspension seat at the seat pan loaded with inert mass exhibited two resonances below 20 Hz while that of the suspension mechanism exhibited one (Figure 5.23). The existence of the extra resonances of the fore-aft and lateral transmissibilities of the suspension seat loaded were possibly related to the dynamic properties of the seat pan cushion.

5.4.2.3 Transmission of the horizontal vibration through the suspension seat with seated subject

With the loaded inert mass, the fundamental resonance frequencies of in-line fore-aft and lateral transmissibilities of the suspension seat were both at around 5 Hz, and the associated moduli were greater than 2, whereas the moduli at the fundamental resonance frequencies of the fore-aft and lateral transmissibility at the seat pan of the suspension seat was close to 1 when the subject was seated (, Figure 5.23). Such a difference may be attributed to the biodynamic properties of the seated human body, such as the relatively high-level damping of the seated human body, and the interaction between the human body and the seat cushion.

5.4.3 The effect of the excitation magnitude on the transmissibilities of the suspension seat under tri-axial translational vibration

5.4.3.1 The effect of the excitation magnitude in the "primary-axis"

The increased excitation magnitude in each axis generally led to the decrease of the resonance frequencies of the seat transmissibility with loaded inert mass and that with seated subject in the same axis. Such a softening behaviour of the suspension-seat-occupant system was observed both under single-axial and tri-axial vibration, and both with upright backrest and inclined backrest.

With the increase of the vertical excitation magnitude, the SEAT value tended to decrease dramatically. This can be explained that when the vertical excitation magnitude increased, the suspension mechanism could better overcome the lock-up effect due to the friction and come to play, so the performance of the suspension seat in terms of the vibration attenuation in the vertical direction got improved.

5.4.3.2 The effect of the excitation magnitude in the "secondary-axes"

The transmissibilities of the suspension mechanism in the horizontal directions were hardly affected by the excitation magnitude in the "secondary-axes". It was found that with the increase of the excitation magnitude in the x and y-axis, the resonance frequency of the vertical transmissibility of the suspension mechanism tended to decrease. For example, with the 45kg inert mass, when the vertical excitation magnitude was 0.25 ms^{-2} r.m.s., the resonance frequency was 10 Hz when the excitation magnitude in the x and y-axis was 0, 8.25 Hz when that excitation magnitude was 0.5 ms^{-2} r.m.s., and 5.75 Hz when that excitation magnitude was 1.0 ms^{-2} r.m.s. This suggests that under tri-axial excitation with relatively high-level magnitude in the "secondary-axes", the suspension mechanism may also overcome the lock-up effect to some extent, even if the vertical excitation magnitude was at a relatively low level (e.g., 0.25 ms^{-2} r.m.s.). The friction that led to the lock-up effect may be in both vertical and horizontal directions.

The effect of the excitation magnitude in the "secondary-axes" on the transmissibilities of the suspension seat loaded with inert mass in different axes was different. The effect of the excitation magnitude in the x and z-axis on the lateral transmissibility was small. The effect of the excitation magnitude in the y and z-axis on the fundamental resonance frequency of the fore-aft transmissibility of the suspension seat with inert mass was evident when the inert mass was 75 kg and with 0.25 ms^{-2} r.m.s. fore-aft excitation (Figure 5.8). The effect of the excitation magnitude in x and y-axis on the vertical transmissibility of the seat with inert mass was also found to be evident when the vertical excitation magnitude was 0.25 ms^{-2} r.m.s. (Figure 5.11). These phenomena indicate that the seat cushion played an important role in the nonlinearity of the suspension seat

in the fore-aft and vertical direction. Similar to the human body, the dynamics of the suspension seat in the fore-aft and vertical directions may also be partly coupled due to its structure. For example, the connection between the backrest and the seat pan allowed the rotational motion of the backrest around the y-axis.

The effect of the excitation magnitude in the "secondary-axes" was also found on the transmissibilities of the suspension seat in all three directions with the seated subjects. For example, the resonances of the in-line fore-aft transmissibilities at the seat pan and backrest of the suspension seat with seated subjects were found to be affected by the excitation magnitude in "secondary-axes", especially when the fore-aft excitation magnitude was at a relatively low level. This was related to the nonlinearity of both the suspension seat and the seated human body in the fore-aft direction. Similar effects of the excitation magnitude in "secondary-axes" have also been found with the lateral seat transmissibilities. It was mainly attributed to the nonlinearity of the seated human body and the interaction between the seat and human body, as the lateral transmissibility of the suspension seat with loaded inert mass was only marginally affected by the excitation magnitude in the "secondary-axes".

With the seated subject, when the backrest was upright and exposed to single-axial vertical vibration, the fundamental resonance frequency of the in-line vertical transmissibility at the backrest was highly correlated with that at the seat pan (p<0.05, Spearman). This indicates that they may be related to a same mode of the seat-occupant system. Under tri-axial vibration, the correlation between the fundamental resonance frequency of the vertical transmissibility at the backrest and that at the seat pan became insignificant under some of the excitation magnitudes, such as when the of excitation magnitudes in the x, y and z-axis were all 1.0 ms^{-2} (p>0.05, Spearman). This indicates that the excitation in the "secondary-axes" affected the coupling of the dynamic response of the seat-occupant system at the seat pan and at the backrest.

The SEAT value of the suspension seat in the vertical direction was also affected by the excitation magnitude in the "secondary-axes" (x and y-axis). When the excitation magnitude in the x and y-axis increased, the SEAT value tended to increase when the magnitude of the vertical excitation was 0.5 and 1.0 ms^{-2} r.m.s. This may be explained that when the excitation magnitude in the x and y-axis increased, the motion of the seated human body in the vertical direction would tend to increase due to coupling of the biodynamic response in the vertical and fore-aft direction (see Chapter 3). With high-level excitation magnitude in the x-axis, the motion of the seated human body in the vertical di-rection may have increased due to such a coupling, so the vertical acceleration measured at the seat pan would increase. As the vertical acceleration at the seat base remained unchanged, the SEAT-value would increase.

5.4.4 The effect of the backrest inclination angle on the transmissibilities of the suspension seat under tri-axial translational vibration

The backrest inclination angle was found to affect the in-line fore-aft transmissibilities both at the seat pan and backrest of the suspension seat in the current study when the subject was seated. When the backrest inclination angle increased, the modulus of the in-line fore-aft transmissibility at the backrest above 10 Hz tended to decrease, suggesting an increase of the system damping in the frequency range above 10 Hz. Similarly, the moduli associated with the second resonance of the in-line lateral transmissibility at the backrest of the suspension seat with subject decreased with the increased backrest inclination angle. These results may be attributed to the increased interaction between the human body and the backrest with the increase of the backrest inclination angle, which means that the damping of the backrest cushion and the human body could play a more important role in affecting the transmissibility at the backrest.

In the current study, when the backrest was upright, the correlation between the frequency of the fundamental resonance of the in-line fore-aft transmissibility at the seat pan and that at the backrest was found to be significant (p<0.05, Spearman) only in 3 out of 9 conditions with different excitation magnitudes, while when the backrest was inclined by 10° and 20°, that correlation was found to be significant in 12 out of 18 conditions. This may be explained that when the backrest was inclined, the coupling between the backrest and the upper human body was stronger, while that between seat pan and the human body was still at a high level. So, the correlation between the fundamental resonance of the fore-aft transmissibility at the seat pan and that at the backrest was significant in more conditions compared to that when the backrest was upright.

The backrest inclination angle also affected the transmission of the vertical vibration through the suspension-seat-occupant system. The modulus associated with the resonance of the in-line vertical transmissibility at the backrest tended to increase with the increase of the backrest inclination angle. Such an increase may be due to the fact that the backrest served as a source of excitation to the seated human body, and the vertical excitation applying to the human body from the backrest would increase with the increase of the backrest inclination angle. On the other hand, the increase of the backrest inclination angle only led to a slight increase of the fundamental resonance frequency of the in-line vertical transmissibility at the seat pan, especially when the vertical excitation magnitude was 0.5 or 1.0 ms^{-2} r.m.s. The change of the seat transmissibility at the seat pan and backrest with the increased backrest inclination may be related the change of the vertical apparent masses at the seat pan and backrest (Chapter 3 and 4), but was also affected by the dynamic behaviour of the seat cushion and the suspension mechanism. When the excitation magnitude at the seat base was low, the suspension mechanism was locked-up due to the friction,

and the vibration transmitted from the seat base to the seat cushion was not much altered by the suspension mechanism at low frequency (Qiu, 2017). So, the dynamic behaviour of the human body and the seat cushion played an important role in determining the dynamic behaviour of the seat-occupant system. Under excitation with high-level magnitudes, the lock-up effect was overcome and the dynamic characteristic of the suspension-seat-occupant system was largely depending on the dynamic behaviour of the suspension mechanism (Qiu, 2017). Meanwhile, the effect of the change in the apparent mass of the human body due to the change of the backrest inclination angle became smaller.

5.4.5 Interactive effects among the influencing factors on the suspension seat transmissibilities under tri-axial translational vibration

Similar to the biodynamic response, interactive effects also existed between the excitation magnitude in the "primary-axis" and that in the "secondary-axes" on the resonances of the transmissibilities of the suspension seat. For example, Table 5.1 and Table 5.2 show the effect of the excitation magnitudes in x and y-axis and the angle of backrest inclination on the degree of the nonlinearity, i.e., the R_{nl_ilmTR} and PC_{ilmTR}, of the in-line vertical transmissibility of the suspension seat at the seat pan with the seated subject.

Table 5.1 Median value (12 subjects) of R_{nl_ilmTR} of the in-line vertical transmissibility of the suspension seat at the seat pan with different excitation magnitudes in x and y-axis and different backrest inclination angles, and the statistical significance of the effects (*p*-value, Friedman) of the excitation magnitudes in x and y-axis and the angle of backrest inclination

Median value of R_{nl_ilmTR}		**Backrest inclination angles**			***p*-value (effect of backrest inclination)**
		0°	**10°**	**20°**	
excitation magnitude in x and y-axis (r.m.s.)	**0 ms^{-2}**	*2.375*	*2.375*	*2.500*	ns
	0.5 ms^{-2}	*-0.125*	*0*	*-0.250*	ns
	1.0 ms^{-2}	*0*	*0*	*0*	ns
***p*-value (effect of the excitation magnitude in x and y-axis)**		**	**	**	

Table 5.2 Median value (12 subjects) of PC_{ilmTR} of the in-line vertical transmissibility of the suspension seat at the seat pan with different excitation magnitudes in x and y-axis and dfferent backrest inclination angles, and the statistical significance of the effects (*p*-value, Friedman) of the excitation magnitudes in x and y-axis and the angle of backrest inclination

Median value of PC_{ilmTR}		**Backrest inclination angles**			***p*-value (effect of backrest inclination)**
		0°	**10°**	**20°**	
excitation magnitude in x and y-axis (r.m.s.)	**0 ms^{-2}**	*10.093%*	*9.804%*	*12.835%*	ns
	0.5 ms^{-2}	*-5.558%*	*-5.875%*	*-4.331%*	ns
	1.0 ms^{-2}	*2.905%*	*2.376%*	*2.109%*	ns
***p*-value (effect of the excitation magnitude in x and y-axis)**		**	**	**	

Table 5.1 and Table 5.2 show that, with the increase of the excitation magnitudes in x and y-axis, the value of the R_{nl_ilmTR} and PC_{ilmTR} at the seat pan tended to decrease, and such an effect was significant (p<0.05) under all backrest inclination angles. Such an interaction between the excitation magnitudes in different directions on the seating dynamics may be attributed to the dynamics of both the suspension seat and the seated human body, as both of them was found to be affected by the excitation magnitudes in both the “primary-axis” and “secondary-axes”. The effect of the backrest inclination angle on the R_{nl_ilmTR} and PC_{ilmTR} of the vertical transmissivity at the seat pan was not significant.

For the seat transmissibility at the backrest in the vertical direction, the effect of the excitation magnitude in the “secondary-axes” on the R_{nl_ilmTR} and PC_{ilmTR} was similar to those at the seat pan, and was significant under all backrest inclination angles. Nevertheless, the effect of backrest inclination angle was found to be significant in 2 out of 6 cases (instead of non-significant for all cases), which indicates that the backrest inclination affected the seating dynamics at the backrest significantly in more cases than that at the seat pan. This indicates the importance of the increased interaction between the backrest and the seated human body when the backrest inclination angle increased.

The interaction between the excitation magnitudes in different directions was also found in the transmissibilities of the suspension seat in the horizontal directions. The decrease of the resonance frequencies due to the increase of the fore-aft excitation magnitude under tri-axial vibration became smaller compared to that under single-axial fore-aft excitation. The effect of the of lateral

excitation magnitude on the resonance frequencies of the lateral transmissibilities of the suspension seat was also affected by the excitation magnitude in “secondary-axes”.

In general, the in-line transmissibility of the suspension seat in either of the three axes was a function of the excitation magnitudes in all the three translational axes. This behaviour is related to the dynamic characteristics of both the suspension seat and the seated human body.

5.5 Conclusion

In the current study, the in-line fore-aft, lateral and vertical transmissibilities of the suspension mechanism, the suspension seat with loaded inert mass, and the suspension seat with the seated subject were measured under single and tri-axial excitations with various excitation magnitudes and with different backrest inclination angles. The results show that similar to the widely studied vertical excitation, the transmission of the horizontal vibration through the suspension-seat-occupant system was also affected by the dynamic characteristics of the suspension mechanism, the seat cushion, and the seated human body.

It was found that with the seated occupant, the resonance of the suspension seat transmissibility in either one of the translational axes was affected by both the excitation magnitude in the same axis and that in the other additional two axes. The increase of the excitation magnitude in either axis would suppress the effect the excitation magnitude in the other two axes on the seat transmissibility, and vice versa. Furthermore, the angle of backrest inclination tended to affect the moduli associated with the resonance frequencies of the seat transmissibilities measured at the backrest.

The results from the current study indicates that when optimizing the dynamic properties of a suspension seat, which will be applied in a tri-axial vibrational environment, the effects of the excitation magnitudes in all three directions and the inclination of the backrest on the seating dynamics should be included in the criteria.

Chapter 6 BIODYNAMIC MODELLING OF THE SEATED HUMAN BODY EXPOSED TO TRI-AXIAL TRANSLATIONAL VIBRATION

6.1 Introduction

The apparent mass of the human body has been widely investigated to understand the response of the seated human body to the WBV and the effect of the influencing factors such as the excitation magnitudes via experimental studies (Mansfield et al., 2006; Qiu and Griffin, 2012; Zheng et al., 2019; Wu et al., 2021) under single- and multi-axis excitations. However, the experimental studies of the biodynamic response are time and expense consuming in terms of the set-up and conduction of the tests. A complementary method to study the biodynamic response to WBV is by developing models of the human body, including finite element (FE) models (e.g., Kitazaki and Griffin, 1997; Liu et al., 2015; Dong et al., 2020), multi-body models (e.g., Qiu and Griffin, 2011; Desai et al., 2018), and lumped parameter models (LPMs) (e.g., Wei and Griffin, 1998; Marzbanrad et al., 2016). Compared to the other two modelling methods, the multi-body biodynamic models appear to be more capable of representing the anatomy of the human body than lumped parameter models, and more computationally effective than FE models.

Although the WBV in three translational axes has important effect on the ride comfort in many heavy vehicles, most of the existing multi-body models of the human body were developed to predict the apparent masses of the human body in the vertical and/or fore-aft directions (Kim et al., 2011; Zheng et al., 2011; Zhang et al., 2015; Desai et al., 2021a). However, biodynamic responses not only include those inside the sagittal plane but also involve the motion and responses outside the sagittal plane. So, the conventional one and two-dimensional models are not sufficient. Wu et al. (2022) developed a model of the seated human body exposed to combined roll, lateral and vertical excitation while the fore-aft excitation was not taken into consideration. A model suitable for studying biodynamics of the human body under tri-axial translational vibration still needs to be developed.

In this chapter, a three-dimensional multi-body model of the seated human body is developed, which included mass elements representing different body segments. The model was verified and calibrated using the apparent masses at the seat pan and backrest in the x, y and z-axis measured when the human body is exposed to tri-axial translational vibration. The experimental data obtained with different excitation magnitudes and backrest inclination angles were used for the

model calibration. With the calibrated model, parameter sensitivity analysis was carried out. Additionally, the modal properties of the human body and the characteristic of the apparent masses were studied.

6.2 Modelling method

For the biodynamic model of the seated human body presented in this chapter, the following assumptions have been made:

1) The human body can be represented by a linear model under a certain excitation magnitude and a certain backrest inclination angle;
2) The dynamic apparent masses of the whole human body can be represented using the rigid multi-body system including the following body segments: pelvis, the thighs, the lower legs, the abdomen, the upper torso including arms, and the head with neck;
3) The vibration input at the feet is much smaller than that at the seat pan and backrest;
4) The vibration inputs to the human body at the seat pan and backrest of the rigid seat are identical;
5) The human body model is symmetric around the sagittal plane.
6) The rigid bodies of the multi-body system perform small oscillations around the corresponding equilibrium position;
7) The contact between the human body and the rigid seat can be represented by pairs of linear spring and damper four contact points between the seat pan and pelvis, between the seat pan and thighs, between the backrest and abdomen, between the backrest and upper torso, respectively.

6.2.1 Structure of the model

The human body model proposed in this chapter is supported by the rigid seat (Figure 6.1). The rigid seat comprises of two rigid bodies (the seat pan B_s and the backrest B_b), which is rigidly connected and always share the same motion. Both of them have three degrees of freedom (DoFs) in x, y, and z-axis. They transmit the excitation to the seated human body.

The human body model consists of six rigid bodies: the pelvis B_1, the thighs B_2, the lower legs B_3, the abdomen B_4, the upper torso including arms B_5, and the head with neck B_6 (Figure 6.1). The feet were not modelled based on the assumption that the influence of the vibration input on the apparent masses at the seat pan and backrest is small. Each of the bodies B_i (i=1, …, 6) has four degrees of freedom (DoFs), i.e., three translational DoFs in the x, y, z-axis, and a rotational DoF around y-axis. The centres of mass of the rigid bodies B_i (i=1, …, 6, s, b) are denoted with O_i. The

origin of the global coordinate system O is at the middle of the intersection line of the seat pan upper surface and the backrest front surface.

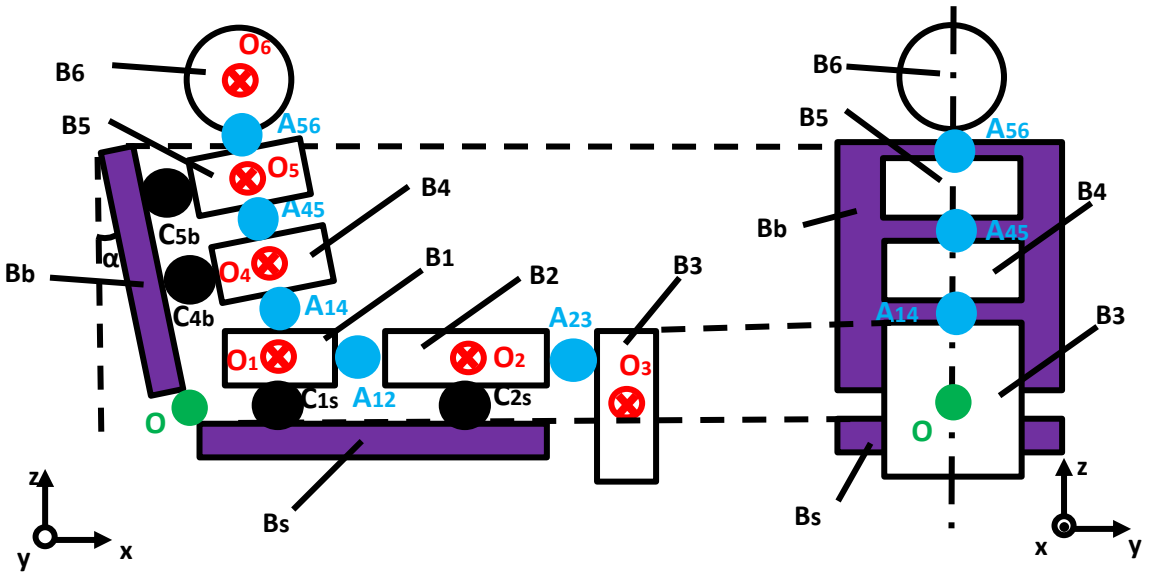

Figure 6.1 Schematic diagram of the model of the human body (with rigid seat). Red ⊗ symbols: The mass centres of the rigid bodies O_i (i=1, …, 6, s, b); Green point ●: Origin point of the global coordinate system O; Black points ●: the contact points between the rigid masses representing the body parts and those representing the seat parts (C_{1s}, C_{2s}, C_{4b}, C_{5b}); Blue points ●: the contact points between the rigid masses representing the body parts (A_{12}, A_{23}, A_{14}, A_{45}, A_{56}). Left: side view (the direction of the y-axis is pointing into the paper); right: front view (the direction of the x-axis is pointing out of the paper).

The contact points between the rigid masses representing the body parts and those representing the seat parts are denoted using the letter C with different subscripts. The contact points between the rigid bodies representing the body parts are denoted using the letter A with different subscripts. Note that the sizes of the contact points are exaggerated to highlight their positions.

For each of the contact points, the subscript denotes the two rigid bodies that it connects. The body parts B_1 and B_2 are in contact with B_s at the contact points C_{1s} and C_{2s}, respectively, and B_4 and B_5 are in contact with B_b at the contact points C_{4b} and C_{5b}, respectively. The body part B_1 is connected with B_2 and B_4 at the contact points A_{12} and A_{14}, respectively. The body part B_2 is also connected with B_3 at the contact point A_{23}. The body part B_4 is connected with B_5 at the contact point A_{45}, and the body part B_5 is connected with B_6 at the contact point A_{56}.

The unit vector of the global coordinate system is expressed as $\boldsymbol{N} = [\boldsymbol{n}_x \quad \boldsymbol{n}_y \quad \boldsymbol{n}_z]^T$, and the rotated unit vector $\breve{\boldsymbol{N}} = [\breve{\boldsymbol{n}}_x \quad \breve{\boldsymbol{n}}_y \quad \breve{\boldsymbol{n}}_z]^T$ denotes the unit vectors of the coordinate systems of some of the rigid bodies when the backrest is inclined by an angle of α (i=4, 5, 6, b). The unit vectors

of the coordinate systems of the rigid bodies are expressed as $\boldsymbol{N_i} = [\boldsymbol{n}_{ix} \quad \boldsymbol{n}_{iy} \quad \boldsymbol{n}_{iz}]^T$ (*i*=1, …, 6, s, b), which are defined as follows:

$$\boldsymbol{N_i} = \begin{cases} \boldsymbol{N}, & (i = s) \\ \breve{\boldsymbol{N}} = \boldsymbol{T}_{br}(\alpha)\boldsymbol{N}, & (i = b) \\ \boldsymbol{T}_{pitch}(\theta_i)\boldsymbol{N}, & (i = 1,2,3) \\ \boldsymbol{T}_{pitch}(\theta_i)\breve{\boldsymbol{N}} = \boldsymbol{T}_{pitch}(\theta_i)\boldsymbol{T}_{br}(\alpha)\boldsymbol{N}, & (i = 4,5,6) \end{cases}$$

Where $\boldsymbol{T}_{br}(\alpha) = \begin{bmatrix} \cos\alpha & 0 & \sin\alpha \\ 0 & 1 & 0 \\ -\sin\alpha & 0 & \cos\alpha \end{bmatrix}$, and $\boldsymbol{T}_{pitch}(\theta_i) = \begin{bmatrix} \cos\theta_i & 0 & -\sin\theta_i \\ 0 & 1 & 0 \\ \sin\theta_i & 0 & \cos\theta_i \end{bmatrix} \cong \begin{bmatrix} 1 & 0 & -\theta_i \\ 0 & 1 & 0 \\ \theta_i & 0 & 1 \end{bmatrix}$ (Linearization as θ_i is small and in radians). $\boldsymbol{T}_{pitch}$ denotes the transformation matrix of the coordinates relative to the global coordinate system subject to the pitch motion, and $\boldsymbol{T}_{br}$ denotes the transformation matrix related to the inclination of backrest.

The excitations are assumed to be applied to the human body segments at the contact points between the seat pan and the human body (C_{1s} and C_{2s}) as well as between the backrest and the human body (C_{4b} and C_{5b}). There are three pairs of translational springs and dampers in the x, y, and z-axis, respectively, for each of the contact points named with letter "C". For each contact point named with letter "A", four pairs of springs and dampers, three in the x, y, and z-axis and one around the y-axis, are allocated. The forces between the human body segments are modelled as linear spring and damping forces in the x, y, z-axis and around the y-axis. The rotational spring and damping forces are proportional to the relative rotational angle and the angular velocity, respectively.

6.2.2 Calculation of the motions and forces

The coordinates of the mass centres in the global coordinate system can be expressed in general as follows:

$$\boldsymbol{O}_i^O = \boldsymbol{O}_{istat}^O + \boldsymbol{O}_{idyn}^O = [x_{i0}\ y_{i0}\ z_{i0}]^T + [x_i\ y_i\ z_i]^T \tag{6.1}$$

Where $\boldsymbol{O}_{istat}^O$ represents the coordinate of the centre of mass of B_i (i=1, …, 6, s, b) in the global coordinate system at static state and $\boldsymbol{O}_{idyn}^O$ represents the dynamic motions of the body Bi in the global coordinate system. The superscript o in the symbol O_i^O indicates that the mass centre of each body Bi is defined in the global coordinate system. On the other hand, the origin of the local coordinate system of each body is fixed at the centre of the mass of the same body.

The relative displacement between the bodies expressed in the global coordinate system can then be derived with the coordinates of the points and the transformation matrices. For example, the relative displacement between the bodies B_1 and B_2 ($\boldsymbol{l}_{12}^O$) is:

$$\boldsymbol{l}_{12}^{O} = \boldsymbol{O}_{2}^{O} + \boldsymbol{A}_{12}^{B_2}\boldsymbol{T}_{pitch}(\theta_2) - \left[\boldsymbol{O}_{1}^{O} + \boldsymbol{A}_{12}^{B_1}\boldsymbol{T}_{pitch}(\theta_1)\right] \tag{6.2}$$

Where the superscript of the contact point represents the rigid body, in whose coordinate system the coordinate of the contact point is defined. For example, B_2 in the symbol $\boldsymbol{A}_{12}^{B_2}$ indicates that the coordinate of the contact point A_{12} is defined in the local system of the rigid body B_2, while the superscript B_1 in the symbol $\boldsymbol{A}_{12}^{B_1}$ indicates that the coordinate of the contact point A_{12} is defined in the local system of the rigid body B_1.

The relative displacements between the bodies B_2 and B_3 ($\boldsymbol{l}_{23}^{O}$), and between the bodies B_1 and B_4 ($\boldsymbol{l}_{14}^{O}$) are derived similarly (see Appendix C). Taking the inclination angle of the backrest α into consideration, the relative displacement between the bodies B4 and B5 $\boldsymbol{l}_{45}^{O}$ is:

$$\boldsymbol{l}_{45}^{O} = \boldsymbol{O}_{5}^{O} + \boldsymbol{A}_{45}^{B_5}\boldsymbol{T}_{pitch}(\theta_5)\boldsymbol{T}_{br}(\alpha) - \left[\boldsymbol{O}_{4}^{O} + \boldsymbol{A}_{45}^{B_4}\boldsymbol{T}_{pitch}(\theta_4)\boldsymbol{T}_{br}(\alpha)\right] \tag{6.3}$$

And the relative displacement between the bodies B_5 and B_6 ($\boldsymbol{l}_{56}^{O}$) is derived similarly.

The relative displacements between the bodies representing the segments of the human body and the seat pan or backrest are also derived similarly. It is defined that $\boldsymbol{O}_{sstat}^{O} = \boldsymbol{O}_{bstat}^{O} = [0\ 0\ 0]^T$, i.e., the mass centres of the seat pan and backrest are set to the origin for the ease of calculation. Similarly, it is defined that $[x_s\ y_s\ z_s]^T = [x_b\ y_b\ z_b]^T$, that is, the excitation at the seat pan and backrest are the same when expressed in the global coordinate system.

Then the relative displacement between the bodies B1 and Bs ($\boldsymbol{l}_{1s}^{O}$) is:

$$\boldsymbol{l}_{1s}^{O} = \boldsymbol{O}_{s}^{O} + \boldsymbol{C}_{1s}^{B_s} - \left[\boldsymbol{O}_{1}^{O} + \boldsymbol{C}_{1s}^{B_1}\boldsymbol{T}_{pitch}(\theta_1)\right] \tag{6.5}$$

The relative displacement between the bodies B_2 and B_s ($\boldsymbol{l}_{2s}^{O}$) is derived similarly. The relative displacement between the bodies B_4 and B_b ($\boldsymbol{l}_{4b}^{O}$) is transformed from the coordinate system associated with the backrest to the global coordinate system, so the inclination of the backrest needs to be included:

$$\boldsymbol{l}_{4b}^{O} = \boldsymbol{O}_{b}^{O} + \boldsymbol{C}_{4b}^{B_b}\boldsymbol{T}_{br}(\alpha) - \left[\boldsymbol{O}_{4}^{O} + \boldsymbol{C}_{4b}^{B_4}\boldsymbol{T}_{pitch}(\theta_4)\boldsymbol{T}_{br}(\alpha)\right] \tag{6.6}$$

And the relative displacement between the bodies B_5 and B_b ($\boldsymbol{l}_{5b}^{O}$) is derived similarly.

The derivatives of the relative displacements, i.e., the relative velocities, are also derived, for example, the relative velocity between the bodies B_1 and B_4 ($\dot{\boldsymbol{l}}_{14}^{O}$):

$$\dot{\boldsymbol{l}}_{14}^{O} = \dot{\boldsymbol{O}}_{4}^{O} + \boldsymbol{A}_{14}^{B_4}\boldsymbol{T}_{pitch}(\dot{\theta}_4)\boldsymbol{T}_{br}(\alpha) - \left[\dot{\boldsymbol{O}}_{1}^{O} + \boldsymbol{A}_{14}^{B_1}\boldsymbol{T}_{pitch}(\dot{\theta}_1)\right] \tag{6.7}$$

Note that each of the contact or contact points may be expressed with the superscript indicating in which local coordinate system are they described, e.g., for the contact point A_{12} between B_1 and B_2, $\boldsymbol{A}_{12}^{B_1}$ and $\boldsymbol{A}_{12}^{B_2}$ represent the coordinate of the point in the local coordinate system of B_1 and B_2, respectively. As the relative positions of the origins of the local coordinate systems are known, the coordinates of a contact or contact points in either local coordinate systems of the two bodies that is connected by it can be derived when its coordinates in the other local coordinate systems is determined, as shown in Table 6.1:

Table 6.1 The coordinates of the contact points expressed in different coordinate systems

Contact point	Coordinates in one local coordinate system	Coordinates in the other local coordinate system
C_{1s}	$\boldsymbol{C}_{1s}^{B_1} = \left[x_{C_{1s}}^{B_1}, y_{C_{1s}}^{B_1}, z_{C_{1s}}^{B_1}\right]$	$\boldsymbol{C}_{1s}^{B_s} = \boldsymbol{C}_{1s}^{B_1} + \boldsymbol{O}_{1stat}^{O} - \boldsymbol{O}_{sstat}^{O}$
C_{2s}	$\boldsymbol{C}_{2s}^{B_2} = \left[x_{C_{2s}}^{B_2}, y_{C_{2s}}^{B_2}, z_{C_{2s}}^{B_2}\right]$	$\boldsymbol{C}_{2s}^{B_s} = \boldsymbol{C}_{2s}^{B_2} + \boldsymbol{O}_{2stat}^{O} - \boldsymbol{O}_{sstat}^{O}$
C_{4b}	$\boldsymbol{C}_{4b}^{B_4} = \left[x_{C_{4b}}^{B_4}, y_{C_{4b}}^{B_4}, z_{C_{4b}}^{B_4}\right]$	$\boldsymbol{C}_{4b}^{B_b} = \boldsymbol{C}_{4b}^{B_4} + (\boldsymbol{O}_{4stat}^{O} - \boldsymbol{O}_{bstat}^{O})\boldsymbol{T}_{br}^{T}(\alpha)$
C_{5b}	$\boldsymbol{C}_{5b}^{B_5} = \left[x_{C_{5b}}^{B_5}, y_{C_{5b}}^{B_5}, z_{C_{5b}}^{B_5}\right]$	$\boldsymbol{C}_{5b}^{B_b} = \boldsymbol{C}_{5b}^{B_5} + (\boldsymbol{O}_{5stat}^{O} - \boldsymbol{O}_{bstat}^{O})\boldsymbol{T}_{br}^{T}(\alpha)$
A_{12}	$\boldsymbol{A}_{12}^{B_1} = \left[x_{A_{12}}^{B_1}, y_{A_{12}}^{B_1}, z_{A_{12}}^{B_1}\right]$	$\boldsymbol{A}_{12}^{B_2} = \boldsymbol{A}_{12}^{B_1} + \boldsymbol{O}_{1stat}^{O} - \boldsymbol{O}_{2stat}^{O}$
A_{23}	$\boldsymbol{A}_{23}^{B_2} = \left[x_{A_{23}}^{B_2}, y_{A_{23}}^{B_2}, z_{A_{23}}^{B_2}\right]$	$\boldsymbol{A}_{23}^{B_3} = \boldsymbol{A}_{23}^{B_2} + \boldsymbol{O}_{2stat}^{O} - \boldsymbol{O}_{3stat}^{O}$
A_{14}	$\boldsymbol{A}_{14}^{B_4} = \left[x_{A_{14}}^{B_4}, y_{A_{14}}^{B_4}, z_{A_{14}}^{B_4}\right]$	$\boldsymbol{A}_{14}^{B_1} = \boldsymbol{A}_{14}^{B_4}\boldsymbol{T}_{br}(\alpha) + \boldsymbol{O}_{4stat}^{O} - \boldsymbol{O}_{1stat}^{O}$
A_{45}	$\boldsymbol{A}_{45}^{B_5} = \left[x_{A_{45}}^{B_5}, y_{A_{45}}^{B_5}, z_{A_{45}}^{B_5}\right]$	$\boldsymbol{A}_{45}^{B_4} = \boldsymbol{A}_{45}^{B_5} + (\boldsymbol{O}_{5stat}^{O} - \boldsymbol{O}_{4stat}^{O})\boldsymbol{T}_{br}^{T}(\alpha)$
A_{56}	$\boldsymbol{A}_{56}^{B_6} = \left[x_{A_{56}}^{B_6}, y_{A_{56}}^{B_6}, z_{A_{56}}^{B_6}\right]$	$\boldsymbol{A}_{56}^{B_5} = \boldsymbol{A}_{56}^{B_6} + (\boldsymbol{O}_{6stat}^{O} - \boldsymbol{O}_{5stat}^{O})\boldsymbol{T}_{br}^{T}(\alpha)$

The coordinates of the contact point between the pelvis and the seat pan C_{1s}, and that between the upper torso and backrest C_{5b}, were calibrated within a small range around the centre position of the SIT-pad as in the experimental study presented in Chapter 3. The coordinates of the contact point between the thighs and the seat pan C_{2s}, and that between the abdomen and the backrest C_{4b}, were calibrated within a small range around the centre position of the contact area between B_2 and the seat pan, and that between B_4 and the backrest, respectively. Similarly, the coordinates of the contact points A_{12}, A_{23}, …, A_{56} were calibrated within a small range around the centre position of the contact area between the two bodies they connected. Note that for each contact point, one of the three coordinates was fixed without calibration as the contact point had to be on the surface of the seat.

The forces between the rigid bodies are then modelled as linear spring and damping forces in the x, y and z-axis at the contact points. For example, the stiffness and damping in the x-axis are represented by k_{xij} or c_{xij}, respectively, where the first letter of the subscript represents the direction of the spring or damper, and the rest of the subscripts i and j indicates the numbering of the bodies that the spring or damper connects. The springs and dampers in other directions are defined similarly, see Table 6.2.

Table 6.2 Definition of the springs and dampers in the human body model

Contact point	Spring	Damper	Direction	The pair of rigid bodies that the point connects
C_{1s}	k_{x1s}	c_{x1s}	x-axis	B_1 and B_s
	k_{y1s}	c_{y1s}	y-axis	
	k_{z1s}	c_{z1s}	z-axis	
C_{2s}	k_{x2s}	c_{x2s}	x-axis	B_2 and B_s
	k_{y2s}	c_{y2s}	y-axis	
	k_{z2s}	c_{z2s}	z-axis	
C_{4b}	k_{x4b}	c_{x4b}	x-axis	B_4 and B_b
	k_{y4b}	c_{y4b}	y-axis	
	k_{z4b}	c_{z4b}	z-axis	
C_{5b}	k_{x5b}	c_{x5b}	x-axis	B_5 and B_b
	k_{y5b}	c_{y5b}	y-axis	
	k_{z5b}	c_{z5b}	z-axis	
A_{12}	k_{x12}	c_{x12}	x-axis	B_1 and B_2
	k_{y12}	c_{y12}	y-axis	
	k_{z12}	c_{z12}	z-axis	
	k_{p12}	c_{p12}	around y-axis	
A_{23}	k_{x23}	c_{x23}	x-axis	B_2 and B_3
	k_{y23}	c_{y23}	y-axis	
	k_{z23}	c_{z23}	z-axis	
	k_{p23}	c_{p23}	around y-axis	
A_{14}	k_{x14}	c_{x14}	x-axis	B_1 and B_4
	k_{y14}	c_{y14}	y-axis	
	k_{z14}	c_{z14}	z-axis	
	k_{p14}	c_{p14}	around y-axis	

Table 6.2 (Continued)

Contact point	Spring	Damper	Direction	The pair of rigid bodies that the point connects
A_{45}	k_{x45}	c_{x45}	x-axis	B_4 and B_5
	k_{y45}	c_{y45}	y-axis	
	k_{z45}	c_{z45}	z-axis	
	k_{p45}	c_{p45}	around y-axis	
A_{56}	k_{x56}	c_{x56}	x-axis	B_5 and B_6
	k_{y56}	c_{y56}	y-axis	
	k_{z56}	c_{z56}	z-axis	
	k_{p56}	c_{p56}	around y-axis	

The forces between the bodies in the biodynamic model proposed in this chapter is proportional to the relative displacements (or their derivatives) between the bodies and are obtained by multiplying the relative displacements (and velocities) in each axis with the corresponding stiffness (or damping). The translational force between the bodies B_1 and B_2 ($\boldsymbol{f}_{12}^{O}$) is:

$$\boldsymbol{f}_{12}^{O} = \boldsymbol{l}_{12}^{O}\begin{bmatrix} k_{x12} & & \\ & k_{y12} & \\ & & k_{z12} \end{bmatrix} + \dot{\boldsymbol{l}}_{12}^{O}\begin{bmatrix} c_{x12} & & \\ & c_{y12} & \\ & & c_{z12} \end{bmatrix} = [f_{12(x)} \quad f_{12(y)} \quad f_{12(z)}]\boldsymbol{N} \qquad (6.8)$$

The translational force between the bodies B_2 and B_3 ($\boldsymbol{f}_{23}^{O}$) and the translational force between the bodies B_1 and B_4 ($\boldsymbol{f}_{14}^{O}$), between the bodies B_1 and B_s ($\boldsymbol{f}_{1s}^{O}$), between the bodies B_2 and B_s ($\boldsymbol{f}_{2s}^{O}$) are derived similarly.

The derivation of the translational force between the bodies B_4 and B_5 ($\boldsymbol{f}_{45}^{O}$) includes the backrest inclination angle:

$$\boldsymbol{f}_{45}^{O} = \boldsymbol{l}_{45}^{O}\boldsymbol{T}_{br}^{T}(\alpha)\begin{bmatrix} k_{x45} & & \\ & k_{y45} & \\ & & k_{z45} \end{bmatrix} + \dot{\boldsymbol{l}}_{45}^{O}\boldsymbol{T}_{br}^{T}(\alpha)\begin{bmatrix} c_{x45} & & \\ & c_{y45} & \\ & & c_{z45} \end{bmatrix}$$

$$= [\check{f}_{45(x)} \quad \check{f}_{45(y)} \quad \check{f}_{45(z)}]\check{\boldsymbol{N}} \qquad (6.9)$$

Where the symbol $\check{f}$ represents the forces in the coordinate system of the inclined backrest. The translational force between the bodies B_4 and B_b ($\boldsymbol{f}_{4b}^{O}$) is derived similarly. The translational force between the bodies B_5 and B_6 ($\boldsymbol{f}_{56}^{O}$) is:

$$\boldsymbol{f}_{56}^{O} = [\check{f}_{56(x)} \quad \check{f}_{56(y)} \quad \check{f}_{56(z)}]\check{\boldsymbol{N}} \qquad (6.10)$$

The translational force between the bodies B_5 and B_b ($\boldsymbol{f}_{5b}^{O}$) is derived similarly. The rotational forces between the bodies are calculated by multiplying the differences (or the deviation of them) between the angles of the bodies.

6.2.3 Equations of motion of the model

With the forces between the rigid bodies, the equations of motion of the bodies representing the human body B_i (i=1, …, 6) can be derived. For example, for the rigid body B_1, four equations of motion in three translational directions and around the y-axis are derived as:

$$m_1\ddot{x}_1 = f_{12(x)} + f_{14(x)} + f_{1s(x)} \tag{6.11}$$

$$m_1\ddot{y}_1 = f_{12(y)} + f_{14(y)} + f_{1s(y)} \tag{6.12}$$

$$m_1\ddot{z}_1 = f_{12(z)} + f_{14(z)} + f_{1s(z)} \tag{6.13}$$

$$\begin{aligned} I_1\ddot{\theta}_1 = {} & k_{p12}(\theta_2 - \theta_1) + c_{p12}\left(\dot{\theta}_2 - \dot{\theta}_1\right) + k_{p14}(\theta_4 - \theta_1) + c_{p14}\left(\dot{\theta}_4 - \dot{\theta}_1\right) \\ & + \boldsymbol{A}_{12}^{B_1} \times [f_{12(x)} \quad f_{12(y)} \quad f_{12(z)}] \begin{bmatrix} 0 \\ 1 \\ 0 \end{bmatrix} + \boldsymbol{A}_{14}^{B_1} \times [f_{14(x)} \quad f_{14(y)} \quad f_{14(z)}] \begin{bmatrix} 0 \\ 1 \\ 0 \end{bmatrix} \\ & + \boldsymbol{C}_{1S}^{B_1} \times [f_{1s(x)} \quad f_{1s(y)} \quad f_{1s(z)}] \begin{bmatrix} 0 \\ 1 \\ 0 \end{bmatrix} \end{aligned} \tag{6.14}$$

For the rigid body B_2 to B_6, the equations of motion are derived similarly (see Appendix C).

6.2.4 Parameters of the model

The parameters in this model include the backrest inclination angle; the masses, moments of inertia, and dimensions of the bodies; the coordinates of the mass centres of the bodies and the contact points; and the stiffness and damping between the bodies. They can be divided into two categories: the (before the calibration) pre-determined parameters, and the parameters to be calibrated.

The values of the pre-determined parameters can be obtained without model calibration by referring to the literature reporting the anthropometric data or by taking measurements, including:

1) The backrest inclination angle α (0°, 10° or 20°);
2) The masses of the rigid bodies representing the human body segments m_i (i=1, …, 6);
3) The length, width and height of the rigid bodies representing the human body segments l_{xi}, l_{yi} and l_{zi} (i=1, …, 6) except for l_{z3} (the height of the body B_3);
4) The coordinates of the centres of the mass of the rigid bodies O_i^O (i=1, …, 6);
5) The moment of inertia of these rigid bodies around y-axis I_i (i=1, …, 6); and
6) Some of the coordinates of the contact points.

6.2.4.1 The masses of the rigid bodies

The masses m_i of the rigid bodies B_i (i=1, …, 6) are related to the masses of the body segments that they are representing. Assume that the total mass of the human body is m_{total}, then the masses of the rigid bodies are: m_1=0.12m_{total}, m_2=0.17m_{total}, m_3=0.03m_{total}, m_4=0.26m_{total}, m_5=0.11m_{total}, m_6=0.08m_{total}. They are determined based on the published anthropometric data (Dempster and Gaughran, 1967) and are adjusted within the range or with small deviation relative to the constrains given by the literature above. It should be pointed out that the mass of the seated human body supported by the seat is roughly 80% of the total mass of the human body (Qiu, 2017), so the sum of the masses of the rigid bodies is smaller than m_{total}. This is partly due to the fact that part of the masses of the lower legs and those of the feet are not supported by the seat, but by the floor.

6.2.4.2 The dimensions of the rigid bodies representing the human body segments

The lengths (l_{xi}), widths (l_{yi}), and heights (l_{zi}) of the rigid bodies are their dimensions in the x, y and z-axis, respectively. Assume that the height of the human body is H, then the dimensions of the rigid bodies B_i (i=1, …, 6) are defined as in Table 6.3, which are determined based on the published anthropometric data of the corresponding body segments (Dempster and Gaughran, 1967). Note that bodies B_1 to B_5 are cuboids, while the head and neck of the human body is represented by body B_6 which is an ellipsoid with its semiaxes equal to half of l_{x6}, l_{y6} and l_{z6}, respectively. The actual height of the body B_3, l_{z3}, still remains to the determined within a range (0.1H to 0.24H) via calibration, as it is not directly corresponding to the full length of the leg (0.24H) in the published data. The actual dimensions of the subjects were used for the parameter optimization when the apparent masses of the same subject were used for model calibration.

Table 6.3 Dimensions of the rigid bodies

Order of body	Length l_{xi}	Width l_{yi}	Height l_{zi}
1	l_{x1}=0.12H	l_{y1}=0.195H	l_{z1}=0.1H
2	l_{x2}=0.24H	l_{y2}=0.195H	l_{z2}=0.1H
3	l_{x3}=0.1H	l_{y3}=0.195H	To be calibrated

Table 6.3 (Continued)

Order of body	Length l_{xi}	Width l_{yi}	Height l_{zi}
4	$l_{x4}=0.1H$	$l_{y4}=0.195H$	$l_{z4}=0.17H$
5	$l_{x5}=0.1H$	$l_{y5}=0.195H$	$l_{z5}=0.16H$
6	$l_{x6}=0.09H$	$l_{y6}=0.09H$	$l_{z6}=0.155H$

Figure 6.2 shows the dimensions of the rigid bodies of the human body model in a more intuitive way.

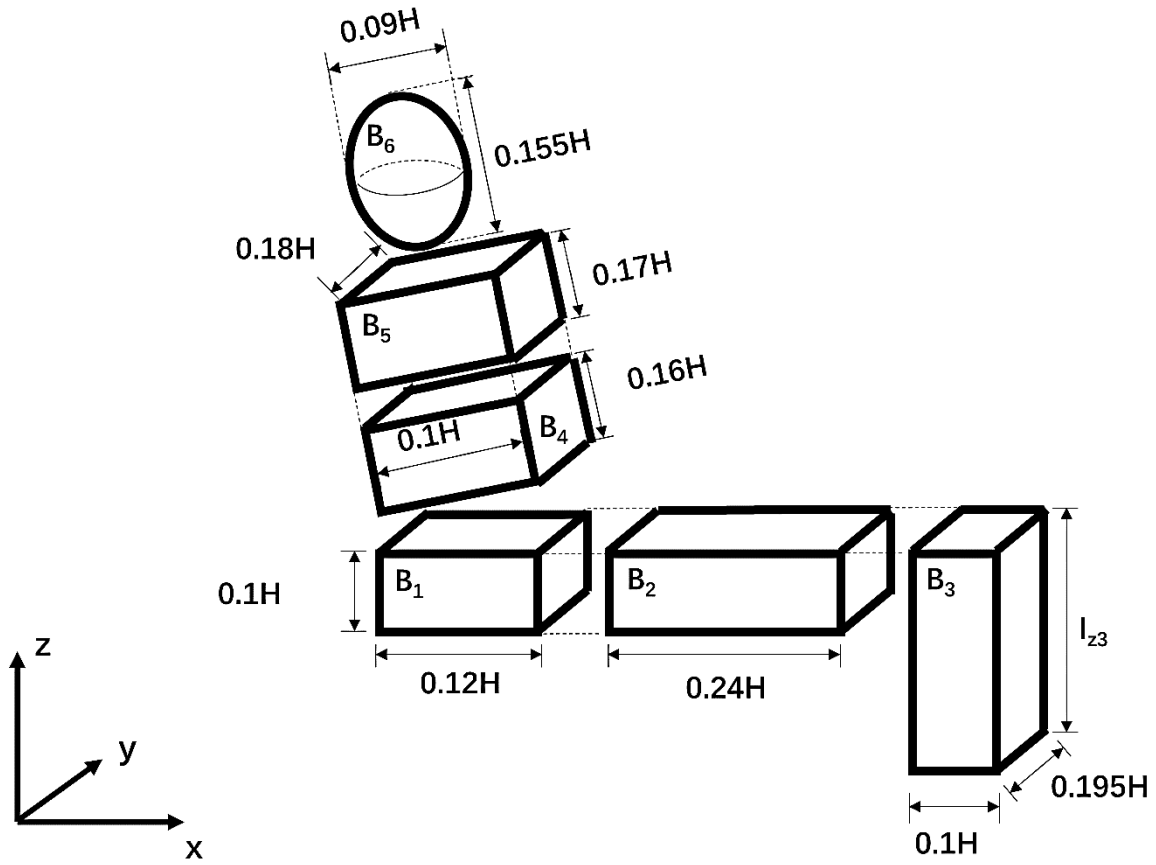

Figure 6.2 Schematic diagram of the dimensions of the rigid bodies of the human body model

6.2.4.3 Coordinates of the mass centres and moments of inertia of the rigid bodies

With the dimensions shown in Figure 6.2, the coordinates of the mass centres x_{i0}, y_{i0}, z_{i0} of the rigid bodies B_i (i=1, …, 6) in three directions, and the moments of inertia of them (about the y-axis) I_i can be derived as shown in Table 6.4, based on the relative position of the mass centres provided by the existing literature (Dempster and Gaughran, 1967; Contini, 1972; Park et al., 1999; Nikolova and Toshev, 2007):

Table 6.4 Coordinates of the mass centres and moments of inertia of the rigid bodies

Order of body	Coordinate in x-axis (x_{i0})	Coordinate in y-axis (y_{i0})	Coordinate in z-axis (z_{i0})	Moment of inertia about y-axis (I_i)
1	$x_{10}=0.5*0.12H$	$y_{10}=0$	$z_{10}=0.5*0.1H$	$I_1=1/12*m_1[(0.12H)^2+(0.1H)^2]$
2	$x_{20}=0.12H+0.43*0.24H$	$y_{20}=0$	$z_{20}=0.5*0.1H$	$I_2=1/12*m_2[(0.24H)^2+(0.1H)^2]$
3	$x_{30}=0.12H+0.24H+0.5*0.1H$	$y_{30}=0$	$z_{30}=0.1H-0.5*l_{z3}$	$I_3=1/12*m_3[(l_{z3})^2+(0.1H)^2]$
4	$x_{40}=(0.1H\cos\alpha+0.5*0.16H)*-\sin\alpha+0.05H\cos\alpha$	$y_{40}=0$	$z_{40}=(0.1H\cos\alpha+0.5*0.16H)*\cos\alpha+0.05H\sin\alpha$	$I_4=1/12*m_4[(0.1H)^2+(0.16H)^2]$
5	$x_{50}=(0.1H\cos\alpha+0.16H+0.5*0.17H)*-\sin\alpha+0.05H\cos\alpha$	$y_{50}=0$	$z_{50}=(0.1H\cos\alpha+0.16H+0.5*0.17H)*\cos\alpha+0.05H\sin\alpha$	$I_2=1/12*m_2[(0.1H)^2+(0.17H)^2]$
6	$x_{60}=(0.1H\cos\alpha+0.33H+0.5*0.155H)*-\sin\alpha+0.05H\cos\alpha$	$y_{60}=0$	$z_{60}=(0.1H\cos\alpha+0.33H+0.5*0.155H)\cos\alpha+0.05H\sin\alpha$	$I_6=1/20*m_6[(0.09H)^2+(0.155H)^2]$

Furthermore, some of the coordinates of the contact points are pre-determined according to the dimensions of the bodies before the calibration of the model, see Table 6.5, since they are located on the contact surface of the rigid bodies when the bodies are at the static position.

Table 6.5 Pre-defined coordinates of some of the contact points

Contact points	Coordinates	Contact points	Coordinates
C_{1s}	$z_{C_{1s}}^{B_1}=0.5*(-0.1H)$	A_{12}	$x_{A_{12}}^{B_1}=0.5*(0.12H)$
C_{2s}	$z_{C_2}^{B_2}=0.5*(-0.1H)$	A_{23}	$x_{A_{23}}^{B_2}=0.5*(0.24H)$
C_{4b}	$x_{C_{4b}}^{B_4}=0.5*(-0.1H)$	A_{14}	$z_{A_{14}}^{B_4}=0.5*(-0.16H)$
C_{5b}	$x_{C_{5b}}^{B_5}=0.5*(-0.1H)$	A_{45}	$z_{A_{45}}^{B_5}=0.5*(-0.17H)$
		A_{56}	$x_{A_{56}}^{B_6}=y_{A_{56}}^{B_6}=0$
		A_{56}	$z_{A_{56}}^{B_6}=0.5*0.155H$

The values of the rest of the parameters of the model are to be calibrated, including all the stiffness and damping at the contact points between the rigid bodies (as listed in Table 6.2), some of the coordinates of the contact points ($x_{C_{1s}}^{B_1}$, $y_{C_{1s}}^{B_1}$, $x_{C_{2s}}^{B_2}$, $y_{C_{2s}}^{B_2}$, $x_{C_{4b}}^{B_4}$, $y_{C_{4b}}^{B_4}$, $x_{C_{5b}}^{B_5}$, $y_{C_{5b}}^{B_5}$, $y_{A_{12}}^{B_1}$, $z_{A_{12}}^{B_1}$, $y_{A_{23}}^{B_2}$, $z_{A_{23}}^{B_2}$, $y_{A_{14}}^{B_4}$, $z_{A_{14}}^{B_4}$, $y_{A_{45}}^{B_5}$, $z_{A_{45}}^{B_5}$), and the height of the body B_3, i.e., l_{z3}.

6.3 Model calibration

The equations of motion of the rigid bodies can be written in the following form:

$$\boldsymbol{M}\ddot{\boldsymbol{X}} + \boldsymbol{C}\dot{\boldsymbol{X}} + \boldsymbol{K}\boldsymbol{X} = \boldsymbol{C}_s\dot{\boldsymbol{X}}_s + \boldsymbol{K}_s\boldsymbol{X}_s \tag{6.15}$$

Where $\boldsymbol{M}$, $\boldsymbol{C}$, $\boldsymbol{K}$ represent the matrices of mass, damping and stiffness of the human body model, respectively, while $\boldsymbol{C_s}$ and $\boldsymbol{K_s}$ represent the damping and stiffness related to the vibration input at the seat-human body interface, respectively. $\boldsymbol{X_s}$ is the vector of vibration input: $[x_s, y_s, z_s]^T$, and $\boldsymbol{X}$ is the vector of the output motion of the body model: $[x_1, y_1, z_1, \theta_1, x_2, y_2, z_2, \theta_2, x_3, y_3, z_3, \theta_3, x_4, y_4, z_4, \theta_4, x_5, y_5, z_5, \theta_5, x_6, y_6, z_6, \theta_6]^T$.

The transfer function $\boldsymbol{T_R}$ between $\boldsymbol{X}$ and $\boldsymbol{X_s}$ can then be derived:

$$\boldsymbol{T}_R(\omega) = \frac{\boldsymbol{X}(\omega)}{\boldsymbol{X}_s(\omega)} = (-\boldsymbol{M}\omega^2 + i\omega\boldsymbol{C} + \boldsymbol{K})^{-1}(i\omega\boldsymbol{C}_s + \boldsymbol{K}_s) \tag{6.16}$$

With the transfer function $\boldsymbol{T_R}$, the apparent masses of the seated human body could be derived. The in-line fore-aft apparent mass at the seat pan M_{sxx} can be calculated as:

$$\begin{aligned} M_{sxx} &= \frac{\mathbf{F}\left(f_{1s(x)} + f_{2s(x)}\right)}{-\omega^2\mathbf{F}(x_s)} \\ &= \frac{k_{x1s}\left[1 - \boldsymbol{T}_R(1,1) - \boldsymbol{T}_R(4,1)z_{C_{1s}}^{B_1}\right] + k_{x2s}\left[1 - \boldsymbol{T}_R(5,1) - \boldsymbol{T}_R(8,1)z_{C_{2s}}^{B_2}\right]}{-\omega^2} \\ &+ \frac{c_{x1s}\left[1 - \boldsymbol{T}_R(1,1) - \boldsymbol{T}_R(4,1)z_{C_{1s}}^{B_1}\right] + c_{x2s}\left[1 - \boldsymbol{T}_R(5,1) - \boldsymbol{T}_R(8,1)z_{C_{2s}}^{B_2}\right]}{j\omega} \end{aligned} \tag{6.17}$$

Where $\boldsymbol{T}_R(a,b)$ represents the entry at the ath row and bth column of the matrix $\boldsymbol{T_R}$.

The in-line lateral apparent mass at the seat pan M_{syy}, the in-line vertical apparent mass at the seat pan M_{szz}, the in-line fore-aft apparent mass at the backrest M_{bxx}, the in-line lateral apparent mass at the backrest M_{byy} and the in-line vertical apparent mass at the backrest M_{bzz} can be calculated similarly (see Appendix C).

The apparent masses in the x, y and z-axis measured at the seat pan and backrest, which are obtained in the experimental study described in Chapter 4 are used to calibrate the parameters of

this human body model. The calibration is carried out by minimizing the sum of the root mean square difference between the real and imaginary parts of the 6 apparent masses calculated using the model and their counterparts obtained via measurements during the experimental study described in Chapter 4. An error function $g_{error\_apms}(f)$ is defined to quantify such a difference as follows:

$$g_{error\_apms}(f) = \sum_{\substack{j=sxx,syy,szz,\\ bxx,byy,bzz}} w_j \left(\sqrt{\frac{\sum_{i=1}^{n} \left(\left(Re\left(M_j(f_i)\right) \right)_{calc} - \left(Re\left(M_j(f_i)\right) \right)_{meas} \right)^2}{n}} + \sqrt{\frac{\sum_{i=1}^{n} \left(\left(Im\left(M_j(f_i)\right) \right)_{calc} - \left(Im\left(M_j(f_i)\right) \right)_{meas} \right)^2}{n}} \right) \quad (6.18)$$

Where the subscripts *calc* and *meas* denotes the apparent masses calculated using the model and obtained via measurement, respectively. *Re* and *Im* stand for the real and imaginary parts of the apparent mass, and *n* is the total number of the frequency points. For the model of the seated human body, the calibration is carried out on the frequency range between 0.5 to 20 Hz with an interval of 0.25 Hz, making the total number of frequency points *n*=79. The subscript *j* distinguishes the direction and position of the apparent masses, and w_j represents the weighting factors for different apparent masses that are adjusted to achieve an optimized result. The weighting factor w_j was manually adjusted for each optimization problem as follows:

1) the value of w_j was set to be the same (e.g., 1) for each apparent mass.
2) Then the optimization was carried out within a limited number of iterations, and the simulation results calculated using the outcome were compared with the measured counterparts.
3) The apparent masses with greater error between the measured and simulated data were allocated with a greater value of the weighting factor w_j' (e.g., $w_j'=2*w_j$).
4) Then the steps 2) and 3) were repeated until each of the six apparent masses was allocated with an individual weighting factor and a satisfactory result of the optimization was achieved.

The Equations (6.2) to (6.17) are solved by generating programmes using MATLAB, which enables a user-defined function comprised with symbolic variables being solved without having to assign exact values to the variables. Thus, the expressions of the apparent masses can be derived which only consist of the variables. Then the expressions of the apparent masses were introduced in Eq. (6.18) together with the measured data to optimize the error function.

To minimize the value of the error function $g_{error}(f)$, two optimization algorithms have been used. The first one is the "fmincon" function provided by MATLAB that is suitable for the minimization of linear and nonlinear multi-variable functions with constrains. Another algorithm is the generic

algorithm (GA), where a group of initial solutions to the optimization problem is randomly chosen and takes part in iterative processes, which is also available in MATLAB. In each iteration, the optimization function is evaluated and the more fit solutions are stochastically selected among all the given solutions (called “generation” in this iteration) and modified (recombined and randomly mutated) to form a new generation to be used in the next iteration of the algorithm (Whitley, 1994). Compared to the “fmincon” function, the GA is more beneficial in finding global optimization solutions, but less efficient in terms of convergence and speed. On the other hand, the “fmincon” function is more suitable for in-depth optimization inside a local area, and is much dependent on the initial values.

To make use of the benefits of both algorithms, two optimization methods have been adopted to calibrate the model. The first one uses the “fmincon” function only by randomly creating different initial solutions and carrying out optimizations with them using this function to obtain a number of candidate solutions, and the best solution is chosen among them. The second method is a combination of both algorithms. An initial solution is randomly created and adopted in the iterations in GA until a certain number of iterations (i.e., generations) is reached to find an intermediate solution which may possibly be located in a local area where the global optimum exists. Then this intermediate solution is adopted in the “fmincon” function to get the optimum faster. The two methods are repeated several times with different sets of initial solutions to get as better solution as possible.

The comparison of the simulated apparent masses using the calibrated model and their counterpart measured during the experimental study under different conditions is shown in Figures 6.3 to 6.6. The results show that with different excitations, backrest inclination angles or different subjects, the model can generally achieve good agreement in terms of the apparent masses at the seat pan and backrest in all three translational directions.

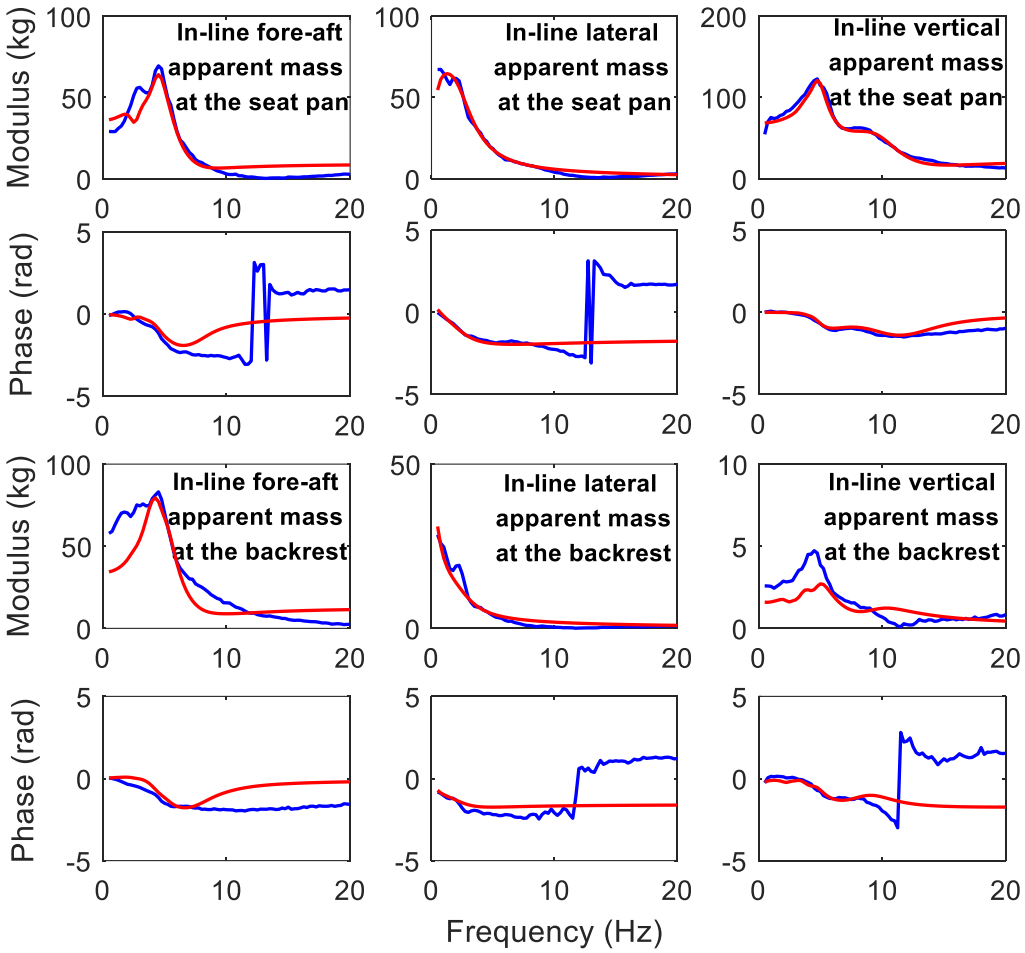

Figure 6.3 The comparison between the measured (—) and simulated (—) apparent masses in the x, y and z-axis at the seat pan and backrest with a subject (1.76m in height and 90.8 kg in weight) under combined 0.5 ms^{-2} fore-aft, 0.5 ms^{-2} lateral, and 0.5 ms^{-2} (r.m.s.) vertical excitation and with an upright backrest

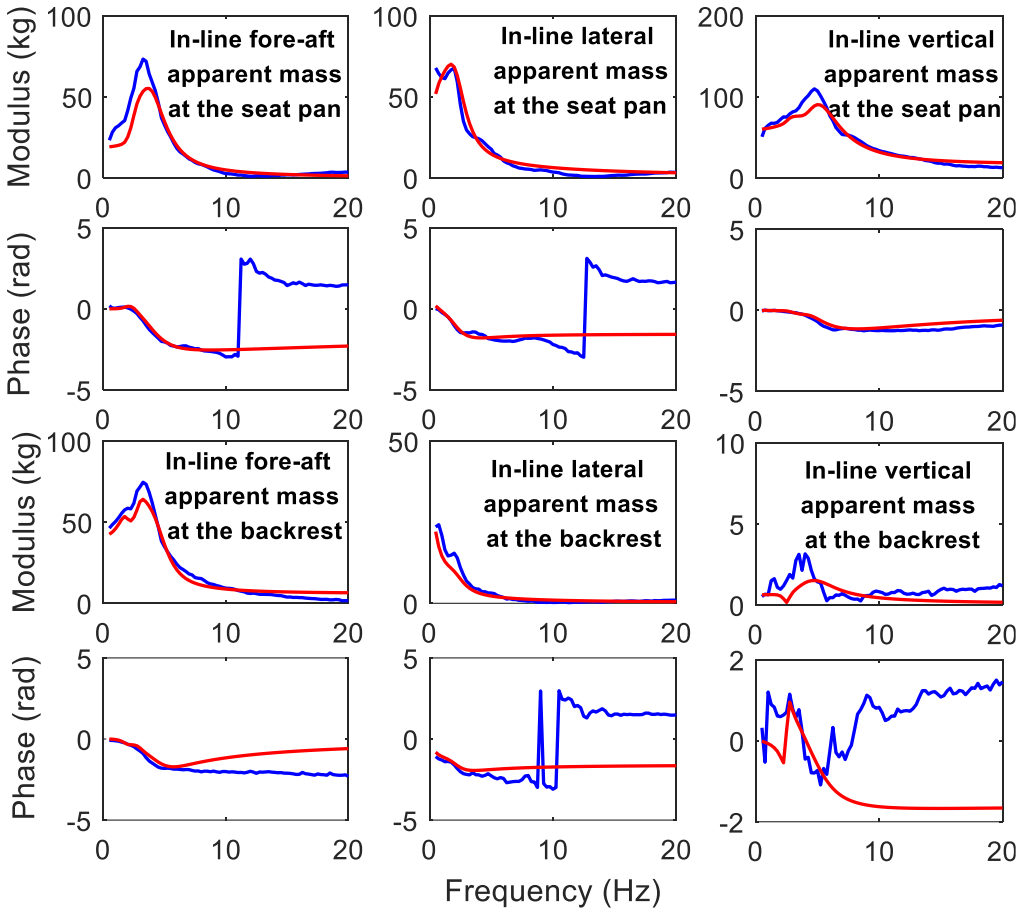

Figure 6.4 The comparison between the measured (—) and simulated (—) apparent masses with a subject (1.75m in height and 78.6 kg in weight) under combined 0.5 ms^{-2} fore-aft, 0.5 ms^{-2} lateral, and 0.5 ms^{-2} (r.m.s.) vertical excitation and with an upright backrest

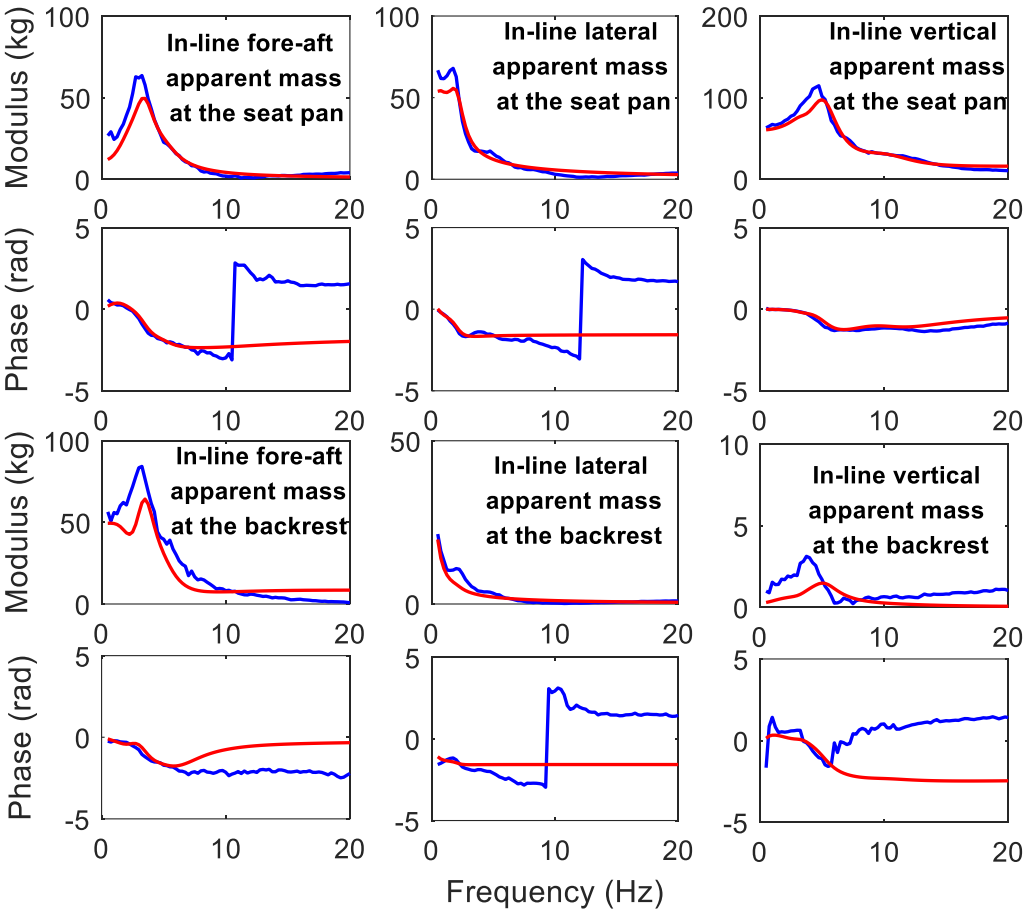

Figure 6.5 The comparison between the measured (—) and simulated (—) apparent masses with a subject (1.75m in height and 78.6 kg in weight) under combined 0.5 ms^{-2} fore-aft, 1.0 ms^{-2} lateral, and 1.0 ms^{-2} (r.m.s.) vertical excitation and with an upright backrest

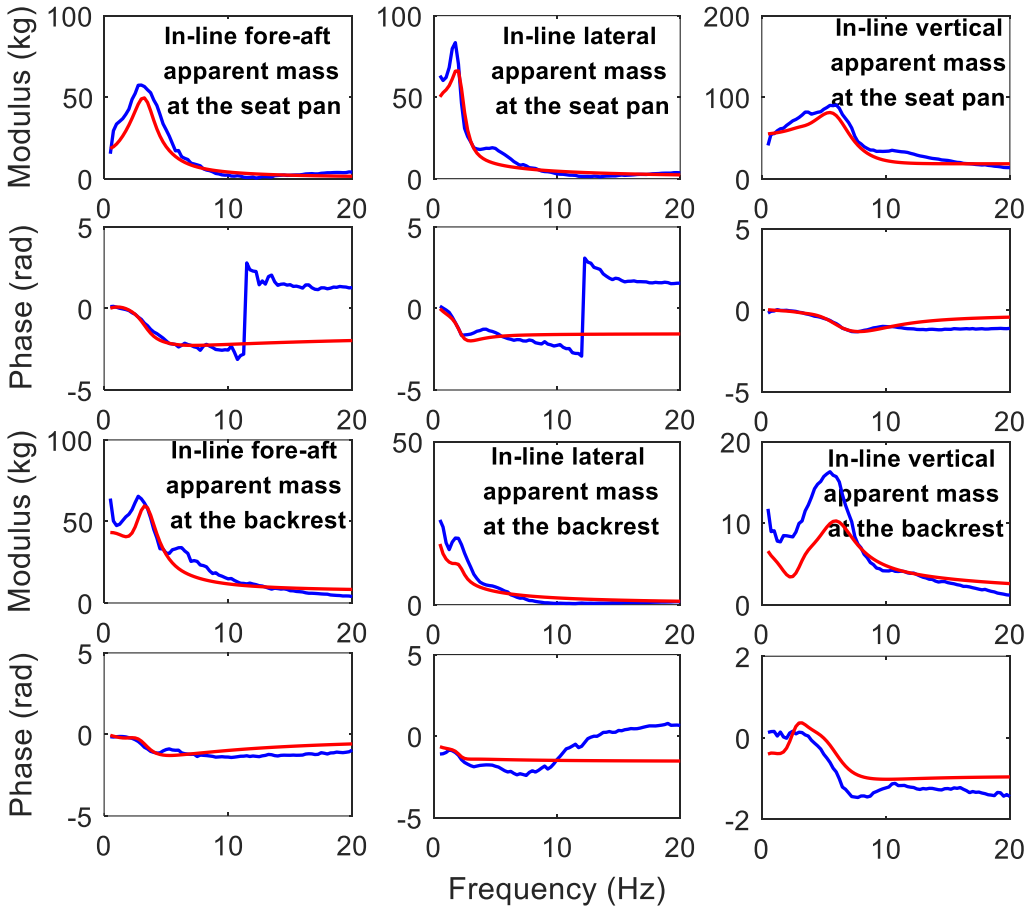

Figure 6.6 The comparison between the measured (—) and simulated (—) apparent masses with a subject (1.75m in height and 78.6 kg in weight) under combined 0.5 ms^{-2} fore-aft, 1.0 ms^{-2} lateral, and 1.0 ms^{-2} (r.m.s.) excitation vibration and with a backrest inclined by 20°

6.4 Modal analysis

After the calibration, modal analysis was performed on the model of the seated human body to investigate on the relationship between the modes represented by the model and the resonances in the apparent masses. To find the undamped free vibration modal properties of the model is to find the solution to the following formula derived from Eq. (6.15):

$$det|\boldsymbol{M}(2\pi if)^2 + \boldsymbol{K}| = 0 \tag{6.19}$$

Where *det* stands for the determinant of the matrix $\boldsymbol{M}(2\pi if)^2 + \boldsymbol{K}$. The solutions of Eq. (6.19) are the eigenvalues of this matrix, which can be used to calculate the undamped natural frequencies of the human body, while the mode shape can be obtained according to the eigenvectors of the matrix. The analysis on the case with a subject of 1.75m and 78.6kg body weight exposed to tri-axial vibration with excitation magnitudes of 0.5 ms^{-2} r.m.s. in the x, y and z-axis and upright backrest is shown in Figure 6.7. There are four modes found below 10 Hz detected with the natural frequencies 0.84, 1.89, 2.88 and 5.76 Hz, respectively. They are corresponding to the four peaks of the fore-aft,

lateral and vertical apparent masses, which are shown in Figure 6.7 in sequence. The four corresponding mode shapes are shown in Figure 6.8.

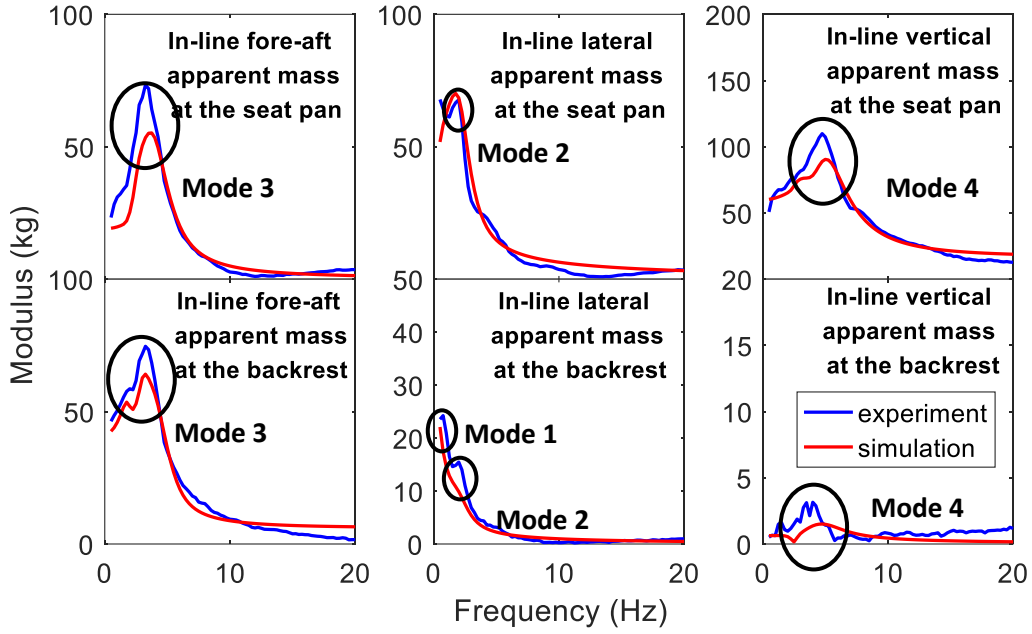

Figure 6.7 The resonance frequencies in the apparent masses that are related to the modes

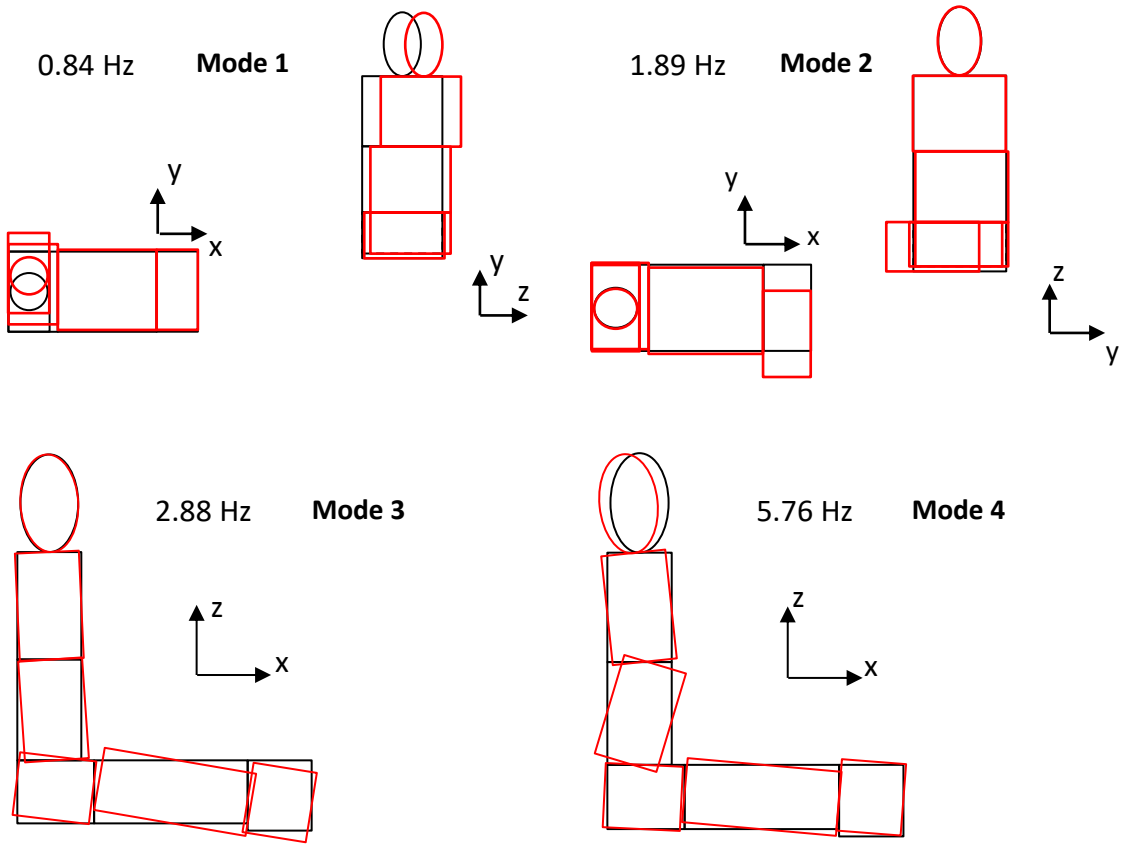

Figure 6.8 The mode shapes of a subject of 1.75m and 78.6kg body weight exposed to tri-axial vibration with excitation magnitudes of 0.5 ms^{-2} r.m.s. in the x, y and z-axis. (Black: undeformed mode shape; red: deformed mode shape)

Figure 6.8 shows that the first mode (0.84 Hz) is related to the lateral motion of the upper body and the head. For the second mode (1.89 Hz), all the body segments exhibit a lateral motion while the motion of the lower body is dominant. The third mode (2.88 Hz) is related to the pitch motion combined with the fore-aft motion of the human body where the motion of the lower body was greater than that of the upper body. The fourth mode (5.76 Hz) involves the combined fore-aft, vertical and pitch motion of all the body segments.

6.5 Parameter sensitivity analysis

The sensitivity analysis was carried out on the parameters of the human body model using the index matrix $\boldsymbol{\Psi}$, with its element defined as follows (Ju and Mansour, 1987):

$$\Psi_{ij} = \frac{\Delta R_i / R_i}{\Delta P_j / P_j} \tag{6.20}$$

Where P_j and ΔP_j represent the j^{th} (j=1, 2, …, 64) parameter being tested and the corresponding change of that parameter respectively; R_i represents the responses obtained with the calibrated parameter values (which are called the "reference values"), on which the effect of the change of parameters was to be examined. Eight responses related to the apparent masses in the x, y and z-axis were chosen to test their sensitivity, with:

1) i=1 being the resonance frequency of the fore-aft apparent mass at the seat pan;
2) i=2 being the modulus associated with the resonance of the fore-aft apparent mass at the seat pan;
3) i=3 being the resonance frequency of the fore-aft apparent mass at the backrest;
4) i=4 being the modulus associated with the resonance of the fore-aft apparent mass at the backrest;
5) i=5 being the resonance frequency of the vertical apparent mass at the seat pan;
6) i=6 being the modulus associated with the resonance of the vertical apparent mass at the seat pan;
7) i=7 being the resonance frequency of the lateral apparent mass at the seat pan; and
8) i=8 being the modulus associated with the resonance of the lateral apparent mass at the seat pan.

ΔR_i represents the difference between the responses obtained with adopting the "reference values" of the parameters and adopting the changed values of the parameters. In the current study, four changed values of the parameters were tested, which were either ±25% or ±50% of the corresponding "reference values", i.e., $\Delta P_j/P_j$=-0.5, -0.25, 0.25, and 0.5. For the analysis on each

parameter, the values of the other parameters were kept the same as their "reference values". The greater the value of Ψ_{ij}, the more sensitive is the response R_i to the parameter P_j.

The sensitivity index Ψ_{ij} defined in Eq. (6.20) can be rewritten as:

$$\Psi_{ij} = \frac{\Delta R_i}{\Delta P_j} \cdot \left(\frac{P_j}{R_i}\right) \tag{6.21}$$

As the P_j and R_i are obtained with the "reference values", which are determined via model calibration, the value of (P_j/R_i) is a constant. So, the value of Ψ_{ij} only depends on the value of $(\Delta P_j/\Delta R_i)$. Assume that the dependent variable, the response (R_i), is linearly correlated with the independent variable, the parameter (P_j):

$$R_i = E_1 P_j + E_0 \tag{6.22}$$

Then the value of $(\Delta P_j/\Delta R_i)$ can be determined by carrying out linear regression analysis, as the correlation coefficient E_1 (i.e., the gradient of the line reflecting the relationship between P_j and R_i) equals to the values of $(\Delta P_j/\Delta R_i)$.

The resultant sensitivity matrix $\boldsymbol{\Psi}$ is a 8×64 matrix (with its elements including the fore-aft, lateral, vertical and pitch stiffness and damping: k_{x12}, c_{x12}, k_{y12}, c_{y12}, k_{z12}, c_{z12}, k_{p12}, c_{p12}, k_{x23}, c_{x23}, k_{y23}, c_{y23}, k_{z23}, c_{z23}, k_{p23}, c_{p23}, k_{x14}, c_{x14}, k_{y14}, c_{y14}, k_{z14}, c_{z14}, k_{p14}, c_{p14}, k_{x45}, c_{x45}, k_{y45}, c_{y45}, k_{z45}, c_{z45}, k_{p45}, c_{p45}, k_{x56}, c_{x56}, k_{y56}, c_{y56}, k_{z56}, c_{z56}, k_{p56}, c_{p56}, k_{x1s}, c_{x1s}, k_{y1s}, c_{y1s}, k_{z1s}, c_{z1s}, k_{x2s}, c_{x2s}, k_{y2s}, c_{y2s}, k_{z2s}, c_{z2s}, k_{x4b}, c_{x4b}, k_{y4b}, c_{y4b}, k_{z4b}, c_{z4b}, k_{x5b}, c_{x5b}, k_{y5b}, c_{y5b}, k_{z5b}, c_{z5b}, see Appendix D).

It is found that the resonance frequency of the fore-aft apparent mass at the seat pan and the associated modulus were most sensitive to the fore-aft stiffness and damping between the seat and the seated human body (such as k_{x1s}, c_{x1s} and k_{x2s}), and the pitch damping between the abdomen and the pelvis c_{p14}. For the fore-aft apparent mass at the backrest, both the resonance frequency and the associated modulus were most sensitive to the fore-aft stiffness between the upper torso and the backrest k_{x5b}.

The resonance frequency of the lateral apparent mass at the seat pan is found to be most sensitive to the lateral stiffness between the thighs and the seat pan (k_{y2s}) and the lateral damping between the pelvis and the thighs (c_{y12}), while the modulus at the resonance frequency was also affected by the lateral stiffness and damping between the upper torso and the backrest k_{y4b} and c_{y4b}.

The resonance frequency and the associated modulus of the vertical apparent mass at the seat pan are most sensitive to the pitch damping between the abdomen and the pelvis c_{p14}. Besides, the fore-aft stiffness and damping between the pelvis and the seat pan (k_{x1s} and c_{x1s}, respectively) also played an important role in affecting the vertical apparent mass.

6.6 Discussion

6.6.1 Design of the model

6.6.1.1 Consideration of the structure of the human body model

The proposed model of the seated human body is represented by 6 rigid bodies. The part above the pelvis of the human body is represented by three rigid bodies: B_6, B_5 and B_4 (Figure 6.1), which represent the head with neck, the upper torso with shoulders and arm, and the abdomen, respectively. This design is similar to the models developed by Zheng et al. (2011), Wu and Qiu (2020), and Desai et al. (2021a), suitable for the prediction of the biodynamic response. The part below the pelvis of the human body is represented by two rigid bodies in this model: the thighs (B_2) and legs (B_3). The contact between the feet and floor is not considered assuming that its effect on the apparent mass is relatively small. This is similar to the model reported by Zheng et al. (2011), while in the models proposed by Zhang et al. (2015) and Desai et al. (2021a), the thighs and legs were modelled separately, but the feet were also included, and the excitation from the floor to the feet was taken into consideration. In the model proposed by Wu and Qiu (2020), the thighs were represented by two rigid bodies on the left and right side, while the legs were not separately represented by rigid bodies, and the masses of the legs were included in the thighs. Such a design seems suitable for predicting the apparent masses of the human body exposed to combined vertical, lateral and roll vibration. In the current model, the legs were added as separate rigid bodies and the joints between the thighs and legs were included. This enables the coupling between the fore-aft and vertical motion at the knee to be taken into consideration, when the body is exposed to combined fore-aft, lateral and vertical vibration.

6.6.1.2 Determination of the model parameters

The parameters of the current model can be divided into two categories. The first one comprises the parameters related to the mass and dimensions of the rigid bodies, including the coordinates of the mass centres and the moments of inertia of the bodies. The values of the these parameters are ultimately determined by two fundamental values: the weight (m) and height (H) of the human body based on the reported anatomy data (Dempster and Gaughran, 1967). Thus, the inter-subject variability can be taken into consideration for the current model by adopting different values of the parameters for different subjects according to their weight and height, which is similar to the method reported in some published literature (Kim et al., 2005; Zheng et al., 2011; Wu and Qiu, 2020). For the model developed by Wu and Qiu (2020), the masses of the rigid bodies representing the body segments were not directly taken from the published data; instead, they were calibrated

within a range around the data, so that the differences due to the inter-subject variabilities among subjects with similar weight or height could be tolerated in such a range. In the model proposed in this chapter, the masses and dimensions of the rigid bodies are treated as pre-defined parameters taken from relevant literature and are kept as constants, so that the complexity of the model is reduced, and the effectiveness of the model is improved without loss of generality. Due to the lack of the universally available data of the moments of inertia for some body segments (e.g., the upper torso and the lumbar segments), the values of these parameters are calculated for different subjects, assuming that they can be represented by those of the cuboid or ellipsoid rigid bodies. This is similar to the method reported by Wu and Qiu (2020).

The second category includes the parameters related to the joints connecting the rigid bodies, i.e., the coordinates of the contact points, and the stiffness and damping at these points. Most of the parameters in this category are to be calibrated except for some coordinates of the contact points that is determined by the dimension of the rigid bodies. The values of these parameters are rarely available in the literature due to the complexity of the human body and the difficulty to carry out measurements on the living human beings, so they are determined by the model calibration based on the measured apparent masses.

6.6.2 Calibration of the model

Relatively sharp changes of the phase of the measured vertical or horizontal apparent masses were observed at around 12 Hz under many conditions (Figures 6.3 to 6.6), while for the phase calculated using the human body model, such sharp changes do not exist. A similar observation has been reported by Wu and Qiu (2020). This phenomenon may be related to the low coherence in the same frequency range, which indicates some errors of the measurement or the estimation of the apparent mass. Additionally, the associated moduli of the apparent masses are also close to zero, where errors in the estimation of the phase of the apparent mass are more likely to take place, due to its sensitivity to small errors of the mass of the rigid seat during mass cancellation.

Due to the existence of such difference between the simulated and measured phase of the horizontal apparent masses, the objective function of the optimization of this model is defined with respect to the real and imaginary parts of the apparent masses similar to that adopted by Wu and Qiu (2020) to reduce the effect of the possible errors in the estimation of the phase, rather than the conventional use of the moduli and phases of the apparent masses (Qiu and Griffin, 2011; Zheng et al., 2011) or merely the moduli of the apparent masses as reported by Marzbanrad et al. (2016) and Desai et al. (2021a).

6.6.3 Modal properties

Most of the reported modal properties of the seated human body so far were obtained by the modal analysis with mathematical models. Four vibration modes below 10 Hz were identified with the current human body model. The first mode (at 0.84 Hz) appears to correspond to the resonance at around 1 Hz of the measured lateral apparent mass at the backrest (Figure 6.7) which involves the lateral motion of the human body, and its mode shape shows that the motion of the upper body is dominant. The second mode (at 1.89 Hz) corresponds to the fundamental resonance of the lateral apparent mass at the seat pan and the second resonance of that at the backrest. The mode shape at this frequency shows that the motion of the lower body is stronger than that of the upper body. The above two modes are comparable with those reported by Wu and Qiu (2020), although with slightly lower modal frequencies. This difference may be due to the fact that the modal analysis conducted by Wu and Qiu (2020) included the damping of the human body, and the modal frequencies and shapes they obtained were from the complex modes.

The third (at 2.88 Hz) and fourth mode (at 5.76 Hz) involves the fore-aft, vertical and pitch motion of the human body, related to the fundamental resonance of the fore-aft apparent mass and that of the vertical apparent mass, respectively. The third mode is close to the mode at 2.81 Hz reported by Kitazaki and Griffin (1997). The fourth mode (at 5.76 Hz) detected from the current model is in general consistent with the widely reported modal resonance at around 5 Hz under vertical excitation (Kitazaki and Griffin, 1997; Zheng et al., 2011; Liu et al., 2015; Wu and Qiu, 2020), The small differences in the mode shapes of the current model and the reported ones may be attributed to the different structure and design of the model. For example, the current model includes three translational and one pitch DoFs for each rigid body, whereas the lateral DoF was missing in most of the models reported previously.

6.6.4 Parameter sensitivity and values

The results of the parameter sensitivity analysis show that the resonance frequencies and the associated moduli of the apparent masses in the x, y and z-axis of the developed model are most sensitive to the stiffness and damping between the human body and the rigid seat, such as the fore-aft stiffness between the abdomen and the seat pan, which affected the resonance frequency of the fore-aft apparent mass the most (k_{x1s}). Additionally, it is found that in the current model, the pitch damping between the abdomen and pelvis, c_{p14} played an important role in affecting the simulated vertical apparent mass, implying that the pitch motion of the pelvis made great contribution to the vertical apparent mass at the seat pan, which is consistent with the previous study (Kitazaki and Griffin, 1997).

The values of the model parameters for one subject exposed to tri-axial translational excitation with a magnitude of 0.5 ms^{-2} r.m.s. in each of the three axes (see Appendix D.2) is used as an example to compare with those reported in the previous models. For the current model, the value of k_{x1s} is 1.53E3 N/m, which is smaller compared to that reported by Desai et al. (2018) (3.45E5 N/m). Such a difference may be explained by the different excitations in the two models. The experimental data used to calibrate the model developed by Desai et al. (2018) was obtained under lower overall excitation magnitude (0.4 ms^{-2} r.m.s.) compared to that in the current study, leading to less softening of the human body.

The resonance frequency and the associated modulus of the lateral apparent mass were much affected by the lateral damping between the seat and the abdomen c_{y12}. The value of c_{y12} in the current model is 3.18E2 Ns/m, which is comparable with that of the model developed by Wu et al. (2022) (2.35E2 Ns/m). In the model presented in this chapter, the value of c_{p14} (9.82 Ns/m) that affected the vertical apparent mass is comparable with those reported by Matsumoto and Griffin (2001), and Nawayseh and Griffin (2009) (6.72 and 6 Ns/m, respectively).

6.7 Conclusions

In this chapter, a three-dimensional linear multi-body biodynamic model of seated human body exposed to tri-axial translational vibration was developed. The model was constructed with six rigid bodies representing the head and neck, upper torso, abdomen, pelvis, thighs, and leg, respectively. The model was calibrated using the apparent masses at the seat pan and backrest in three translational directions measured in the experimental study described in Chapter 4. The model was capable of capturing the biodynamic responses of different subjects under various experimental conditions, including multi-axis excitations with different magnitudes, and different backrest inclination angles. Four vibration modes of the seated human body were found from the modal analysis, corresponding to one resonance in the measured fore-aft apparent mass, two resonances in the measured lateral apparent mass, and one resonance in the measured vertical apparent mass, respectively. The modal frequencies and mode shapes are comparable with those reported previously. The contact stiffness or damping at the seat and human body interface and the pitch damping between the abdomen and the pelvis were found to affect the apparent masses predicted using the model the most. This model can be further combined with a model of the suspension seat to study the seating dynamics under tri-axial translational excitation.

Chapter 7 DYNAMIC MODELLING OF THE SUSPENSION SEAT AND THE SEAT-OCCUPANT SYSTEM EXPOSED TO TRI-AXIAL TRANSLATIONAL VIBRATION

7.1 Introduction

On heavy vehicles, the effect of the WBV in multi-axis excitation on the ride comfort of the drivers and passengers is not to be underestimated. Most of the suspension seats currently used on the heavy vehicles or construction machinery are designed to attenuate the vertical vibration transmitted to the seated human body, whereas the suspension seat dynamics with horizontal excitations has not been often studied. The spectra of the vibration at the seat base of construction machinery are noticed to distribute in a relatively narrow frequency range (ISO 7096:2008), which requires the suspension seat to have its best performance of vibration attenuation in such a range. A mismatch of the seating dynamics (such as the resonance frequency of the seat-occupant system) with the excitation will significantly affect the WBV exposure of the seated human body and the ride comfort. Hence, how the seat-occupant system behaves under multi-axial excitation needs to be investigated.

The existing experimental studies on the seating dynamics were primarily focus on the single-axis vertical excitation, and are limited by the tolerance of the human body to the high-dose exposure of WBV (e.g., Smith et al., 2008; Qiu, 2017). Many mathematical models of the suspension-seat-occupant system in studying the seating dynamics have been proposed to overcome such limitations (e.g., Gunston et al., 2004; Qiu, 2012; Shahzad and Qiu, 2012; Olausson and Garme, 2015; Shukla et al., 2021, Yin et al., 2021). However, the majority of the developed models were designed to predict the vertical transmissibility of the suspension seat under single-axial vertical excitation, whereas a model capable of capturing the seat transmissibilities in both the vertical and horizontal directions under tri-axial vibration has not been reported.

In this chapter, a multi-body model of the suspension seat including the suspension mechanism, the seat pan, and the backrest was developed and calibrated using the seat transmissibilities measured in the seat loaded with inert mass under tri-axial translational excitation. The initially calibrated suspension seat model was then integrated with the human body model developed in Chapter 6. The combined seat-occupant model was further calibrated using the tri-axial seat

transmissibilities measured in the experimental study described and discussed in Chapter 5. With the verified suspension-seat-human body model, parameter sensitivity analysis was also carried out to find the parameters that influence the seat transmissibility the most.

7.2 Dynamic modelling of the suspension seat

The suspension seat model is developed in the following procedure. First, a lumped parameter model of the suspension mechanism is developed and calibrated using the transmissibilities of the suspension mechanism in the x, y and z-axis measured under tri-axial vibration. Then the rigid bodies representing the seat cushion and backrest were added to the suspension mechanism model. The calibrated parameters of the suspension mechanism remained unchanged, and values of the rest of the parameters of the seat were determined via the calibration of the integrated seat model using the transmissibility of the suspension seat at the seat pan in three translational directions, which were measured with loaded inert masses under tri-axial vibration.

For the suspension seat model presented in this chapter, the following assumptions have been made:

1) The suspension seat is assumed to be a linear system under a certain excitation magnitude and backrest inclination angle;
2) The dynamic transmissibility of the suspension seat can be captured using the rigid multi-body system including the following seat components: suspension top plate the supporting mass of the suspension mechanism, the seat pan cushion and the backrest;
3) The rigid bodies representing the suspension seat perform small oscillations around the corresponding equilibrium position;
4) The inert mass loaded on the suspension mechanism is assumed to be rigidly connected with the suspension top plate and move with the latter as a whole.
5) The suspension seat is symmetric around the sagittal plane.
6) The mass distribution of the human body when seated on the rigid seat is assumed to be the same as that when seated in the suspension seat.

7.2.1 Design of the model of the suspension mechanism

Consider a suspension mechanism loaded with an inert mass. The model of the suspension mechanism consists of three rigid bodies, which is shown in Figure 7.1. The body B_{sp} represents the combination of the sprung mass of the suspension top plate and the loaded inert mass. The sprung mass of the suspension top plate and the inert mass are assumed to be a unity and have the same motion (highlighted in orange in Figure 7.1). Each of the bodies B_l and B_r represents half of the

combination of the unsprung mass (which is a small amount) of the suspension top plate and the supporting mass of the suspension mechanism (such as the scissors-linkage) on the left or right-hand side. The left and right-hand side of the suspension mechanism are assumed to be symmetric, and the masses and dimensions of the bodies B_l and B_r are assumed to be the same. In addition, for the ease of the derivation of the equations of motion, the floor supporting the suspension mechanism is also modelled as a rigid body B_f with infinite dimension and 3 translational DoFs. The centre of the floor is defined to be at the origin O_f, which is located at the middle point of the line between the rear left corner and the rear right corner of the seat base.

The bodies B_l and B_r have 3 DoFs in the fore-aft, lateral and vertical directions each, whereas the body B_{sp} has 4 DoFs, including three translational DoFs in the x, y, and z-axis as well as a rotational DOF around the x-axis.

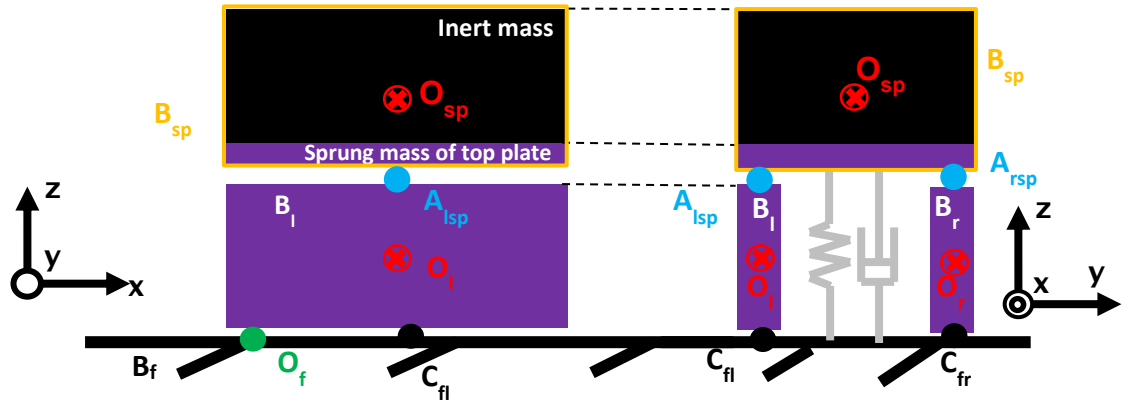

Figure 7.1 Schematic diagram of the model of the suspension mechanism. Red ⊗ symbols: The mass centres of the rigid bodies O_i (i=l, r, sp, f); Green point: Origin point of the global coordinate system O_f; Black points: the contact points between the floor and rigid bodies B_l and B_r (C_{fl} and C_{fr}, respectively); Blue points: the contact points between the rigid bodies representing the structure of the suspension mechanism (A_{lsp} and A_{rsp}). Gray graphic: the springs and dampers in three translational directions between the floor and B_{sp}. Left: side view (the direction of the y-axis is pointing into the paper); right: front view (the direction of the x-axis is pointing out of the paper)

The contact points between the rigid bodies B_l and B_r and the floor are denoted as C_{fl} and C_{fr}, respectively. The body B_s is in contact with B_l and B_r at the contact points A_{lsp} and A_{rsp}, respectively. The mass centres of the bodies are defined as O_{sp}, O_l and O_r, respectively, and the centre point O_{sp} is at the geometry centre of the unity of the sprung mass of the suspension top plate and the inert mass.

For the suspension mechanism model, the unit vectors of the coordinate systems of the rigid bodies are expressed as $\boldsymbol{N_i} = [\boldsymbol{n}_{ix} \quad \boldsymbol{n}_{iy} \quad \boldsymbol{n}_{iz}]^T$ (i=l, r, s). The unit vectors are defined as follows:

$$\boldsymbol{N_i} = \begin{cases} \boldsymbol{N}, & (i = l, r) \\ \boldsymbol{T}_{roll}(\beta_i)\boldsymbol{N}, & (i = sp) \end{cases}$$

Where $\boldsymbol{T}_{roll}(\gamma_{sp}) = \begin{bmatrix} 1 & 0 & 0 \\ 0 & \cos\beta_{sp} & \sin\beta_{sp} \\ 0 & -\sin\beta_{sp} & \cos\beta_{sp} \end{bmatrix} \cong \begin{bmatrix} 1 & 0 & 0 \\ 0 & 1 & \beta_{sp} \\ 0 & -\beta_{sp} & 1 \end{bmatrix}$ (Linearization as β_{sp} is small and in radians) denotes the transformation matrix of the coordinates of body B_s relative to the global coordinate system subject to the roll motion.

The excitations are assumed to be applied from the floor to the suspension mechanism at the contact points between the floor and the bodies B_l and B_r (C_{fl} and C_{fr}, respectively). The top plate of the suspension mechanism was connected with the seat base not only with the cross-linkage on both sides, but also with the air spring and damper in reality. So, the body B_{sp} and the floor is also connected by the springs and dampers in three translational directions (Gray graphic in Figure 7.1).

7.2.2 Equations of motion of the model of the suspension mechanism

7.2.2.1 Displacements and forces of the suspension mechanism model

The coordinates of the mass centres in the global coordinate system can be expressed using Eq. (6.1). Similar to the human body model developed in Chapter 6, the origin of the local coordinate system of each body in the suspension model is fixed at the mass centre of the same body.

The relative displacement between the bodies B_f and B_l ($\boldsymbol{l}_{fl}^{O}$) is:

$$\boldsymbol{l}_{fl}^{O} = \boldsymbol{O}_{l}^{O} + \boldsymbol{C}_{fl}^{B_l} - \left(\boldsymbol{O}_{f}^{O} + \boldsymbol{C}_{fl}^{B_f}\right) \tag{7.1}$$

The relative displacement between the bodies B_f and B_r ($\boldsymbol{l}_{fr}^{O}$) is derived similarly. Taking the roll motion of the suspension top plate into consideration, the relative displacement between the bodies B_l and B_{sp} ($\boldsymbol{l}_{lsp}^{O}$) is:

$$\boldsymbol{l}_{lsp}^{O} = \boldsymbol{O}_{sp}^{O} + \boldsymbol{A}_{lsp}^{B_{sp}}\boldsymbol{T}_{roll}(\gamma_{sp}) - \left(\boldsymbol{O}_{l}^{O} + \boldsymbol{A}_{lsp}^{B_l}\right) \tag{7.2}$$

The relative displacement between the bodies B_r and B_{sp} ($\boldsymbol{l}_{rsp}^{O}$) is derived similarly.

The relative displacement between the bodies B_f and B_{sp} can be directly written as:

$$\boldsymbol{l}_{fsp}^{O} = \left[x_{sp} - x_f, y_{sp} - y_f, z_{sp} - z_f\right] \tag{7.3}$$

The derivatives of the relative displacements, i.e., the velocities of the rigid bodies are derived using Eq. (6.7).

The coordinates of a contact or contact points in one local coordinate systems of the two bodies which it connects can be derived when its coordinates in the other local coordinate systems is determined, as shown in Table 7.1:

Table 7.1 The coordinates of the contact points expressed in different coordinate systems

Contact point	Coordinates in one local coordinate system	Coordinates in the other local coordinate system
C_{fl}	$\boldsymbol{C}_{fl}^{B_l} = \left[x_{C_{fl}}^{B_l}, y_{C_{fl}}^{B_l}, z_{C_{fl}}^{B_l}\right]$	$\boldsymbol{C}_{fl}^{B_f} = \boldsymbol{C}_{fl}^{B_l} + \boldsymbol{O}_{lstat}^{O} - \boldsymbol{O}_{fstat}^{O}$
C_{fr}	$\boldsymbol{C}_{fr}^{B_r} = \left[x_{C_{fr}}^{B_r}, y_{C_{fr}}^{B_r}, z_{C_{fr}}^{B_r}\right]$	$\boldsymbol{C}_{fr}^{B_f} = \boldsymbol{C}_{fr}^{B_r} + \boldsymbol{O}_{rstat}^{O} - \boldsymbol{O}_{fstat}^{O}$
A_{lsp}	$\boldsymbol{A}_{lsp}^{B_{sp}} = \left[x_{A_{lsp}}^{B_{sp}}, y_{A_{lsp}}^{B_{sp}}, z_{A_{lsp}}^{B_{sp}}\right]$	$\boldsymbol{A}_{lsp}^{B_l} = \boldsymbol{A}_{lsp}^{B_{sp}} + \boldsymbol{O}_{spstat}^{O} - \boldsymbol{O}_{lstat}^{O}$
A_{rsp}	$\boldsymbol{A}_{rsp}^{B_{sp}} = \left[x_{A_{rsp}}^{B_{sp}}, y_{A_{rsp}}^{B_{sp}}, z_{A_{rsp}}^{B_{sp}}\right]$	$\boldsymbol{A}_{rsp}^{B_r} = \boldsymbol{A}_{rsp}^{B_{sp}} + \boldsymbol{O}_{spstat}^{O} - \boldsymbol{O}_{rstat}^{O}$

The forces between the bodies are modelled as linear springs and dampers in three translational directions at the contact points C_{fl}, C_{fr}, A_{lsp}, and A_{rsp}. The stiffness and damping between the rigid bodies in either direction are represented by k_{qij} or c_{qij}, respectively, where the first letter of the subscript q represents the direction of the spring or damper (q=x, y, z), and the subscripts i and j indicates the numbering of the two bodies that the spring or damper connects (Table 7.2).

Table 7.2 Definition of the springs and dampers in the model of the suspension mechanism

Contact point	Spring	Damper	Direction	The pair of bodies that the point connects
C_{fl}	k_{xfl}	c_{xfl}	x-axis	B_f and B_1
	k_{yfl}	c_{yfl}	y-axis	
	k_{zfl}	c_{zfl}	z-axis	
C_{fr}	k_{xfr}	c_{xfr}	x-axis	B_f and B_r
	k_{yfr}	c_{yfr}	y-axis	
	k_{zfr}	c_{zfr}	z-axis	
A_{lsp}	k_{xlsp}	c_{xlsp}	x-axis	B_l and B_{sp}
	k_{ylsp}	c_{ylsp}	y-axis	
	k_{zlsp}	c_{zlsp}	z-axis	
A_{rsp}	k_{xrsp}	c_{xrsp}	x-axis	B_r and B_{sp}
	k_{yrsp}	c_{yrsp}	y-axis	
	k_{zrsp}	c_{zrsp}	z-axis	

Note that the values of some parameters are restricted that $k_{xfl}=k_{xfr}$, $k_{yfl}=k_{yfr}$, $k_{zfl}=k_{zfr}$, $c_{xfl}=c_{xfr}$, $c_{yfl}=c_{yfr}$, $c_{zfl}=c_{zfr}$, $k_{xlsp}=k_{xrsp}$, $k_{ylsp}=k_{yrsp}$, $k_{zlsp}=k_{zrsp}$, $c_{xlsp}=c_{xrsp}$, $c_{ylsp}=c_{yrsp}$, and $c_{zflp}=c_{zrsp}$, so that the roll motion of the body B_{sp} due to the vertical motion of the supporting masses B_l and B_r only affects the lateral transmissibility of the suspension mechanism, which is in accordance with the test results.

The spring and damping forces between the rigid bodies of the suspension mechanism model are derived by multiplying the relative displacements (and velocities) in each axis with the corresponding stiffness (or damping) respectively. For example, the force between the bodies B_f and B_l ($\boldsymbol{f}_{fl}^{O}$) is:

$$\boldsymbol{f}_{fl}^{O} = \boldsymbol{l}_{fl}^{O}\begin{bmatrix} k_{xfl} & & \\ & k_{yfl} & \\ & & k_{zfl} \end{bmatrix} + \dot{\boldsymbol{l}}_{fl}^{O}\begin{bmatrix} c_{xfl} & & \\ & c_{yfl} & \\ & & c_{zfl} \end{bmatrix} = [f_{fl(x)} \quad f_{fl(y)} \quad f_{fl(z)}]\boldsymbol{N} \tag{7.4}$$

The force between the bodies B_f and B_r ($\boldsymbol{f}_{fr}^{O}$), the force between the bodies B_l and B_{sp} ($\boldsymbol{f}_{lsp}^{O}$), the force between the bodies B_r and B_{sp} ($\boldsymbol{f}_{rsp}^{O}$), and the force between the bodies B_f and B_{sp} ($\boldsymbol{f}_{fsp}^{O}$) are derived similarly.

7.2.2.2 Equations of motion of the suspension mechanism model

The equations of motion of the rigid bodies B_i (i=l, r, sp) can be derived using the forces between the bodies.

For the rigid body B_l, the equations of motion are derived as:

$$m_l\ddot{x}_l = -f_{fl(x)} + f_{lsp(x)} \tag{7.5}$$

$$m_l\ddot{y}_l = -f_{fl(y)} + f_{lsp(y)} \tag{7.6}$$

$$m_l\ddot{z}_l = -f_{fl(z)} + f_{ls(z)} \tag{7.7}$$

For the rigid body B_r, the equations of motion are derived similarly.

For the rigid body B_{sp}, an additional equation of motion is included representing the roll motion:

$$m_{sp}\ddot{x}_{sp} = -f_{lsp(x)} - f_{rsp(x)} - f_{fsp(x)} \tag{7.8}$$

$$m_{sp}\ddot{y}_{sp} = -f_{lsp(y)} - f_{rsp(y)} - f_{fsp(z)} \tag{7.9}$$

$$m_{sp}\ddot{z}_{sp} = -f_{lsp(z)} - f_{rsp(z)} - f_{fsp(z)} \tag{7.10}$$

$$I_{sp}\ddot{\beta}_{sp} = -\boldsymbol{A}_{lsp}^{B_{sp}} \times \{[f_{lsp(x)} \quad f_{lsp(y)} \quad f_{lsp(z)}]\}\begin{bmatrix}1\\0\\0\end{bmatrix}$$

$$-\boldsymbol{A}_{rsp}^{B_{sp}} \times \{[f_{rsp(x)} \quad f_{rsp(y)} \quad f_{rsp(z)}]\} \begin{bmatrix} 1 \\ 0 \\ 0 \end{bmatrix} \tag{7.11}$$

7.2.2.3 Parameters of the suspension mechanism model

By expanding the equations of motion, it is found that only the parameters including the stiffness and damping (Table 7.2), the masses of the rigid bodies, the moment of inertia of the rigid body B_{sp}, some of the dimensions of the rigid bodies, and the coordinates of the contact points A_{lsp} and A_{rsp}, are included in these equations.

The dimensions of the rigid bodies included in the equations of the motion are the width (l_{ysp}) and height (l_{zsp}) of the rigid body B_{sp}, and the widths of the bodies B_l and B_r, i.e., l_{yl} and l_{yr}, respectively. The width (l_{ysp}) and height (l_{zsp}) of the rigid body B_{sp} are determined based on the measured dimensions of the inert mass and the suspension top plate. The width of the sprung mass of the suspension top plate is assumed to identical to those of the inert mass, and the height of the sprung mass of the suspension top plate, l_{zp}, is assumed to be the same as the height of the suspension top plate measured in reality. The widths of the bodies B_l and B_r, i.e., l_{yl} and l_{yr} are assumed to be the same due to the symmetricity, which are determined by the measured width of the crossbar linkage of the suspension mechanism. Then the coordinates of the contact points are determined with regard to the determined dimensions of the rigid body B_{sp}.

The values of the parameters mentioned above are determined before the model calibration. Table 7.3 shows the determined dimensions of the inert mass and the determined coordinates of the contact points of the suspension mechanism model when the inert mass loaded was 60kg as an example.

Table 7.3 Determined dimensions of the inert mass and the determined coordinates of the contact points of the suspension mechanism model when the loaded with 60kg inert mass

Dimensions	Values (m)	Contact points	Coordinates (m)
l_{ysp}	0.33	A_{lsp}	$x_{A_{lsp}}^{B_{sp}} = 0$
l_{zsp}	0.33	A_{lsp}	$y_{A_{lsp}}^{B_{sp}} = -0.5(l_{\mathrm{ysp}} - l_{yl})$
l_{yl}/l_{yr}	0.03	A_{lsp}	$z_{A_{lsp}}^{B_{sp}} = -0.5 l_{\mathrm{zsp}}$
l_{zp}	0.15	A_{rsp}	$x_{A_{rsp}}^{B_{sp}} = 0$
		A_{rsp}	$y_{A_{rsp}}^{B_{sp}} = 0.5(l_{\mathrm{ysp}} - l_{yr})$
		A_{rsp}	$z_{A_{rsp}}^{B_{sp}} = -0.5 l_{\mathrm{zsp}}$

The rest of the parameters whose values remain to be optimized and determined via calibration are:

1) All the stiffness and damping (Table 7.2),
2) The masses of the rigid bodies B_{sp} and B_l (which is assumed to be identical to that of the body B_r), which are represented by m_{sp} and m_l, respectively.

The values of the masses of the three rigid bodies are constrained by the following equation:

$$m_{sp} + 2m_l = \left(m_p + 2m_l\right) + m_{in} = m_{mech} + m_{in} \tag{7.12}$$

Where m_{mech} (which was 25.5kg) together with the inert mass m_{in} represent the total mass of the suspension mechanism and the mass of the loaded inert mass. Furthermore, the sprung mass of the suspension top plate, m_p, is assumed to be taking relatively small proportion of the mass of the complete suspension mechanism and is hence calibrated within a small range. The moment of inertia I_{sp} of the rigid body B_{sp} about the x-axis is calculated as follows:

$$I_{sp} = \frac{1}{12} m_{sp} \left(\left(l_{ysp}\right)^2 + \left(l_{zsp}\right)^2\right) \tag{7.13}$$

7.2.3 Calibration of the suspension mechanism model

The equations of motion of the rigid bodies can be written in the following form:

$$\boldsymbol{M}_{susp}\ddot{\boldsymbol{X}}_{susp} + \boldsymbol{C}_{susp}\dot{\boldsymbol{X}}_{susp} + \boldsymbol{K}_{susp}\boldsymbol{X}_{susp} = \boldsymbol{C}_f\dot{\boldsymbol{X}}_f + \boldsymbol{K}_f\boldsymbol{X}_f \tag{7.14}$$

Where $\boldsymbol{M}_{susp}$, $\boldsymbol{C}_{susp}$, $\boldsymbol{K}_{susp}$ represent the matrices of mass, damping and stiffness of the model of the suspension mechanism, respectively, while $\boldsymbol{C}_f$ and $\boldsymbol{K}_f$ represent the damping and stiffness related to the vibration input at the floor, respectively. $\boldsymbol{X}_f$ is the vector of vibration input: $[x_f, y_f, z_f]^T$, and $\boldsymbol{X}_{susp}$ is the vector of the output motion of the suspension mechanism model: $[x_l, y_l, z_l, x_r, y_r, z_r, x_{sp}, y_{sp}, z_{sp}, \theta_{sp}]^T$.

Then the transfer function $\boldsymbol{T}_{Rsusp}$ between $\boldsymbol{X}_{susp}$ and $\boldsymbol{X}_f$ is:

$$\boldsymbol{T}_{Rsusp}(\omega) = \frac{\boldsymbol{X}_{susp}(\omega)}{\boldsymbol{X}_f(\omega)} = \left(-\boldsymbol{M}_{susp}\omega^2 + i\omega\boldsymbol{C}_{susp} + \boldsymbol{K}_{susp}\right)^{-1}\left(i\omega\boldsymbol{C}_f + \boldsymbol{K}_f\right) \tag{7.15}$$

With the transfer function $\boldsymbol{T}_{Rsusp}$, the transmissibilities of the suspension mechanism could be derived. Note that the transmissibilities of the suspension mechanism used to calibrate this model were measured at the interface between the suspension upper plate and the inert mass instead of at the mass centre of the inert-mass-and-top-plate assembly, so the lateral displacement of the measurement point should include both the pure lateral motion of the rigid body and the lateral motion that is due to the roll motion of the body B_{sp}. Then the transmissibilities of the suspension mechanism in three directions could hence be derived as:

$$\begin{cases} \boldsymbol{T}_{Rsusp_x} = \boldsymbol{T}_{Rsusp}(7,1) \\ \boldsymbol{T}_{Rsusp_y} = \boldsymbol{T}_{Rsusp}(8,2) + 0.5\left(l_{zsp} - l_{zp}\right) \cdot \boldsymbol{T}_{Rsusp}(10,2) \\ \boldsymbol{T}_{Rsusp_z} = \boldsymbol{T}_{Rsusp}(9,3) \end{cases} \tag{7.16}$$

Where $\boldsymbol{T}_{Rsusp}(i,j)$ represents the element at the ith row and jth column in the 10*3 transfer function $\boldsymbol{T}_{Rsusp}$.

The calculated transmissibilities of the suspension mechanism in the x, y and z-axis, which are obtained in the experimental study described in Chapter 5 are used to calibrate the suspension mechanism model. The calibration is carried out by minimizing the value of the error function $g_{error\_susp}(f)$ is defined to quantify such a difference as follows:

$$g_{error\_susp}(f) = \sum_{j=x,y,z} w_{susp_j} \sqrt{\frac{\sum_{i=1}^{n} \left(\left(Re\left(\boldsymbol{T}_{Rsusp_j}(f_i) \right) \right)_{calc} - \left(Re\left(\boldsymbol{T}_{Rsusp_j}(f_i) \right) \right)_{meas} \right)^2}{n}}$$
$$+ \sum_{j=x,y,z} w_{susp_j} \sqrt{\frac{\sum_{i=1}^{n} \left(\left(Im\left(\boldsymbol{T}_{Rsusp_j}(f_i) \right) \right)_{calc} - \left(Im\left(\boldsymbol{T}_{Rsusp_j}(f_i) \right) \right)_{meas} \right)^2}{n}} \tag{7.17}$$

Where the subscripts *calc* and *meas* denotes the transmissibilities of the suspension mechanism calculated using the model and via measurement, respectively. *Re* and *Im* stand for the real and imaginary parts of the transmissibilities of the suspension mechanism, and *n* is the total number of the frequency points (*n*=119). The subscript *j* distinguishes the direction of the transmissibilities of the suspension mechanism, and w_{susp_j} represents the weighting factors for different transmissibilities that are adjusted to achieve an optimized result. The model is then calibrated using the same method as described in Chapter 5.

A good agreement between the measured and simulated transmissibilities of the suspension mechanism in three translational directions was achieved. Figures 7.2, for example, shows the comparison of the moduli and phases of the simulated transmissibilities of the suspension mechanism using the calibrated model (▬)and their counterpart measured during the experimental study (▬).

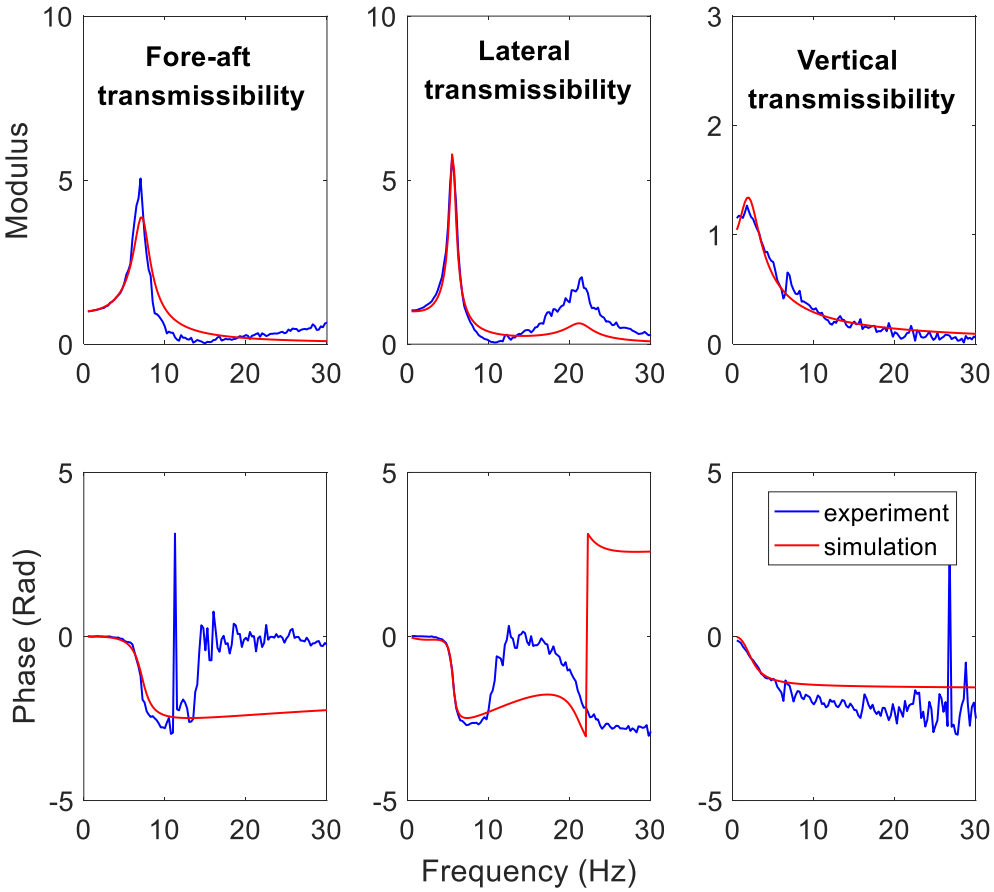

Figure 7.2 The comparison between the transmissibilities of the suspension mechanism measured via experiment and calculated via simulation in the x, y and z-axis when loaded with an inert mass of 60 kg under combined 0.5 ms^{-2} fore-aft, 0.5 ms^{-2} lateral, and 0.5 ms^{-2} (r.m.s.) vertical excitation

7.2.4 Design of the model of the suspension seat

The model of the complete suspension seat was developed by first removing the inert mass from the suspension mechanism model and connecting the rigid bodies representing the seat cushion B_c and the backrest B_{br} to the suspension top plate B_p, and then adding the rigid body representing the inert mass B_m, which is shown in Figure 7.3.

Each of the bodies B_i (i=l, r, p) has 3 DoFs in the x, y, and z-axis, while each of the bodies B_c, B_m, and B_{br} has 5 DoFs, including 3 translational DoFs in the x, y, z-axis, and 2 rotational DoFs around x and y-axis. The mass centres of the rigid bodies B_i (i= l, r, p, c, m, br) are denoted with O_i at the geometry centres. The origin of the global coordinate system O_{seat} is defined at the middle of the intersection line of the seat pan upper surface and backrest front surface when the backrest is upright (Figure 7.3). Note that the thickness of the backrest (i.e., the dimension of the backrest in the x-axis) is not ignored, so this intersection line is not at the left edge of the seat cushion. The body B_p is in

contact with B_l, B_r and B_c at the contact points A_{lsp}, A_{rsp}, and A_{pc}, respectively. The body B_c is in contact with B_m and B_{br} at the contact points A_{cm} and A_{cb}, respectively.

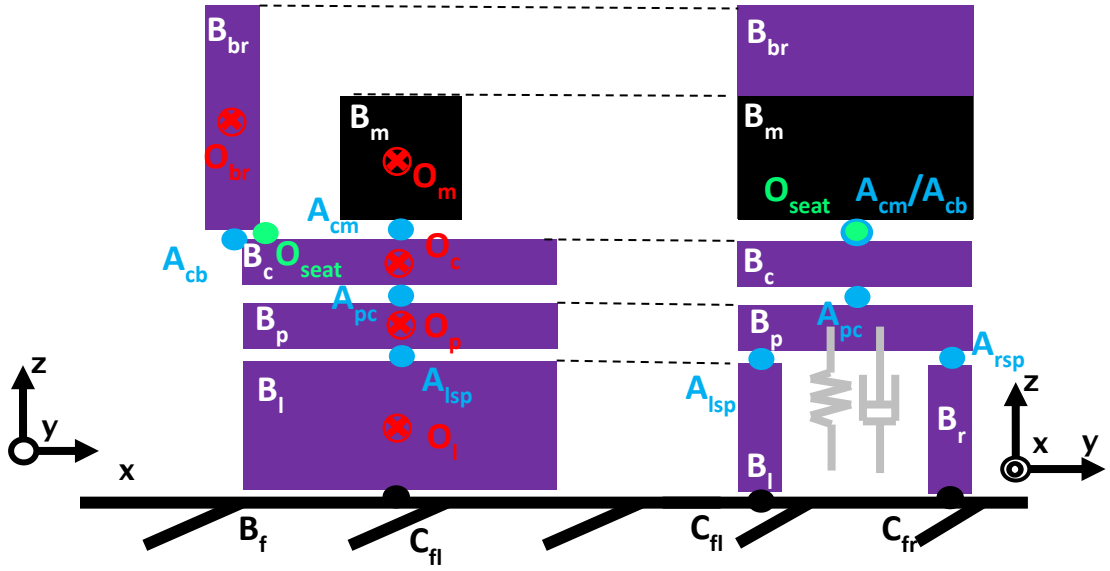

Figure 7.3 Schematic graph of the model of the suspension seat. Red ⊗ symbols: The mass centres of the rigid bodies O_i (*i*=l, r, p, c, m, br); Green point: Origin of the global coordinate system O_{seat}; Black points: the contact points between the floor and rigid bodies B_l and B_r (C_{fl} and C_{fr}, respectively); Blue points: the contact points between the rigid bodies representing the suspension seat (A_{lsp}, A_{rsp}, A_{pc}, A_{cm} and A_{cb}). Gray graphic: the springs and dampers in three translational directions between the floor and B_p. Left: side view; right: front view

The unit vectors of the coordinate systems of the rigid bodies are expressed as $\boldsymbol{N_i} = [\boldsymbol{n}_{ix} \quad \boldsymbol{n}_{iy} \quad \boldsymbol{n}_{iz}]^T$ (i=l, r, p, c, m, br). All the unit vectors are defined as follows:

$$\boldsymbol{N_i} = \begin{cases} \begin{bmatrix} \boldsymbol{n}_x \\ \boldsymbol{n}_y \\ \boldsymbol{n}_z \end{bmatrix}, & (i = l, r) \\ \boldsymbol{T}_{roll}(\beta_i) \begin{bmatrix} \boldsymbol{n}_x \\ \boldsymbol{n}_y \\ \boldsymbol{n}_z \end{bmatrix}, & (i = s) \\ \boldsymbol{T}_{pitch}(\theta_i)\boldsymbol{T}_{roll}(\beta_i) \begin{bmatrix} \boldsymbol{n}_x \\ \boldsymbol{n}_y \\ \boldsymbol{n}_z \end{bmatrix}, & (i = c, m) \\ \boldsymbol{T}_{pitch}(\theta_i)\boldsymbol{T}_{roll}(\beta_i)\boldsymbol{T}_{br}(\alpha) \begin{bmatrix} \boldsymbol{n}_x \\ \boldsymbol{n}_y \\ \boldsymbol{n}_z \end{bmatrix}, & (i = b) \end{cases}$$

Where $\boldsymbol{T}_{br}(\alpha) = \begin{bmatrix} \cos\alpha & 0 & \sin\alpha \\ 0 & 1 & 0 \\ -\sin\alpha & 0 & \cos\alpha \end{bmatrix}$, $\boldsymbol{T}_{roll}(\gamma_i) = \begin{bmatrix} 1 & 0 & 0 \\ 0 & \cos\beta_i & \sin\beta_i \\ 0 & -\sin\beta_i & \cos\beta_i \end{bmatrix} \cong \begin{bmatrix} 1 & 0 & 0 \\ 0 & 1 & \beta_i \\ 0 & -\beta_i & 1 \end{bmatrix}$, and $\boldsymbol{T}_{pitch}(\theta_i) = \begin{bmatrix} \cos\theta_i & 0 & -\sin\theta_i \\ 0 & 1 & 0 \\ \sin\theta_i & 0 & \cos\theta_i \end{bmatrix} \cong \begin{bmatrix} 1 & 0 & -\theta_i \\ 0 & 1 & 0 \\ \theta_i & 0 & 1 \end{bmatrix}$ (linearization as β_i and θ_i are small and in

radians). Furthermore, with second-order linearization ($\beta_i\theta_i \approx 0$), it is simplified that $\boldsymbol{T}_{pitch}(\theta_i)\boldsymbol{T}_{roll}(\beta_i) \cong \begin{bmatrix} 1 & 0 & -\theta_i \\ 0 & 1 & \beta_i \\ \theta_i & -\beta_i & 1 \end{bmatrix}$. Here, $\boldsymbol{T}_{roll}$ denotes the transformation matrix of the coordinates relative to the global coordinate system subject to the roll motion, $\boldsymbol{T}_{pitch}$ denotes the transformation matrix of the coordinates relative to the global coordinate system subject to the pitch motion, and $\boldsymbol{T}_{br}$ denotes the transformation matrix related to the inclination of backrest. As the test results of the seat transmissibilities with loaded inert masses were obtained with an upright backrest, the value of the backrest inclination angle α in the current seat model is 0°.

Same as the suspension mechanism model, the excitations are assumed to be applied at the contact points C_{fl} and C_{fr}. The forces between the bodies representing the suspension mechanism are kept the same as defined in Section 7.2.2. In the complete seat model, the forces between the bodies B_p, B_c, B_m and B_{br} are modelled as linear springs and dampers in three translational directions and around the x and y-axis at the contact points A_{pc}, A_{cm}, and A_{cb}, respectively.

7.2.5 Equations of motion of the suspension seat model

7.2.5.1 Displacements and forces of the suspension seat model

The coordinates of the mass centres in the global coordinate system can be expressed similar to Eq. (6.1). Substituting B_{sp} with B_p, the relative displacements between the bodies B_f and B_l, B_f and B_r, B_l and B_p, B_r and B_p and B_f and B_p are the same as those derived in Section 7.2.2. The rest of the relative displacements are derived as follows:

Due to the additional pitch motion of the body B_c, the relative displacement between the bodies B_p and B_c ($\boldsymbol{l}_{pc}^{O}$) is:

$$\boldsymbol{l}_{pc}^{O} = \boldsymbol{O}_{c}^{O} + \boldsymbol{A}_{pc}^{B_c}\boldsymbol{T}_{pitch}(\theta_c)\boldsymbol{T}_{roll}(\beta_c) - \left[\boldsymbol{O}_{p}^{O} + \boldsymbol{A}_{pc}^{B_p}\boldsymbol{T}_{roll}(\beta_p)\right] \tag{7.18}$$

The relative displacement between the bodies B_c and B_m ($\boldsymbol{l}_{cm}^{O}$) is:

$$\boldsymbol{l}_{cm}^{O} = \boldsymbol{O}_{m}^{O} + \boldsymbol{A}_{cm}^{B_m}\boldsymbol{T}_{pitch}(\theta_m)\boldsymbol{T}_{roll}(\beta_m) - \left[\boldsymbol{O}_{c}^{O} + \boldsymbol{A}_{cm}^{B_c}\boldsymbol{T}_{pitch}(\theta_c)\boldsymbol{T}_{roll}(\beta_c)\right] \tag{7.19}$$

And the relative displacement between the bodies B_c and B_b ($\boldsymbol{l}_{cbr}^{O}$) is derived similarly. The derivatives of the relative displacements, i.e., the velocities of the rigid bodies are also derived.

The coordinates of each of the newly introduced contact points expressed in different local coordinate systems of the bodies that it connects are shown in Table 7.4. The contact points C_{fl}, C_{fr}, A_{lsp}, A_{rsp}, and their coordinates are the same as shown in Table 7.1.

The newly introduced springs and dampers in the suspension seat model are shown in Table 7.5. The springs and dampers at the contact points C_{fl}, C_{fr}, A_{lsp}, A_{rsp} are the same as shown in Table 7.2.

Table 7.4 The coordinates of the introduced contact points expressed in different coordinate systems

Contact point	Coordinates in one local coordinate system	Coordinates in the other local coordinate system
A_{pc}	$\boldsymbol{A}_{pc}^{B_c} = \left[x_{A_{pc}}^{B_c}, y_{A_{pc}}^{B_c}, z_{A_{pc}}^{B_c}\right]$	$\boldsymbol{A}_{pc}^{B_p} = \boldsymbol{A}_{pc}^{B_c} + \boldsymbol{O}_{cstat}^{O} - \boldsymbol{O}_{pstat}^{O}$
A_{cm}	$\boldsymbol{A}_{cm}^{B_m} = \left[x_{A_{cm}}^{B_m}, y_{A_{cm}}^{B_m}, z_{A_{cm}}^{B_m}\right]$	$\boldsymbol{A}_{cm}^{B_c} = \boldsymbol{A}_{cm}^{B_m} + \boldsymbol{O}_{mstat}^{O} - \boldsymbol{O}_{cstat}^{O}$
A_{cb}	$\boldsymbol{A}_{cbr}^{B_{br}} = \left[x_{A_{cbr}}^{B_{br}}, y_{A_{cbr}}^{B_{br}}, z_{A_{cbr}}^{B_{br}}\right]$	$\boldsymbol{A}_{cbr}^{B_c} = \boldsymbol{A}_{cbr}^{B_{br}}\boldsymbol{T}_{br}(\alpha) + \boldsymbol{O}_{brstat}^{O} - \boldsymbol{O}_{cstat}^{O}$

Table 7.5 Definition of the introduced springs and dampers in the model of the suspension seat

Contact point	Spring	Damper	Direction	The pair of rigid bodies that the point connects
A_{pc}	k_{xpc}	c_{xpc}	x-axis	B_p and B_c
	k_{ypc}	c_{ypc}	y-axis	
	k_{zpc}	c_{zpc}	z-axis	
	k_{rpc}	c_{rpc}	around y-axis	
	k_{ppc}	c_{ppc}	around x-axis	
A_{cm}	k_{xcm}	c_{xcm}	x-axis	B_c and B_m
	k_{ycm}	c_{ycm}	y-axis	
	k_{zcm}	c_{zcm}	z-axis	
	k_{rcm}	c_{rcm}	around y-axis	
	k_{pcm}	c_{pcm}	around x-axis	
A_{cb}	k_{xcbr}	c_{xcbr}	x-axis	B_c and B_{br}
	k_{ycbr}	c_{ycbr}	y-axis	
	k_{zcbr}	c_{zcbr}	z-axis	
	k_{rcbr}	c_{rcbr}	around y-axis	
	k_{pcbr}	c_{pcbr}	around x-axis	

Then the spring and damping forces between the rigid bodies of the suspension seat model are derived by multiplying the relative displacements (and velocities) in each axis with the corresponding stiffness (or damping), respectively. Substituting B_{sp} with B_p, the forces between the bodies B_f and B_l, B_f and B_r, B_l and B_p, B_r and B_p and B_f and B_p are the same as those derived in Section 7.2.2. For example, the translational force between the bodies B_p and B_c ($\boldsymbol{f}_{pc}^{O}$) is:

$$\boldsymbol{f}_{pc}^{O} = \boldsymbol{l}_{pc}^{O}\begin{bmatrix} k_{xpc} & & \\ & k_{ypc} & \\ & & k_{zpc} \end{bmatrix} + \dot{\boldsymbol{l}}_{sc}^{O}\begin{bmatrix} c_{xpc} & & \\ & c_{ypc} & \\ & & c_{zpc} \end{bmatrix} = [f_{pc(x)} \quad f_{pc(y)} \quad f_{pc(z)}]\boldsymbol{N} \qquad (7.20)$$

The translational force between the bodies B_c and B_m ($\boldsymbol{f}_{cm}^{O}$) and the translational force between the bodies B_c and B_m ($\boldsymbol{f}_{cbr}^{O}$) are derived similarly.

7.2.5.2 Equations of motion of the suspension seat model

The equations of motion of the rigid bodies B_i (i=l, r, p, c, m, br) can then be derived using the forces between the bodies. The equations of motion of the rigid bodies B_l and B_r are the same as those derived in Section 7.2.2. For the rigid body B_c, the equations of motion in three translational axes and around the x and y-axis are derived as:

$$m_c\ddot{x}_c = -f_{pc(x)} + f_{cm(x)} + f_{cbr(x)} \qquad (7.21)$$

$$m_c\ddot{y}_c = -f_{pc(y)} + f_{cm(y)} + f_{cbr(y)} \qquad (7.22)$$

$$m_c\ddot{z}_c = -f_{pc(z)} + f_{cm(y)} + f_{cbr(y)} \qquad (7.23)$$

$$\begin{aligned} I_{rc}\ddot{\gamma}_c = {} & -k_{rpc}(\beta_c - \beta_p) - c_{rpc}(\dot{\beta}_c - \dot{\beta}_p) + k_{rcm}(\beta_m - \beta_c) + c_{rcm}(\dot{\beta}_m - \dot{\beta}_c) \\ & + k_{rcbr}(\beta_{br} - \beta_c) + c_{rcbr}(\dot{\beta}_{br} - \dot{\beta}_c) - \boldsymbol{A}_{pc}^{B_c} \times \{[f_{pc(x)} \quad f_{pc(y)} \quad f_{pc(z)}]\}\begin{bmatrix}1\\0\\0\end{bmatrix} \\ & + \boldsymbol{A}_{cm}^{B_c} \times \{[f_{cm(x)} \quad f_{cm(y)} \quad f_{cm(z)}]\}\begin{bmatrix}1\\0\\0\end{bmatrix} + \boldsymbol{A}_{cbr}^{B_c} \times \{[f_{cbr(x)} \quad f_{cbr(y)} \quad f_{cbr(z)}]\}\begin{bmatrix}1\\0\\0\end{bmatrix} \end{aligned} \qquad (7.24)$$

$$\begin{aligned} I_{pc}\ddot{\theta}_c = {} & -k_{ppc}\theta_c - c_{ppc}\dot{\theta}_c + k_{pcm}(\theta_m - \theta_c) + c_{pcm}(\dot{\theta}_m - \dot{\theta}_c) + k_{pcbr}(\theta_{br} - \theta_c) \\ & + \boldsymbol{A}_{cm}^{B_c} \times \{[f_{cm(x)} \quad f_{cm(y)} \quad f_{cm(z)}]\}\begin{bmatrix}0\\1\\0\end{bmatrix} + \boldsymbol{A}_{cbr}^{B_c} \times \{[f_{cbr(x)} \quad f_{cbr(y)} \quad f_{cbr(z)}]\}\begin{bmatrix}0\\1\\0\end{bmatrix} \end{aligned} \qquad (7.25)$$

The equations of motion of the rigid body B_p, B_m, and B_{br} are derived similarly.

7.2.5.3 Parameters of the suspension seat model

The masses of the bodies B_l and B_r; the stiffness, damping and coordinates of the contact points that are linked with the bodies B_l and B_r are determined in the suspension mechanism model in Section 7.2.3 are kept unchanged in the seat model.

The masses and dimensions of the bodies B_p, B_c, B_m and B_{br} are determined before model calibration via measurements. Figure 7.4 shows the dimensions (l_{xi}, l_{yi} and l_{zi}) of the body B_i (*i*=p, c, m, br) when the seat was loaded with 60kg inert mass as an example. Then the moments of inertia, and the coordinates of the centres of the mass and the rest of the contact points are calculated based on the masses and dimensions of the bodies. Table 7.6 shows the masses m_i (*i*=p, c, m, br) and the moments of inertia around x-axis I_{ri} (i=p, c, m, br) and y-axis I_{pi} (i=c, m, br). Table 7.7 shows the coordinates of the centres of the mass O_i^O (*i*=p, c, m, br) and the coordinates of the contact points expressed in certain local axes.

The values of the rest of the parameters, i.e., all the stiffness and damping listed in Table 7.5, need to be determined via the calibration of the suspension seat model.

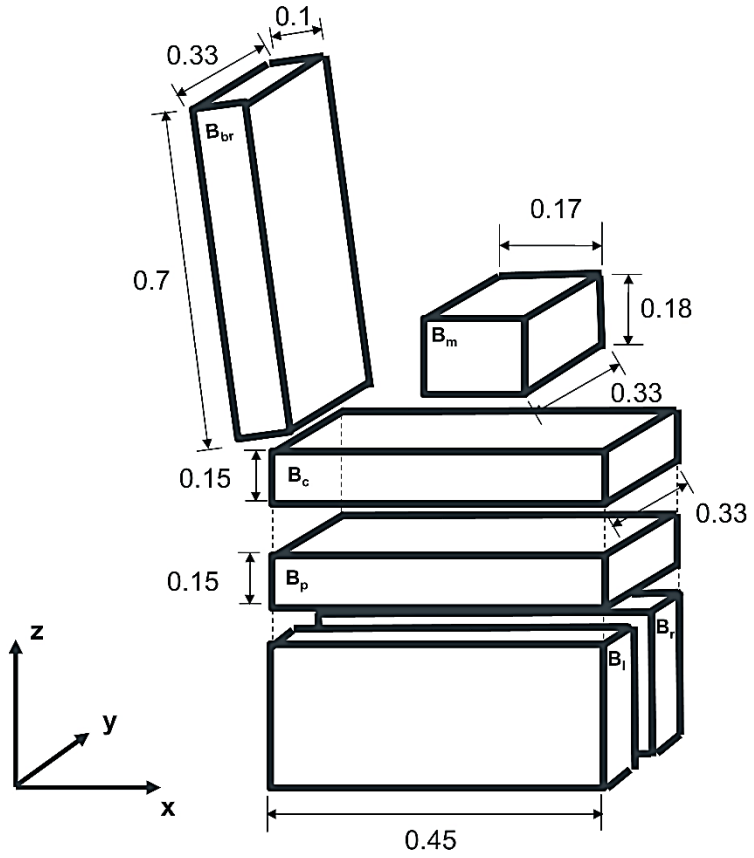

Figure 7.4 Dimensions of the rigid bodies B_p, B_c, B_m and B_{br} of the suspension seat model (unit: m)

Table 7.6 The determined masses and the moments of inertia around x-axis and y-axis I_{pi} of the bodies B_p, B_c, B_m and B_{br} of the suspension seat model

Body	Mass (kg)	Moment of inertia around x-axis	Moment of inertia around y-axis
B_p	m_p =3	$I_{rp} = \frac{m_p}{12}\left[\left(l_{yp}\right)^2 + \left(l_{zp}\right)^2\right]$	Not applicable
B_c	m_c =8.15	$I_{rc} = \frac{m_c}{12}\left[\left(l_{yc}\right)^2 + (l_{zc})^2\right]$	$I_{pc} = \frac{m_c}{12}[(l_{xc})^2 + (l_{zc})^2]$
B_m	m_m =60	$I_{rm} = \frac{m_m}{12}\left[\left(l_{ym}\right)^2 + (l_{zm})^2\right]$	$I_{pm} = \frac{m_m}{12}[(l_{xm})^2 + (l_{zm})^2]$
B_{br}	m_{br} =10.53	$I_{rbr} = \frac{m_{br}}{12}\left[\left(l_{ybr}\right)^2 + (l_{zbr})^2\right]$	$I_{pbr} = \frac{m_{br}}{12}[(l_{xbr})^2 + (l_{zbr})^2]$

Table 7.7 The determined coordinates of the centres of the mass O_i^O (i=p, c, m, br) and contact points of the suspension seat model

Point	Coordinate in x-axis	Coordinate in y-axis	Coordinate in z-axis
O_p^O	$x_{p0} = 0.5l_{xp} - 0.5l_{xbr}$	$y_{p0} = 0$	$z_{s0} = -l_{zc} - 0.5l_{zp}$
O_c^O	$x_{c0} = 0.5l_{xc} - 0.5l_{xbr}$	$y_{c0} = 0$	$z_{s0} = -0.5l_{zc}$
O_m^O	$x_{c0} = 0.5l_{xm} - 0.5l_{xbr}$	$y_{m0} = 0$	$z_{s0} = 0.5l_{zm}$
O_{br}^O	$x_{c0} = -0.5l_{xbr} - 0.5l_{zbr}\sin\alpha$	$y_{br0} = 0$	$z_{br0} = 0.5l_{zbr}\cos\alpha$
A_{pc}	$x_{A_{pc}}^{B_c} = 0$	$y_{A_{pc}}^{B_c} = 0$	$z_{A_{pc}}^{B_c} = -0.5l_{zc}$
A_{cm}	$x_{A_{cm}}^{B_m} = 0$	$y_{A_{cm}}^{B_m} = 0$	$z_{A_{cm}}^{B_m} = -0.5l_{zm}$
A_{cbr}	$x_{A_{cb}}^{B_b} = 0$	$y_{A_{cb}}^{B_b} = 0$	$z_{A_{cb}}^{B_b} = -0.5l_{zbr}$

7.2.6 Calibration of the model of the suspension seat

The equations of motion of the rigid bodies can be written in the following form:

$$\boldsymbol{M}_{seat\_inert}\ddot{\boldsymbol{X}}_{seat\_inert} + \boldsymbol{C}_{seat\_inert}\dot{\boldsymbol{X}}_{seat\_inert} + \boldsymbol{K}_{seat\_inert}\boldsymbol{X}_{seat\_inert} = \boldsymbol{C}_f\dot{\boldsymbol{X}}_f + \boldsymbol{K}_f\boldsymbol{X}_f \quad (7.26)$$

Where $\boldsymbol{M}_{seat\_inert}$, $\boldsymbol{C}_{seat\_inert}$, and $\boldsymbol{K}_{seat\_inert}$ represent the matrices of mass, damping and stiffness of the model of the suspension seat, respectively. $\boldsymbol{X}_{seat\_inert}$ is the vector of the output motion of the suspension seat model: $[x_l, y_l, z_l, x_r, y_r, z_r, x_p, y_p, z_p, \beta_p, x_c, y_c, z_c, \beta_c, \theta_c, x_m, y_m, z_m, \beta_m, \theta_m, x_{br}, y_{br}, z_{br}, \beta_{br}, \theta_{br}]^T$. The transfer function $\boldsymbol{T}_{Rseat\_inert}$ between $\boldsymbol{X}_{sp}$ and $\boldsymbol{X}_f$ is derived as:

$$\boldsymbol{T}_{Rseat\_inert}(\omega) = \frac{\boldsymbol{X}_{seat\_inert}(\omega)}{\boldsymbol{X}_{f}(\omega)} = \frac{i\omega\boldsymbol{C}_f + \boldsymbol{K}_f}{-\boldsymbol{M}_{seat\_inert}\omega^2 + i\omega\boldsymbol{C}_{seat\_inert} + \boldsymbol{K}_{seat\_inert}} \tag{7.27}$$

With the transfer function $\boldsymbol{T}_{Rseat\_inert}$, the transmissibilities of the suspension seat at the seat pan and backrest in three translational directions could be derived. Since the transmissibilities of the suspension seat used to calibrate this model were measured at the surface of the seat pan and backrest, the displacements of the measurement point should include both the translational motion at the centre of the mass and that due to the rotational motion. Then the transmissibilities of the suspension seat in three directions at the seat pan and backrest when loaded with inert mass could hence be derived as:

$$\begin{cases} \boldsymbol{T}_{Rseat\_inert\_sx} = \boldsymbol{T}_{Rseat\_inert}(16,1) + 0.5l_{zm}\boldsymbol{T}_{Rseat\_inert}(20,1) \\ \boldsymbol{T}_{Rseat\_inert\_sy} = \boldsymbol{T}_{Rseat\_inert}(17,2) - 0.5l_{zm}\boldsymbol{T}_{Rseat\_inert}(19,2) \\ \boldsymbol{T}_{Rseat\_inert\_sz} = \boldsymbol{T}_{Rseat\_inert}(18,3) \\ \boldsymbol{T}_{Rseat\_inert\_bx} = \boldsymbol{T}_{Rseat\_inert}(21,1) + 0.07\boldsymbol{T}_{Rseat\_inert}(25,1)c\alpha \\ \quad +0.05\boldsymbol{T}_{Rseat\_inert}(25,1)s\alpha \\ \boldsymbol{T}_{Rseat\_inert\_by} = \boldsymbol{T}_{Rseat\_inert}(22,2) - 0.07\boldsymbol{T}_{Rseat\_inert}(24,2) \\ \boldsymbol{T}_{Rseat\_inert\_bz} = \boldsymbol{T}_{Rseat\_inert}(23,3) + 0.07\boldsymbol{T}_{Rseat\_inert}(25,3)s\alpha \\ \quad -0.05\boldsymbol{T}_{Rseat\_inert}(25,3)c\alpha \end{cases} \tag{7.28}$$

The transmissibilities of the suspension seat at the seat pan and backrest in the x, y and z-axis when loaded with inert mass, which were obtained in the experimental study described in Chapter 5, are used to calibrate the suspension seat model. The calibration is carried out by minimizing the value of the error function $g_{error\_seatinert}(f)$ is defined to quantify such a difference as follows:

$$\begin{aligned} & g_{error\_seatinert}(f) \\ & = \sum_{\substack{j=sx,sy,sz,\\ bx,by,bz}} w_{seatinert\_j} \sqrt{\frac{\sum_{i=1}^{n}\left(\left(Re(\boldsymbol{T}_{Rseat\_inert\_j}(f_i))\right)_{calc} - \left(Re(\boldsymbol{T}_{Rseat\_inert\_j}(f_i))\right)_{meas}\right)^2}{n}} \\ & + \sum_{\substack{j=sx,sy,sz,\\ bx,by,bz}} w_{seatinert\_j} \sqrt{\frac{\sum_{i=1}^{n}\left(\left(Im(\boldsymbol{T}_{Rseat\_inert\_j}(f_i))\right)_{calc} - \left(Im(\boldsymbol{T}_{Rseat\_inert\_j}(f_i))\right)_{meas}\right)^2}{n}} \end{aligned} \tag{7.29}$$

Where the subscript *j* distinguishes the position and direction of the transmissibilities of the suspension seat, and $w_{seatinert\_j}$ represents the weighting factors for different seat transmissibilities that are adjusted to achieve an optimized result. The model is then calibrated using the same method as described in Chapter 5.

Good agreements were achieved between the measured and simulated transmissibilities of the suspension seat at the seat pan and backrest in the x and z-axis (Figures 7.5), and the resonance

frequency and the associated modulus of the lateral transmissibilities (Figures 7.6). The transmissibilities of the suspension seat were obtained under the same excitation as that in Figure 7.2.

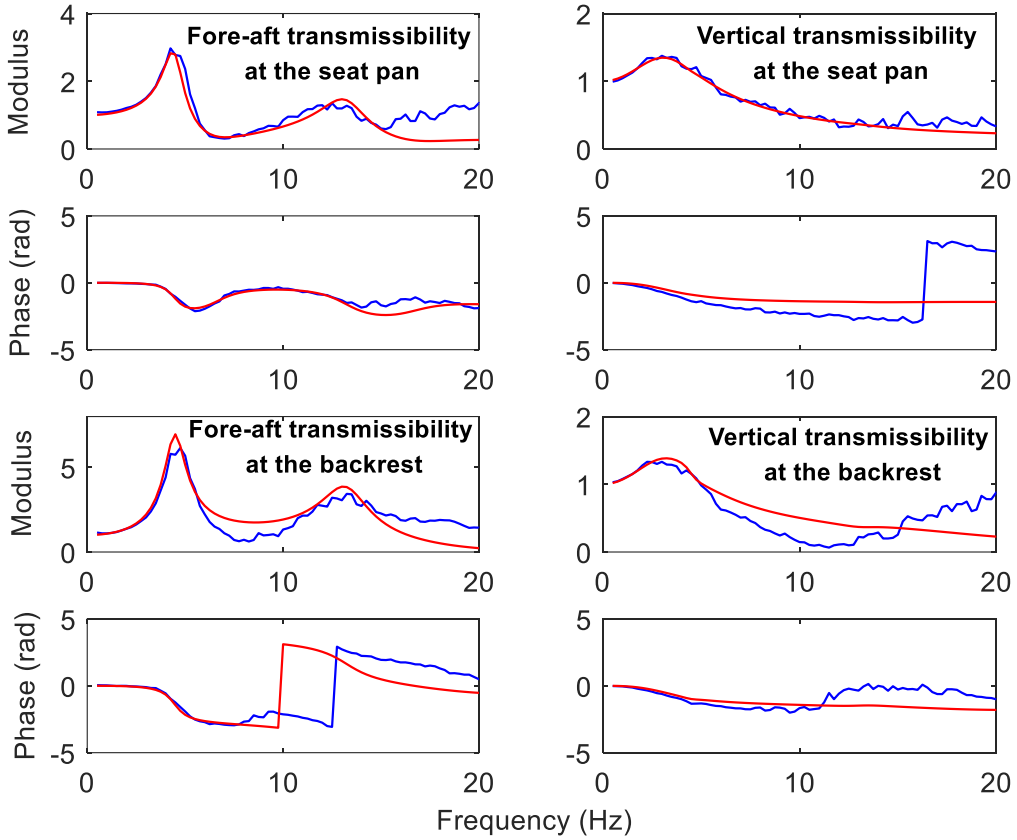

Figure 7.5 The comparison between the measured (▬) and simulated (▬) transmissibilities of the suspension seat at the seat pan and backrest in the x and z-axis with loaded inert mass of 60kg under combined 0.5 ms^{-2} fore-aft, 0.5 ms^{-2} lateral, and 0.5 ms^{-2} (r.m.s.) vertical excitation

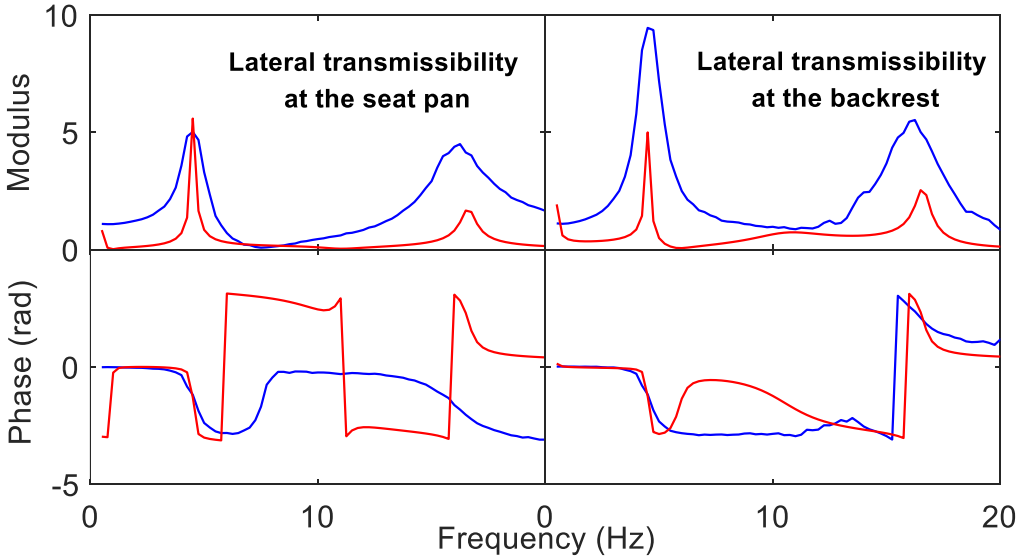

Figure 7.6 The comparison between the measured (▬) and simulated (▬) transmissibilities of the suspension seat at the seat pan and backrest in the y-axis with loaded inert

mass of 60kg under combined 0.5 ms^{-2} fore-aft, 0.5 ms^{-2} lateral, and 0.5 ms^{-2} (r.m.s.) vertical excitation

7.3 Dynamic modelling of the coupled suspension-seat-occupant system

The assumptions for the suspension-seat-occupant model include those for the seated human body model (Section 6.2) and those for the suspension seat model (Section 7.2). Additionally, it is assumed that the coordinates of the contact points between the human body and the suspension seat at the seat pan and backrest are the same as those between the human body and the rigid seat, which were determined in Chapter 6.

7.3.1 The coupling of the human body model and the suspension seat model

The coupled suspension-seat-occupant model is shown in Figure 7.7. Note that it provides a side view, so B_r and the connection points related to it are not shown.

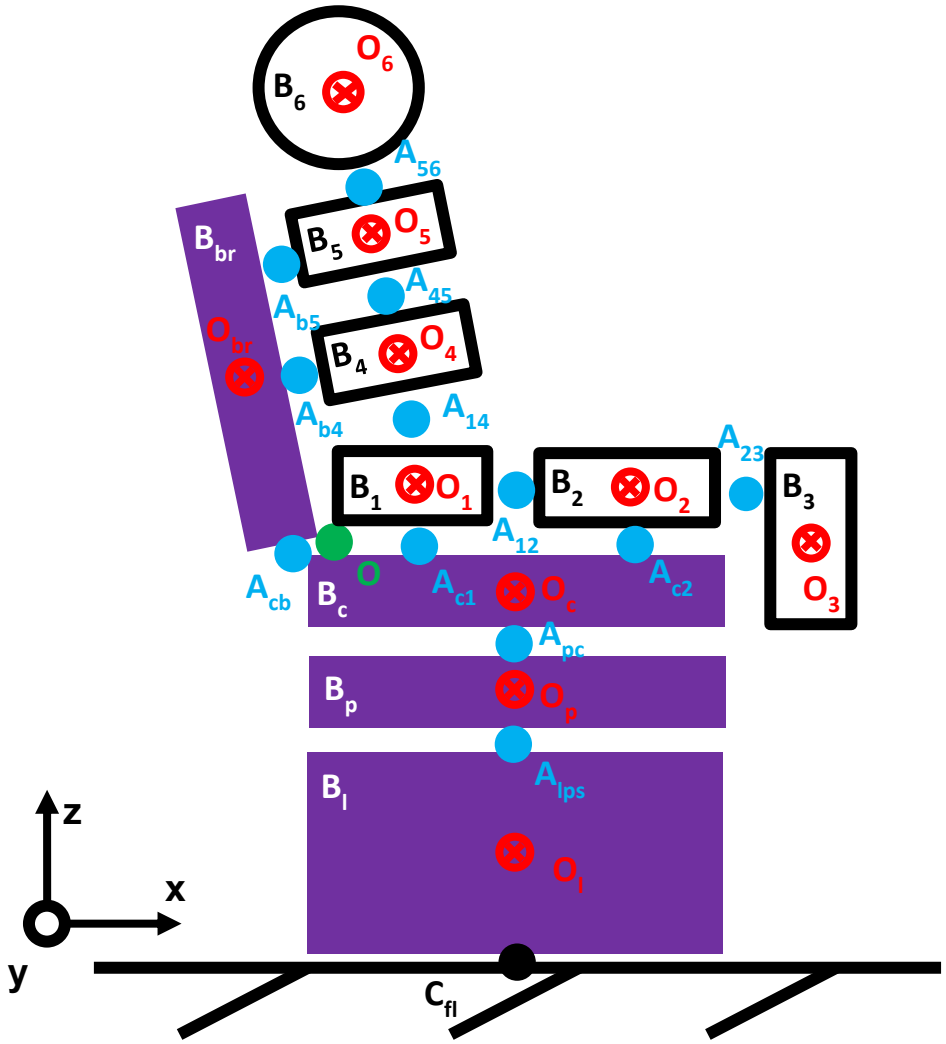

Figure 7.7 Schematic diagram of the model of the suspension-seat-occupant system.

The inert mass in the suspension seat model is removed. The model of the seated human body (developed in Chapter 6) is supported by the model of the suspension seat. The origin of the global coordinate system O is the same as that in the suspension seat model. This makes the coordinates of the mass centres of the rigid bodies and the contact points remain the same as those defined in the human body model and the suspension seat model. The masses, dimensions, and the numbers of DoF of the bodies B_i (i=1, 2, …6, l, r, p, c, br) are also kept the same as those defined in the corresponding original models.

In this suspension-seat-occupant model, the symbols representing the rigid bodies, the mass centres, and the contact points related to the human body model and the suspension seat model are kept the same as those in Figure 6.1 and Figure 7.3, respectively, expect the four contact points between the seat and the human body. The rigid bodies B_1 and B_2 are in contact with B_c at the contact points A_{c1} and A_{c2}, respectively, and the rigid bodies B_4 and B_5 are in contact with B_{br} at the contact points A_{b4} and A_{b5}, respectively.

It is assumed that the mass distribution of the human body when seated on the rigid seat and the suspension seat are the same. However, due to the difference between the material of the suspension seat cushion and that of the rigid seat, the contact stiffness and damping between the seated human body and the suspension seat would be different from those between the human body and the rigid seat. Hence, the parameters related to the stiffness and damping at the contact points between the seat and the human body (see Table 7.8) are re-calibrated in the suspension-seat-occupant model, while the values of the rest of the parameters are the kept the same as those in the human body model and the suspension seat model.

Table 7.8 The introduced springs and dampers to be calibrated in the model of the suspension-seat-occupant model

Contact point	Spring	Damper	Direction	The pair of rigid bodies that the point connects
A_{c1}	k_{xc1}	c_{xc1}	x-axis	B_c and B_1
	k_{yc1}	c_{yc1}	y-axis	
	k_{zc1}	c_{zc1}	z-axis	
	k_{pc1}	c_{pc1}	around x-axis	

Table 7.8 (Continued)

Contact point	Spring	Damper	Direction	The pair of rigid bodies that the point connects
A_{c2}	k_{xc2}	c_{xc2}	x-axis	B_c and B_2
	k_{yc2}	c_{yc2}	y-axis	
	k_{zc2}	c_{zc2}	z-axis	
	k_{pc2}	c_{pc2}	around x-axis	
A_{b4}	k_{xb4}	c_{xb4}	x-axis	B_{br} and B_4
	k_{yb4}	c_{yb4}	y-axis	
	k_{zb4}	c_{zb4}	z-axis	
	k_{pb4}	c_{pb4}	around x-axis	
A_{b5}	k_{xb5}	c_{xb5}	x-axis	B_{br} and B_5
	k_{yb5}	c_{yb5}	y-axis	
	k_{zb5}	c_{zb5}	z-axis	
	k_{pb5}	c_{pb5}	around x-axis	

7.3.2 Equations of motion of the model

Due to the changed contact dynamics between the seated human body and the suspension seat at the contact points (A_{c1}, A_{c2}, A_{b4} and A_{b5}), the relative displacements between the bodies connected by these points, the forces at these points and the equations of motion of the bodies that are connected with these contact points need to be re-defined and calculated. The equations of motion of the rest of the bodies, B_l, B_r, B_p, B_3 and B_6 are kept the same as defined in Sections 6.2.3 and 7.2.3, respectively.

The relative displacement between the bodies B_c and B_1 ($\boldsymbol{l}_{c1}^{O}$) is:

$$\boldsymbol{l}_{c1}^{O} = \boldsymbol{O}_{1}^{O} + \boldsymbol{A}_{c1}^{B_1}\boldsymbol{T}_{pitch}(\theta_1) - \left[\boldsymbol{O}_{c}^{O} + \boldsymbol{A}_{c1}^{B_c}\boldsymbol{T}_{pitch}(\theta_c)\boldsymbol{T}_{roll}(\beta_c)\right] \tag{7.30}$$

The relative displacement between the bodies B_c and B_2 ($\boldsymbol{l}_{c2}^{O}$) derived similarly.

The relative displacement between the bodies B_b and B_4 ($\boldsymbol{l}_{b4}^{O}$) is:

$$\boldsymbol{l}_{b4}^{O} = \boldsymbol{O}_{4}^{O} + \boldsymbol{A}_{b4}^{B_4}\boldsymbol{T}_{pitch}(\theta_4)\boldsymbol{T}_{br}(\alpha) - \left[\boldsymbol{O}_{b}^{O} + \boldsymbol{A}_{b4}^{B_{br}}\boldsymbol{T}_{pitch}(\theta_{br})\boldsymbol{T}_{roll}(\beta_{br})\boldsymbol{T}_{br}(\alpha)\right] \tag{7.31}$$

The relative displacement between the bodies B_{br} and B_5 ($\boldsymbol{l}_{b5}^{O}$) is derived similarly.

The spring and damping forces related to these relative displacements (and their derivations) are then derived. The translational force between the bodies B_c and B_1 ($\boldsymbol{f}_{c1}^{O}$) is:

$$\boldsymbol{f}_{c1}^{O} = \boldsymbol{l}_{c1}^{O}\begin{bmatrix} k_{xc1} & & \\ & k_{yc1} & \\ & & k_{zc1} \end{bmatrix} + \dot{\boldsymbol{l}}_{c1}^{O}\begin{bmatrix} c_{xc1} & & \\ & c_{yc1} & \\ & & c_{zc1} \end{bmatrix} = [f_{c1(x)} \quad f_{c1(y)} \quad f_{c1(z)}]\boldsymbol{N} \qquad (7.32)$$

The translational force between the bodies B_c and B_2 ($\boldsymbol{f}_{c2}^{O}$) is derived similarly.

The translational force between the bodies B_{br} and B_4 ($\boldsymbol{f}_{b4}^{O}$) is:

$$\boldsymbol{f}_{b4}^{O} = \boldsymbol{l}_{b4}^{O}\boldsymbol{T}_{br}^{T}(\alpha)\begin{bmatrix} k_{xb4} & & \\ & k_{yb4} & \\ & & k_{zb4} \end{bmatrix} + \dot{\boldsymbol{l}}_{b4}^{O}\boldsymbol{T}_{br}^{T}(\alpha)\begin{bmatrix} c_{xb4} & & \\ & c_{yb4} & \\ & & c_{zb4} \end{bmatrix}$$

$$= [\check{f}_{b4(x)} \quad \check{f}_{b4(y)} \quad \check{f}_{b4(z)}]\check{\boldsymbol{N}} \qquad (7.33)$$

The translational force between the bodies B_{br} and B_5 ($\boldsymbol{f}_{b5}^{O}$) is derived similarly. Then the updated equations of motion of the rigid bodies B_1, B_2, B_4, B_5, B_c and B_{br} in the suspension-seat-occupant model are derived similar to Eqs (6.11) to (6.14).

7.3.3 Model calibration

The equations of motion of the rigid bodies can be written in the following form:

$$\boldsymbol{M}_{seat\_body}\ddot{\boldsymbol{X}}_{seat\_body} + \boldsymbol{C}_{seat\_body}\dot{\boldsymbol{X}}_{seat\_body} + \boldsymbol{K}_{seat\_body}\boldsymbol{X}_{seat\_body} = \boldsymbol{C}_f\dot{\boldsymbol{X}}_f + \boldsymbol{K}_f\boldsymbol{X}_f \quad (7.34)$$

Where $\boldsymbol{M}_{seat\_body}$, $\boldsymbol{C}_{seat\_body}$, and $\boldsymbol{K}_{seat\_body}$ represent the matrices of mass, damping and stiffness of the model of the suspension-seat-occupant system, respectively. $\boldsymbol{X}_{seat\_body}$ is the vector of the output motion of the suspension seat model: [x_l, y_l, z_l, x_r, y_r, z_r, x_p, y_p, z_p, θ_p, x_c, y_c, z_c, θ_c, θ_c, x_{br}, y_{br}, z_{br}, θ_{br}, θ_{br}, x_1, y_1, z_1, θ_1, x_2, y_2, z_2, θ_2, x_3, y_3, z_3, θ_3, x_4, y_4, z_4, θ_4, x_5, y_5, z_5, θ_5, x_6, y_6, z_6, θ_6]^T. Hence, the transfer function $\boldsymbol{T}_{Rseat\_body}$ between $\boldsymbol{X}_{sp}$ and $\boldsymbol{X}_f$ is:

$$\boldsymbol{T}_{Rseat\_body}(\omega) = \frac{\boldsymbol{X}_{seat\_body}(\omega)}{\boldsymbol{X}_f(\omega)} = \frac{i\omega\boldsymbol{C}_f + \boldsymbol{K}_f}{-\boldsymbol{M}_{seat\_body}\omega^2 + i\omega\boldsymbol{C}_{seat\_body} + \boldsymbol{K}_{seat\_body}} \qquad (7.35)$$

With the transfer function $\boldsymbol{T}_{Rseat\_body}$, the transmissibilities of the suspension seat at the seat pan and backrest in three translational directions when the human body is seated could be derived. The transmissibilities of the suspension seat in three directions at the seat pan and backrest could hence be derived as:

$$\begin{cases} \boldsymbol{T}_{Rseat\_body\_sx} = \boldsymbol{T}_{Rseat\_body}(21,1) + \boldsymbol{z}_{A_{c1}}^{B_1} * \boldsymbol{T}_{Rseat\_body}(24,1) \\ \boldsymbol{T}_{Rseat\_body\_sy} = \boldsymbol{T}_{Rseat\_body}(22,2) \\ \boldsymbol{T}_{Rseat\_body\_sz} = \boldsymbol{T}_{Rseat\_body}(23,3) - \boldsymbol{x}_{A_{c1}}^{B_1} * \boldsymbol{T}_{Rseat\_body}(24,3) \\ \boldsymbol{T}_{Rseat\_body\_bx} = \boldsymbol{T}_{Rseat\_body}(37,1) + \left(\boldsymbol{z}_{A_{c1}}^{B_1} c\alpha + \boldsymbol{x}_{A_{c1}}^{B_1} s\alpha\right)\boldsymbol{T}_{Rseat\_body}(40,1) \\ \boldsymbol{T}_{Rseat\_body\_by} = \boldsymbol{T}_{Rseat\_body}(38,2) \\ \boldsymbol{T}_{Rseat\_body\_bz} = \boldsymbol{T}_{Rseat\_body}(39,3) + \left(\boldsymbol{z}_{A_{c1}}^{B_1} s\alpha - \boldsymbol{x}_{A_{c1}}^{B_1} c\alpha\right)\boldsymbol{T}_{Rseat\_body}(40,3) \end{cases} \quad (7.36)$$

Where $\boldsymbol{T}_{Rseat\_body}(i,j)$ represents the element at the i[th] row and j[th] column in the 25*3 transfer function $\boldsymbol{T}_{Rseat\_body}$.

The measured transmissibilities of the suspension seat at the seat pan and backrest in the x, y and z-axis when the human body (Chapter 5) is seated are used to calibrate the parameters of the suspension seat model. The calibration is carried out by minimizing the value of the error function $g_{error\_seatbody}(f)$ is defined to quantify such a difference as follows:

$$g_{error\_seatbody}(f) = \sum_{\substack{j=sx,sy,sz,\\ bx,by,bz}} w_{seatbody\_j} \sqrt{\frac{\sum_{i=1}^{n}\left(\left(Re(\boldsymbol{T}_{Rseat\_body\_j}(f_i))\right)_{calc} - \left(Re(\boldsymbol{T}_{Rseat\_body\_j}(f_i))\right)_{meas}\right)^2}{n}} + \sum_{\substack{j=sx,sy,sz,\\ bx,by,bz}} w_{seatbody\_j} \sqrt{\frac{\sum_{i=1}^{n}\left(\left(Im(\boldsymbol{T}_{Rseat\_body\_j}(f_i))\right)_{calc} - \left(Im(\boldsymbol{T}_{Rseat\_body\_j}(f_i))\right)_{meas}\right)^2}{n}} \quad (7.37)$$

Where $w_{seatbody\_j}$ represents the weighting factors for different seat transmissibilities that are adjusted to achieve an optimized result. The model is then calibrated using the same method as described in Chapter 6.

The seat transmissibilities obtained using the calibrated suspension-seat-occupant model (▬) could in general achieve good agreement with the experiment results (▬) in the x and z-axis at the seat pan and backrest when the human body is seated under different excitation magnitudes and backrest inclination angles (Figure 7.8 to 7.10).

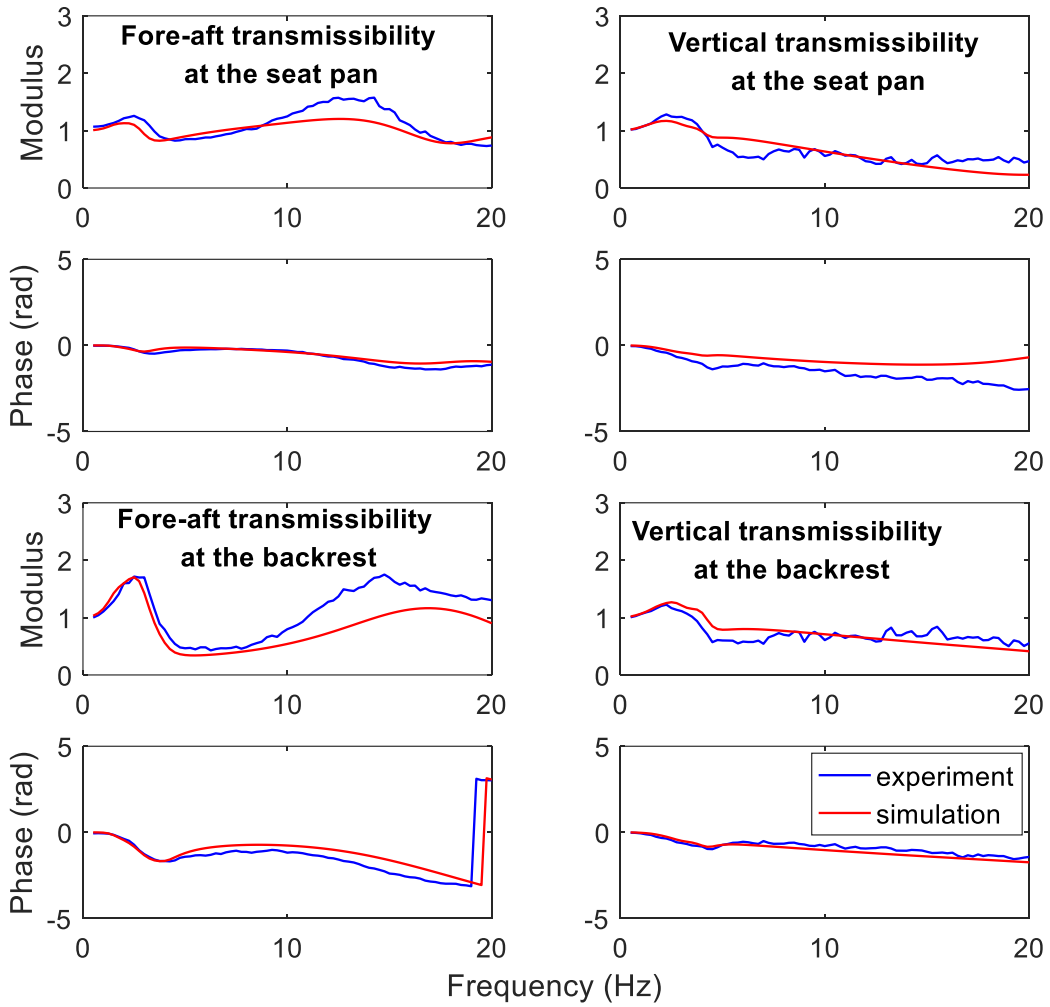

Figure 7.8 The comparison between the measured (▬) and simulated (▬) transmissibilities of the suspension seat at the seat pan and backrest in the x and z-axis under combined 0.5 ms^{-2} fore-aft, 0.5 ms^{-2} lateral, and 0.5 ms^{-2} (r.m.s.) vertical excitation when a subject (1.75m in height and 78.6 kg in weight) was seated and with upright backrest

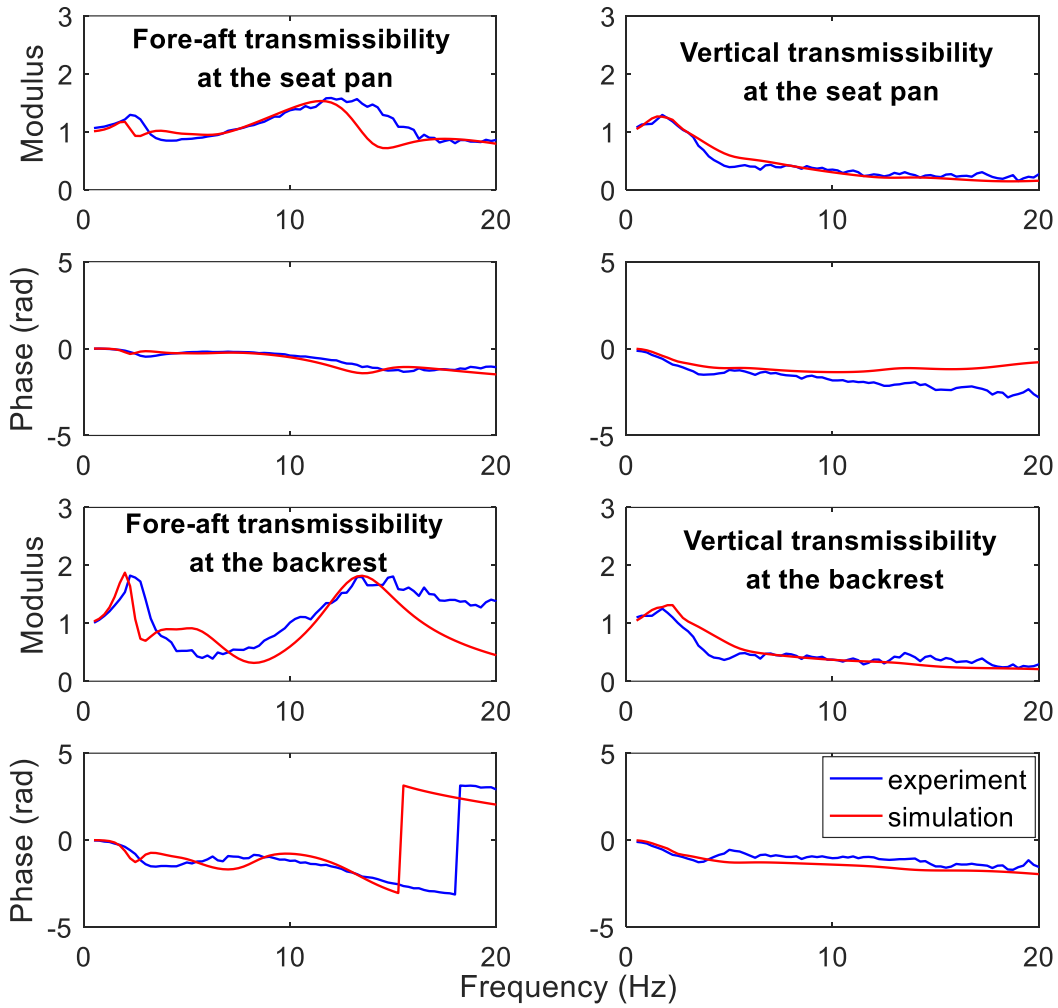

Figure 7.9 The comparison between the measured ( ) and simulated ( ) transmissibilities of the suspension seat at the seat pan and backrest in the x and z-axis under combined 0.5 ms^{-2} fore-aft, 1.0 ms^{-2} lateral, and 1.0 ms^{-2} (r.m.s.) vertical excitation when a subject (1.75m in height and 78.6 kg in weight) was seated and with upright backrest

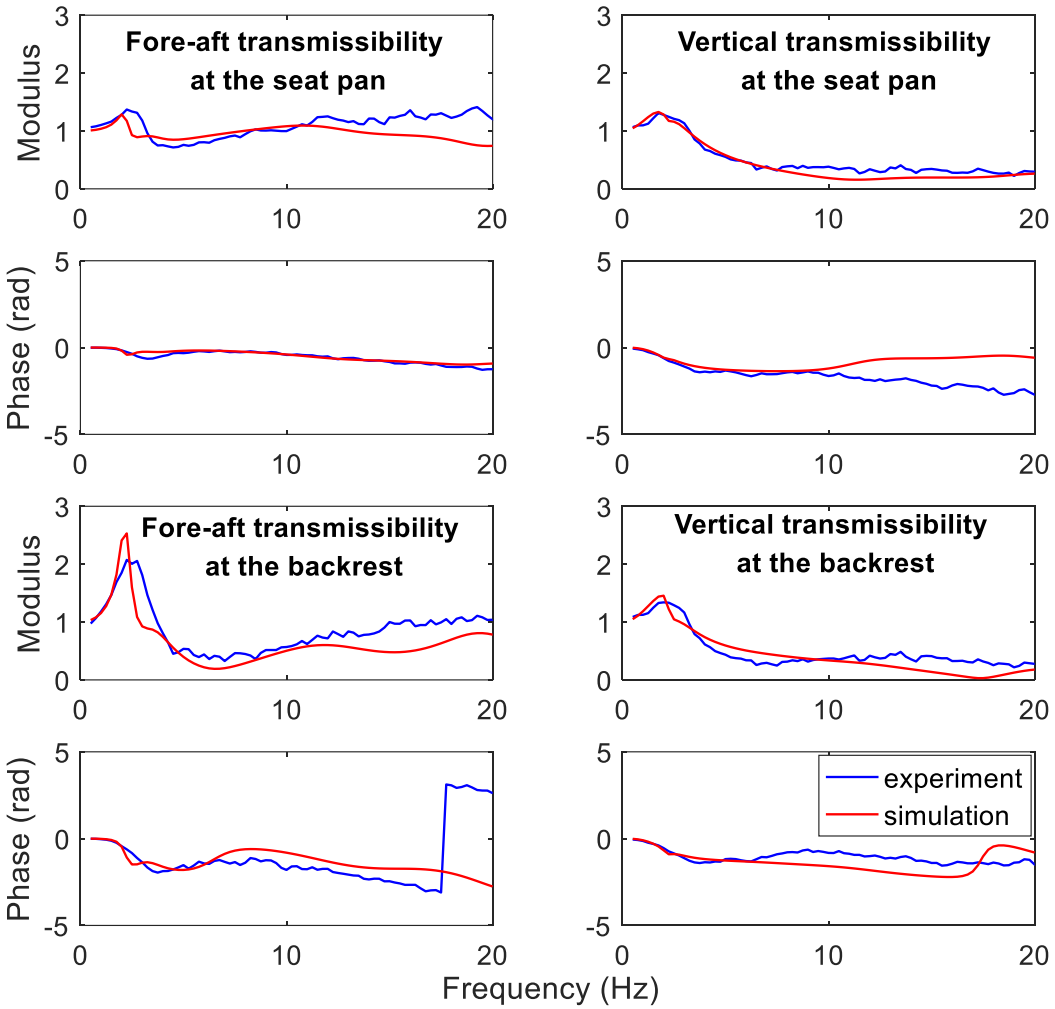

Figure 7.10 The comparison between the measured (▬) and simulated (▬) transmissibilities of the suspension seat at the seat pan and backrest in the x and z-axis under combined 0.5 ms^{-2} fore-aft, 1.0 ms^{-2} lateral, and 1.0 ms^{-2} (r.m.s.) vertical excitation when a subject (1.75m in height and 78.6 kg in weight) was seated and with backrest inclined by 20°

Figure 7.11 shows that for the seat transmissibilities at the seat pan and backrest in the y-axis, the error simulated results (▬) was relatively greater, whereas they had the same number of resonances occurring at the same frequencies as their measured counterparts (▬). The excitation for the results shown in Figures 7.8 and 7.11 was the same as the those shown in Figure 7.2, and the subject for the results shown in Figures 7.8 to 7.11 was the same as the one whose apparent masses were shown in Figure 6.4.

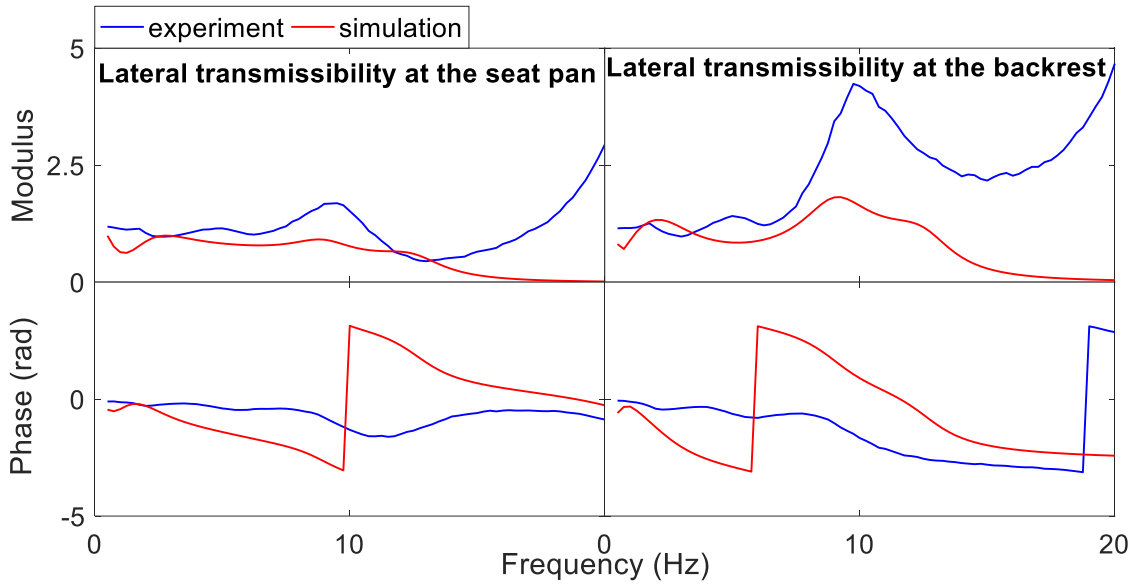

Figure 7.11 The comparison between the measured (▬) and simulated (▬) transmissibilities of the suspension seat at the seat pan and backrest in the y -axis under combined 0.5 ms^{-2} fore-aft, 0.5 ms^{-2} lateral, and 0.5 ms^{-2} (r.m.s.) vertical excitation when a subject (1.75m in height and 78.6 kg in weight) was seated and with upright backrest

7.4 Parameter sensitivity analysis

The sensitivity analysis was carried out on the parameters of the suspension seat using the same method as introduced in Section 6.5 and Eqs. (6.20) to (6.22). Four responses at the seat pan and backrest closely related to the ride comfort were chosen, with i=1 being the resonance frequency of the vertical transmissibility at the seat pan with the seated subject, i=2 being the modulus associated with the resonance of the vertical transmissibility at the seat pan, i=3 the fundamental resonance frequency of the fore-aft transmissibility at the backrest, and i=4 the modulus associated with the fundamental resonance of the fore-aft transmissibility at the backrest.

The resultant sensitivity matrix $\boldsymbol{\Psi}_{seat}$ can be written as:

$$\boldsymbol{\Psi}_{seat} = [\boldsymbol{\Psi}_{susp} \quad \boldsymbol{\Psi}_{seatpan} \quad \boldsymbol{\Psi}_{backrest}]_{4\times 52} \tag{7.38}$$

Where $\boldsymbol{\Psi}_{susp}$, $\boldsymbol{\Psi}_{seatpan}$ and $\boldsymbol{\Psi}_{backrest}$ represent the sensitivity matrices of the parameters related to the suspension mechanism (k_{xfl}, c_{xfl}, k_{zfl}, c_{zfl}, k_{xlp}, c_{xlp}, k_{zlp}, c_{zlp}, k_{xfp}, c_{xfp}, k_{zfp}, c_{zfp}), the seat pan (k_{xpc}, c_{xpc}, k_{zpc}, c_{zpc}, k_{rpc}, c_{rpc}, k_{ppc}, c_{ppc}, k_{xcbr}, c_{xcbr}, k_{zcbr}, c_{zcbr}, k_{rcbr}, c_{rcbr}, k_{pcbr}, c_{pcbr}, k_{xc1}, c_{xc1}, k_{zc1}, c_{zc1}, k_{pc1}, c_{pc1}, k_{xc2}, c_{xc2}, k_{zc2}, c_{zc2}, k_{pc2}, c_{pc2}) and the backrest (k_{xb4}, c_{xb4}, k_{zb4}, c_{zb4}, k_{pb4}, c_{pb4}, k_{xb5}, c_{xb5}, k_{zb5}, c_{zb5}, k_{p5}, c_{pb5}), respectively (see Appendix D).

It is found that for the parameters related to the suspension mechanism, the resonance frequency of the vertical seat transmissibility at the seat pan and the associated modulus were most sensitive

to the vertical stiffness and damping between the floor and the suspension top plate k_{zfp} and c_{zfp} (in the descending order of the sensitivities). The modulus associated with the fundamental resonance frequency of the fore-aft transmissibility at the backrest was most sensitive to the fore-aft stiffness and damping between the floor and the suspension supporting linkage k_{zlp}.

For the parameters related to the seat pan, all of the four responses were most sensitive to the rotational stiffness around y-axis (i.e., the pitch stiffness) between the seat cushion and the suspension top plate k_{ppc}. Additionally, the fundamental resonance frequency of the fore-aft seat transmissibility at the backrest and the associated modulus were also sensitive (but to a smaller degree) to the rotational damping around y-axis between the seat cushion and the suspension top plate c_{ppc} and that between the seat cushion and the thighs of the human body c_{pc2}.

For the parameters related to the backrest, all of the four responses were most sensitive to the rotational damping around y-axis between the backrest and the upper torso of the human body c_{pb5}. Furthermore, the resonance frequency of the vertical seat transmissibility at the seat pan and the modulus associated with the fundamental resonance frequency of the fore-aft seat transmissibility at the backrest were also sensitive (but to a smaller degree) to the fore-aft stiffness between the backrest and the upper torso of the human body k_{xb5}.

7.5 Discussion

7.5.1 The structure of the seat model

A suspension seat model suitable for the prediction of seat transmissibility with tri-axis translational excitation has been rarely seen in the literature. The suspension seat model developed in this chapter included rigid bodies representing the seat structure including the suspension and the seat-pan-and-backrest assembly. Similar to the human body model, the rigid masses representing different parts of the suspension seat were connected with each other with pairs of spring and damper at the contact points. This is based on the assumption that the forces at the surfaces can be treated as concentrated forces acting at the contact point. The suspension seat model was established by calibrating the suspension mechanism model first, and then adding the rigid bodies representing the seat pan cushion and backrest and calibrating the newly-introduced parameters. Such a development method is the same as that suggested by Qiu (2012), which improves the rationality of the determination of the model parameters systematically by calibrating the parameters using the measurement data step by step.

The masses of the three bodies (B_p, B_l and B_r) in the model of the suspension mechanism were treated as the parameters to be optimised in the calibration procedure. The values of the masses

after calibration were the effective masses of the rigid bodies, as B_p included part of the sprung mass of the top plate and the supporting structure which were difficult to measure in the dynamic conditions.

In the suspension mechanism model, the dimensions in the x and y-axis of inert mass used to apply the preload on the seat were not considered, whereas in the suspension seat model, the length and width of the rigid body representing the inert mass B_m were defined (Figure 7.4). This is due to the fact that the inert mass was rigidly connected with the suspension mechanism in the experimental study (Figure 5.2), while when the inert mass was connected with the seat pan cushion of the suspension seat, the interaction between the seat and inert mass system was affected by the seat pan cushion (Figure 5.23), and the rotational motion of the inert mass needed to be taken into consideration. Hence, the dimensions of the inert mass were adopted in the development of the suspension seat model for the calculation of its moments of inertia.

The complete seat model was developed by connecting the rigid bodies representing the seat pan cushion and backrest to the suspension mechanism model. The springs and dampers between the bodies B_p and B_c were used to model the dynamic forces between the suspension top plate and the seat pan cushion instead of the dynamic stiffness and damping of the cushion, as the latter was included in the contact forces between the seat and the seated human body determined via calibration of the suspension-seat-occupant model. This makes the stiffness and damping of the human body and the seat cushion, and the interaction between them, be represented by one set of springs and dampers, which simplified the modelling of the coupling of the seat and occupant. The forces between the suspension top plate and the seat pan cushion also enables the interaction between the seat cushion and the suspension mechanism to be modelled. These two seat components were assumed to be rigidly connected in some models developed previously, and the parameter sensitivity analysis revealed that such an interaction could affect the seating dynamics, which will be discussed in Section 7.5.3.

The friction between the suspension seat components may affect the seating dynamics. The modelling of suspension seat and human body system in this study is focused on the linear dynamics of the suspension seat and occupant system when the seat is in normal operation after the friction is overcome. Once the suspension overcame the lock-up and starts to play, the effect of the friction between seat components on the seating dynamics becomes small. Hence, the friction was not considered in the current suspension-seat model.

7.5.2 The DoFs of the seat model

The degrees of freedom (DoF) of the suspension seat model were decided based on the observed dynamic behaviour of the suspension seat and the measurement data from the experimental study. For the model of the suspension mechanism, the transmissibilities in the x and z-directions possess one resonance each, while in the y-direction, two distinctive peaks were found in the frequency range considered (up to 30 Hz). Hence, in addition to the DoFs in the three translational directions, an extra DoF in the x-axis was introduced to the body B_p to capture the secondary resonance of the lateral transmissibility, which seemed to be related to the roll motion from the experimental observation (Figure 7.2). When the suspension seat model was constructed by connecting the seat pan cushion (B_c) and backrest (B_{br}) with the suspension mechanism, an extra DoF around the y-axis was added to these two rigid bodies apart from the DoF around the x-axis. The purpose of this design was to enable the seat model capable of capturing the secondary resonance of the fore-aft transmissibility of the suspension seat with inert mass located between 10 and 20 Hz (Figure 7.5).

The experimental results indicated that the transmissibilities of the suspension-seat-occupant system in the horizontal directions exhibited more than one resonance below 20 Hz. Figures 7.8 to 7.10 show that the coupled suspension seat and human body model proposed in this chapter can achieve reasonably good agreement with the fore-aft transmissibility at the seat pan and backrest, although a discrepancy was observed at the secondary resonance of the fore-aft transmissibility at the backrest. It is noticed the current model predicted transmissibility in the lateral direction at the seat pan and backrest deviated from the corresponding experimental results. The rigid bodies designed to represent the seat pan and backrest of the suspension seat have five DoFs each (translational in the x, y and z-axis, and rotational around the x and y-axis), considering that the dynamic response of the suspension seat and occupant system also involved rotational motion in addition to the translational motion when exposed to tri-axis translational vibration. On the other hand, the constituent parts of the human body model only had four DoFs each, without the rolling DoF around the x-axis, already achieved good agreement with the measured apparent masses. The lack of the roll DoF in the current human body model may be the reason causing the discrepancy between the model-predicted and experimentally measured transmissibilities in the lateral direction at the seat pan and backrest.

7.5.3 Parameter sensitivity

The result of parameter sensitivity analysis indicated that the vertical seat transmissibility at the seat pan was largely affected by the vertical stiffness and damping of the suspension. This reveals

that the main air spring and the damper of the suspension, between the suspension top plate and the floor (Figure 7.12, on the right), played an important role in the vertical transmissibility.

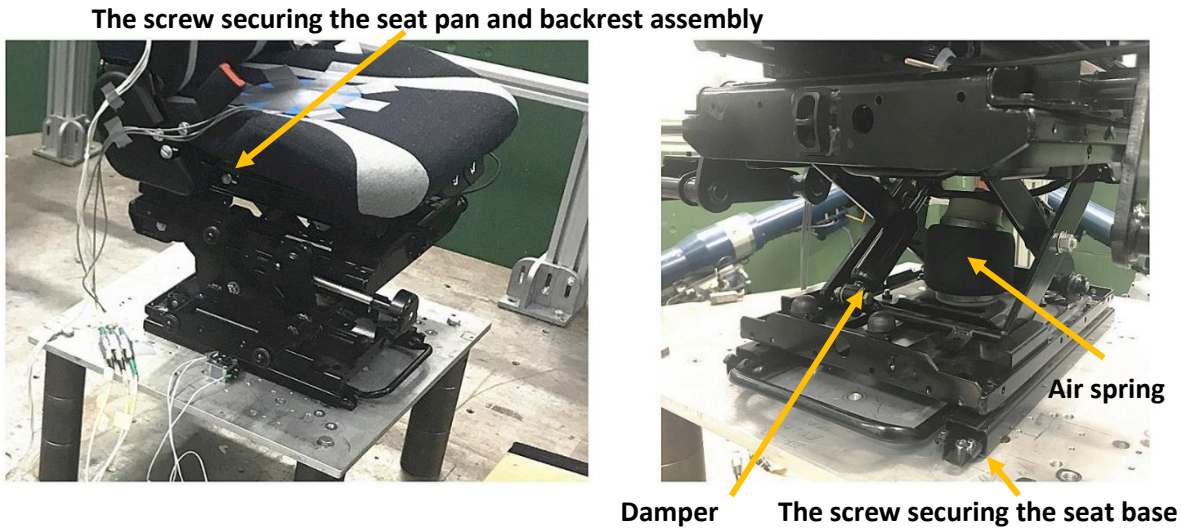

Figure 7.12 The screws and the air spring and damper of the suspension seat used in the current study

It was found that the fore-aft contact stiffness between the floor and the supporting masses of the suspension mechanism k_{xfl}, which may be related to the deformation of the linkage, affected the fore-aft transmissibility at the backrest. As the suspension bottom plate is bolted on the floor, the shear stiffness of the bolt screws and the elastic deformation of the linkage played an important role in affecting the fore-aft seat transmissibility. Similarly, the seat pan and the suspension top plate were firmly connected using vertical screws for the seat in the current study (Figure 7.12, on the left). The result of parameter sensitivity analysis suggests that attention may need to paid to the structure constraints against the fore-aft or pitch motion of the seat components, because the rotational stiffness or damping between the seat pan cushion and suspension top plate can affect the vertical and fore-aft seat transmissibilities.

The rotational (pitch) stiffness or damping between the thighs and seat pan cushion k_{pc2} and c_{pc2}, and that between the upper torso and the backrest k_{pb5} and c_{pb5}, were also found to affect the vertical and fore-aft seat transmissibilities. This reveals the importance of the pitch motion of the suspension-seat-occupant system which could affect the seating dynamics in both x and z-directions. The effect of the contact stiffness and damping around the y-axis may be a result of the interacted pitch motion of both the seat and the human body.

7.6 Conclusions

In this chapter, a multi-body model of the suspension seat exposed to tri-axis translational excitation is developed and calibrated. The model comprises five rigid bodies, three of which represent the suspension mechanism and the other two rigid bodies represent the seat pan cushion and the backrest, respectively. The model was calibrated using the transmissibilities in three translational directions measured when the suspension mechanism or the complete seat was loaded with inert mass during the experimental study described in Chapter 5. The suspension seat model was then coupled with the multi-body model of the human body developed in Chapter 6 to form the suspension-seat-occupant model, and was calibrated using the tri-axis seat transmissibilities at the seat pan and backrest measured with tri-axis excitation. Sensitivity analysis was conducted with the seat-occupant model. The results showed that the seat transmissibility in fore-aft and vertical directions were most sensitive to the rotational stiffness and damping between the human body and the seat, the fore-aft stiffness at the connection points between the seat pan and suspension, and the vertical stiffness and damping of the suspension. These results indicate that more attention may need to be paid in the interaction between the seat and human body in the rotational direction, and the structure constraints against the motion of the seat components in the fore-aft direction in the seat design.

Chapter 8 GENERAL DISCUSSION

In this chapter, the main findings of the current study in response to the research questions (Chapter 2) that were generated based on the review of relevant studies are summarised and remarked.

8.1 The effect of the backrest inclination angle on the apparent masses and seat transmissibilities in different directions

In general, the effect of the backrest inclination on the apparent masses measured with the rigid seat and the seating dynamics measured with the suspension seat was found under various excitation magnitudes in the current study. The change related to the resonance of the apparent masses and the suspension seat transmissibilities with the increased backrest inclination angle varied between different axes.

Effect of the backrest inclination angle on the apparent masses

It was revealed from the current study that the increase of the backrest inclination angle generally led to increasing moduli of the in-line vertical and lateral apparent masses at the backrest over a frequency range of 0.5-10 Hz (Figure 3.7 and Figure 3.9), which was mainly explained by the increased body mass supported by the backrest. However, the effects of the backrest inclination angle on the apparent masses at the seat pan in these two axes showed differences.

With the increased backrest inclination, the resonance frequency of the in-line vertical apparent mass at the seat pan increased and the associated modulus decreased (Figure 3.9). The resonance frequency of the in-line lateral apparent mass at the seat pan was marginally affected by the backrest angle, while the modulus associated with the resonance tended to increase with the increase of the backrest inclination angle, and the resonance frequency hardly changed (Figure 3.7). Although changing the backrest angle resulted in a redistribution of the body mass at the seat pan, the changes of the resonance frequencies of the lateral and vertical apparent masses were different. It appears that increasing the backrest inclination has resulted in increased effective stiffness and damping of the seat pan and body system in the vertical direction but led to reduced effective damping of the seat pan and body system in the lateral direction. Similarly, the change of the fore-aft apparent mass at the seat pan due to the increase of the backrest inclination angle also seemed to be related to the change in the effective damping (Chapter 3).

Comparison between the effect of the backrest inclination angle on the suspension seat transmissibilities and on the apparent masses

The effect of the backrest inclination on the transmissibility of the suspension seat with seated subject involved the dynamic properties of both the seated human body and the suspension seat.

When the backrest inclination angle increased, the tendency of the change in the resonance frequency of the vertical seat transmissibility at the seat pan was similar to that of the vertical apparent mass at the seat pan: they both increased slightly (Figure 3.9 and Figure 5.22, respectively). The effect of the backrest inclination angle on the resonance frequency of the fore-aft apparent mass at the seat pan and that of the fore-aft seat transmissibility measured at the seat pan were both relatively small (Figure 3.5 and Figure 5.15, respectively).

However, the moduli associated with the resonances of the in-line lateral seat transmissibility at the seat pan tended to decrease when the backrest inclination angle increased (Figure 5.18), while the modulus associated with the resonance of the in-line lateral apparent mass at the seat pan increased (Figure 3.7). The different trend between the change of the lateral apparent mass and that of the seat transmissibility due to the increased backrest inclination may be related to the dynamic properties of the cushion. As the modulus in the vicinity of the resonance frequency of the lateral apparent mass increased with the increased backrest inclination angle, the load on the seat pan cushion in that frequency range increased. Thus, the friction force in the lateral direction tended to increase, leading to an increase of the damping ratio at the contact between the seat pan and the seated human body in the lateral direction, and a decrease of the modulus associated with the resonance frequency of the seat transmissibility in the y-axis.

8.2 The effect of the excitation magnitude on the apparent masses and the suspension seat transmissibilities under tri-axial translational vibration

When exposed to tri-axial vibration, the nonlinearity of the human body was affected by the increase of the excitation magnitude in both the “primary-axis” and the “secondary-axes” (see Chapter 4). The weighting factors of the excitation magnitude in the “secondary-axes” were generally at relatively high level for the calculation of the overall excitation magnitude (Table 4.8), indicating its importance in affecting the biodynamic response.

The effect of the excitation magnitude in different directions on the transmissibility of the suspension seat and occupant system is in general related to the characteristics of both the seat dynamics and the human body biodynamics. Similar to the biodynamic response, it is found that

the nonlinearity of the suspension-seat-occupant system in one axis could be observed with the increase of the excitation magnitude in the corresponding "primary-axis" or "secondary-axes" under tri-axial excitation, and interaction existed between them. Nevertheless, in contrast to the important effect of excitation in the "secondary-axes" on the in-line apparent masses, the effect of the excitation magnitude in the x and y-axis on the transmissibility of the suspension seat in the vertical direction were much smaller than that in the z-axis. With the seated subject, the change of the resonance frequency of the vertical suspension seat transmissibility at the seat pan due to the change of the excitation magnitude in the "secondary-axes" was only significant when the vertical excitation magnitude was at a low-level (0.25 ms^{-2} r.m.s., Figure 5.11 and Figure 5.20). On the other hand, the effect of the vertical excitation magnitude on the vertical transmissibility was still significant even when the excitation magnitude in the "secondary-axes" was 1.0 ms^{-2} r.m.s. (Figure 5.10 and Figure 5.19). This may be related to the lock-up effect due to the friction within the suspension mechanism. Although it was concluded that the increase of the excitation magnitude in the horizontal directions may also help the suspension mechanism overcome the lock-up effect in the vertical direction, such an effect was still smaller than a direct increase of the vertical excitation magnitude.

In the current study, the interaction between the excitation magnitudes in different axes was investigated by fixing the excitation magnitude in the "secondary-axes" at the same level (0.5 or 1.0 ms^{-2} r.m.s.). This may explain some insignificant results found with the linear regression analysis shown in Section 4.4.5. In the future, more combinations of the excitation magnitudes in each of the two additional axes may be tested. Then the contribution of the magnitude of excitation in each of the three translational axes on the overall excitation magnitude could be more thoroughly investigated.

8.3 The calibration of the human body model and the suspension-seat-occupant model

The human body model and the suspension-seat-occupant model were developed to meet the needs of representing the apparent masses and the seat transmissibilities under tri-axial translational excitation, respectively.

Each part of the multi-body model of the seated human body proposed in Chapter 6 has four DoFs (three translational DoFs in the x, y and z-axis, and one rotational DOF around the y-axis). The good agreement achieved between the model prediction and the experimental data suggests that the developed human body model could sufficiently represent the apparent masses in three directions when exposed to tri-axis excitation in the current study.

In the current study, the excitations used to measure apparent masses of the human body on a rigid seat were the same as those applied to measure the transmissibilities of the suspension-seat-occupant system. With the rigid seat, the tri-axis translational vibration to the human body was assumed to be identical to the tri-axis excitation on the floor, as mentioned in Chapter 3. On the other hand, due to the dynamics of the suspension seat and the interaction between the seat and the human body, the vibration at the seat pan may be different from excitation at the seat base. Hence, there may be difference between the vibration transmitted to the human body with a rigid seat and that with a suspension seat, despite the identical excitation on the floor. Due to the nonlinear behaviour of the seated human body and the seat-occupant system, such a difference may require the values of the model parameters of the human body to be modified accordingly.

In the models proposed in Chapters 6 and 7, the stiffness and damping between human body segments, and the coordinates of the contact points between the seat and human body are assumed to remain the same with both types of seats. Compared to the suspension seat with cushion, the surface of the seat used for the measurement of the apparent masses was rigid and the friction coefficient was smaller. This may result in small changes in the position of the contact points between the body segments and the seat. Besides, the orientation of the pelvis of the seated human body may be different when sitting on a rigid seat compared to that when sitting on a seat with soft cushion.

The effect of the difference between the rigid seat and suspension seat may be taken into consideration in the future study. To improve the accuracy of the model, the experimental data used for the calibration of the human body model and the coupled seat-occupant model may need be coordinated. For example, the acceleration measured at the seat pan of the suspension seat with the seated human body may be used as the input to the rigid seat to measure the apparent mass, then the excitation transmitted to the human body in the two types of seats would be the same. An alternative approach is to develop nonlinear models of the human body and the suspension seat so that the nonlinearity of them can be better captured.

Chapter 9 CONCLUSIONS AND RECOMMENDATIONS

9.1 The effect of the backrest inclination angle on the biodynamic response

- The backrest inclination angle affected the apparent mass of the seated human body measured at the seat pan and backrest of the rigid seat in all the three translational directions under various magnitudes of single-axial vibration (0.25, 0.5 and 1.0 ms^{-2} r.m.s.). The effect of the backrest inclination angle (changing between 0°, 10° and 20°) on the biodynamic response was found to be generally similar to single-axial and tri-axial excitations.

- With the increase of the inclination angle, the modulus associated with the resonance of the in-line vertical apparent masses at the backrest increased, while that at the seat pan tended to decrease.

- The moduli associated with the resonances of the in-line lateral apparent masses at the seat pan and at the backrest above 2 Hz tended to increase with the increased backrest inclination angle. In the fore-aft direction, the changes of the apparent masses did not exhibit the same tendency when the backrest inclination angle increased from 0° to 10° and from 10° to 20°. The changes of the resonance frequencies and the associated moduli of the apparent masses in the horizontal directions indicated that the inclination of the backrest not only affected the distribution of the body mass on the seat pan and backrest, but also led to the change in the stiffness or the damping of the human body.

- Interaction was found to exist between the backrest inclination and the excitation magnitude, especially for the in-line apparent masses at the backrest. The study suggests that when studying the effect of the backrest inclination angle, the excitation magnitude must be taken into consideration.

9.2 The effect of the excitation magnitudes on the apparent masses under tri-axial translational vibration

- Under tri-axial translational excitation with the magnitude in each axis up to 1.0 ms^{-2} r.m.s., the in-line apparent mass of the human body seated in the rigid seat in each translational axis behaved in a nonlinear manner, i.e., the resonance frequency decreased with the increased

excitation magnitude in the same axis and in the other two axes, which was observed with both upright and inclined backrest.

- Besides, the degree of nonlinearity of the apparent mass in one axis tended to become smaller when the excitation magnitude in the other axes was at a high level. This suggests that the biodynamic response of the seated human body is affected by the overall excitation magnitude under tri-axial translational vibration. For the effect on the resonance frequency of the apparent mass in one axis, the excitation magnitude in the same direction in general contributed more than that in the other two directions to the overall magnitude.

9.3 The effect of the excitation magnitudes and the backrest inclination on the suspension seat transmissibilities under tri-axial translational vibration

- When loaded with inert mass, the nonlinear dynamic behaviour of the suspension seat was found to exist in both vertical and horizontal directions with the change of the excitation magnitude in the same direction. The effect of the excitation magnitude in the x and y-axis on the in-line vertical transmissibility of the suspension seat was also noticeable, partly because of the strong lock-up effect arising from the friction of the suspension mechanism.

- Under tri-axial translational excitation with the magnitude in each axis up to 1.0 ms^{-2} r.m.s., the transmissibilities of the suspension seat with the seated human body in the x, y and z-axis were affected by the excitation magnitude in both the same axis and the other two axes, which was attributed to the nonlinearity of both the seated human body and the suspension seat.

- The SEAT value of the suspension seat with the seated subject was found to be affected by the excitation magnitude not only in the vertical but also in the horizontal directions. The result suggests that the evaluation of ride comfort of the suspension seat in the current international standards using the SEAT value as an important index should also include tri-axial translational excitations rather than under the vertical excitation only as defined in, e.g., ISO 7096 and ISO 5007.

- The backrest inclination angle was also found to affect the transmissibility of the suspension seat at the backrest, which may be attributed to its effect on the apparent masses of the human body and on the interaction between the suspension seat and the human body.

9.4 Modelling of the seated human body exposed to tri-axial translational vibration

- The proposed three-dimensional multi-body model of the seated human body exposed to tri-axial translational vibration consists of the head and neck, upper torso, abdomen, pelvis, thighs, and leg of the human body. The values of the anthropometry-related model parameters were determined based on the literature. The values of the rest model parameters were determined by a procedure of model calibration based on the apparent masses at the seat pan and backrest in three translational directions measured in the experimental study.

- The developed model was capable of giving a satisfactory prediction of the apparent masses of the human body exposed to tri-axial vibration of different excitation magnitudes and varied backrest inclination angles.

- The results of the modal analysis with the calibrated model revealed four modes of the seated human body below 10 Hz in the x, y and z directions, which were comparable with those reported in the previous studies.

- The parameter sensitivity analysis showed that the apparent masses in the x, y and z-axis simulated using the model were sensitive to the contact stiffness or damping at the seat and human body interface in the fore-aft or lateral direction. Additionally, the pitch damping between the abdomen and the pelvis also affected the fore-aft and vertical apparent mass.

9.5 Modelling of the suspension-seat-occupant system under tri-axial translational vibration

- A three-dimensional multi-body model of the suspension-seat-occupant system exposed to tri-axial excitation was developed. The suspension seat model was constructed with five rigid bodies representing the main components of the suspension mechanism, the seat pan cushion and the backrest. The values of the seat model parameters were optimized using the measured three-dimensional transmissibilities of the suspension mechanism and the suspension seat with loaded inert masses, respectively.

- The proposed suspension seat-occupant model was further calibrated using the transmissibilities in x, y and z-axis at the seat pan and backrest of the suspension-seat-occupant system exposed to tri-axial translational vibration. The result showed that the developed suspension-seat-occupant model is capable of predicting the fore-aft and vertical transmissibilities of the system exposed to tri-axial vibration.

- The parameter sensitivity analysis showed that the vertical transmissibility at the seat pan and the fore-aft transmissibility at the backrest were most sensitive to the stiffness and damping of the seat suspension, the stiffness and damping between the seat components, and the contact stiffness and damping between the seat cushion and the seated human body. This study provided useful information for the design of the suspension seat and the optimization of ride comfort.

9.6 Recommendations for the future study

Experimental study

- The apparent mass is good at reflecting the overall biodynamic response of the human body. It does not however provide sufficient information on the dynamics of individual body segments. The local effect of the excitation on the motions of the body segments, such as the spine and head, is also related to its effect on comfort and health. It is recommended to investigate in the future the dynamic behaviour of important body segments, such as the seat-to-head-transmissibility, under combined fore-aft, lateral and vertical vibration, and how are they affected by the excitation magnitude and backrest inclination angle.

- In the current study, the magnitude of the broadband random excitation in each of the three translational axes was set to be up to 1.0 ms^{-2} r.m.s. In the reality, the vibration on some types of off-road heavy vehicles may be of even higher magnitudes and may include shock. How the nonlinear behaviour of the seated human body and the suspension-seat-occupant system is affected by the higher-level magnitude of excitation or the shock, should be investigated in the future.

Modelling study

- The human body model and the suspension-seat-occupant model proposed in this study are both linear multi-body models. Due to the nonlinear characteristics of the human body and the seat, the values of the model parameters may need to be recalibrated for different excitation magnitudes. The future modelling of the seated human body and the seat-occupant system should seek to apply nonlinear modelling methods to better characterize their nonlinear behaviour with the vibration of higher magnitudes and shock.

- The modelling of the interaction between the seated human body and the suspension seat with tri-axial translational excitation may be further studied, so as to achieve a better agreement with the measured lateral transmissibilities of the suspension seat exposed to tri-axial translational excitation.

Appendix A THE EFFECT OF THE BACKREST INCLINATION COMBINED WITH DIFFERENT EXCITATION MAGNITUDES ON THE APPARENT MASSES OF THE SEATED HUMAN BODY

A.1 Cross-axis apparent masses

Nonlinearity has been found on the cross-axis behaviour of the seated human body when the excitation magnitude increased. For example, the resonance frequency of the cross-axis fore-aft apparent mass at the seat pan under single-axial vertical excitation decreased with the increase of the vertical excitation magnitude (p<0.05). The backrest inclination angle was also found to affect the cross-axis apparent masses in the vertical and fore-aft directions. Under single-axial fore-aft excitation, the modulus of the cross-axis vertical apparent mass at the backrest became dramatically greater when the backrest inclination angle increased from 10° to 20° compared to that when the backrest changed from upright to inclined by 10° (Figure A.1).

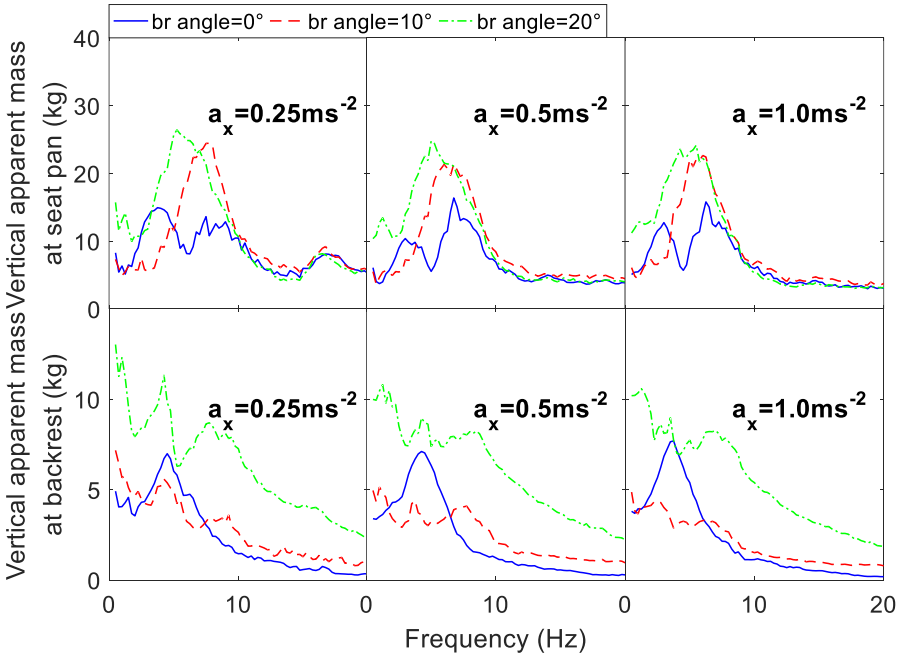

Figure A.1 Median cross-axis vertical apparent mass at the seat pan and backrest under single-axial fore-aft excitation: the effect of backrest inclination angle

Under single-axial vertical excitation, the increase of the backrest inclination angle led to an increase of the resonance frequency and the associated modulus of the cross-axis fore-aft apparent

mass at the backrest under all excitation magnitudes (p<0.05) (Figure A.2). On the other hand, the moduli of the cross-axis fore-aft and vertical apparent masses measured under single-axial lateral excitation were small under all the excitation magnitudes. The effect of the increase of the backrest inclination angle on the cross-axis fore-aft and vertical apparent masses was small (Figure A.3).

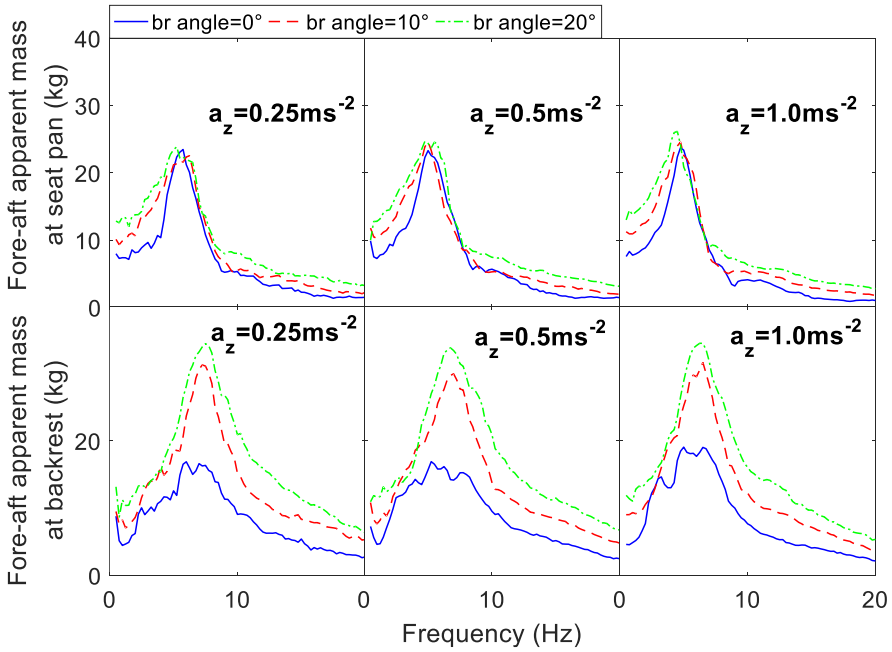

Figure A.2 Median cross-axis fore-aft apparent mass at the seat pan and backrest under single-axial vertical excitation: the effect of backrest inclination angle

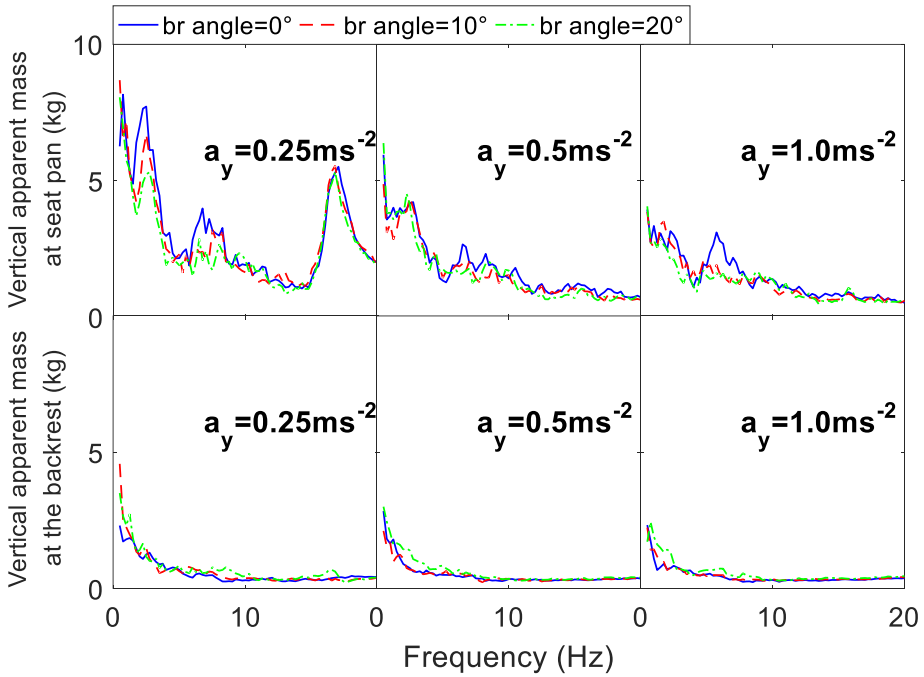

Figure A.3 Median cross-axis vertical apparent mass measured at the seat pan and backrest under lateral excitation: the effect of the backrest inclination

A.2 The effect of the excitation magnitude in the "secondary-axes" on the apparent masses

Table A.1 Statistical significance (*p*-value, Friedman) of the effect of the magnitude of y and z-axis excitations on the resonance frequency (red) and the associated modulus (blue) of the in-line fore-aft apparent masses at the backrest, with different inclination angles of the backrest and different in-line fore-aft excitation magnitudes (r.m.s.)

Angle of backrest inclination \ Excitation magnitude (x-axis)	0.25 ms^{-2}	0.5 ms^{-2}	1.0 ms^{-2}
0°	** / ns	** / ns	ns / ns
10°	** / *	** / *	* / ns
20°	** / *	** / ns	** / ns

Table A.2 Statistical significance (*p*-value, Friedman) of the effect of the magnitude of y and z-axis excitations on the resonance frequency and the associated modulus of the in-line fore-aft apparent masses at the seat pan, with different inclination angles of the backrest and different in-line fore-aft excitation magnitudes (r.m.s.)

Angle of backrest inclination \ Excitation magnitude (x-axis)	0.25 ms^{-2}	0.5 ms^{-2}	1.0 ms^{-2}
0°	** / **	** / **	** / ns
10°	** / **	** / **	ns / *
20°	** / ns	** / *	* / ns

Table A.3 Statistical significance (*p*-value, Friedman) of the effect of the magnitude of x and z-axis excitations on the resonance frequency and the associated modulus of the in-line lateral apparent masses at the seat pan, with different inclination angles of the backrest and different in-line lateral excitation magnitudes (r.m.s.)

Angle of backrest inclination \ Excitation magnitude (y-axis)	0.25 ms^{-2}	0.5 ms^{-2}	1.0 ms^{-2}
0°	** / *	* / ns	ns / *
10°	** / **	** / *	* / *
20°	** / *	* / ns	ns / ns

A.4 Statistical significance (*p*-value, Friedman) of the effect of the magnitude of x and y-axis excitations on the resonance frequency and the modulus of the associated in-line vertical apparent masses at the backrest, with different inclination angles of the backrest and different in-line vertical excitation magnitudes (r.m.s.)

Angle of backrest inclination \ Excitation magnitude (z-axis)	0.25 ms^{-2}	0.5 ms^{-2}	1.0 ms^{-2}
0°	** / **	** / ns	** / *
10°	** / *	** / **	** / **
20°	** / **	** / *	** / **

Table A.5 Statistical significance (*p*-value, Friedman) of the effect of the magnitude of x and y-axis excitations on the resonance frequency and the associated modulus of the in-line vertical apparent masses at the seat pan, with different inclination angles of the backrest and different in-line vertical excitation magnitudes (r.m.s.)

Excitation magnitude (z-axis) / Angle of backrest inclination	0.25 ms^{-2}	0.5 ms^{-2}	1.0 ms^{-2}
0°	** / ns	** / ns	* / ns
10°	** / ns	** / ns	** / ns
20°	ns / ns	ns / ns	* / ns

A.3 The effect of the backrest inclination angle on the apparent masses

Table A.6 Statistical significance (*p*-value, Friedman) of the effect of the angle of backrest inclination on the modulus of the in-line lateral apparent masses at the backrest at 0.75 Hz, with different in-line lateral excitation magnitudes and different excitation magnitudes in x and z-axis (r.m.s.)

Excitation magnitude (x and z-axis) / Excitation magnitude (y-axis)	0 ms^{-2}	0.5 ms^{-2}	1.0 ms^{-2}
0.25 ms^{-2}	*	**	*
0.5 ms^{-2}	**	*	**
1.0 ms^{-2}	ns	*	*

Table A.7 Statistical significance (*p*-value, Friedman) of the effect of the angle of backrest inclination on the resonance frequency and the associated modulus of the in-line lateral apparent masses at the seat pan, with different in-line lateral excitation magnitudes and different excitation magnitudes in x and z-axis (r.m.s.)

Excitation magnitude (x and z-axis) / **Excitation magnitude (y-axis)**	**0 ms^{-2}**	**0.5 ms^{-2}**	**1.0 ms^{-2}**
0.25 ms^{-2}	** / *	ns / ns	* / **
0.5 ms^{-2}	ns / ns	* / **	ns / **
1.0 ms^{-2}	ns / ns	* / **	ns / *

Table A.8 Statistical significance (*p*-value, Friedman) of the effect of the angle of backrest inclination on the resonance frequency and the associated modulus of the in-line vertical apparent masses at the backrest, with different in-line vertical excitation magnitudes and different excitation magnitudes in x and y-axis (r.m.s.)

Excitation magnitude (z-axis)	**0 ms^{-2}**	**0.5 ms^{-2}**	**1.0 ms^{-2}**
0.25 ms^{-2}	** / **	** / **	** / **
0.5 ms^{-2}	* / **	** / **	** / **
1.0 ms^{-2}	** / **	* / **	** / **

Table A.9 Statistical significance (*p*-value, Friedman) of the effect of the angle of backrest inclination on the resonance frequency and the associated modulus of the in-line vertical apparent masses at the seat pan, with different in-line vertical excitation magnitudes and different excitation magnitude in x and y-axis (r.m.s.)

Excitation magnitude (x and y-axis) / Excitation magnitude (z-axis)	0 ms^{-2}	0.5 ms^{-2}	1.0 ms^{-2}
0.25 ms^{-2}	ns / **	* / **	ns / **
0.5 ms^{-2}	ns / *	ns / **	ns / **
1.0 ms^{-2}	ns / **	ns / **	ns / **

A.4 Interactive effect between the excitation magnitudes and the backrest inclination angle

Table A.10 Median value (12 subjects) of R_{nl_ilm} of the in-line fore-aft apparent mass at the backrest, and the statistical significance of the effects (*p*-value, Friedman) of the angle of backrest inclination and the excitation magnitude in y and z-axis (r.m.s.)

Median value of R_{nl_ilm}		Angles of backrest inclination			*p*-value (effect of backrest inclination)
		0°	10°	20°	
magnitude of y and z-axis excitation	0 ms^{-2}	*1.250*	*1.367*	*1.250*	ns
	0.5 ms^{-2}	*1.113*	*1.185*	*1.182*	ns
	1.0 ms^{-2}	*1.033*	*1.079*	*1.191*	ns
p-value (effect of the excitation magnitude in y and z-axis)		*	*	ns	

Table A.11 Median value of PC_{ilm} of the in-line fore-aft apparent mass at the backrest, and the statistical significance of the effects (*p*-value, Friedman) of the angle of backrest inclination and the excitation magnitude in y and z-axis

Median value of PC_{ilm}		**Angles of backrest inclination**			***p*-value (effect of backrest inclination)**
		0°	**10°**	**20°**	
magnitude of y and z-axis excitation	**0 ms^{-2}**	*-3.698%*	*6.511%*	*9.398%*	*
	0.5 ms^{-2}	*0.716%*	*0.230%*	*3.255%*	ns
	1.0 ms^{-2}	*-1.758%*	*1.319%*	*1.265%*	ns
***p*-value (effect of the excitation magnitude in y and z-axis)**		ns	ns	*	

Table A.12 Median valueof R_{nl_ilm} of the in-line fore-aft apparent mass at the seat pan, and the statistical significance of the effects (*p*-value, Friedman) of the angle of backrest inclination and the excitation magnitude in y and z-axis (r.m.s.)

Median value of R_{nl_ilm}		**Angles of backrest inclination**			***p*-value (effect of backrest inclination)**
		0°	**10°**	**20°**	
magnitude of y and z-axis excitation	**0 ms^{-2}**	*1.225*	*1.385*	*1.310*	ns
	0.5 ms^{-2}	*1.188*	*1.199*	*1.223*	ns
	1.0 ms^{-2}	*1.113*	*1.087*	*1.083*	ns
***p*-value (effect of the excitation magnitude in y and z-axis)**		**	*	**	

Table A.13 Median value of PC_{ilm} of the in-line fore-aft apparent mass at the seat pan, and the statistical significance of the effects (*p*-value, Friedman) of the angle of backrest inclination and the excitation magnitude in y and z-axis (r.m.s.)

Median value of PC_{ilm}		**Angles of backrest inclination**			***p*-value (effect of backrest inclination)**
		0°	**10°**	**20°**	
magnitude of y and z-axis excitation	**0 ms^{-2}**	*15.984%*	*16.588%*	*13.318%*	ns
	0.5 ms^{-2}	*9.795%*	*11.572%*	*13.860%*	ns
	1.0 ms^{-2}	*4.196%*	*5.117%*	*7.352%*	ns
***p*-value (effect of the excitation magnitude in y and z-axis)**		*	**	ns	

Table A.14 Median value of R_{nl_ilm} of the in-line lateral apparent mass at the seat pan, and the statistical significance of the effects (*p*-value, Friedman) of the angle of backrest inclination and the excitation magnitude in x and z-axis (r.m.s.)

Median value of R_{nl_ilm}		**Angles of backrest inclination**			***p*-value (effect of backrest inclination)**
		0°	**10°**	**20°**	
magnitude of x- and z-axis excitation	**0 ms^{-2}**	*1.550*	*1.464*	*1.479*	ns
	0.5 ms^{-2}	*1.900*	*1.500*	*1.381*	ns
	1.0 ms^{-2}	*1.183*	*1.350*	*1.167*	ns
***p*-value (effect of the excitation magnitude in x and z-axis)**		ns	ns	*	

Table A.15 Median value of PC_{lm} of the in-line lateral apparent mass at the seat pan, and the statistical significance of the effects (*p*-value, Friedman) of the angle of backrest inclination and the excitation magnitude in x and z-axis (r.m.s.)

Median value of PC_{ilm}		**Angles of backrest inclination**			***p*-value (effect of backrest inclination)**
		0°	**10°**	**20°**	
magnitude of x and z-axis excitation	**0 ms^{-2}**	*2.884%*	*9.516%*	*7.748%*	ns
	0.5 ms^{-2}	*4.469%*	*7.580%*	*6.026%*	ns
	1.0 ms^{-2}	*-2.799%*	*5.134%*	*12.417%*	**
***p*-value (effect of the excitation magnitude in x and z-axis)**		ns	ns	ns	

Table A.16 Median value of R_{nl_ilm} of the in-line vertical apparent mass at the backrest, and the statistical significance of the effects (*p*-value, Friedman) of the angle of backrest inclination and the excitation magnitude in x and y-axis (r.m.s.)

Median value of R_{nl_ilm}		**Angles of backrest inclination**			***p*-value (effect of backrest inclination)**
		0°	**10°**	**20°**	
magnitude of x and y-axis excitation	**0 ms^{-2}**	*1.211*	*1.184*	*1.193*	ns
	0.5 ms^{-2}	*1.000*	*1.155*	*1.127*	*
	1.0 ms^{-2}	*1.081*	*0.978*	*1.000*	ns
***p*-value (effect of the excitation magnitude in x and y-axis)**		*	*	*	

Table A.17 Median value of PC_{ilm} of the in-line vertical apparent mass at the backrest, and the statistical significance of the effects (*p*-value, Friedman) of the angle of backrest inclination and the excitation magnitude in x and y-axis (r.m.s.)

Median value of PC_{ilm}		**Angles of backrest inclination**			***p*-value (effect of backrest inclination)**
		0°	**10°**	**20°**	
magnitude of x and y-axis excitation	**0 ms^{-2}**	*15.452%*	*13.465%*	*4.793%*	ns
	0.5 ms^{-2}	*-0.065%*	*-4.022%*	*1.471%*	ns
	1.0 ms^{-2}	*28.950%*	*7.306%*	*5.942%*	**
***p*-value (effect of the excitation magnitude in x and y-axis)**		*	*	ns	

Table A.18 Median value of R_{nl_ilm} of the in-line vertical apparent mass at the seat pan, and the statistical significance of the effects (*p*-value, Friedman) of the angle of backrest inclination and the excitation magnitude in x and y-axis (r.m.s.)

Median value of R_{nl_ilm}		**Angles of backrest inclination**			***p*-value (effect of backrest inclination)**
		0°	**10°**	**20°**	
magnitude of x and y-axis excitation	**0 ms^{-2}**	*1.143*	*1.156*	*1.190*	ns
	0.5 ms^{-2}	*1.046*	*1.120*	*1.175*	ns
	1.0 ms^{-2}	*1.048*	*1.000*	*1.049*	ns
***p*-value (effect of the excitation magnitude in x and y-axis)**		ns	*	ns	

Table A.19 Median value of R_{nl_sec} of the in-line fore-aft apparent mass at the backrest, and the statistical significance of the effects (*p*-value, Friedman) of the excitation magnitude in x-axis (r.m.s.)

Median value of R_{nl_sec}		**Angles of backrest inclination**		
		0°	**10°**	**20°**
magnitude of x-axis excitation	**0 ms^{-2}**	*1.385*	*1.349*	*1.336*
	0.5 ms^{-2}	*1.113*	*1.215*	*1.214*
	1.0 ms^{-2}	*1.000*	*1.000*	*1.133*
***p*-value (effect of the excitation magnitude in x-axis)**		*	*	*

Table A.20 Median value of R_{nl_sec} of the in-line fore-aft apparent mass at the seat pan, and the statistical significance of the effects (*p*-value, Friedman) of the excitation magnitude in x-axis (r.m.s.)

Median value of R_{nl_sec}		**Angles of backrest inclination**		
		0°	**10°**	**20°**
magnitude of x-axis excitation	**0 ms^{-2}**	*1.243*	*1.230*	*1.385*
	0.5 ms^{-2}	*1.077*	*1.194*	*1.243*
	1.0 ms^{-2}	*1.071*	*1.036*	*1.167*
***p*-value (effect of the excitation magnitude in x-axis)**		ns	**	**

Table A.21 Median value of PC_{sec} of the in-line fore-aft apparent mass at the seat pan, and the statistical significance of the effects (*p*-value, Friedman) of the excitation magnitude in x-axis (r.m.s.)

Median value of PC_{sec}		**Angles of backrest inclination**		
		0°	**10°**	**20°**
magnitude of x-axis excitation	**0 ms^{-2}**	*11.181%*	*15.984%*	*7.459%*
	0.5 ms^{-2}	*9.282%*	*8.967%*	*5.865%*
	1.0 ms^{-2}	*-0.610%*	*5.222%*	*-1.674%*
***p*-value (effect of the excitation magnitude in x-axis)**		*	**	ns

Table A.22 Median value of R_{nl_sec} of the in-line vertical apparent mass at the backrest, and the statistical significance of the effects (*p*-value, Friedman) of the excitation magnitude in z-axis (r.m.s.)

Median value of R_{nl_sec}		**Angles of backrest inclination**		
		0°	**10°**	**20°**
magnitude of z-axis excitation	**0 ms^{-2}**	*1.324*	*1.264*	*1.250*
	0.5 ms^{-2}	*1.243*	*1.262*	*1.195*
	1.0 ms^{-2}	*1.177*	*1.047*	*1.098*
***p*-value (effect of the excitation magnitude in z-axis)**		ns	**	**

Table A.23 Median value of R_{nl_sec} of the in-line vertical apparent mass at the seat pan, and the statistical significance of the effects (*p*-value, Friedman) of the excitation magnitude in z-axis (r.m.s.)

Median value of R_{nl_sec}		**Angles of backrest inclination**		
		0°	**10°**	**20°**
magnitude of z-axis excitation	**0 ms^{-2}**	*1.191*	*1.294*	*1.187*
	0.5 ms^{-2}	*1.124*	*1.149*	*1.107*
	1.0 ms^{-2}	*1.054*	*1.085*	*1.090*
***p*-value (effect of the excitation magnitude in z-axis)**		ns	**	ns

Table A.24 Median value of PC_{br} of the in-line fore-aft apparent mass at the backrest, and the statistical significance of the effects (*p*-value, Friedman) of the excitation magnitude in x-axis and the excitation magnitude in the y and z-axis (r.m.s.)

Median value of PC_{br}		**magnitude of y and z-axis excitation**			***p*-value (effect of the excitation magnitude in y and z-axis)**
		0 ms^{-2}	**0.5 ms^{-2}**	**1.0 ms^{-2}**	
magnitude of x-axis excitation	**0.25 ms^{-2}**	*7.479%*	*13.504%*	*12.089%*	ns
	0.5 ms^{-2}	*9.494%*	*0.012%*	*19.196%*	ns
	1.0 ms^{-2}	*16.825%*	*8.328%*	*10.979%*	ns
***p*-value (effect of the excitation magnitude in x-axis)**		*	ns	ns	

Table A.25 Median value of PC_{br} of the in-line lateral apparent mass at the seat pan, and the statistical significance of the effects (*p*-value, Friedman) of the excitation magnitude in y-axis and the excitation magnitude in the x and z-axis (r.m.s.)

Median value of PC_{br}		**magnitude of x and z-axis excitation**			***p*-value (effect of the excitation magnitude in x and z-axis)**
		0 ms^{-2}	**0.5 ms^{-2}**	**1.0 ms^{-2}**	
magnitude of y-axis excitation	**0.25 ms^{-2}**	*-24.113%*	*-12.296%*	*-27.462%*	**
	0.5 ms^{-2}	*-15.298%*	*-21.441%*	*-24.237%*	ns
	1.0 ms^{-2}	*-8.489%*	*-12.740%*	*-12.430%*	ns
***p*-value (effect of the excitation magnitude in y-axis)**		*	ns	**	

Table A.26 Median value of R_{nl_br} of the in-line vertical apparent mass at the backrest, and the statistical significance of the effects (*p*-value, Friedman) of the excitation magnitude in z-axis and the excitation magnitude in the x and y-axis (r.m.s.)

Median value of R_{nl_br}		**magnitude of x and y-axis excitation**			***p*-value (effect of the excitation magnitude in x and y-axis)**
		0 ms^{-2}	**0.5 ms^{-2}**	**1.0 ms^{-2}**	
magnitude of z-axis excitation	**0.25 ms^{-2}**	*0.750*	*0.630*	*0.658*	ns
	0.5 ms^{-2}	*0.753*	*0.668*	*0.715*	ns
	1.0 ms^{-2}	*0.822*	*0.780*	*0.714*	*
***p*-value (effect of the excitation magnitude in z-axis)**		ns	*	ns	

Appendix B THE EFFECT OF THE BACKREST INCLINATION COMBINED WITH EXCITATION MAGNITUDES ON THE TRANSMISSIBILITIES OF THE SUSPENSION SEAT

B.1 The effect of the excitation magnitude in the "primary-axis" on the seat transmissibilities

Table B.1 Statistical significance (p-value, Friedman) of the effect of the in-line fore-aft excitation magnitude on the frequency and the associated modulus of the fundamental resonance of the in-line fore-aft seat transmissibility at the backrest, with different inclination angles of the backrest and different excitation magnitudes in y and z-axis (r.m.s.)

Angle of backrest inclination \ Excitation magnitude (y and z-axis)	0 ms^{-2}	0.5 ms^{-2}	1.0 ms^{-2}
0°	** / **	** / ns	* / **
10°	** / **	* / ns	ns / *
20°	** / ns	ns / *	* / ns

Table B.2 Statistical significance (p-value, Friedman) of the effect of the in-line fore-aft excitation magnitude on the frequency and the associated modulus of the fundamental resonance of the in-line fore-aft seat transmissibility at the seat pan, with different inclination angles of the backrest and different excitation magnitudes in y and z-axis (r.m.s.)

Angle of backrest inclination \ Excitation magnitude (y and z-axis)	0 ms^{-2}	0.5 ms^{-2}	1.0 ms^{-2}
0°	** / **	** / **	** / **
10°	** / **	* / ns	* / **
20°	** / *	ns / ns	* / ns

Table B.3 Statistical significance (p-value, Friedman) of the effect of the magnitude in y and z-axis on the frequency and the associated modulus of the fundamental resonance of the in-line fore-aft seat transmissibility at the backrest, with different inclination angles of the backrest and different excitation magnitudes in x-axis (r.m.s.)

Angle of backrest inclination \ Excitation magnitude (x-axis)	0.25 ms^{-2}	0.5 ms^{-2}	1.0 ms^{-2}
0°	** / **	** / **	ns / ns
10°	** / **	** / *	ns / *
20°	** / **	** / *	ns / ns

Table B.4 Statistical significance (p-value, Friedman) of the effect of the lateral excitation magnitude on the frequency and the associated modulus of the second resonance of the in-line lateral seat transmissibility at the backrest, with different inclination angles of the backrest and different excitation magnitudes in x and z-axis (r.m.s.)

Angle of backrest inclination \ Excitation magnitude (x and z-axis)	0 ms^{-2}	0.5 ms^{-2}	1.0 ms^{-2}
0°	** / *	** / **	** / ns
10°	** / *	** / **	** / ns
20°	** / ns	** / **	** / *

Table B.5 Statistical significance (p-value, Friedman) of the effect of the lateral excitation magnitude on the frequency and the associated modulus of the second resonance of the in-line lateral seat transmissibility at the seat pan, with different inclination angles of the backrest and different excitation magnitudes in y and z-axis (r.m.s.)

Angle of backrest inclination \ Excitation magnitude (x and z-axis)	0 ms^{-2}	0.5 ms^{-2}	1.0 ms^{-2}
0°	** / ns	** / **	ns / ns
10°	** / **	* / ns	ns / ns
20°	** / ns	* / *	ns / *

Table B.6 Statistical significance (p-value, Friedman) of the effect of the in-line vertical excitation magnitude on the frequency and the associated modulus of the fundamental resonance of the in-line vertical seat transmissibility at the backrest, with different inclination angles of the backrest and different excitation magnitudes in x and y-axis (r.m.s.)

Angle of backrest inclination \ Excitation magnitude (x and y-axis)	0 ms^{-2}	0.5 ms^{-2}	1.0 ms^{-2}
0°	** / **	** / **	** / ns
10°	** / **	** / **	** / *
20°	** / ns	** / *	** / *

Table B.7 Statistical significance (p-value, Friedman) of the effect of the in-line vertical excitation magnitude on the frequency and the modulus of the associated second resonance of the in-line vertical seat transmissibility at the backrest, with different inclination angles of the backrest and different excitation magnitudes in x and y-axis (r.m.s.)

Angle of backrest inclination \ Excitation magnitude (x and y-axis)	0 ms^{-2}	0.5 ms^{-2}	1.0 ms^{-2}
0°	** / **	** / **	** / **
10°	** / **	** / **	** / **
20°	** / **	** / **	** / **

Table B.8 Statistical significance (p-value, Friedman) of the effect of the in-line vertical excitation magnitude on the frequency and the associated modulus of the fundamental resonance of the in-line vertical seat transmissibility at the seat pan, with different inclination angles of the backrest and different excitation magnitudes in x and y-axis (r.m.s.)

Angle of backrest inclination \ Excitation magnitude (x and y-axis)	0 ms^{-2}	0.5 ms^{-2}	1.0 ms^{-2}
0°	** / ns	** / ns	** / **
10°	** / *	** / *	** / *
20°	** / *	** / *	** / **

Table B.9 Statistical significance (*p*-value, Friedman) of the effect of the magnitude of vertical excitations on the vertical SEAT value of the suspension seat, with different inclination angles of the backrest and different excitation magnitudes in x and y-axis (r.m.s.)

Angle of backrest inclination \ Excitation magnitude (x and y-axis)	0 ms^{-2}	0.5 ms^{-2}	1.0 ms^{-2}
0°	**	**	**
10°	**	**	**
20°	**	**	**

B.2 The effect of the excitation magnitude in the "secondary-axes" on the seat transmissibilities

Table B.10 Statistical significance (p-value, Friedman) of the effect of the magnitude of excitation in y and z-axis on the frequency and the associated modulus of the fundamental resonance of the in-line fore-aft seat transmissibility at the seat pan, with different inclination angles of the backrest and different excitation magnitudes in x-axis (r.m.s.)

Angle of backrest inclination \ Excitation magnitude (x-axis)	0.25 ms^{-2}	0.5 ms^{-2}	1.0 ms^{-2}
0°	* / **	* / **	ns / **
10°	* / **	* / **	ns / *
20°	** / **	** / **	ns / **

Table B.11 Statistical significance (p-value, Friedman) of the effect of the magnitude of excitation in x and z-axis on the frequency and the associated modulus of the secondary resonance of the in-line lateral seat transmissibility at the backrest, with different inclination angles of the backrest and different excitation magnitudes in y-axis (r.m.s.)

Angle of backrest inclination \ Excitation magnitude (y-axis)	0.25 ms^{-2}	0.5 ms^{-2}	1.0 ms^{-2}
0°	** / *	** / ns	** / **
10°	** / *	** / ns	* / **
20°	** / ns	** / ns	* / **

Table B.12 Statistical significance (p-value, Friedman) of the effect of the magnitude of excitation in x and z-axis on the frequency and the associated modulus of the secondary resonance of the in-line lateral seat transmissibility at the seat pan, with different inclination angles of the backrest and different excitation magnitudes in y-axis (r.m.s.)

Angle of backrest inclination \ Excitation magnitude (y-axis)	0.25 ms^{-2}	0.5 ms^{-2}	1.0 ms^{-2}
0°	** / *	** / *	* / ns
10°	** / **	** / **	** / *
20°	** / ns	** / **	ns / *

Table B.13 Statistical significance (p-value, Friedman) of the effect of the magnitude of excitation in x and y-axis on the frequency and the associated modulus of the fundamental resonance of the in-line vertical seat transmissibility at the backrest, with different inclination angles of the backrest and different excitation magnitudes in z-axis (r.m.s.)

Angle of backrest inclination \ Excitation magnitude (z-axis)	0.25 ms^{-2}	0.5 ms^{-2}	1.0 ms^{-2}
0°	** / **	** / **	** / **
10°	** / *	** / **	* / **
20°	** / **	** / **	* / **

Table B.14 Statistical significance (p-value, Friedman) of the effect of the magnitude of excitation in x and y-axis on the frequency and the associated modulus of the second resonance of the in-line vertical seat transmissibility at the backrest, with different inclination angles of the backrest and different excitation magnitudes in z-axis (r.m.s.)

Angle of backrest inclination \ Excitation magnitude (z-axis)	0.25 ms^{-2}	0.5 ms^{-2}	1.0 ms^{-2}
0°	** / **	** / **	ns / ns
10°	** / **	ns / **	ns / ns
20°	* / **	ns / ns	ns / ns

Table B.15 Statistical significance (p-value, Friedman) of the effect of the magnitude of excitation in x and y-axis on the frequency and the associated modulus of the fundamental resonance of the in-line vertical seat transmissibility at the seat pan, with different inclination angles of the backrest and different excitation magnitudes in z-axis (r.m.s.)

Angle of backrest inclination \ Excitation magnitude (z-axis)	0.25 ms^{-2}	0.5 ms^{-2}	1.0 ms^{-2}
0°	** / **	** / **	* / **
10°	** / **	ns / **	ns / **
20°	** / **	ns / **	* / **

Table B.16 Statistical significance (*p*-value, Friedman) of the effect of the magnitude of x and y-axis excitations on the vertical SEAT value of the suspension seat, with different inclination angles of the backrest and different in-line vertical excitation magnitudes (r.m.s.)

Angle of backrest inclination \ Excitation magnitude (z-axis)	0.25 ms^{-2}	0.5 ms^{-2}	1.0 ms^{-2}
0°	**	**	**
10°	**	**	**
20°	**	**	**

B.3 The effect of the backrest inclination angle on the seat transmissibilities

Table B.17 Statistical significance (p-value, Friedman) of the effect of the inclination angles of the backrest on the frequency and the associated modulus of the fundamental resonance of the in-line fore-aft seat transmissibility at the seat pan, with different excitation magnitudes in x-axis and different excitation magnitude in y and z-axis (r.m.s.)

Excitation magnitude (y and z-axis) / Excitation magnitude (x-axis)	0 ms^{-2}	0.5 ms^{-2}	1.0 ms^{-2}
0.25 ms^{-2}	** / ns	ns / ns	ns / ns
0.5 ms^{-2}	** / ns	ns / ns	ns / ns
1.0 ms^{-2}	ns / ns	ns / ns	ns / ns

Table B.18 Statistical significance (p-value, Friedman) of the effect of the inclination angles of the backrest on the frequency and the associated modulus of the secondary resonance of the in-line lateral seat transmissibility at the backrest, with different excitation magnitudes in y-axis and different excitation magnitude in x and z-axis (r.m.s.)

Excitation magnitude (x and z-axis) / Excitation magnitude (y-axis)	0 ms^{-2}	0.5 ms^{-2}	1.0 ms^{-2}
0.25 ms^{-2}	ns / **	ns / **	** / **
0.5 ms^{-2}	* / **	* / **	* / **
1.0 ms^{-2}	ns / **	ns / **	ns / **

Table B.19 Statistical significance (p-value, Friedman) of the effect of the inclination angles of the backrest on the frequency and the associated modulus of the secondary resonance of the in-line lateral seat transmissibility at the seat pan, with different excitation magnitudes in y-axis and different excitation magnitude in x and z-axis (r.m.s.)

Excitation magnitude (x and z-axis) / **Excitation magnitude (y-axis)**	**0 ms^{-2}**	**0.5 ms^{-2}**	**1.0 ms^{-2}**
0.25 ms^{-2}	ns / *	ns / **	ns / **
0.5 ms^{-2}	ns / **	ns / **	ns / **
1.0 ms^{-2}	ns / **	ns / **	ns / **

Table B.20 Statistical significance (p-value, Friedman) of the effect of the inclination angles of the backrest on the frequency and the associated modulus of the fundamental resonance of the in-line vertical seat transmissibility at the backrest, with different excitation magnitudes in z-axis and different excitation magnitude in x and y-axis (r.m.s.)

Excitation magnitude (x and y-axis) / **Excitation magnitude (z-axis)**	**0 ms^{-2}**	**0.5 ms^{-2}**	**1.0 ms^{-2}**
0.25 ms^{-2}	ns / **	ns / **	ns / **
0.5 ms^{-2}	** / **	** / **	* / **
1.0 ms^{-2}	** / **	** / **	* / **

Table B.21 Statistical significance (p-value, Friedman) of the effect of the inclination angles of the backrest on the frequency and the associated modulus of the second resonance of the in-line vertical seat transmissibility at the backrest, with different excitation magnitudes in z-axis and different of excitation magnitude in x and y-axis (r.m.s.)

Excitation magnitude (x and y-axis) / Excitation magnitude (z-axis)	0 ms^{-2}	0.5 ms^{-2}	1.0 ms^{-2}
0.25 ms^{-2}	** / **	ns / **	* / **
0.5 ms^{-2}	ns / **	ns / **	* / **
1.0 ms^{-2}	ns / ns	ns / **	ns / **

Table B.22 Statistical significance (p-value, Friedman) of the effect of the inclination angles of the backrest on the frequency and the associated modulus of the fundamental resonance of the in-line vertical seat transmissibility at the seat pan, with different excitation magnitudes in z-axis and different excitation magnitude in x and y-axis (r.m.s.)

Excitation magnitude (x and y-axis) / Excitation magnitude (z-axis)	0 ms^{-2}	0.5 ms^{-2}	1.0 ms^{-2}
0.25 ms^{-2}	ns / ns	ns / ns	ns / ns
0.5 ms^{-2}	* / ns	* / ns	* / ns
1.0 ms^{-2}	** / ns	ns / ns	ns / ns

Table B.23 Statistical significance (*p*-value, Friedman) of the effect of the inclination angles of the backrest on the vertical SEAT value of the suspension seat, with different excitation magnitudes in z-axis and different excitation magnitude in x and y-axis (r.m.s.)

Excitation magnitude (x and y-axis) / **Excitation magnitude (z-axis)**	**0 ms^{-2}**	**0.5 ms^{-2}**	**1.0 ms^{-2}**
0.25 ms^{-2}	*	ns	ns
0.5 ms^{-2}	ns	ns	ns
1.0 ms^{-2}	*	*	ns

Appendix C EQUATIONS OF THE BIODYNAMIC MODEL OF THE SEATED HUMAN BODY EXPOSED TO TRI-AXIAL TRANSLATIONAL VIBRATION

The relative displacements between the bodies B_2 and B_3:

$$\boldsymbol{l}_{23}^{O} = \boldsymbol{O}_{3}^{O} + \boldsymbol{A}_{23}^{B_3}\boldsymbol{T}_{pitch}(\theta_3) - \left[\boldsymbol{O}_{2}^{O} + \boldsymbol{A}_{23}^{B_2}\boldsymbol{T}_{pitch}(\theta_2)\right]$$

The relative displacements between the bodies B_1 and B_4:

$$\boldsymbol{l}_{14}^{O} = \boldsymbol{O}_{4}^{O} + \boldsymbol{A}_{14}^{B_4}\boldsymbol{T}_{pitch}(\theta_4)\boldsymbol{T}_{br}(\alpha) - \left[\boldsymbol{O}_{1}^{O} + \boldsymbol{A}_{14}^{B_1}\boldsymbol{T}_{pitch}(\theta_1)\right]$$

The relative displacement between the bodies B_5 and B_6:

$$\boldsymbol{l}_{56}^{O} = \boldsymbol{O}_{6}^{O} + \boldsymbol{A}_{56}^{B_6}\boldsymbol{T}_{pitch}(\theta_6)\boldsymbol{T}_{br}(\alpha) - \left[\boldsymbol{O}_{5}^{O} + \boldsymbol{A}_{56}^{B_5}\boldsymbol{T}_{pitch}(\theta_5)\boldsymbol{T}_{br}(\alpha)\right]$$

The relative displacement between the bodies B_2 and B_s is:

$$\boldsymbol{l}_{2s}^{O} = \boldsymbol{O}_{s}^{O} + \boldsymbol{C}_{2s}^{B_s} - \left[\boldsymbol{O}_{2}^{O} + \boldsymbol{C}_{2s}^{B_2}\boldsymbol{T}_{pitch}(\theta_2)\right]$$

the relative displacement between the bodies B_5 and B_b is:

$$\boldsymbol{l}_{5b}^{O} = \boldsymbol{O}_{b}^{O} + \boldsymbol{C}_{5b}^{B_b}\boldsymbol{T}_{br}(\alpha) - \left[\boldsymbol{O}_{5}^{O} + \boldsymbol{C}_{5b}^{B_5}\boldsymbol{T}_{pitch}(\theta_5)\boldsymbol{T}_{br}(\alpha)\right]$$

The translational force between the bodies B_2 and B_3 is:

$$\boldsymbol{f}_{23}^{O} = \boldsymbol{l}_{23}^{O}\begin{bmatrix} k_{x23} & & \\ & k_{y23} & \\ & & k_{z23} \end{bmatrix} + \dot{\boldsymbol{l}}_{23}^{O}\begin{bmatrix} c_{x23} & & \\ & c_{y23} & \\ & & c_{z23} \end{bmatrix} = [f_{23(x)} \quad f_{23(y)} \quad f_{23(z)}]\boldsymbol{N}$$

The translational force between the bodies B_1 and B_4 is:

$$\boldsymbol{f}_{14}^{O} = \boldsymbol{l}_{14}^{O}\begin{bmatrix} k_{x14} & & \\ & k_{y14} & \\ & & k_{z14} \end{bmatrix} + \dot{\boldsymbol{l}}_{14}^{O}\begin{bmatrix} c_{x14} & & \\ & c_{y14} & \\ & & c_{z14} \end{bmatrix} = [f_{14(x)} \quad f_{14(y)} \quad f_{14(z)}]\boldsymbol{N}$$

The translational force between the bodies B_1 and B_s is:

$$\boldsymbol{f}_{1s}^{O} = \boldsymbol{l}_{1s}^{O}\begin{bmatrix} k_{x1s} & & \\ & k_{y1s} & \\ & & k_{z1s} \end{bmatrix} + \dot{\boldsymbol{l}}_{1s}^{O}\begin{bmatrix} c_{x1s} & & \\ & c_{y1s} & \\ & & c_{z1s} \end{bmatrix} = [f_{1s(x)} \quad f_{1s(y)} \quad f_{1s(z)}]\boldsymbol{N}$$

The translational force between the bodies B_2 and B_s is:

$$\boldsymbol{f}_{2s}^{O} = \boldsymbol{l}_{2s}^{O}\begin{bmatrix} k_{x2s} & & \\ & k_{y2s} & \\ & & k_{z2s} \end{bmatrix} + \dot{\boldsymbol{l}}_{2s}^{O}\begin{bmatrix} c_{x2s} & & \\ & c_{y2s} & \\ & & c_{z2s} \end{bmatrix} = [f_{2s(x)} \quad f_{2s(y)} \quad f_{2s(z)}]\boldsymbol{N}$$

The translational force between the bodies B_4 and B_b is:

$$\boldsymbol{f}_{4b}^{O} = \boldsymbol{l}_{4b}^{O}\boldsymbol{T}_{br}^{T}(\alpha)\begin{bmatrix} k_{x4b} & & \\ & k_{y4b} & \\ & & k_{z4b} \end{bmatrix} + \dot{\boldsymbol{l}}_{4b}^{O}\boldsymbol{T}_{br}^{T}(\alpha)\begin{bmatrix} c_{x4b} & & \\ & c_{y4b} & \\ & & c_{z4b} \end{bmatrix}$$

$$= \begin{bmatrix} \check{f}_{4b(x)} & \check{f}_{4b(y)} & \check{f}_{4b(z)} \end{bmatrix}\check{\boldsymbol{N}}$$

And the translational force between the bodies B_5 and B_b is:

$$\boldsymbol{f}_{5b}^{O} = \begin{bmatrix} \check{f}_{5b(x)} & \check{f}_{5b(y)} & \check{f}_{5b(z)} \end{bmatrix}\check{\boldsymbol{N}}$$

For the rigid body B_2, the equations of motion are derived as:

$$m_2\ddot{x}_2 = -f_{12(x)} + f_{23(x)} + f_{2s(x)}$$

$$m_2\ddot{y}_2 = -f_{12(y)} + f_{23(y)} + f_{2s(y)}$$

$$m_2\ddot{z}_2 = -f_{12(z)} + f_{23(z)} + f_{2s(z)}$$

$$I_2\ddot{\theta}_2 = k_{p23}(\theta_3 - \theta_2) + c_{p23}\left(\dot{\theta}_3 - \dot{\theta}_2\right) - k_{p12}(\theta_2 - \theta_1) - c_{p12}\left(\dot{\theta}_2 - \dot{\theta}_1\right)$$
$$- \boldsymbol{A}_{12}^{B_2} \times \begin{bmatrix} f_{12(x)} & f_{12(y)} & f_{12(z)} \end{bmatrix}\begin{bmatrix} 0 \\ 1 \\ 0 \end{bmatrix} + \boldsymbol{A}_{23}^{B_2} \times \begin{bmatrix} f_{23(x)} & f_{23(y)} & f_{23(z)} \end{bmatrix}\begin{bmatrix} 0 \\ 1 \\ 0 \end{bmatrix}$$
$$+ \boldsymbol{C}_{2s}^{B_2} \times \begin{bmatrix} f_{2s(x)} & f_{2s(y)} & f_{2s(z)} \end{bmatrix}\begin{bmatrix} 0 \\ 1 \\ 0 \end{bmatrix}$$

For the rigid body B_3, the equations of motion are derived as:

$$m_3\ddot{x}_3 = -f_{23(x)}$$

$$m_3\ddot{y}_3 = -f_{23(y)}$$

$$m_3\ddot{z}_3 = -f_{23(z)}$$

$$I_3\ddot{\theta}_3 = -k_{p23}(\theta_3 - \theta_2) - c_{p23}\left(\dot{\theta}_3 - \dot{\theta}_2\right) - \boldsymbol{A}_{23}^{B_3} \times \begin{bmatrix} f_{23(x)} & f_{23(y)} & f_{23(z)} \end{bmatrix}\begin{bmatrix} 0 \\ 1 \\ 0 \end{bmatrix}$$

For the rigid body B_4, the equations of motion are derived as:

$$m_4\ddot{x}_4 = -f_{14(x)} + \begin{bmatrix} \check{f}_{45(x)} & \check{f}_{45(y)} & \check{f}_{45(z)} \end{bmatrix}\boldsymbol{T}_{br}(\alpha)\begin{bmatrix} 1 \\ 0 \\ 0 \end{bmatrix} + \begin{bmatrix} \check{f}_{4b(x)} & \check{f}_{4b(y)} & \check{f}_{4b(z)} \end{bmatrix}\boldsymbol{T}_{br}(\alpha)\begin{bmatrix} 1 \\ 0 \\ 0 \end{bmatrix}$$

$$m_4\ddot{y}_4 = -f_{14(y)} + \begin{bmatrix} \check{f}_{45(x)} & \check{f}_{45(y)} & \check{f}_{45(z)} \end{bmatrix}\boldsymbol{T}_{br}(\alpha)\begin{bmatrix} 0 \\ 1 \\ 0 \end{bmatrix} + \begin{bmatrix} \check{f}_{4b(x)} & \check{f}_{4b(y)} & \check{f}_{4b(z)} \end{bmatrix}\boldsymbol{T}_{br}(\alpha)\begin{bmatrix} 0 \\ 1 \\ 0 \end{bmatrix}$$

$$m_4\ddot{z}_4 = -f_{14(z)} + \begin{bmatrix} \check{f}_{45(x)} & \check{f}_{45(y)} & \check{f}_{45(z)} \end{bmatrix}\boldsymbol{T}_{br}(\alpha)\begin{bmatrix} 0 \\ 0 \\ 1 \end{bmatrix} + \begin{bmatrix} \check{f}_{4b(x)} & \check{f}_{4b(y)} & \check{f}_{4b(z)} \end{bmatrix}\boldsymbol{T}_{br}(\alpha)\begin{bmatrix} 0 \\ 0 \\ 1 \end{bmatrix}$$

$$I_4\ddot{\theta}_4 = -k_{p14}(\theta_4 - \theta_1) - c_{p14}\left(\dot{\theta}_4 - \dot{\theta}_1\right) - k_{p45}(\theta_4 - \theta_5) - c_{p45}\left(\dot{\theta}_4 - \dot{\theta}_5\right)$$
$$+ \boldsymbol{A}_{14}^{B_4} \times \left\{\begin{bmatrix} -f_{14(x)} & -f_{14(y)} & -f_{14(z)} \end{bmatrix}\boldsymbol{T}_{br}^{T}(\alpha)\right\}\begin{bmatrix} 0 \\ 1 \\ 0 \end{bmatrix}$$
$$+ \boldsymbol{A}_{45}^{B_4} \times \begin{bmatrix} \check{f}_{45(x)} & \check{f}_{45(y)} & \check{f}_{45(z)} \end{bmatrix}\begin{bmatrix} 0 \\ 1 \\ 0 \end{bmatrix} + \boldsymbol{C}_{4b}^{B_4} \times \begin{bmatrix} \check{f}_{4b(x)} & \check{f}_{4b(y)} & \check{f}_{4b(z)} \end{bmatrix}\begin{bmatrix} 0 \\ 1 \\ 0 \end{bmatrix}$$

For the rigid body B_5, the equations of motion are derived as:

$$m_5\ddot{x}_5 = -\begin{bmatrix}\check{f}_{45(x)} & \check{f}_{45(y)} & \check{f}_{45(z)}\end{bmatrix}\boldsymbol{T}_{br}(\alpha)\begin{bmatrix}1\\0\\0\end{bmatrix} + \begin{bmatrix}\check{f}_{5b(x)} & \check{f}_{5b(y)} & \check{f}_{5b(z)}\end{bmatrix}\boldsymbol{T}_{br}(\alpha)\begin{bmatrix}1\\0\\0\end{bmatrix} + \begin{bmatrix}\check{f}_{56(x)} & \check{f}_{56(y)} & \check{f}_{56(z)}\end{bmatrix}\boldsymbol{T}_{br}(\alpha)\begin{bmatrix}1\\0\\0\end{bmatrix}$$

$$m_5\ddot{y}_5 = -\begin{bmatrix}\check{f}_{45(x)} & \check{f}_{45(y)} & \check{f}_{45(z)}\end{bmatrix}\boldsymbol{T}_{br}(\alpha)\begin{bmatrix}0\\1\\0\end{bmatrix} + \begin{bmatrix}\check{f}_{5b(x)} & \check{f}_{5b(y)} & \check{f}_{5b(z)}\end{bmatrix}\boldsymbol{T}_{br}(\alpha)\begin{bmatrix}0\\1\\0\end{bmatrix} + \begin{bmatrix}\check{f}_{56(x)} & \check{f}_{56(y)} & \check{f}_{56(z)}\end{bmatrix}\boldsymbol{T}_{br}(\alpha)\begin{bmatrix}0\\1\\0\end{bmatrix}$$

$$m_5\ddot{z}_5 = -\begin{bmatrix}\check{f}_{45(x)} & \check{f}_{45(y)} & \check{f}_{45(z)}\end{bmatrix}\boldsymbol{T}_{br}(\alpha)\begin{bmatrix}0\\0\\1\end{bmatrix} + \begin{bmatrix}\check{f}_{5b(x)} & \check{f}_{5b(y)} & \check{f}_{5b(z)}\end{bmatrix}\boldsymbol{T}_{br}(\alpha)\begin{bmatrix}0\\0\\1\end{bmatrix} + \begin{bmatrix}\check{f}_{56(x)} & \check{f}_{56(y)} & \check{f}_{56(z)}\end{bmatrix}\boldsymbol{T}_{br}(\alpha)\begin{bmatrix}0\\0\\1\end{bmatrix}$$

$$I_5\ddot{\theta}_5 = -k_{p45}(\theta_5-\theta_4) - c_{p45}(\dot{\theta}_5-\dot{\theta}_4) - k_{p56}(\theta_5-\theta_6) - c_{p56}(\dot{\theta}_5-\dot{\theta}_6) - \boldsymbol{A}_{45}^{B_5}\times\begin{bmatrix}\check{f}_{45(x)} & \check{f}_{45(y)} & \check{f}_{45(z)}\end{bmatrix}\begin{bmatrix}0\\1\\0\end{bmatrix} + \boldsymbol{C}_{5b}^{B_5}\times\begin{bmatrix}\check{f}_{5b(x)} & \check{f}_{5b(y)} & \check{f}_{5b(z)}\end{bmatrix}\begin{bmatrix}0\\1\\0\end{bmatrix} + \boldsymbol{A}_{56}^{B_5}\times\begin{bmatrix}\check{f}_{56(x)} & \check{f}_{56(y)} & \check{f}_{56(z)}\end{bmatrix}\begin{bmatrix}0\\1\\0\end{bmatrix}$$

For the rigid body B_6, the equations of motion are derived as:

$$m_6\ddot{x}_6 = -\begin{bmatrix}\check{f}_{56(x)} & \check{f}_{56(y)} & \check{f}_{56(z)}\end{bmatrix}\boldsymbol{T}_{br}(\alpha)\begin{bmatrix}1\\0\\0\end{bmatrix}$$

$$m_6\ddot{y}_6 = -\begin{bmatrix}\check{f}_{56(x)} & \check{f}_{56(y)} & \check{f}_{56(z)}\end{bmatrix}\boldsymbol{T}_{br}(\alpha)\begin{bmatrix}0\\1\\0\end{bmatrix}$$

$$m_6\ddot{z}_6 = -\begin{bmatrix}\check{f}_{56(x)} & \check{f}_{56(y)} & \check{f}_{56(z)}\end{bmatrix}\boldsymbol{T}_{br}(\alpha)\begin{bmatrix}0\\0\\1\end{bmatrix}$$

$$I_6\ddot{\theta}_6 = -k_{p56}(\theta_6-\theta_5) - c_{p56}(\dot{\theta}_6-\dot{\theta}_5) - \boldsymbol{A}_{56}^{B_6}\times\begin{bmatrix}\check{f}_{56(x)} & \check{f}_{56(y)} & \check{f}_{56(z)}\end{bmatrix}\begin{bmatrix}0\\1\\0\end{bmatrix}$$

The in-line lateral apparent mass at the seat pan M_{syy} can be calculated as:

$$M_{syy} = \frac{\mathbf{F}(f_{1s(y)}+f_{2s(y)})}{-\omega^2\mathbf{F}(y_s)} = \frac{k_{y1s}[1-\boldsymbol{T}_R(2,2)]+k_{y2s}[1-\boldsymbol{T}_R(6,2)]}{-\omega^2} + \frac{c_{y1s}[1-\boldsymbol{T}_R(2,2)]+c_{y2s}[1-\boldsymbol{T}_R(6,2)]}{j\omega}$$

The in-line vertical apparent mass at the seat pan M_{szz} can be calculated as:

$$M_{szz} = \frac{\mathbf{F}(f_{1s(z)} + f_{2s(z)})}{-\omega^2 \mathbf{F}(z_s)}$$

$$= \frac{k_{z1s}\left[1 - \boldsymbol{T}_R(3,3) + \boldsymbol{T}_R(4,3)x_{C_{1s}}^{B_1}\right] + k_{z2s}\left[1 - \boldsymbol{T}_R(7,3) + \boldsymbol{T}_R(8,3)x_{C_{2s}}^{B_2}\right]}{-\omega^2}$$

$$+ \frac{c_{z1s}\left[1 - \boldsymbol{T}_R(3,3) + \boldsymbol{T}_R(4,3)x_{C_{1s}}^{B_1}\right] + c_{z2s}\left[1 - \boldsymbol{T}_R(7,3) + \boldsymbol{T}_R(8,3)x_{C_{2s}}^{B_2}\right]}{j\omega}$$

The in-line fore-aft apparent mass at the backrest M_{bxx} can be calculated as:

$$M_{bxx} = \frac{\mathbf{F}(f_{4b(x)} + f_{5b(x)})}{-\omega^2 \mathbf{F}(x_s)} = \frac{\mathbf{F}(\check{f}_{4b(x)}c\alpha - \check{f}_{4b(z)}s\alpha + \check{f}_{5b(x)}c\alpha - \check{f}_{5b(z)}s\alpha)}{-\omega^2 \mathbf{F}(x_s)}$$

$$= \frac{\begin{Bmatrix} k_{x4b}\left[c\alpha - \boldsymbol{T}_R(13,1)c\alpha - \boldsymbol{T}_R(15,1)s\alpha - \boldsymbol{T}_R(16,1)z_{C_{4b}}^{B_4}\right]c\alpha \\ -k_{z4b}\left[-s\alpha + \boldsymbol{T}_R(13,1)s\alpha - \boldsymbol{T}_R(15,1)c\alpha + \boldsymbol{T}_R(16,1)x_{C_{4b}}^{B_4}\right]s\alpha \\ +k_{x5b}\left[c\alpha - \boldsymbol{T}_R(17,1)c\alpha - \boldsymbol{T}_R(19,1)s\alpha - \boldsymbol{T}_R(20,1)z_{C_{5b}}^{B_5}\right]c\alpha \\ -k_{z5b}\left[-s\alpha + \boldsymbol{T}_R(17,1)s\alpha - \boldsymbol{T}_R(19,1)c\alpha + \boldsymbol{T}_R(20,1)x_{C_{5b}}^{B_5}\right]s\alpha \end{Bmatrix}}{-\omega^2}$$

$$+ \frac{\begin{Bmatrix} c_{x4b}\left[c\alpha - \boldsymbol{T}_R(13,1)c\alpha - \boldsymbol{T}_R(15,1)s\alpha - \boldsymbol{T}_R(16,1)z_{C_{4b}}^{B_4}\right]c\alpha \\ -c_{z4b}\left[-s\alpha + \boldsymbol{T}_R(13,1)s\alpha - \boldsymbol{T}_R(15,1)c\alpha + \boldsymbol{T}_R(16,1)x_{C_{4b}}^{B_4}\right]s\alpha \\ +c_{x5b}\left[c\alpha - \boldsymbol{T}_R(17,1)c\alpha - \boldsymbol{T}_R(19,1)s\alpha - \boldsymbol{T}_R(20,1)z_{C_{5b}}^{B_5}\right]c\alpha \\ -c_{z5b}\left[-s\alpha + \boldsymbol{T}_R(17,1)s\alpha - \boldsymbol{T}_R(19,1)c\alpha + \boldsymbol{T}_R(20,1)x_{C_{5b}}^{B_5}\right]s\alpha \end{Bmatrix}}{j\omega}$$

The in-line lateral apparent mass at the backrest M_{byy} can be calculated as:

$$M_{byy} = \frac{\mathbf{F}(f_{4b(y)} + f_{5b(y)})}{-\omega^2 \mathbf{F}(y_s)}$$

$$= \frac{k_{y4b}[1 - \boldsymbol{T}_R(14,2)] + k_{y5b}[1 - \boldsymbol{T}_R(18,2)]}{-\omega^2}$$

$$+ \frac{c_{y4b}[1 - \boldsymbol{T}_R(14,2)] + c_{y5b}[1 - \boldsymbol{T}_R(18,2)]}{j\omega}$$

The in-line vertical apparent mass at the backrest M_{bzz} can be calculated as:

$$M_{bzz} = \frac{\mathbf{F}(f_{4b(z)} + f_{5b(z)})}{-\omega^2 \mathbf{F}(z_s)} = \frac{\mathbf{F}(\check{f}_{4b(x)} s\alpha + \check{f}_{4b(z)} c\alpha + \check{f}_{5b(x)} s\alpha + \check{f}_{5b(z)} c\alpha)}{-\omega^2 \mathbf{F}(z_s)}$$

$$= \frac{\left\{\begin{array}{l} k_{x4b}\left[-\boldsymbol{T}_R(13,3)c\alpha + s\alpha - \boldsymbol{T}_R(15,3)s\alpha - \boldsymbol{T}_R(16,3)z_{C_{4b}}^{B_4}\right]s\alpha \\ +k_{z4b}\left[\boldsymbol{T}_R(13,3)s\alpha + c\alpha - \boldsymbol{T}_R(15,3)c\alpha + \boldsymbol{T}_R(16,3)x_{C_{4b}}^{B_4}\right]c\alpha \\ +k_{x5b}\left[-\boldsymbol{T}_R(17,3)c\alpha + s\alpha - \boldsymbol{T}_R(19,3)s\alpha - \boldsymbol{T}_R(20,3)z_{C_{5b}}^{B_5}\right]s\alpha \\ +k_{z5b}\left[\boldsymbol{T}_R(17,3)s\alpha + c\alpha - \boldsymbol{T}_R(19,3)c\alpha + \boldsymbol{T}_R(20,3)x_{C_{5b}}^{B_5}\right]c\alpha \end{array}\right\}}{-\omega^2}$$

$$+ \frac{\left\{\begin{array}{l} c_{x4b}\left[-\boldsymbol{T}_R(13,3)c\alpha + s\alpha - \boldsymbol{T}_R(15,3)s\alpha - \boldsymbol{T}_R(16,3)z_{C_{4b}}^{B_4}\right]s\alpha \\ +c_{z4b}\left[\boldsymbol{T}_R(13,3)s\alpha + c\alpha - \boldsymbol{T}_R(15,3)c\alpha + \boldsymbol{T}_R(16,3)x_{C_{4b}}^{B_4}\right]c\alpha \\ +c_{x5b}\left[-\boldsymbol{T}_R(17,3)c\alpha + s\alpha - \boldsymbol{T}_R(19,3)s\alpha - \boldsymbol{T}_R(20,3)z_{C_{5b}}^{B_5}\right]s\alpha \\ +c_{z5b}\left[\boldsymbol{T}_R(17,3)s\alpha + c\alpha - \boldsymbol{T}_R(19,3)c\alpha + \boldsymbol{T}_R(20,3)x_{C_{5b}}^{B_5}\right]c\alpha \end{array}\right\}}{j\omega}$$

Appendix D EQUATIONS OF THE DYNAMIC MODEL OF THE SUSPENSION-SEAT-OCCUPANT SYSTEM EXPOSED TO TRI-AXIAL TRANSLATIONAL VIBRATION AND THE PARAMETER SENSITIVITY ANALYSIS

D.1 Equations

The relative displacement between the bodies B_f and B_r is:

$$\boldsymbol{l}_{fr}^{O} = \boldsymbol{O}_{r}^{O} + \boldsymbol{C}_{fr}^{B_r} - \left(\boldsymbol{O}_{f}^{O} + \boldsymbol{C}_{fr}^{B_f}\right)$$

The relative displacement between the bodies B_r and B_{sp} is:

$$\boldsymbol{l}_{rsp}^{O} = \boldsymbol{O}_{sp}^{O} + \boldsymbol{A}_{rsp}^{B_{sp}}\boldsymbol{T}_{roll}(\beta_{sp}) - \left(\boldsymbol{O}_{r}^{O} + \boldsymbol{A}_{rsp}^{B_r}\right)$$

The force between the bodies B_f and B_r is:

$$\boldsymbol{f}_{fr}^{O} = \boldsymbol{l}_{fr}^{O}\begin{bmatrix} k_{xfr} & & \\ & k_{yfr} & \\ & & k_{zfr} \end{bmatrix} + \dot{\boldsymbol{l}}_{fr}^{O}\begin{bmatrix} c_{xfr} & & \\ & c_{yfr} & \\ & & c_{zfr} \end{bmatrix} = [f_{fr(x)} \quad f_{fr(y)} \quad f_{fbr(z)}]\boldsymbol{N}$$

The force between the bodies B_l and B_{sp} is:

$$\boldsymbol{f}_{lsp}^{O} = \boldsymbol{l}_{lsp}^{O}\begin{bmatrix} k_{xlsp} & & \\ & k_{ylsp} & \\ & & k_{zlsp} \end{bmatrix} + \dot{\boldsymbol{l}}_{lsp}^{O}\begin{bmatrix} c_{xlsp} & & \\ & c_{ylsp} & \\ & & c_{zlsp} \end{bmatrix} = [f_{lsp(x)} \quad f_{lsp(y)} \quad f_{lsp(z)}]\boldsymbol{N}$$

The force between the bodies B_r and B_{sp} is:

$$\boldsymbol{f}_{rsp}^{O} = \boldsymbol{l}_{rsp}^{O}\begin{bmatrix} k_{xrsp} & & \\ & k_{yrsp} & \\ & & k_{zrsp} \end{bmatrix} + \dot{\boldsymbol{l}}_{rsp}^{O}\begin{bmatrix} c_{xrsp} & & \\ & c_{yrsp} & \\ & & c_{zrsp} \end{bmatrix} = [f_{rsp(x)} \quad f_{rsp(y)} \quad f_{rsp(z)}]\boldsymbol{N}$$

The force between the bodies B_f and B_{sp} is:

$$\boldsymbol{f}_{fsp}^{O} = \boldsymbol{l}_{fsp}^{O}\begin{bmatrix} k_{xfsp} & & \\ & k_{yfsp} & \\ & & k_{zfsp} \end{bmatrix} + \dot{\boldsymbol{l}}_{fsp}^{O}\begin{bmatrix} c_{xfsp} & & \\ & c_{yfsp} & \\ & & c_{zfsp} \end{bmatrix} = [f_{fsp(x)} \quad f_{fsp(y)} \quad f_{fsp(z)}]\boldsymbol{N}$$

For the rigid body B_r, the equations of motion are derived as:

$$m_r\ddot{x}_r = -f_{fr(x)} + f_{rsp(x)}$$

$$m_r\ddot{y}_r = -f_{fr(y)} + f_{rsp(y)}$$
$$m_r\ddot{z}_r = -f_{fr(z)} + f_{rs(z)}$$

And the relative displacement between the bodies B_c and B_b is:

$$\boldsymbol{l}^O_{cbr} = \boldsymbol{O}^O_{br} + \boldsymbol{A}^{B_{br}}_{cbr}\boldsymbol{T}_{pitch}(\theta_{br})\boldsymbol{T}_{roll}(\beta_{br})\boldsymbol{T}_{br}(\alpha) - \left[\boldsymbol{O}^O_c + \boldsymbol{A}^{B_c}_{cbr}\boldsymbol{T}_{pitch}(\theta_c)\boldsymbol{T}_{roll}(\beta_c)\right]$$

The translational force between the bodies B_c and B_m is:

$$\boldsymbol{f}^O_{cm} = \boldsymbol{l}^O_{cm}\begin{bmatrix} k_{xcm} & & \\ & k_{ycm} & \\ & & k_{zcm} \end{bmatrix} + \dot{\boldsymbol{l}}^O_{cm}\begin{bmatrix} c_{xcm} & & \\ & c_{ycm} & \\ & & c_{zcm} \end{bmatrix} = [f_{cm(x)} \quad f_{cm(y)} \quad f_{cm(z)}]\boldsymbol{N}$$

And the translational force between the bodies B_c and B_m is:

$$\boldsymbol{f}^O_{cbr} = \boldsymbol{l}^O_{cbr}\begin{bmatrix} k_{xcbr} & & \\ & k_{ycbr} & \\ & & k_{zcbr} \end{bmatrix} + \dot{\boldsymbol{l}}^O_{cbr}\begin{bmatrix} c_{xcbr} & & \\ & c_{ycbr} & \\ & & c_{zcbr} \end{bmatrix} = [f_{cbr(x)} \quad f_{cbr(y)} \quad f_{cbr(z)}]\boldsymbol{N}$$

For the rigid body B_p, the equations of motion are derived as:

$$m_p\ddot{x}_p = -f_{lsp(x)} - f_{rsp(x)} - f_{fsp(x)} + f_{pc(x)}$$
$$m_p\ddot{y}_p = -f_{lsp(y)} - f_{rsp(y)} - f_{fsp(z)} + f_{pc(y)}$$
$$m_p\ddot{z}_p = -f_{lsp(z)} - f_{rsp(z)} - f_{fsp(z)} + f_{pc(z)}$$

$$I_p\ddot{\beta}_p = k_{rpc}(\beta_c - \beta_p) + c_{rpc}(\dot{\beta}_c - \dot{\beta}_p) - \boldsymbol{A}^{B_p}_{lsp} \times \{[f_{lsp(x)} \quad f_{lsp(y)} \quad f_{lsp(z)}]\}\begin{bmatrix}1\\0\\0\end{bmatrix}$$
$$- \boldsymbol{A}^{B_p}_{rsp} \times \{[f_{rsp(x)} \quad f_{rsp(y)} \quad f_{rsp(z)}]\}\begin{bmatrix}1\\0\\0\end{bmatrix} + \boldsymbol{A}^{B_p}_{pc} \times \{[f_{pc(x)} \quad f_{pc(y)} \quad f_{pc(z)}]\}\begin{bmatrix}1\\0\\0\end{bmatrix}$$

For the rigid body B_m, the equations of motion are derived as:

$$m_m\ddot{x}_m = -f_{cm(x)}$$
$$m_m\ddot{y}_m = -f_{cm(y)}$$
$$m_m\ddot{z}_m = -f_{cm(y)}$$

$$I_{rm}\ddot{\beta}_m = -k_{rcm}(\beta_m - \beta_c) - c_{rcm}(\dot{\beta}_m - \dot{\beta}_c) - \boldsymbol{A}^{B_m}_{cm} \times \{[f_{cm(x)} \quad f_{cm(y)} \quad f_{cm(z)}]\}\begin{bmatrix}1\\0\\0\end{bmatrix}$$

$$I_{pm}\ddot{\theta}_m = -k_{pcm}(\theta_m - \theta_c) - c_{pcm}(\dot{\theta}_m - \dot{\theta}_c) - \boldsymbol{A}^{B_m}_{cm} \times \{[f_{cm(x)} \quad f_{cm(y)} \quad f_{cm(z)}]\}\begin{bmatrix}0\\1\\0\end{bmatrix}$$

And for the rigid body B_{br}, the equations of motion are derived as:

$$m_{br}\ddot{x}_{br} = -f_{cbr(x)}$$
$$m_{br}\ddot{y}_{br} = -f_{cbr(y)}$$
$$m_{br}\ddot{z}_{br} = -f_{cbr(z)}$$

$$I_{rbr}\ddot{\beta}_{br} = -k_{rcbr}(\beta_{br} - \beta_c) - c_{rcb}\left(\dot{\beta}_{br} - \dot{\beta}_c\right) - \boldsymbol{A}_{cbr}^{B_{br}} \times \left\{[f_{cbr(x)} \quad f_{cbr(y)} \quad f_{cbr(z)}]\boldsymbol{T}_{br}^{T}(\alpha)\right\}\begin{bmatrix}1\\0\\0\end{bmatrix}$$

$$I_{pbr}\ddot{\theta}_{br} = -k_{rcbr}(\theta_{br} - \theta_c) - c_{rcbr}\left(\dot{\theta}_{br} - \dot{\theta}_c\right) - \boldsymbol{A}_{cbr}^{B_{br}} \times \left\{[f_{cbr(x)} \quad f_{cbr(y)} \quad f_{cbr(z)}]\boldsymbol{T}_{br}^{T}(\alpha)\right\}\begin{bmatrix}0\\1\\0\end{bmatrix}$$

The relative displacement between the bodies B_c and B_2 is:

$$\boldsymbol{l}_{c2}^{O} = \boldsymbol{O}_2^{O} + \boldsymbol{A}_{c2}^{B_2}\boldsymbol{T}_{pitch}(\theta_2) - \left[\boldsymbol{O}_c^{O} + \boldsymbol{A}_{c2}^{B_c}\boldsymbol{T}_{pitch}(\theta_c)\boldsymbol{T}_{roll}(\beta_c)\right]$$

The relative displacement between the bodies B_{br} and B_5 is:

$$\boldsymbol{l}_{b5}^{O} = \boldsymbol{O}_5^{O} + \boldsymbol{A}_{b5}^{B_5}\boldsymbol{T}_{pitch}(\theta_5)\boldsymbol{T}_{br}(\alpha) - \left[\boldsymbol{O}_b^{O} + \boldsymbol{A}_{b5}^{B_{br}}\boldsymbol{T}_{pitch}(\theta_{br})\boldsymbol{T}_{roll}(\beta_{br})\boldsymbol{T}_{br}(\alpha)\right]$$

The translational force between the bodies B_c and B_2 is

$$\boldsymbol{f}_{c2}^{O} = \boldsymbol{l}_{c2}^{O}\begin{bmatrix}k_{xc2} & & \\ & k_{yc2} & \\ & & k_{zc2}\end{bmatrix} + \dot{\boldsymbol{l}}_{c2}^{O}\begin{bmatrix}c_{xc2} & & \\ & c_{yc2} & \\ & & c_{zc2}\end{bmatrix} = [f_{c2(x)} \quad f_{c2(y)} \quad f_{c2(z)}]\boldsymbol{N}$$

The translational force between the bodies B_{br} and B_5 is:

$$\boldsymbol{f}_{b5}^{O} = \boldsymbol{l}_{b5}^{O}\boldsymbol{T}_{br}^{T}(\alpha)\begin{bmatrix}k_{xb5} & & \\ & k_{yb5} & \\ & & k_{zb5}\end{bmatrix} + \dot{\boldsymbol{l}}_{b5}^{O}\boldsymbol{T}_{br}^{T}(\alpha)\begin{bmatrix}c_{xb5} & & \\ & c_{yb5} & \\ & & c_{zb5}\end{bmatrix}$$
$$= \left[\check{f}_{b5(x)} \quad \check{f}_{b5(y)} \quad \check{f}_{b5(z)}\right]\check{\boldsymbol{N}}$$

The updated equations of motion of B_1 are derived as:

$$m_1\ddot{x}_1 = -f_{c1(x)} + f_{12(x)} + f_{14(x)}$$
$$m_1\ddot{y}_1 = -f_{c1(y)} + f_{12(y)} + f_{14(y)}$$
$$m_1\ddot{z}_1 = -f_{c1(z)} + f_{12(z)} + f_{14(z)}$$
$$I_1\ddot{\theta}_1 = k_{p12}(\theta_2 - \theta_1) + c_{p12}\left(\dot{\theta}_2 - \dot{\theta}_1\right) + k_{p14}(\theta_4 - \theta_1) + c_{p14}\left(\dot{\theta}_4 - \dot{\theta}_1\right) + k_{pc1}(\theta_c - \theta_1)$$
$$+ c_{pc1}\left(\dot{\theta}_c - \dot{\theta}_1\right) - \boldsymbol{A}_{c1}^{B_1} \times [f_{c1(x)} \quad f_{c1(y)} \quad f_{c1(z)}]\begin{bmatrix}0\\1\\0\end{bmatrix}$$
$$+ \boldsymbol{A}_{12}^{B_1} \times [f_{12(x)} \quad f_{12(y)} \quad f_{12(z)}]\begin{bmatrix}0\\1\\0\end{bmatrix} + \boldsymbol{A}_{14}^{B_1} \times [f_{14(x)} \quad f_{14(y)} \quad f_{14(z)}]\begin{bmatrix}0\\1\\0\end{bmatrix}$$

The updated equations of motion of B_2 are derived as:

$$m_2\ddot{x}_2 = -f_{c2(x)} - f_{12(x)} + f_{23(x)}$$
$$m_2\ddot{y}_2 = -f_{c2(y)} - f_{12(y)} + f_{23(y)}$$
$$m_2\ddot{z}_2 = -f_{c2(z)} - f_{12(z)} + f_{23(z)}$$

$$I_2\ddot{\theta}_2 = k_{p23}(\theta_3 - \theta_2) + c_{p23}(\dot{\theta}_3 - \dot{\theta}_2) - k_{p12}(\theta_2 - \theta_1) - c_{p12}(\dot{\theta}_2 - \dot{\theta}_1) + k_{pc2}(\theta_c - \theta_2)$$
$$+ c_{pc2}(\dot{\theta}_c - \dot{\theta}_2) - \boldsymbol{A}_{c2}^{B_2} \times [f_{c2(x)} \quad f_{c2(y)} \quad f_{c2(z)}] \begin{bmatrix}0\\1\\0\end{bmatrix}$$
$$- \boldsymbol{A}_{12}^{B_2} \times [f_{12(x)} \quad f_{12(y)} \quad f_{12(z)}] \begin{bmatrix}0\\1\\0\end{bmatrix} + \boldsymbol{A}_{23}^{B_2} \times [f_{23(x)} \quad f_{23(y)} \quad f_{23(z)}] \begin{bmatrix}0\\1\\0\end{bmatrix}$$

The updated equations of motion of B_4 are derived as:

$$m_4\ddot{x}_4 = -f_{14(x)} + [\check{f}_{45(x)} \quad \check{f}_{45(y)} \quad \check{f}_{45(z)}]\boldsymbol{T}_{br}(\alpha) \begin{bmatrix}1\\0\\0\end{bmatrix} - [\check{f}_{b4(x)} \quad \check{f}_{b4(y)} \quad \check{f}_{b4(z)}]\boldsymbol{T}_{br}(\alpha) \begin{bmatrix}1\\0\\0\end{bmatrix}$$
$$m_4\ddot{y}_4 = -f_{14(y)} + [\check{f}_{45(x)} \quad \check{f}_{45(y)} \quad \check{f}_{45(z)}]\boldsymbol{T}_{br}(\alpha) \begin{bmatrix}0\\1\\0\end{bmatrix} - [\check{f}_{b4(x)} \quad \check{f}_{b4(y)} \quad \check{f}_{b4(z)}]\boldsymbol{T}_{br}(\alpha) \begin{bmatrix}0\\1\\0\end{bmatrix}$$
$$m_4\ddot{z}_4 = -f_{14(z)} + [\check{f}_{45(x)} \quad \check{f}_{45(y)} \quad \check{f}_{45(z)}]\boldsymbol{T}_{br}(\alpha) \begin{bmatrix}0\\0\\1\end{bmatrix} - [\check{f}_{b4(x)} \quad \check{f}_{b4(y)} \quad \check{f}_{b4(z)}]\boldsymbol{T}_{br}(\alpha) \begin{bmatrix}0\\0\\1\end{bmatrix}$$
$$I_4\ddot{\theta}_4 = -k_{p14}(\theta_4 - \theta_1) - c_{p14}(\dot{\theta}_4 - \dot{\theta}_1) - k_{p45}(\theta_4 - \theta_5) - c_{p45}(\dot{\theta}_4 - \dot{\theta}_5) + k_{pb4}(\theta_{br} - \theta_4)$$
$$+ c_{pb4}(\dot{\theta}_{br} - \dot{\theta}_4) - \boldsymbol{A}_{14}^{B_4} \times \{[f_{14(x)} \quad f_{14(y)} \quad f_{14(z)}]\boldsymbol{T}_{br}^{T}(\alpha)\} \begin{bmatrix}0\\1\\0\end{bmatrix}$$
$$+ \boldsymbol{A}_{45}^{B_4} \times [\check{f}_{45(x)} \quad \check{f}_{45(y)} \quad \check{f}_{45(z)}] \begin{bmatrix}0\\1\\0\end{bmatrix} - \boldsymbol{A}_{b4}^{B_4} \times [\check{f}_{b4(x)} \quad \check{f}_{b4(y)} \quad \check{f}_{b4(z)}] \begin{bmatrix}0\\1\\0\end{bmatrix}$$

The updated equations of motion of B_5 are derived as:

$$m_5\ddot{x}_5 = -[\check{f}_{45(x)} \quad \check{f}_{45(y)} \quad \check{f}_{45(z)}]\boldsymbol{T}_{br}(\alpha) \begin{bmatrix}1\\0\\0\end{bmatrix} - [\check{f}_{b5(x)} \quad \check{f}_{b5(y)} \quad \check{f}_{b5(z)}]\boldsymbol{T}_{br}(\alpha) \begin{bmatrix}1\\0\\0\end{bmatrix}$$
$$+ [\check{f}_{56(x)} \quad \check{f}_{56(y)} \quad \check{f}_{56(z)}]\boldsymbol{T}_{br}(\alpha) \begin{bmatrix}1\\0\\0\end{bmatrix}$$
$$m_5\ddot{y}_5 = -[\check{f}_{45(x)} \quad \check{f}_{45(y)} \quad \check{f}_{45(z)}]\boldsymbol{T}_{br}(\alpha) \begin{bmatrix}0\\1\\0\end{bmatrix} - [\check{f}_{b5(x)} \quad \check{f}_{b5(y)} \quad \check{f}_{b5(z)}]\boldsymbol{T}_{br}(\alpha) \begin{bmatrix}0\\1\\0\end{bmatrix}$$
$$+ [\check{f}_{56(x)} \quad \check{f}_{56(y)} \quad \check{f}_{56(z)}]\boldsymbol{T}_{br}(\alpha) \begin{bmatrix}0\\1\\0\end{bmatrix}$$
$$m_5\ddot{z}_5 = -[\check{f}_{45(x)} \quad \check{f}_{45(y)} \quad \check{f}_{45(z)}]\boldsymbol{T}_{br}(\alpha) \begin{bmatrix}0\\0\\1\end{bmatrix} - [\check{f}_{b5(x)} \quad \check{f}_{b5(y)} \quad \check{f}_{b5(z)}]\boldsymbol{T}_{br}(\alpha) \begin{bmatrix}0\\0\\1\end{bmatrix}$$
$$+ [\check{f}_{56(x)} \quad \check{f}_{56(y)} \quad \check{f}_{56(z)}]\boldsymbol{T}_{br}(\alpha) \begin{bmatrix}0\\0\\1\end{bmatrix}$$

$$I_5\ddot{\theta}_5 = k_{p45}(\theta_4 - \theta_5) + c_{p45}(\dot{\theta}_4 - \dot{\theta}_5) - k_{p56}(\theta_5 - \theta_6) - c_{p56}(\dot{\theta}_5 - \dot{\theta}_6) + k_{pb5}(\theta_{br} - \theta_5) + c_{pb5}(\dot{\theta}_{br} - \dot{\theta}_5) - \boldsymbol{A}_{45}^{B_5} \times \begin{bmatrix} \check{f}_{45(x)} & \check{f}_{45(y)} & \check{f}_{45(z)} \end{bmatrix} \begin{bmatrix} 0 \\ 1 \\ 0 \end{bmatrix} - \boldsymbol{A}_{b5}^{B_5} \times \begin{bmatrix} \check{f}_{b5(x)} & \check{f}_{b5(y)} & \check{f}_{b5(z)} \end{bmatrix} \begin{bmatrix} 0 \\ 1 \\ 0 \end{bmatrix} + \boldsymbol{A}_{56}^{B_5} \times \begin{bmatrix} \check{f}_{56(x)} & \check{f}_{56(y)} & \check{f}_{56(z)} \end{bmatrix} \begin{bmatrix} 0 \\ 1 \\ 0 \end{bmatrix}$$

The updated equations of motion of B_c are derived as:

$$m_c\ddot{x}_c = -f_{pc(x)} + f_{c1(x)} + f_{c2(x)} + f_{cbr(x)}$$

$$m_c\ddot{y}_c = -f_{pc(y)} + f_{c1(y)} + f_{c2(y)} + f_{cbr(y)}$$

$$m_c\ddot{z}_c = -f_{pc(z)} + f_{c1(z)} + f_{c2(z)} + f_{cbr(z)}$$

$$I_{rc}\ddot{\beta}_c = -k_{rpc}(\beta_c - \beta_p) - c_{rpc}(\dot{\beta}_c - \dot{\beta}_p) + k_{rcbr}(\beta_{br} - \beta_c) + c_{rcbr}(\dot{\beta}_{br} - \dot{\beta}_c) - \boldsymbol{A}_{pc}^{B_c} \times \{[f_{pc(x)} \quad f_{pc(y)} \quad f_{pc(z)}]\} \begin{bmatrix} 1 \\ 0 \\ 0 \end{bmatrix} + \boldsymbol{A}_{c1}^{B_c} \times \{[f_{c1(x)} \quad f_{c1(y)} \quad f_{c1(z)}]\} \begin{bmatrix} 1 \\ 0 \\ 0 \end{bmatrix} + \boldsymbol{A}_{c2}^{B_c} \times \{[f_{c2(x)} \quad f_{c2(y)} \quad f_{c2(z)}]\} \begin{bmatrix} 1 \\ 0 \\ 0 \end{bmatrix} + \boldsymbol{A}_{cbr}^{B_c} \times \{[f_{cbr(x)} \quad f_{cbr(y)} \quad f_{cbr(z)}]\} \begin{bmatrix} 1 \\ 0 \\ 0 \end{bmatrix}$$

$$I_{pc}\ddot{\theta}_c = -k_{ppc}\theta_c - c_{ppc}\dot{\theta}_c + k_{pc1}(\theta_1 - \theta_c) + c_{pc1}(\dot{\theta}_1 - \dot{\theta}_c) + k_{pc2}(\theta_2 - \theta_c) + c_{pc1}(\dot{\theta}_2 - \dot{\theta}_c) + k_{pcbr}(\theta_{br} - \theta_c) + c_{pcbr}(\dot{\theta}_{br} - \dot{\theta}_c) - \boldsymbol{A}_{pc}^{B_c} \times \{[f_{pc(x)} \quad f_{pc(y)} \quad f_{pc(z)}]\} \begin{bmatrix} 0 \\ 1 \\ 0 \end{bmatrix} + \boldsymbol{A}_{c1}^{B_c} \times \{[f_{c1(x)} \quad f_{c1(y)} \quad f_{c1(z)}]\} \begin{bmatrix} 0 \\ 1 \\ 0 \end{bmatrix} + \boldsymbol{A}_{c2}^{B_c} \times \{[f_{c2(x)} \quad f_{c2(y)} \quad f_{c2(z)}]\} \begin{bmatrix} 0 \\ 1 \\ 0 \end{bmatrix} + \boldsymbol{A}_{cbr}^{B_c} \times \{[f_{cbr(x)} \quad f_{cbr(y)} \quad f_{cbr(z)}]\} \begin{bmatrix} 0 \\ 1 \\ 0 \end{bmatrix}$$

The updated equations of motion of B_{br} are derived as:

$$m_{br}\ddot{x}_{br} = -f_{cbr(x)} + \begin{bmatrix} \check{f}_{b4(x)} & \check{f}_{b4(y)} & \check{f}_{b4(z)} \end{bmatrix} \boldsymbol{T}_{br}(\alpha) \begin{bmatrix} 1 \\ 0 \\ 0 \end{bmatrix} + \begin{bmatrix} \check{f}_{b5(x)} & \check{f}_{b5(y)} & \check{f}_{b5(z)} \end{bmatrix} \boldsymbol{T}_{br}(\alpha) \begin{bmatrix} 1 \\ 0 \\ 0 \end{bmatrix}$$

$$m_{br}\ddot{y}_{br} = -f_{cbr(y)} + \begin{bmatrix} \check{f}_{b4(x)} & \check{f}_{b4(y)} & \check{f}_{b4(z)} \end{bmatrix} \boldsymbol{T}_{br}(\alpha) \begin{bmatrix} 0 \\ 1 \\ 0 \end{bmatrix} + \begin{bmatrix} \check{f}_{b5(x)} & \check{f}_{b5(y)} & \check{f}_{b5(z)} \end{bmatrix} \boldsymbol{T}_{br}(\alpha) \begin{bmatrix} 0 \\ 1 \\ 0 \end{bmatrix}$$

$$m_{br}\ddot{z}_{br} = -f_{cbr(y)} + \begin{bmatrix} \check{f}_{b4(x)} & \check{f}_{b4(y)} & \check{f}_{b4(z)} \end{bmatrix} \boldsymbol{T}_{br}(\alpha) \begin{bmatrix} 0 \\ 0 \\ 1 \end{bmatrix} + \begin{bmatrix} \check{f}_{b5(x)} & \check{f}_{b5(y)} & \check{f}_{b5(z)} \end{bmatrix} \boldsymbol{T}_{br}(\alpha) \begin{bmatrix} 0 \\ 0 \\ 1 \end{bmatrix}$$

$$I_{rbr}\ddot{\beta}_{br} = -k_{rcbr}(\beta_{br} - \beta_c) - c_{rcbr}(\dot{\beta}_{br} - \dot{\beta}_c) - \boldsymbol{A}_{cbr}^{B_{br}} \times \{[f_{cbr(x)} \quad f_{cbr(y)} \quad f_{cbr(z)}]\boldsymbol{T}_{br}^{T}(\alpha)\} \begin{bmatrix} 1 \\ 0 \\ 0 \end{bmatrix} + \boldsymbol{A}_{b4}^{B_{br}} \times \{[\check{f}_{b4(x)} \quad \check{f}_{b4(y)} \quad \check{f}_{b4(z)}]\} \begin{bmatrix} 1 \\ 0 \\ 0 \end{bmatrix} + \boldsymbol{A}_{b5}^{B_{br}} \times \{[\check{f}_{b5(x)} \quad \check{f}_{b5(y)} \quad \check{f}_{b5(z)}]\} \begin{bmatrix} 1 \\ 0 \\ 0 \end{bmatrix}$$

$$I_{pbr}\ddot{\theta}_{br} = -k_{rcbr}(\theta_{br} - \theta_c) - c_{rcb}\left(\dot{\theta}_{br} - \dot{\theta}_c\right) + k_{pb4}(\theta_4 - \theta_{br}) + c_{pb4}\left(\dot{\theta}_4 - \dot{\theta}_{br}\right)$$
$$+ k_{pb5}(\theta_5 - \theta_{br}) + c_{pb5}\left(\dot{\theta}_5 - \dot{\theta}_{br}\right)$$
$$- \boldsymbol{A}_{cbr}^{B_{br}} \times \left\{[f_{cb(x)} \quad f_{cb(y)} \quad f_{cb(z)}]\boldsymbol{T}_{br}^{T}(\alpha)\right\}\begin{bmatrix}0\\1\\0\end{bmatrix}$$
$$+ \boldsymbol{A}_{b4}^{B_{br}} \times \left\{\left[\check{f}_{b4(x)} \quad \check{f}_{b4(y)} \quad \check{f}_{b4(z)}\right]\right\}\begin{bmatrix}0\\1\\0\end{bmatrix} + \boldsymbol{A}_{b5}^{B_{br}} \times \left\{\left[\check{f}_{b5(x)} \quad \check{f}_{b5(y)} \quad \check{f}_{b5(z)}\right]\right\}\begin{bmatrix}0\\1\\0\end{bmatrix}$$

D.2 Parameters of the suspension-seat-occupant model (e.g., a 1.75m and 78.6 kg subject under the combined 0.5 ms^{-2} fore-aft, 0.5 ms^{-2} lateral, and 0.5 ms^{-2} r.m.s. vertical excitation)

Notation	Parameter (Unit)	Value	Notation	Parameter (Unit)	Value
k_{x12}	Stiffness between B_1 and B_2 in x-axis (N/m)	1.58E3	c_{x12}	Damping between B_1 and B_2 in x-axis (Ns/m)	5.28E3
k_{y12}	Stiffness between B_1 and B_2 in y-axis (N/m)	4.44E2	c_{y12}	Damping between B_1 and B_2 in y-axis (Ns/m)	3.18E2
k_{z12}	Stiffness between B_1 and B_2 in z-axis (N/m)	1.33E2	c_{z12}	Damping between B_1 and B_2 in z-axis (Ns/m)	4.70
k_{p12}	Stiffness between B_1 and B_2 around y-axis (Nm/rad)	3.13E2	c_{p12}	Damping between B_1 and B_2 around y-axis (Nms/rad)	2.12
k_{x23}	Stiffness between B_2 and B_3 in x-axis (N/m)	2.54E2	c_{x12}	Damping between B_2 and B_3 in x-axis (Ns/m)	2.00E4
k_{y23}	Stiffness between B_2 and B_3 in y-axis (N/m)	3.69E2	c_{y23}	Damping between B_2 and B3 in y-axis (Ns/m)	7.4E7
k_{z23}	Stiffness between B_2 and B_3 in z-axis (N/m)	1.63E8	c_{z23}	Damping between B_2 and B_3 in z-axis (Ns/m)	1.76E2
k_{p23}	Stiffness between B_2 and B_3 around y-axis (Nm/rad)	3.10E7	c_{p23}	Damping between B_2 and B_3 around y-axis (Nms/rad)	1.65E2
k_{x14}	Stiffness between B_1 and B_4 in x-axis (N/m)	1.76E8	c_{x14}	Damping between B_1 and B_4 in x-axis (Ns/m)	2.24E2
k_{y14}	Stiffness between B_1 and B_4 in y-axis (N/m)	6.53E3	c_{y14}	Damping between B_1 and B_4 in y-axis (Ns/m)	5.37E3
k_{z14}	Stiffness between B_1 and B_4 in z-axis (N/m)	1.04E7	c_{z14}	Damping between B_1 and B_4 in z-axis (Ns/m)	3.28E2
k_{p14}	Stiffness between B_1 and B_4 around y-axis (Nm/rad)	2.03E2	c_{p14}	Damping between B_1 and B_4 around y-axis (Nms/rad)	9.82
k_{x45}	Stiffness between B_4 and B_5 in x-axis (N/m)	1.81E3	c_{x45}	Damping between B_4 and B_5 in x-axis (Ns/m)	1.32
k_{y45}	Stiffness between B_4 and B_5 in y-axis (N/m)	2.98E2	c_{y45}	Damping between B_4 and B_5 in y-axis (Ns/m)	1.42E8
k_{z45}	Stiffness between B_4 and B_5 in z-axis (N/m)	1.29E8	c_{z45}	Damping between B_4 and B_5 in z-axis (Ns/m)	2.30E2
k_{p45}	Stiffness between B_4 and B_5 around y-axis (Nm/rad)	4.52E1	c_{p45}	Damping between B_4 and B_5 around y-axis (Nms/rad)	2.78
k_{x56}	Stiffness between B_5 and B_6 in x-axis (N/m)	1.34E2	c_{x56}	Damping between B_5 and B_6 in x-axis (Ns/m)	1.74E8
k_{y56}	Stiffness between B_5 and B_6 in y-axis (N/m)	3.64E3	c_{y56}	Damping between B_5 and B_6 in y-axis (Ns/m)	2.76E3
k_{z56}	Stiffness between B_5 and B_6 in z-axis (N/m)	9.18E1	c_{z56}	Damping between B_5 and B_6 in z-axis (Ns/m)	5.18E7

k_{p56}	Stiffness between B_5 and B_6 around y-axis (Nm/rad)	9.26E7	c_{p56}	Damping between B_5 and B_6 around y-axis (Nms/rad)	2.42E2
$x_{A_{c1}}^{B_1}$	Coordinate of A_{c1} in x-axis in the coordinate system of B_1 (m)	5E-2	$y_{A_{c1}}^{B_1}$	Coordinate of A_{c1} in y-axis in the coordinate system of B_1 (m)	-1E-2
$x_{A_{c2}}^{B_2}$	Coordinate of A_{c2} in x-axis in the coordinate system of B_2 (m)	-1.1E-1	$y_{A_{c2}}^{B_2}$	Coordinate of A_{c2} in y-axis in the coordinate system of B_2 (m)	-1E-2
$y_{A_{b4}}^{B_4}$	Coordinate of A_{b4} in y-axis in the coordinate system of B_4 (m)	-1E-2	$z_{A_{b4}}^{B_4}$	Coordinate of A_{b4} in z-axis in the coordinate system of B_4 (m)	7E-2
$y_{A_{b5}}^{B_5}$	Coordinate of A_{b5} in y-axis in the coordinate system of B_5 (m)	-1.5E-3	$z_{A_{b5}}^{B_5}$	Coordinate of A_{b5} in z-axis in the coordinate system of B_5 (m)	0.07
$y_{A_{12}}^{B_1}$	Coordinate of A_{12} in y-axis in the coordinate system of B_1 (m)	-2.9E-3	$z_{A_{12}}^{B_1}$	Coordinate of A_{12} in z-axis in the coordinate system of B_1 (m)	4.7E-3
$y_{A_{23}}^{B_2}$	Coordinate of A_{23} in y-axis in the coordinate system of B_2 (m)	-2.7E-4	$z_{A_{23}}^{B_2}$	Coordinate of A_{23} in z-axis in the coordinate system of B_2 (m)	-2E-2
$x_{A_{14}}^{B_4}$	Coordinate of A_{14} in x-axis in the coordinate system of B_4 (m)	-4E-2	$y_{A_{14}}^{B_4}$	Coordinate of A_{14} in y-axis in the coordinate system of B_4 (m)	-3E-2
$x_{A_{45}}^{B_5}$	Coordinate of A_{45} in x-axis in the coordinate system of B_5 (m)	7.8E-3	$y_{A_{45}}^{B_5}$	Coordinate of A_{45} in y-axis in the coordinate system of B_5 (m)	-1E-2
l_{z3}	Length of B_3 in the z-axis (m)	1.9E-1			
k_{xfl}	Stiffness between B_f and B_l in x-axis (N/m)	3.52E6	c_{xfl}	Damping between B_f and B_l in x-axis (Ns/m)	6.04E5
k_{yfl}	Stiffness between B_f and B_l in y-axis (N/m)	1.2E-3	c_{yfl}	Damping between B_f and B_l in y-axis (Ns/m)	4.12E1
k_{zfl}	Stiffness between B_f and B_l in z-axis (N/m)	4.71E5	c_{zfl}	Damping between B_f and B_l in z-axis (Ns/m)	1.16E5
k_{xlp}	Stiffness between B_l and B_p in x-axis (N/m)	8.5E4	c_{xlp}	Damping between B_l and B_p in x-axis (Ns/m)	2.14
k_{ylp}	Stiffness between B_l and B_p in y-axis (N/m)	1.23E5	c_{ylp}	Damping between B_l and B_p in y-axis (Ns/m)	1E-3
k_{zlp}	Stiffness between B_l and B_p in z-axis (N/m)	1.5E-3	c_{zlp}	Damping between B_l and B_p in z-axis (Ns/m)	1.1E-3
k_{xfp}	Stiffness between B_f and B_p in x-axis (N/m)	1E2	c_{xfp}	Damping between B_f and B_p in x-axis (Ns/m)	1E3
k_{yfp}	Stiffness between B_f and B_p in y-axis (N/m)	1.36E5	c_{yfp}	Damping between B_f and B_p in y-axis (Ns/m)	3.33E2
k_{zfp}	Stiffness between B_f and B_p in z-axis (N/m)	4.57E3	c_{zfp}	Damping between B_f and B_p in z-axis (Ns/m)	2.33E3

m_l	Mass of the supporting linkage in one side (kg)	1E1	m_s	Mass of the sprung mass of the suspension top plate (kg)	3
k_{xpc}	Stiffness between B_p and B_c in x-axis (N/m)	3.33E6	c_{xpc}	Stiffness between B_p and B_c in x-axis (N/m)	1.01E6
k_{ypc}	Stiffness between B_p and B_c in y-axis (N/m)	7.38E3	c_{ypc}	Damping between B_p and B_c in y-axis (N/m)	6.6E-2
k_{zpc}	Stiffness between B_p and B_c in z-axis (N/m)	1.35E6	c_{zpc}	Damping between B_p and B_c in z-axis (N/m)	3.71E6
k_{rpc}	Stiffness between B_p and B_c around x-axis (Nm/rad)	1.96E1	c_{rpc}	Damping between B_p and B_c around x-axis (Nm/rad)	4E1
k_{ppc}	Stiffness between B_p and B_c around y-axis (Nm/rad)	9E3	c_{ppc}	Damping between B_p and B_c around y-axis (Nms/rad)	9E1
k_{xcbr}	Stiffness between B_c and B_{br} in x-axis (N/m)	6E4	c_{xcbr}	Damping between B_c and B_{br} in x-axis (N/m)	5
k_{ycbr}	Stiffness between B_c and B_{br} in y-axis (N/m)	1.76E4	c_{ycbr}	Damping between B_c and B_{br} in y-axis (N/m)	3.42E5
k_{zcbr}	Stiffness between B_c and B_{br} in z-axis (N/m)	2.46E6	c_{zcbr}	Damping between B_c and B_{br} in z-axis (N/m)	1.066E7
k_{rcbr}	Stiffness between B_c and B_{br} around x-axis (Nm/rad)	4.34E3	c_{rcbr}	Damping between B_c and B_{br} around x-axis (Nm/rad)	8.35E-1
k_{pcbr}	Stiffness between B_c and B_{br} around y-axis (Nm/rad)	5.18E4	c_{pcbr}	Damping between B_c and B_{br} around y-axis (Nms/rad)	1.92E6
k_{xc1}	Stiffness between B_1 and B_c in x-axis (N/m)	1.83E8	c_{xc1}	Damping between B_1 and B_c in x-axis (N/m)	5.73E7
k_{yc1}	Stiffness between B_1 and B_c in y-axis (N/m)	9E1	c_{yc1}	Damping between B_1 and B_c in y-axis (N/m)	9
k_{zc1}	Stiffness between B_1 and B_c in z-axis (N/m)	4.14	c_{zc1}	Damping between B_1 and B_c in z-axis (N/m)	4.1E-1
k_{pc1}	Stiffness between B_1 and B_c around y-axis (Nm/rad)	1.5E-1	c_{pc1}	Damping between B_1 and B_c around y-axis (Nms/rad)	4.62E-2
k_{xc2}	Stiffness between B_2 and B_c in x-axis (N/m)	1.54	c_{xc2}	Damping between B_2 and B_c in x-axis (N/m)	3.55
k_{yc2}	Stiffness between B_2 and B_c in y-axis (N/m)	1E4	c_{yc2}	Damping between B_2 and B_c in y-axis (N/m)	3E2
k_{zc2}	Stiffness between B_2 and B_c in z-axis (N/m)	7.15	c_{zc2}	Damping between B_2 and B_c in z-axis (N/m)	1.46
k_{pc2}	Stiffness between B_2 and B_c around y-axis (Nm/rad)	1	c_{pc2}	Damping between B_2 and B_c around y-axis (Nms/rad)	2
k_{xb4}	Stiffness between B_4 and B_b in x-axis (N/m)	8.92E-1	c_{xb4}	Damping between B_4 and B_b in x-axis (N/m)	1.13E-1
k_{yb4}	Stiffness between B_4 and B_b in y-axis (N/m)	1E1	c_{yb4}	Damping between B_4 and B_b in y-axis (N/m)	1.2E2

k_{zb4}	Stiffness between B_4 and B_b in z-axis (N/m)	4.24	c_{zb4}	Damping between B_4 and B_b in z-axis (N/m)	8.98E-1
k_{pb4}	Stiffness between B_4 and B_b around y-axis (Nm/rad)	7.25E-1	c_{pb4}	Damping between B_4 and B_b around y-axis (Nms/rad)	9.03E-2
k_{xb5}	Stiffness between B_5 and B_b in x-axis (N/m)	5E4	c_{xb5}	Damping between B_5 and B_b in x-axis (N/m)	1E2
k_{yb5}	Stiffness between B_5 and B_b in y-axis (N/m)	1.6E4	c_{yb5}	Damping between B_5 and B_b in y-axis (N/m)	8.79
k_{zb5}	Stiffness between B_5 and B_b in z-axis (N/m)	1.78E8	c_{zb5}	Damping between B_5 and B_b in z-axis (N/m)	4.16E-1
k_{pb5}	Stiffness between B_5 and B_b around y-axis (Nm/rad)	1.40E1	c_{pb5}	Damping between B_5 and B_b around y-axis (Nms/rad)	2.33E1

D.3 Sensitivity matrix of the parameters of the human body model

$$\boldsymbol{\Psi} = \begin{bmatrix} 0 & 0 & 0 & 0 & 0 & 0 & 0 & 0 & 0 & 0 & 0 & 0 & 0 & 0 & 0 & 0 & 0 & 0 & 0 & 0 & 0 & 0 & 0 & 0 & 0.11 & 0 & 0 & 0 & 0 & 0 & 0 & 0 & 0 & \cdots \\ 0 & 0 & 0 & 0 & 0 & 0 & 0 & 0 & 0 & 0 & 0 & 0 & 0 & 0 & 0.26 & 0 & 0 & 0 & 0 & 0 & 0 & 0 & 0.15 & -0.16 & 0.13 & 0 & 0 & 0 & 0 & 0 & -0.07 & -0.11 & \\ 0 & 0 & 0 & 0 & 0 & 0 & 0 & 0 & 0 & 0 & 0 & 0 & 0 & 0 & 0 & 0 & 0 & 0 & 0 & 0 & 0 & 0 & -0.09 & 0 & 0.21 & 0 & 0 & 0 & 0 & 0 & 0 & 0 & \\ 0 & 0 & 0 & 0 & 0 & 0 & 0 & 0 & 0 & 0 & 0 & 0 & 0 & 0 & 0 & 0 & 0 & 0 & 0 & 0 & 0 & 0 & 0 & 0 & 0.26 & 0 & 0 & 0 & 0 & 0 & 0 & 0 & \\ 0 & 0 & 0 & 0 & 0 & 0 & 0 & 0 & 0 & 0 & 0 & 0 & 0 & 0 & 0 & 0 & 0 & 0 & 0 & 0 & 0 & 0 & 0 & 0 & -0.1 & 0 & 0 & 0 & 0 & 0 & 0 & 0 & \\ 0 & 0 & 0 & 0 & 0 & 0 & 0 & 0 & 0 & 0 & 0 & 0 & 0 & 0 & 0.19 & -0.07 & 0 & 0 & 0 & 0 & 0 & 0 & 0.06 & -0.28 & 0 & 0 & 0 & 0 & 0 & 0 & 0 & 0 & \\ 0 & 0 & 0 & -0.14 & 0 & 0 & 0 & 0 & 0 & 0 & 0 & 0 & 0 & 0 & 0 & 0 & 0 & 0 & 0 & 0 & 0 & 0 & 0 & 0 & 0 & 0 & 0 & 0 & 0 & 0 & 0 & 0 & \\ 0 & 0 & 0 & 0.05 & 0 & 0 & 0 & 0 & 0 & 0 & 0 & 0 & 0 & 0 & 0 & 0 & 0 & 0 & 0 & 0 & 0 & 0 & 0 & 0 & 0 & 0 & 0 & 0 & 0 & 0 & 0 & 0 & \\ \hline 0 & 0 & 0 & 0 & 0 & 0 & 0 & 0 & 0.43 & -0.11 & 0 & 0 & 0 & 0 & 0.16 & 0 & 0 & 0 & 0 & 0 & 0 & 0 & 0 & 0 & 0 & 0 & 0 & 0 & 0 & 0 & 0 & 0 & \\ 0 & 0 & 0 & 0 & 0 & 0 & 0 & 0 & 0 & -0.47 & 0 & 0 & 0 & 0 & 0.41 & 0 & 0 & 0 & 0 & 0 & 0 & 0 & 0 & 0 & 0 & 0 & 0 & 0 & -0.04 & 0 & 0 & 0 & \\ 0 & 0 & 0 & 0 & 0 & 0 & 0 & 0 & 0 & 0 & 0 & 0 & 0 & 0 & 0 & 0 & 0 & 0 & 0 & 0 & 0 & 0 & 0 & 0 & 0 & 0 & 0.58 & 0 & 0 & 0 & 0 & 0 & \\ 0 & 0 & 0 & 0 & 0 & 0 & 0 & 0 & -0.35 & 0 & 0 & 0 & 0 & 0 & -0.25 & 0 & 0 & 0 & 0 & 0 & 0 & 0 & 0 & 0 & 0 & 0 & 0.48 & 0.48 & 0 & 0 & 0 & 0 & \\ \cdots & 0 & 0 & 0 & 0 & 0 & 0 & 0 & 0.26 & 0 & 0 & 0 & 0 & 0 & 0 & 0 & 0 & 0 & 0 & 0 & 0 & 0 & 0 & 0 & 0 & 0 & 0 & 0 & 0 & 0 & 0 & 0 & \\ & 0 & 0 & 0 & 0 & 0 & 0 & 0 & 0 & 0 & -0.09 & 0 & 0 & 0 & 0 & 0 & 0 & 0 & 0 & 0 & 0 & 0 & 0 & 0 & 0 & 0 & 0 & 0 & 0 & 0 & 0 & 0 & \\ & 0 & 0 & 0 & 0 & 0 & 0 & 0 & 0 & 0 & 0 & 0 & 0 & 0 & 0 & 0 & 0 & 0 & 0 & 0 & 0.2 & 0 & 0 & 0 & 0 & 0 & 0 & 0 & 0 & 0 & 0 & 0 & \\ & 0 & 0 & 0 & 0 & 0 & 0 & 0 & 0 & 0 & 0 & 0 & 0 & 0 & 0 & 0 & 0 & 0 & 0 & 0 & 0 & 0 & 0 & 0 & -0.05 & 0 & 0 & 0 & 0 & 0 & 0 & 0 & \end{bmatrix}_{8\times 64}$$

D.4 Sensitivity matrices of the parameters of the suspension-seat-occupant model

$$\boldsymbol{\Psi}_{susp} = \begin{bmatrix} 0 & 0 & 0 & 0 & 0.07 & 0 & 0 & 0 & 0 & 0 & 0.66 & -0.40 \\ 0 & 0 & 0 & 0 & 0 & 0 & 0 & 0 & 0 & 0 & 0.08 & -0.27 \\ 0 & 0 & 0 & 0 & 0 & 0 & 0 & 0 & 0 & 0 & 0 & 0 \\ 0 & 0 & 0 & 0 & -0.21 & 0 & 0 & 0 & 0 & -0.03 & 0 & 0 \end{bmatrix}_{4\times 12}$$

$$\boldsymbol{\Psi}_{seatpan} = \begin{bmatrix} 0 & 0 & 0 & 0 & 0 & 0 & 0.11 & 0 & 0 & 0 & 0 & 0 & 0 & 0 \\ 0 & 0 & 0 & 0 & 0 & 0 & 0.01 & -0.002 & 0 & 0 & 0 & 0 & 0 & 0 \\ 0 & 0 & 0 & 0 & 0 & 0 & 0.7 & -0.1 & 0 & 0 & 0 & 0 & 0 & 0 \\ 0 & 0 & 0 & 0 & 0 & 0 & 0 & -0.23 & -0.13 & 0 & 0 & 0 & 0 & 0 \\ \hline 0 & 0 & 0 & 0 & 0 & 0 & 0 & 0 & 0 & 0 & 0 & 0 & 0 & 0 \\ 0 & 0 & 0 & 0 & 0 & 0 & 0 & 0 & 0 & 0 & 0 & 0 & 0 & -0.003 \\ 0 & 0 & 0 & 0 & 0 & 0 & 0 & 0 & 0 & 0 & 0 & 0 & 0 & 0.1 \\ 0 & 0 & 0 & 0 & 0 & 0 & 0 & 0 & 0 & 0 & 0 & -0.002 & 0.004 & 0.013 \end{bmatrix}_{4\times 28} \cdots \cdots$$

$$\boldsymbol{\Psi}_{backrest} = \begin{bmatrix} 0 & 0 & 0 & 0 & 0 & 0 & 0.07 & 0 & 0 & 0 & 0 & 0.11 \\ 0 & 0 & 0 & 0 & 0 & 0 & 0 & 0 & 0 & 0 & 0 & 0.03 \\ 0 & 0 & 0 & 0 & 0 & 0 & 0 & 0 & 0 & 0 & 0 & -0.1 \\ 0 & 0 & 0 & 0 & 0 & 0 & -0.04 & -0.004 & 0 & 0 & -0.003 & -0.03 \end{bmatrix}_{4\times 12}$$

LIST OF REFERENCES

Adam, S. A., Jalil, N. A., Razali, K. M. and Ng, Y. (2019a) The Effects of Posture on Suspension Seat Transmissibility during Exposure to Vertical Whole-Body Vibration. *Journal of Physics: Conference Series*. IOP Publishing, 012026.

Adam, S. A., Jalil, N. A., Razali, K. M., Ng, Y. and Aladdin, M. (2019b) Mathematical model of suspension seat-person exposed to vertical vibration for off-road vehicles. *International Journal of Automotive and Mechanical Engineering,* 16**,** 6773-6782.

Alperovitch-Najenson, D., Santo, Y., Masharawi, Y., Katz-Leurer, M., Ushvaev, D. and Kalichman, L. (2010) Low back pain among professional bus drivers: ergonomic and occupational-psychosocial risk factors. *Sat,* 2**,** 18.

Bendat, J. S. and Piersol, A. G. (2011) *Random data: analysis and measurement procedures*, John Wiley & Sons.

Bernard, B. P. and Putz-Anderson, V. (1997) Musculoskeletal disorders and workplace factors; a critical review of epidemiologic evidence for work-related musculoskeletal disorders of the neck, upper extremity, and low back.

Blood, R., Ploger, J., Yost, M., Ching, R. and Johnson, P. (2010) Whole body vibration exposures in metropolitan bus drivers: A comparison of three seats. *Journal of Sound and Vibration,* 329**,** 109-120.

Chaudhary, D., Bhattacherjee, A. and Patra, A. (2015) Analysis of whole-body vibration exposure of drill machine operators in open pit iron ore mines. *Procedia Earth and Planetary Science,* 11**,** 524-530.

Contini, R. (1972) Body segment parameters, Part II. *Artificial limbs,* 16**,** 1-19.

D'amore, F. and Qiu, Y. (2021) Vibration Transmission at Seat Cushion and Sitting Comfort in Next-Generation Cars. *Congress of the International Ergonomics Association*. Springer, 615-622.

Dempster, W. T. and Gaughran, G. R. (1967) Properties of body segments based on size and weight. *American journal of anatomy,* 120**,** 33-54.

Desai, R., Guha, A. and Seshu, P. (2018) Multibody Biomechanical Modelling of Human Body Response to Direct and Cross Axis Vibration. *Procedia computer science,* 133**,** 494-501.

Desai, R., Guha, A. and Seshu, P. (2021a) An appropriate biomechanical model of seated human subjects exposed to whole-body vibration. *Proceedings of the Institution of Mechanical Engineers, Part K: Journal of Multi-body Dynamics***,** 14644193211039406.

Desai, R., Guha, A. and Seshu, P. (2021b) A comparison of different models of passive seat suspensions. *Proceedings of the institution of mechanical engineers, Part D: journal of automobile engineering,* 235**,** 2585-2604.

Dong, R.-C., Guo, Q.-J., Yuan, W., Du, W., Yang, X.-H. and Zhao, Y.-J. (2020) The finite element model of seated whole human body for vibration investigations of lumbar spine in complex system. *IEEE Access,* 8**,** 125046-125055.

Du, B. B., Bigelow, P. L., Wells, R. P., Davies, H. W., Hall, P. and Johnson, P. W. (2018) The impact of different seats and whole-body vibration exposures on truck driver vigilance and discomfort. *Ergonomics,* 61**,** 528-537.

Fairley, T. and Griffin, M. (1990) The apparent mass of the seated human body in the fore-and-aft and lateral directions. *Journal of Sound and Vibration,* 139**,** 299-306.

Fritz, M. (2000) Description of the relation between the forces acting in the lumbar spine and whole-body vibrations by means of transfer functions. *Clinical Biomechanics,* 15**,** 234-240.

Gao, K., Li, C., Xiao, Y. and Zhang, Z. (2021) Finite element modeling and parameter identification of the seated human body exposed to vertical vibration. *Biomechanics and Modeling in Mechanobiology,* 20**,** 1789-1803.

Gong, W. and Griffin, M. J. (2018) Measuring, evaluating and assessing the transmission of vibration through the seats of railway vehicles. *Proceedings of the Institution of Mechanical Engineers, Part F: Journal of Rail and Rapid Transit,* 232**,** 384-395.

Griffin, M. J. (1990) *Handbook of human vibration*, Academic press.

Gunston, T., Rebelle, J. and Griffin, M. (2004) A comparison of two methods of simulating seat suspension dynamic performance. *Journal of Sound and Vibration,* 278**,** 117-134.

Houghton, T. (2003) The effect of backrest inclination on the transmission of vertical vibration through an automotive seat. *United Kingdom Conference on Human Response to Vibration, held at Institute of Naval Medicine*. 17-19.

Huang, Y. and Griffin, M. J. (2006) Effect of voluntary periodic muscular activity on nonlinearity in the apparent mass of the seated human body during vertical random whole-body vibration. *Journal of sound and vibration,* 298**,** 824-840.

Huang, Y., Zhang, P. and Liang, S. (2020) Apparent mass of the seated human body during vertical vibration in the frequency range 2–100 Hz. *Ergonomics,* 63**,** 1150-1163.

Ittianuwat, R., Fard, M. and Kato, K. (2014) The transmission of vibration at various locations on vehicle seat to seated occupant body. *INTER-NOISE and NOISE-CON Congress and Conference Proceedings*. Institute of Noise Control Engineering, 2062-2073.

Jalil, N. a. A. and Griffin, M. J. (2007) Fore-and-aft transmissibility of backrests: Effect of backrest inclination, seat-pan inclination, and measurement location. *Journal of sound and vibration,* 299**,** 99-108.

Jalil, N. a. A. and Griffin, M. J. (2008) Fore-and-aft apparent mass of the back: nonlinearity and variation with vertical location. *Journal of Sound and Vibration,* 318**,** 1348-1363.

Johanning, E. (1998) Back Disorder Intervention Strategies for Mass Transit Operators Exposed to

Whole-Body Vibration—comparison of Two Transit System Approaches and Practices. *Journal of Sound and Vibration,* 215**,** 629-634.

Johnson, P. W., Ibbotson-Brown, J., Menocal, S. and Parison, J. (2019) Comparison of Whole-Body Vibration Exposures When Operating a City Bus with an Active, Passive and Static Suspension Bus Seat. *Proceedings of the Human Factors and Ergonomics Society Annual Meeting,* 63**,** 1052-1056.

Jonsson, P. M., Rynell, P. W., Hagberg, M. and Johnson, P. W. (2015) Comparison of whole-body vibration exposures in buses: effects and interactions of bus and seat design. *Ergonomics,* 58**,** 1133-1142.

Ju, M.-S. and Mansour, J. M. (1987) APPLICATION OF SIMULATION SENSITIVITY ANALYSIS TO FUNCTIONAL NEUROMUSCULAR STIMULATION OF GAIT. *American Society of Mechanical Engineers, Applied Mechanics Division, AMD,* 84**,** 327-330.

Kabir, M. S. N., Chung, S.-O., Kim, Y.-J., Sung, N.-S. and Hong, S.-J. (2017) Measurement and evaluation of whole body vibration of agricultural tractor operator. *International Journal of Agricultural and Biological Engineering,* 10**,** 248-255.

Kim, J. H., Dennerlein, J. T. and Johnson, P. W. (2018) The effect of a multi-axis suspension on whole body vibration exposures and physical stress in the neck and low back in agricultural tractor applications. *Applied ergonomics,* 68**,** 80-89.

Kim, K.-S., Kim, J. and Kim, K.-J. (2011) Dynamic modeling of seated human body based on measurements of apparent inertia matrix for fore-and-aft/vertical/pitch motion. *Journal of Sound and Vibration,* 330**,** 5716-5735.

Kim, T.-H., Kim, Y.-T. and Yoon, Y.-S. (2005) Development of a biomechanical model of the human body in a sitting posture with vibration transmissibility in the vertical direction. *International Journal of Industrial Ergonomics,* 35**,** 817-829.

Kitazaki, S. and Griffin, M. J. (1997) A modal analysis of whole-body vertical vibration, using a finite element model of the human body. *Journal of Sound and Vibration,* 200**,** 83-103.

Krajnak, K. (2018) Health effects associated with occupational exposure to hand-arm or whole body vibration. *Journal of Toxicology and Environmental Health, Part B,* 21**,** 320-334.

Krumm, D., Schwanitz, S. and Odenwald, S. (2020) Seat cushions made of warp knitted spacer fabrics influence seat transmissibility. *Applied Ergonomics,* 86**,** 103099.

Kumar, V. and Saran, V. H. (2019) Biodynamic model of the seated human body under the vertical whole body vibration exposure. *International Journal of Acoustics & Vibration,* 24.

Liu, C. (2017) *Localised biodynamic responses of the seated human body during excitation by vertical vibration.* PhD dissertation, University of Southampton.

Liu, C. and Qiu, Y. (2020) Nonlinearity in the localised apparent masses of the seated human body exposed to vertical vibration. *Mechanical Systems and Signal Processing,* 135**,** 106394.

Liu, C. and Qiu, Y. (2021) Mechanism associated with the effect of backrest inclination on biodynamic responses of the human body sitting on a rigid seat exposed to vertical vibration. *Journal of Sound and Vibration***,** 116299.

Liu, C., Qiu, Y. and Griffin, M. J. (2015) Finite element modelling of human-seat interactions: vertical in-line and fore-and-aft cross-axis apparent mass when sitting on a rigid seat without backrest and exposed to vertical vibration. *Ergonomics,* 58**,** 1207-1219.

Mandapuram, S., Rakheja, S., Boileau, P.-É. and Maeda, S. (2012) Apparent mass and head vibration transmission responses of seated body to three translational axis vibration. *International Journal of Industrial Ergonomics,* 42**,** 268-277.

Mandapuram, S., Rakheja, S. and Boileau, P. (2010) Analysis of Coupling Effects in Seated Body Biodynamic Responses to Multi-Axis Vibration.

Mandapuram, S. C., Rakheja, S., Demont, R. G. and Boileau, P.-É. (2005) Influence of back support conditions on the apparent mass of seated occupants under horizontal vibration. *Industrial Health,* 43**,** 421-435.

Mansfield, N., Holmlund, P., Lundström, R., Lenzuni, P. and Nataletti, P. (2006) Effect of vibration magnitude, vibration spectrum and muscle tension on apparent mass and cross axis transfer functions during whole-body vibration exposure. *Journal of biomechanics,* 39**,** 3062-3070.

Mansfield, N. J. and Lundström, R. (1999) Orthogonal force response of the seated person when exposed to horizontal whole-body vibration. *the 34th United Kingdom Group Meeting on Human Response to Vibration.* Dunton, Essex, England.

Mansfield, N. J. and Maeda, S. (2006) Comparison of the apparent masses and cross-axis apparent masses of seated humans exposed to single-and dual-axis whole-body vibration. *Journal of Sound and Vibration,* 298**,** 841-853.

Mansfield, N. J. and Maeda, S. (2007) The apparent mass of the seated human exposed to single-axis and multi-axis whole-body vibration. *Journal of Biomechanics,* 40**,** 2543-2551.

Marzbanrad, J., Jamali, S. and Afkar, A. (2016) Calculation of APMS and STHT Responses in Three Translational Axis Vibration for Human Body Using Biomechanical Modeling and Matrix Method. *Computational Research Progress in Applied Science & Engineering,* 2**,** 150-157.

Matsumoto, Y. and Griffin, M. J. (2001) Modelling the dynamic mechanisms associated with the principal resonance of the seated human body. *Clinical Biomechanics,* 16**,** S31-S44.

Nawayseh, N. and Griffin, M. (2003) Non-linear dual-axis biodynamic response to vertical whole-body vibration. *Journal of Sound and Vibration,* 268**,** 503-523.

Nawayseh, N. and Griffin, M. (2005) Non-linear dual-axis biodynamic response to fore-and-aft whole-body vibration. *Journal of Sound and Vibration,* 282**,** 831-862.

Nawayseh, N. and Griffin, M. J. (2009) A model of the vertical apparent mass and the fore-and-aft cross-axis apparent mass of the human body during vertical whole-body vibration. *Journal*

of Sound and Vibration, 319**,** 719-730.

Nikolova, G. S. and Toshev, Y. E. (2007) Estimation of male and female body segment parameters of the Bulgarian population using a 16-segmental mathematical model. *Journal of biomechanics,* 40**,** 3700-3707.

Ning, D., Sun, S., Du, H., Li, W. and Zhang, N. (2018) Vibration control of an energy regenerative seat suspension with variable external resistance. *Mechanical Systems and Signal Processing,* 106**,** 94-113.

Park, S. J., Park, S. C., Kim, J. H. and Kim, C.-B. (1999) Biomechanical parameters on body segments of Korean adults. *International Journal of Industrial Ergonomics,* 23**,** 23-31.

Phate, M., Toney, S. and Phate, V. (2019) Prediction and Analysis of Apparent Masses (AM) of Anthropometric Based Human Seated Posture. *Industrial Engineering Journal,* 12**,** 1-14.

Qiu, Y. (2012) A procedure for developing a generic model of a suspenison seat with occupant for predicting seat transmissibility. *47th United Kingdom Conference on Human Responses to Vibration.* ISVR, University of Southampton, Southampton, England.

Qiu, Y. (2017) Dynamic Characteristics of a Suspension Seat Determined in Laboratory Study. *J Ergonomics,* 7**,** 220-225.

Qiu, Y. and Griffin, M. (2003) Transmission of fore–aft vibration to a car seat using field tests and laboratory simulation. *Journal of sound and vibration,* 264**,** 135-155.

Qiu, Y. and Griffin, M. (2004) Transmission of vibration to the backrest of a car seat evaluated with multi-input models. *Journal of Sound and Vibration,* 274**,** 297-321.

Qiu, Y. and Griffin, M. J. (2010) Biodynamic responses of the seated human body to single-axis and dual-axis vibration. *Industrial Health,* 48**,** 615-627.

Qiu, Y. and Griffin, M. J. (2011) Modelling the fore-and-aft apparent mass of the human body and the transmissibility of seat backrests. *Vehicle System Dynamics,* 49**,** 703-722.

Qiu, Y. and Griffin, M. J. (2012) Biodynamic response of the seated human body to single-axis and dual-axis vibration: effect of backrest and non-linearity. *Industrial health,* 50**,** 37-51.

Rakheja, S., Dewangan, K. N., Dong, R. G. and Marcotte, P. (2020a) Whole-body vibration biodynamics-a critical review: I. Experimental biodynamics. *International journal of vehicle performance,* 6**,** 1-51.

Rakheja, S., Dewangan, K. N., Dong, R. G., Marcotte, P. and Pranesh, A. (2020b) Whole-body vibration biodynamics-a critical review: II. Biodynamic modelling. *International journal of vehicle performance,* 6**,** 52-84.

Rakheja, S., Stiharu, I., Zhang, H. and Boileau, P.-É. (2006) Seated occupant interactions with seat backrest and pan, and biodynamic responses under vertical vibration. *Journal of Sound and Vibration,* 298**,** 651-671.

Rao, M., Sivapirakasam, S. and Sankaranarayanasamy, K. (2018) Whole body vibration of the midibus

driver with different seating condition. *IOP Conference Series: Materials Science and Engineering*. IOP Publishing, 012115.

Robb, M. J. and Mansfield, N. J. (2007) Self-reported musculoskeletal problems amongst professional truck drivers. *Ergonomics,* 50**,** 814-827.

Sayed, M., Shahrin, H. and Adawy, M. (2013) Whole-body-vibration measurement and assessment for Cairo subway (metro), car and bus passengers. *Int J Elect, Commun Instru Engin Res Develop,* 3**,** 185-202.

Shahzad, F. and Qiu, Y. (2012) A nonlinear multi-body dynamic model of a suspension seat with occupant correlated with experimental results. *47th United Kingdom Conference on Human Responses to Vibration.* ISVR, University of Southampton, Southampton, England.

Singh, A., Nawayseh, N., Singh, L., Singh, S. and Singh, H. (2019) Investigation of compressive stress on lumbar spine due to whole body vibration exposure in rotary tillage operation. *International Journal of Automotive and Mechanical Engineering,* 16**,** 6684-6696.

Singh, A., Singh, H., Singh, I., Kalsi, S. and Saran, V. (2021). Effect of Variant Seat Suspension Systems on Human Subject in Agricultural Conditions. *Advances in Systems Engineering.* Springer, 869-879.

Tiemessen, I. J., Hulshof, C. T. and Frings-Dresen, M. (2008) Low back pain in drivers exposed to whole body vibration: analysis of a dose–response pattern. *Occupational and environmental medicine,* 65**,** 667-675.

Toward, M. G. and Griffin, M. J. (2009) Apparent mass of the human body in the vertical direction: Effect of seat backrest. *Journal of Sound and Vibration,* 327**,** 657-669.

Toward, M. G. and Griffin, M. J. (2011) The transmission of vertical vibration through seats: Influence of the characteristics of the human body. *Journal of Sound and Vibration,* 330**,** 6526-6543.

Tufano, S. and Griffin, M. J. (2013) Nonlinearity in the vertical transmissibility of seating: the role of the human body apparent mass and seat dynamic stiffness. *Vehicle System Dynamics,* 51**,** 122-138.

Wei, L. and Griffin, M. (1998) Mathematical models for the apparent mass of the seated human body exposed to vertical vibration. *Journal of Sound and Vibration,* 212**,** 855-874.

Whitley, D. (1994) A genetic algorithm tutorial. *Statistics and computing,* 4**,** 65-85.

Wu, J. and Qiu, Y. (2020) Modelling of seated human body exposed to combined vertical, lateral and roll vibrations. *Journal of Sound and Vibration,* 485**,** 115509.

Wu, J. and Qiu, Y. (2021) Modeling and analysis of a train seat with occupant exposed to combined lateral, vertical and roll vibration. *Journal of Sound and Vibration,* 496**,** 115920.

Wu, J., Qiu, Y. and Sun, C. (2022) Modelling and analysis of coupled vibration of human body in the sagittal and coronal planes exposed to vertical, lateral and roll vibrations and the comparison with modal test. *Mechanical Systems and Signal Processing,* 166**,** 108439.

Wu, J., Qiu, Y. and Zhou, H. (2021) Biodynamic response of seated human body to vertical and added lateral and roll vibrations. *Ergonomics***,** 1-32.

Yang, M. (2016) *Effects of sitting posture and seat backrest on the biodynamic response of the human body and the prediction of spinal forces during vertical whole-body vibration.* PhD dissertation, University of Southampton.

Yang, M. and Qiu, Y. (2015) Effect of backrest inclination on apparent mass at the seat and the backrest during vertical whole-body vibration. *50th United Kingdom Conference on Human Responses to Vibration.* University of Southampton.

Yin, W., Ding, J. and Qiu, Y. (2021) Nonlinear Dynamic Modelling of a Suspension Seat for Predicting the Vertical Seat Transmissibility. *Mathematical Problems in Engineering, 2021***,** 1-10.

Zhang, W., Ma, Z., Jin, A., Yang, J. and Zhang, Y. (2015) An improved human biodynamic model considering the interaction between feet and ground. *SAE International Journal of Commercial Vehicles,* 8**,** 13-19.

Zhang, X. (2014) *Measurement and modelling of seating dynamics to predict seat transmissibility.* PhD dissertation, University of Southampton.

Zhang, X., Qiu, Y. and Griffin, M. J. (2016) Transmission of fore-and-aft vibration to the seat pan, the backrest and the headrest of a car seat. *Proceedings of the Institution of Mechanical Engineers, Part D: Journal of Automobile Engineering,* 230**,** 736-744.

Zhang, X., Yu, P., Li, Y., Qiu, Y., Sun, C., Wang, Z. and Liu, C. (2021) Dynamic interaction between the human body and the seat during vertical vibration: effect of inclination of the seat pan and the backrest on seat transmissibilities. *Ergonomics***,** 1-54.

Zheng, G. (2012) *Biodynamics of the seated human body with dual-axis excitation: nonlinearity and cross-axis coupling.* PhD dissertation, University of Southampton.

Zheng, G., Qiu, Y. and Griffin, M. J. (2011) An analytic model of the in-line and cross-axis apparent mass of the seated human body exposed to vertical vibration with and without a backrest. *Journal of sound and vibration,* 330**,** 6509-6525.

Zheng, G., Qiu, Y. and Griffin, M. J. (2012) Vertical and dual-axis vibration of the seated human body: Nonlinearity, cross-axis coupling, and associations between resonances in transmissibility and apparent mass. *Journal of Sound and Vibration,* 331**,** 5880-5894.

Zheng, G., Qiu, Y. and Griffin, M. J. (2019) Fore-and-aft and dual-axis vibration of the seated human body: Nonlinearity, cross-axis coupling, and associations between resonances in the transmissibility and apparent mass. *International Journal of Industrial Ergonomics,* 69**,** 58-65.

Zou, K., Fard, M., Davy, J. and Robinson, S. (2021) Effects of Vibration on Seated Human Drowsiness/Alertness. *Vibration Engineering for a Sustainable Future: Numerical and Analytical Methods to Study Dynamical Systems, Vol. 3***,** 381.